

Controlled Release System for Delivery of GET peptide and its Application for Transcription Factor Delivery for Bone Regeneration

Hosam Al-Deen M. Abu Awwad, BSc, MRes

Department of Regenerative Medicine and Cellular Therapies

School of Pharmacy

Thesis submitted to the University of Nottingham

for the degree of Doctor of Philosophy

March 2018

Abstract

The repair of bone defects and non-union fractures is a significant challenge for clinicians as it requires tissue replacement. The current graft approaches used to treat these injuries have limitations with regard to quality and availability. This has resulted in research efforts to develop alternative synthetic materials that are able to aid tissue regeneration. These materials usually combined with biological factors to induce cells proliferation and differentiation. Transcription factors can provide specific regulatory effect, however, these transcription factors are very difficult to be delivered intracellularly. A recent work, conducted at Tissue Engineering group – University of Nottingham, has shown that recombinant transcription factors can be expressed, purified and delivered efficiently to control cell behaviour for further tissue engineering applications. Efficient delivery of these factors can be achieved by using Glycosaminoglycan-binding enhanced transduction (GET) peptides, which are multi-domain peptides comprising a GAG-binding peptide (to promote cell interaction) and a cell-penetrating peptide (CPP) for high efficiency membrane transduction.

The aim of the work presented in this thesis was to develop a poly-(lactic-co-glycolic acid) (PLGA) based delivery system to release RUNX2 transcription factor, which is significantly involved in osteogenesis. GET peptide was utilised to enhance the intracellular delivery of RUNX2. The advantage of this system is to control the dose and localisation of the released RUNX2 as well as providing a biodegradable scaffold to support the newly formed tissue.

Reproducible procedures were developed to manufacture spherical PLGA microparticles (MPs) using Solid-in-oil-in-water (S/O/W) emulsion method. Red florescent protein (RFP) coupled with GET peptide was used as model

protein to evaluate the stability of peptide during microparticles fabrication and release. Efficient encapsulation (~65%) and tailored protein release profiles could be achieved, however intracellular transduction was significantly inhibited post-release. Co-encapsulation of L-Histidine, which may form a complex with the PLGA degradation products under acidic conditions, was used as a strategy to retain GET peptide activity. Simulations of the polymer microclimate showed that hydrolytic acidic PLGA degradation products directly inhibited GET peptide transduction activity, use of L-Histidine significantly enhanced released protein delivery.

GET-RUNX2 was efficiently encapsulated (~60%) within PLGA MPs using the developed S/O/W method and release profile was adopted to match the optimal RUNX2 dose needed to induce osteogenesis of hMSCs (i.e. 60µg in the first 7 days of the study). GET-RUNX2 activity post release was evaluated. Results showed comparable transduction and transfection activities (compared to experimental control) throughout the release period. GET-RUNX2 loaded MPs were mixed with temperature-sensitive PLGA/PEG particles to provide scaffold structures.

hMSCs were used for an in-vitro differentiation assessments. Osteogenesis gene markers were comparable to experimental controls for both early and late markers. Moreover, the scaffold formula was optimised to be 3D printable to provide complex and irregular shape scaffolds matching defect size.

The ability to control intracellular transduction of functional proteins into cells will facilitate localised delivery of therapeutics, with minimised risk of systemic dosing that may lead to non-targeted activity, and allow approaches to direct cellular behaviour for regenerative medicine applications.

Publications and Presentations

Publications in Peer-Reviewed Journals:

Abu-Awwad HA-DM, Thiagarajan L, Dixon JE. Controlled release of GAG-binding enhanced transduction (GET) peptides for sustained and highly efficient intracellular delivery. Acta Biomaterialia 2017;57:225-37.

Thiagarajan L, **Abu-Awwad HA-DM**, Dixon JE. Osteogenic Programming of Human Mesenchymal Stem Cells with Highly Efficient Intracellular Delivery of RUNX2. Stem cells translational medicine 2017;6:2146-59.

Poster presentations:

- ''Controlled release of GET peptide for targeted delivery of runx2 for osteogenic programing of hMSCs'' Hosam M. Abu Awwad, Lalitha Thiagarajan, Kevin M. Shakesheff and James E. Dixon **TERMIS-EU, Davos, Switzerland 26 – 30 June 2017**

- Osteogenic Programming of human Mesenchymal Stem cells with highly efficient intracellular delivery of RUNX2'' Lalitha Thiagarajan, Hosam M. Abu Awwad and James E. Dixon
  TERMIS-EU, Davos, Switzerland 26 – 30 June 2017

- ''Controlled release of GET peptide and enhanced intracellular delivery of therapeutics'' H. M. Abu Awwad, K. M. Shakesheff and J. E. Dixon
  APS 2016, Glasgow 5 – 7 September 2016
  Commended and received poster award

- ‘’Controlled release of GET peptide and enhanced intracellular delivery of therapeutics’’ Hosam M. Abu Awwad, Kevin M. Shakesheff and James E. Dixon **TCES 2016, London 4 – 6 July 2016**

- ‘’Controlled release of GET peptide and enhanced intracellular delivery of therapeutics’’ Hosam M. Abu Awwad, Kevin M. Shakesheff and James E. Dixon **UKICRS 2016, Cardiff 21 – 22 April 2016** Commended and received poster award

Acknowledgment

I would like to express my gratitude to my supervisors, Dr James Dixon and Professor Kevin Shakesheff, who supported me during my PhD journey with advice and guidance. I am, as well, grateful to Dr. Lalitha Thiagarajan for the training, advice and support she provided throughout my PhD.

Moreover, I would like to thank Dr. Marta Alvares, Dr. Mahetab Amer, Dr. Gizem Osman, Dr. Omar Quatchi, for training and discussions on various things during different stages of my PhD.

I am greatly thankful to the staff and members of the tissue engineering group in the school of pharmacy, University of Nottingham, especially Dr. Abdulrahman Baki, Dr. Omar Hamid and Dr. Ahmed Aied. They were like a second family to me during my study.

Last, but not least, my words won't suffice the gratitude I have towards my family who has always provided support, enthusiasm, inspiration and motivation that kept me going during the journey.

Table of Contents

Abstract I

Publications and Presentations III

Acknowledgment V

List of Figures XI

List of Tables XXXII

1. Introduction 2

1.1. Bone physiology and structure 2

1.2. Bone development and growth 5

1.3. Bone repair 6

1.4. Clinical interventions for non-union bone Fracture 7

1.5. Growth factors for bone regeneration 10

1.5.1. BMP-2 signalling pathway 11

1.6. Transcription factor (RUNX2) 13

1.7. Glycosaminoglycan Enhanced Transduction (GET) Peptides 16

1.7.1. RUNX2 delivery using GET peptides 20

1.8. Therapeutic molecules delivery from microparticles 23

1.8.1. Polymers used for controlled drug release systems 24

1.8.2. PLGA use in controlled drug release systems 26

1.8.3. Physico-chemical characteristics of PLGA 27

1.8.4. Factors Affecting Polymer Degradation 27

1.8.5. Microparticle fabrication techniques 29

1.8.6. Factors affecting protein stability during MPs fabrication 33

1.9. Scaffolds for bone regeneration applications 34

1.9.1. Scaffold Materials 34

1.9.2. Injection of the Scaffold 37

1.9.3. 3D printing of scaffolds for bone tissue engineering 39

1.10. Thesis Aims 40
2. Development of a method to fabricate GET-protein loaded PLGA microparticles 43
2.1. Introduction 43
2.1.1. Aims 46
2.2. Materials and methods 47
2.2.1. Expression and purification of P21-mR-8R 47
2.2.2. Microparticles fabrication using S/O/W 48
2.2.3. Microparticles fabrication using W/O/W 50
2.2.4. Microparticles characterisation 50
2.2.5. Protein extraction from PLGA microparticles by acetone precipitation 51
2.2.6. Cell Culture 52
2.2.7. GET peptide transduction activity 52
2.2.8. Flow cytometry and microscopy 52
2.3. Results 53
2.3.1. Microparticles fabrication using W/O/W and S/O/W methods 53
2.3.2. Protein activity upon extraction from microparticles produced by W/O/W and S/O/W 61
2.3.3. Protein stability at shear stress 64
2.4. Discussion 68
2.5. Conclusions 70
3. Control of protein delivery and bioactivity assessment of released GET peptide 72
3.1. Introduction 72
3.1.1. Aims 74
3.2. Materials and Methods 75
3.2.1. Porous PLGA microparticles preparation using S/O/W method 75

3.2.2. MP characterization: Size, charge and morphology 75
3.2.3. Protein release from PLGA microparticles prepared using S/O/W ……76
3.2.4. Cell culture..... 76
3.2.5. GET peptide stability at various pH conditions..... 77
3.2.6. GET peptide transduction activity assessment 77
3.2.7. GET peptide interaction with blank PLGA microparticles 77
3.2.8. GET peptide interaction with PLGA degradation product 78
3.2.9. Flow cytometry and Microscopy 78
3.2.10. Statistical analysis..... 78
3.3. Results and Discussion 79
3.3.1. Protein release from PLGA microparticles prepared using S/O/W ……79
3.3.2. Acceleration of protein release using porous PLGA microparticles..... 82
3.3.3. Released GET peptide transduction activity assessment..... 84
3.3.4. Building a hypothesis for GET peptide loss of activity..... 88
3.3.5. Validation of GET peptide loss of activity hypothesis..... 88
3.3.6. Building a hypothesis for protein inactivation and stabilisation approach of GET peptide using L-histidine..... 105
3.3.7. Validation of L-Histidine stabilisation approach..... 106
3.3.8. L-Histidine does not neutralize carboxyl group acidity 118
3.3.9. Co-incubation with L-Histidine is required to prevent inhibition of GET transduction by carboxylic acid 119
3.3.10. L-Histidine dose is important to preserve GET transduction ... 121
3.3.11. Co-encapsulation of L-Histidine during fabrication of porous PLGA MPs..... 123
3.3.12. L-Histidine has no effect on sustained release of GET proteins from porous MPs..... 125

3.3.13. Released GET peptide transduction activity assessment 126
3.4. Conclusions 130
4. Development of Injectable Bone system to Study the Effect of GET Peptide Loaded Microparticles on Bone Regeneration 132
4.1. Introduction 132
4.1.1. Aims 135
4.2. Materials and Methods 136
4.2.1. Protein synthesis and FITC tagging 136
4.2.2. PLGA Microparticles fabrication 136
4.2.3. MP characterization: size and morphology 137
4.2.4. MP characterization: Determination of protein loading (loading efficiency) 137
4.2.5. MP characterization: P21-RUNX2-8R release 138
4.2.6. Cell culture 138
4.2.7. GET peptide transduction activity 138
4.2.8. Luciferase reporter assay 139
4.2.9. Flow cytometry and microscopy 139
4.2.10. PLGA/PEG particle production 139
4.2.11. Scaffold preparation 140
4.2.12. Cell seeding on scaffolds 140
4.2.13. Osteogenesis assay 141
4.2.14. Cell viability assay 141
4.2.15. Alkaline phosphatase (ALP) assay 141
4.2.16. Osteocalcin immunostaining 142
4.2.17. Von kossa staining 142
4.2.18. Gene Expression analysis 142
4.2.19. µCT 143
4.2.20. 3D printing of PLGA/PEG composites 143

4.2.21. Statistical analysis 144
4.3. Results 145
4.3.1. RUNX2-GET peptide loaded PLGA microparticles characterisation: morphology, size & entrapment efficiency 145
4.3.2. RUNX2-GET peptide release from PLGA microparticle 147
4.3.3. Biological activity evaluation of the released GET-RUNX2 using hMSC 149
4.3.4. Injectable bone scaffolds formation and characterisation: cell attachment and proliferation 155
4.3.5. Cell differentiation on injectable bone scaffolds containing RUNX2-GET peptide loaded PLGA microparticles 158
4.3.6. Scaffold characterisation: SEM and Micro-CT 165
4.3.7. PF-127 concentration and quantity affects the printing quality 168
4.3.8. Tri-acetin can be used to accelerate scaffolds sintering 171
4.3.9. Mixing pluronic and tri-acetin to enhance printing and sintering properties 173
4.3.10. Scaffold washing post-sintering 175
4.3.11. Cell proliferation on scaffolds 177
4.3.12. 3D printing of injectable bone mixed with pluronic and tri-acetin ……...179
4.3.13. Bio-printing and assessment of cell viability 181
4.4. Discussion 183
4.5. Conclusions 189
5. Final Conclusion and Future Work 191
5.1. Conclusions 191
5.2. Future Directions 195
6. References 197

List of Figures

Figure 1.1 Basic structure of bone. The cortical or compact bone structure is shown at the circumference with the more porous cancellous or spongy bone structure within the centre of the bone. [11]..... 4

Figure 1.2 Schematic showing the stages of normal bone fracture repair. Secondary fracture healing: bridging of a fracture by external callus. Adopted from Jahagirdar et. al. [13]. 8

Figure 1.3 The main components of the SMAD signalling pathways of BMP-2 in osteogenesis. Phosphorylation steps are highlighted by [ ][27]. 12

Figure 1.4 P21 improves PTD-mediated cellular uptake. (*A*) Schematic of the proteins created after screening domains that improve efficiency of protein delivery to cells. P21-mR is mRFP with an *N*-terminal fusion of the P21 domain of HB-EGF. P21-mR-8R is mRFP with N-terminal fusion of P21 and C-terminal fusion of 8R. (*B*) Fluorescence microscopy images of NIH3t3 cells treated with proteins (20 μg/mL) for 12 h in standard media conditions. (Scale bar, 100 μm.) (*C*) P21-mR-8R is efficiently taken into hESCs and mESCs (HUES7 and CGR-8, respectively) and hiPSCs (IPS2) and mouse cardiomyocyte cell line HL1. Flow cytometry analyses of the mR-8R inefficiently delivered cell lines treated with proteins mR-8R (20 μg/mL) for 12 h. (*D*) P21-mR-8R initially strongly interacts with cell membranes and progressively is taken up and localized perinuclearly. Fluorescence (*Top*) and confocal laser scanning microscopy (*Bottom*) images of NIH3t3 cells treated with P21-mR-8R (20 μg/mL) for 1 h, 1 h with washes and a further 5 h incubation (in serum-free media), or 6 h treatment. Cells were pre-incubated for 1 h in serum-free media and transduced

for the desired time in serum-free media. (Scale bars, top, 50 μm; bottom, 10 μm). Printed from Dixon et. al. [81]..... 19

Figure 1.5 (A) Design of the osteogenic constructs. P21-RUNX2-8R is a RUNX2 transcription factor with an N-terminal fusion of P21 and a C-terminal fusion of 8R. P21-RUNT-8R contains only the DNA binding domain, RUNT, sandwiched between P21 and 8R. (B) To assess the delivery of the fusion peptide, the proteins were labelled with FITC and delivered at different concentrations overnight. Flow cytometry analysis of percentage positivity and relative fluorescence unit (RFU) of hMSCs treated with different concentrations of P21-RUNX2-8R-FITC (10, 30, 50 μg/ml) overnight. Statistical significance was determined using the Holm-Sidak method, α=0.05. (C) Viability of hMSCs measured using trypan blue at day 1 and 7 after overnight treatment with 30 μg/ml of P21-RUNX2-8R. 30 μg/ml of P21-RUNX2-8R was used as the optimal concentration on further experiments. Statistical significance determined using the Holm-Sidak method, with alpha=5.000%. (D) Fluorescence microscopy images of hMSCs treated with 10, 30 and 50 μg/ml P21-RUNX2-8R-FITC overnight. As the concentration increases, fluorescence intensity of P21-RUNX2-8R-FITC inside hMSCs increases. Scale bar is 50 μm. (E) For the first week, hMSCs were treated overnight with P21-RUNX2-8R (30 μg/ml) every other night (3x), every three days (2x) or treated only once (1x). Viability of hMSCs measured using trypan blue at day 1 and 7 after overnight treatment with 30 μg/ml of P21-RUNX2-8R once, twice and thrice per week. Statistical significance determined using the Holm-Sidak method, with alpha=5.000%. (F) Treated hMSCs were cultured in osteo-permissive medium for three weeks, stained with Alizarin Red S (ARS) for matrix mineralization and quantified

using a microplate reader. 30 μg/ml of P21-RUNX2-8R treated twice during the first week was identified as the optimal dose and the same conditions were used in the subsequent assays. Statistical significance was determined using one way ANOVA. Error bars indicate standard deviation (SD). 21

Figure 1.6 Chemical Structure of PLGA (x is the repeat of lactic acid units and y is repeat of glycolic acid units). 28

Figure 1.7 Hydrolysis of PLGA 28

Figure 1.8 The principle of oil in water emulsion 30

Figure 1.9 Schematic showing the water-in-oil-in-water double emulsion method of polymer microparticles manufacture [119]. 32

Figure 2.1 Phases of MP formation using W/O/W and S/O/W methods and factors affecting MP morphology and possible factors affecting protein stability during MP fabrication. 45

Figure 2.2 Schematic showing the solid-in-oil-in-water emulsion method of PLGA MPs manufacturing. 49

Figure 2.3 Schematic of P21-mR-8R structure (A). P21-mR-8R characterisation through SDS-PAGE gel electrophoresis (B). Protein sample was ran through against ladder to confirm molecular weight. 53

Figure 2.4 (A) MP size distribution comparing MPs manufactured by W/O/W (grey line) and S/O/W (black line). The mean MP size for the W/O/W batch was 31.9± 4.3 μm and for the S/O/W batch 42.5 ± 2.5 μm. (B) 0.25% methylcellulose solution and 0.3% PVA solution viscosity measured at various shear rates at 25°C. Error bars indicate SD (n = 3). 55

Figure 2.5 Size distribution of MPs manufactured by W/O/W (A) and by S/O/W (B). Black line is blank MPs and blue line is P21-mR-8R loaded MPs (0.5% w/w). 57

Figure 2.6 Scanning electron images comparing blank PLGA MPs manufactured by the W/O/W emulsion method (left) and the S/O/W emulsion method (right). Scale bars are as indicated. 59

Figure 2.7 Scanning electron images comparing P21-mR-8R loaded PLGA MPs manufactured by the W/O/W emulsion method (left) and the S/O/W emulsion method (right). Scale bars are as indicated. 60

Figure 2.8 P21-mR-8R activity after extraction from PLGA MPs prepared using W/O/W and S/O/W methods. Protein was quantified and added to pre-plated NIH3t3 cells. Protein transduction activity was evaluated. (A) Fluorescence microscopy images of the NIH3t3 cells treated with the sampled P21-mR-8R (Scale bar 10 μm). (B) Flow cytometry histograms showing cellular uptake of P21-mR-8R after application of the samples to NIH3t3 cells. The red histograms are the P21-mR-8R samples, while the black histograms are the experimental control. (C) Relative biological activity of the sampled P21-mR-8R. Protein transduction activity was compared to the experiment control. Error bars indicate SD (n = 3). 63

Figure 2.9 P21-mR-8R activity upon exposure to various homogenisation speeds. P21-mR-8R was then added to pre-plated NIH3t3 cells. P21-mR-8R transduction activity was evaluated. (A) Fluorescence microscopy images of the NIH3t3 cells treated with the sampled P21-mR-8R (Scale bar 10μm). (B) Flow cytometry histograms showing cellular uptake of P21-mR-8R after application of the samples to NIH3t3 cells. The red histograms are the P21-mR-8R samples,

while the black histograms are the experimental control. (C) Relative biological activity of the sampled P21-mR-8R. Protein transduction activity was compared to the experiment control. Error bars indicate SD (n = 3). 66

Figure 2.10 PLGA MPs characterisation upon preparation using W/O/W method without homogenisation and activity of P21-mR-8R extracted from these microparticles. (A) SEM analyses for prepared MPs (scale bars as indicated). (B) Fluorescence microscopy images of the NIH3t3 cells treated with the sampled P21-mR-8R (Scale bar 10 μm) (Left) and flow cytometry histograms showing cellular uptake of P21-mR-8R after application of the samples to NIH3t3 cells (right). The red histograms are the P21-mR-8R samples, while the black histograms are the experimental control. 67

Figure 3.1 MP characterization; SEM and size analyses. MPs were loaded with P21-mR-8R (0.5% (w/w)). SEM analyses for MPs (scale bars represent 50 μm on left image, and 10 μm on right image). Representative size distribution, average of three different loaded PLGA microparticles batches (n=3). 80

Figure 3.2 In vitro release profiles of P21-mR-8R from PLGA MPs (pH 7.4 at 37°C) MPs were prepared using S/O/W method loaded with P21-mR-8R (0.5% (w/w)). (A) Protein was quantified using Micro BCA assay kit. (B) Protein was quantified using fluorescence intensity. Error bars indicate SD (n = 3). 81

Figure 3.3 MP characterization; SEM and size analyses. MPs were prepared with addition of 200μL PBS to the primary emulsion. MPs were loaded with P21-mR-8R (0.5% (w/w)). SEM analyses for MPs (scale bars represent 50 μm on left image, and 10 μm on right image). Representative size distribution, average of three different loaded PLGA microparticles batches (n=3). 83

Figure 3.4 In vitro release profiles of P21-mR-8R from PLGA MPs (pH 7.4 at 37°C) MPs were prepared with addition of 200µL PBS to the primary emulsion. MPs were loaded with P21-mR-8R (0.5% (w/w)). Protein was quantified using Micro BCA assay kit. Error bars indicate SD (n = 3)..... 84

Figure 3.5 Transduction activity of the released P21-mR-8R. MPs were prepared using S/O/W method and loaded with P21-mR-8R (0.5% (w/w)), mixed with PBS. Transduction activity of the released protein was assessed by addition to plated NIH3t3 cells. (A) Schematic showing the sampling of the released protein and quantification. (B) Fluorescence microscopy images of the NIH3t3 cells treated with the sampled P21-mR-8R (Scale bar 10 µm). (C)Flow cytometry histograms showing cellular uptake of P21-mR-8R after application of the samples to NIH3t3 cells. The red histograms are the P21-mR-8R samples, while the black histograms are the experimental control. 86

Figure 3.6 Relative biological activity of the sampled P21-mR-8R. GET Protein transduction activity was compared to the experiment control. Error bars indicate SD (n = 3). 87

Figure 3.7 GET peptide interaction with blank PLGA MPs at pH 7.4 PLGA MPs were suspended in solution and P21-mR-8R was then added, the solution was then centrifuged and the P21-mR-8R quantity in the supernatant was measured. Error bars indicate SD (n = 3). 91

Figure 3.8 GET peptide interaction with blank PLGA MPs at pH. PLGA MPs were suspended in solution of pH 3 and P21-mR-8R was then added, the solution was then centrifuged and the P21-mR-8R quantity in the supernatant was measured. Error bars indicate SD (n = 3). 93

Figure 3.9 Effect of PLGA degradants containing media on GET peptide stability. Blank PLGA MPs were left to degrade in media, after that P21-mR-8R was mixed with the media. Protein was then transduced into cells by addition to plated NIH3t3 cells. Fluorescence microscopy images of the NIH3t3 cells treated with the sampled P21-mR-8R (left) (Scale bar 10μm) and flow cytometry histograms showing cellular uptake of P21-mR-8R after application of the samples to NIH3t3 cells (right). The red histograms represent P21-mR-8R samples while black histograms are the experiment control. 95

Figure 3.10 Schematic of the protein storage and sampling, 200μg/ml P21-mR-8R solution prepared with various pH values (3, 5 &7) and stored at 37ºC. A sample was taken from each solution, at defined time points, and diluted 1:10 in fresh cell culture media. Protein was then transduced into cells by addition to plated NIH3t3 cells. 97

Figure 3.11 GET-peptide stability at various pH values mimicking the PLGA Microenvironment. P21-mR-8R stability in cell culture media of various pH values (3, 5 & 7), pH was adjusted using 1M lactic acid solution Protein sample was transduced into cells by addition to plated NIH3t3 cells. (A) Fluorescence microscopy images of the NIH3t3 cells treated with the protein samples (Scale bar 10μm). (B) Flow cytometry histograms showing cellular uptake of P21-mR-8R after application of the samples to NIH3t3 cells. The red histograms represent P21-mR-8R samples taken at day 1, while the grey histograms represent day 7 samples, black histograms are the experiment control. (C) Relative transduction activity of the samples. Protein transduction activity was compared to the experiment control. Error bars indicate SD (n = 3). * is $p<0.05$, ** is $p<0.01$. 98

Figure 3.12 GET-peptide stability at various pH values mimicking the PLGA Microenvironment. P21-mR-8R stability in cell culture media of various pH values (3, 5 & 7), pH was adjusted using 1M glycolic acid solution Protein sample was transduced into cells by addition to plated NIH3t3 cells. (A) Fluorescence microscopy images of the NIH3t3 cells treated with the protein samples (Scale bar 10μm). (B) Flow cytometry histograms showing cellular uptake of P21-mR-8R after application of the samples to NIH3t3 cells. The red histograms represent P21-mR-8R samples taken at day 1, while the grey histograms represent day 7 samples, black histograms are the experiment control. (C) Relative transduction activity of the samples. Protein transduction activity was compared to the experiment control. Error bars indicate SD (n = 3). * is $p<0.05$, ** is $p<0.01$. 99

Figure 3.13 GET-peptide stability at various pH values mimicking the PLGA Microenvironment. P21-mR-8R stability in cell culture media of various pH values (3, 5 & 7), pH was adjusted using 1M acetic acid solution Protein sample was transduced into cells by addition to plated NIH3t3 cells. (A) Fluorescence microscopy images of the NIH3t3 cells treated with the protein samples (Scale bar 10μm). (B) Flow cytometry histograms showing cellular uptake of P21-mR-8R after application of the samples to NIH3t3 cells. The red histograms represent P21-mR-8R samples taken at day 1, while the grey histograms represent day 7 samples, black histograms are the experiment control. (C) Relative transduction activity of the samples. Protein transduction activity was compared to the experiment control. Error bars indicate SD (n = 3). * is $p<0.05$. 100

Figure 3.14 P21-mR-8R stability in cell culture media of various pH values (3, 5 & 7). pH was adjusted using 1M phosphoric acid solution. (A) Fluorescence

microscopy images of the NIH3t3 cells treated with the samples contain P21-mR-8R (Scale bar 10μm). (B) Flow cytometry histograms showing cellular uptake of P21-mR-8R after application of the samples to NIH3t3 cells. The red histograms represent P21-mR-8R samples taken at day 1, while the grey histograms represent day 7 samples, black histograms are the experiment control. (C) Relative biological activity of the P21-mR-8R. Protein transduction activity was compared to the experiment control. Error bars indicate SD (n = 3). * is $p<0.05$, ** is $p<0.01$. 102

Figure 3.15 P21-mR-8R stability in cell culture media of various pH values (3, 5 & 7). pH was adjusted using 1M hydrochloric acid solution. (A) Fluorescence microscopy images of the NIH3t3 cells treated with the samples contain P21-mR-8R (Scale bar 10μm). (B) Flow cytometry histograms showing cellular uptake of P21-mR-8R after application of the samples to NIH3t3 cells. The red histograms represent P21-mR-8R samples taken at day 1, while the grey histograms represent day 7 samples, black histograms are the experiment control. (C) Relative biological activity of the P21-mR-8R. Protein transduction activity was compared to the experiment control. Error bars indicate SD (n = 3). * is $p<0.05$. 103

Figure 3.16 P21-mR-8R stability in cell culture media of various pH values (3, 5 & 7). pH was adjusted using 1M sulfuric acid solution. (A) Fluorescence microscopy images of the NIH3t3 cells treated with the samples contain P21-mR-8R (Scale bar 10μm). (B) Flow cytometry histograms showing cellular uptake of P21-mR-8R after application of the samples to NIH3t3 cells. The red histograms represent P21-mR-8R samples taken at day 1, while the grey histograms represent day 7 samples, black histograms are the experiment

control. (C) Relative biological activity of the P21-mR-8R. Protein transduction activity was compared to the experiment control. Error bars indicate SD (n = 3). * is p<0.05. 104

Figure 3.17 GET peptide interaction with 25mg PLGA MPs at various pH conditions in presence of different L-Histidine quantities. PLGA MPs were suspended in solution of different pH values and P21-mR-8R with L-Histidine was then added, the solution was then centrifuged and the P21-mR-8R quantity in the supernatant was measured. Error bars indicate SD (n = 3)..... 107

Figure 3.18 Effect of L-Histidine on GET peptide stability in media contains PLGA degradation product. Blank PLGA MPs were left to degrade in media, after that P21-mR-8R was mixed with the media and different quantities of L-Histidine. Protein was then transduced into cells by addition to plated NIH3t3 cells. (A) Fluorescence microscopy images of the NIH3t3 cells treated with the sampled P21-mR-8R (Scale bar 10μm) and flow cytometry histograms showing cellular uptake of P21-mR-8R after application of the samples to NIH3t3 cells. The red histograms represent P21-mR-8R samples while black histograms are the experiment control. (B) Relative transduction activity of the sampled P21-mR-8R. Protein transduction activity was compared to the experiment control. Error bars indicate SD (n = 3). * is p<0.05..... 109

Figure 3.19 GET-peptide stability at various pH values mimicking the PLGA Microenvironment. P21-mR-8R with L-Histidine stability in cell culture media of various pH values (3, 5 & 7), pH was adjusted using 1M lactic acid solution Protein sample was transduced into cells by addition to plated NIH3t3 cells. (A) Fluorescence microscopy images of the NIH3t3 cells treated with the protein samples (Scale bar 10μm). (B) Flow cytometry histograms showing cellular

uptake of P21-mR-8R after application of the samples to NIH3t3 cells. The red histograms represent P21-mR-8R samples taken at day 1, while the grey histograms represent day 7 samples, black histograms are the experiment control. (C) Relative transduction activity of the samples. Protein transduction activity was compared to the experiment control. Error bars indicate SD (n = 3). 111

Figure 3.20 GET-peptide stability at various pH values mimicking the PLGA Microenvironment. P21-mR-8R with L-Histidine stability in cell culture media of various pH values (3, 5 & 7), pH was adjusted using 1M glycolic acid solution Protein sample was transduced into cells by addition to plated NIH3t3 cells. (A) Fluorescence microscopy images of the NIH3t3 cells treated with the protein samples (Scale bar 10μm). (B) Flow cytometry histograms showing cellular uptake of P21-mR-8R after application of the samples to NIH3t3 cells. The red histograms represent P21-mR-8R samples taken at day 1, while the grey histograms represent day 7 samples, black histograms are the experiment control. (C) Relative transduction activity of the samples. Protein transduction activity was compared to the experiment control. Error bars indicate SD (n = 3). 112

Figure 3.21 GET-peptide stability at various pH values mimicking the PLGA Microenvironment. P21-mR-8R with L-Histidine stability in cell culture media of various pH values (3, 5 & 7), pH was adjusted using 1M acetic acid solution Protein sample was transduced into cells by addition to plated NIH3t3 cells. (A) Fluorescence microscopy images of the NIH3t3 cells treated with the protein samples (Scale bar 10μm). (B) Flow cytometry histograms showing cellular uptake of P21-mR-8R after application of the samples to NIH3t3 cells. The red

histograms represent P21-mR-8R samples taken at day 1, while the grey histograms represent day 7 samples, black histograms are the experiment control. (C) Relative transduction activity of the samples. Protein transduction activity was compared to the experiment control. Error bars indicate SD (n = 3). 113

Figure 3.22 GET-peptide stability at various pH values mimicking the PLGA Microenvironment. P21-mR-8R with L-Histidine stability in cell culture media of various pH values (3, 5 & 7), pH was adjusted using 1M phosphoric acid solution Protein sample was transduced into cells by addition to plated NIH3t3 cells. (A) Fluorescence microscopy images of the NIH3t3 cells treated with the protein samples (Scale bar 10μm). (B) Flow cytometry histograms showing cellular uptake of P21-mR-8R after application of the samples to NIH3t3 cells. The red histograms represent P21-mR-8R samples taken at day 1, while the grey histograms represent day 7 samples, black histograms are the experiment control. (C) Relative transduction activity of the samples. Protein transduction activity was compared to the experiment control. Error bars indicate SD (n = 3). 115

Figure 3.23 GET-peptide stability at various pH values mimicking the PLGA Microenvironment. P21-mR-8R with L-Histidine stability in cell culture media of various pH values (3, 5 & 7), pH was adjusted using 1M hydrochloric acid solution Protein sample was transduced into cells by addition to plated NIH3t3 cells. (A) Fluorescence microscopy images of the NIH3t3 cells treated with the protein samples (Scale bar 10μm). (B) Flow cytometry histograms showing cellular uptake of P21-mR-8R after application of the samples to NIH3t3 cells. The red histograms represent P21-mR-8R samples taken at day 1, while the grey

histograms represent day 7 samples, black histograms are the experiment control. (C) Relative transduction activity of the samples. Protein transduction activity was compared to the experiment control. Error bars indicate SD (n = 3). * is p<0.05. 116

Figure 3.24 GET-peptide stability at various pH values mimicking the PLGA Microenvironment. P21-mR-8R with L-Histidine stability in cell culture media of various pH values (3, 5 & 7), pH was adjusted using 1M sulfuric acid solution Protein sample was transduced into cells by addition to plated NIH3t3 cells. (A) Fluorescence microscopy images of the NIH3t3 cells treated with the protein samples (Scale bar 10μm). (B) Flow cytometry histograms showing cellular uptake of P21-mR-8R after application of the samples to NIH3t3 cells. The red histograms represent P21-mR-8R samples taken at day 1, while the grey histograms represent day 7 samples, black histograms are the experiment control. (C) Relative transduction activity of the samples. Protein transduction activity was compared to the experiment control. Error bars indicate SD (n = 3). * is p<0.05. 117

Figure 3.25 pH values for media before and after addition of L-Histidine (200μg/ml). pH was initially adjusted using 1M acetic acid solution. Error bars indicate SD (n = 3)..... 118

Figure 3.26 Effect of L-Histidine on P21-mR-8R stability upon storage in cell culture media of pH 3, adjusted using 1M acetic acid solution. 200μg/ml P21-mR-8R solution of pH 3 was prepared and stored at 37ºC for 7 days. A sample was taken from the solution, after 7 days, and diluted 1:10 in fresh cell culture media, producing a P21-mR-8R solution of 20μg/ml. 20μg of L-Histidine was then added to the solution. Protein was then transduced into cells by addition to

plated NIH3t3 cells. (A) Fluorescence microscopy images of the NIH3t3 cells treated with the sampled P21-mR-8R (Scale bar 10μm). (B) Flow cytometry histograms showing cellular uptake of P21-mR-8R after application of the sample to NIH3t3 cells. The red histograms represent P21-mR-8R sample, black histogram is the experiment control. 120

Figure 3.27 Dose of L-Histidine required to promote GET-peptide activity. Effect of different quantities of L-Histidine on P21-mR-8R stability upon storage in cell culture media of pH 3 (pH was adjusted using 1M acetic acid solution). 200μg/ml P21-mR-8R solution was prepared with various quantities L-Histidine (0 – 200μg) and stored at 37ºC. A sample was taken from each solution, at defined time points, and diluted 1:10 in fresh cell culture media. Protein was then transduced into cells by addition to plated NIH3t3 cells. (A) Fluorescence microscopy images of the NIH3t3 cells treated with the sampled P21-mR-8R (Scale bar 10μm). (B) Flow cytometry histograms showing cellular uptake of P21-mR-8R after application of the samples to NIH3t3 cells. The red histograms represent P21-mR-8R samples taken at day 1, while the grey histograms represent day 7 samples, black histograms are the experiment control. (C) Relative transduction activity of the sampled P21-mR-8R. Protein transduction activity was compared to the experiment control. Error bars indicate SD (n = 3). * is $p<0.05$. 122

Figure 3.28 MP characterization; SEM and size analyses. MPs were prepared with addition of 200μL PBS to the primary emulsion. MPs were loaded with P21-mR-8R (0.5% (w/w)) mixed with L-Histidine (25% (w/w)). SEM analyses for MPs (scale bars represent 50 μm on left image, and 10 μm on right image).

Representative size distribution, average of three different loaded PLGA microparticles batches (n=3). 124

Figure 3.29 In vitro release profiles of P21-mR-8R from porous PLGA MPs (pH 7.4 at 37°C) MPs were prepared using S/O/W method loaded with P21-mR-8R (0.5% (w/w)) mixed with L-Histidine (25% (w/w)). Protein was quantified using Micro BCA assay kit. Error bars indicate SD (n = 3)..... 125

Figure 3.30 Transduction activity of the released P21-mR-8R. Porous MPs were prepared using S/O/W method and loaded with P21-mR-8R (0.5% (w/w)) mixed with L-Histidine (0.25% (w/w)). Transduction activity of the released protein was assessed by addition to plated NIH3t3 cells. (A) Fluorescence microscopy images of the NIH3t3 cells treated with the sampled P21-mR-8R (Scale bar 10 µm). (B) Flow cytometry histograms showing cellular uptake of P21-mR-8R after application of the samples to NIH3t3 cells. The red histograms are the P21-mR-8R samples, while the black histograms are the experimental control.... 127

Figure 3.31 Relative biological activity of P21-mR-8R released from PLGA MPs prepared using S/O/W (0.5% w/w) and containing L-Histidine (25% w/w). GET Protein transduction activity was compared to the experiment control. Error bars indicate SD (n = 3). 128

Figure 3.32 Schematic for hypothesis of GET peptide interaction with Carboxyl groups and L-Histidine. Interaction between GET peptide released from MPs and cells in presence of carboxyl groups resulted from PLGA degradation, with and without L-Histidine. (A) pH 7 without L-Histidine. (B) pH 7 with L-Histidine. (C) pH 3 without L-Histidine. (D) pH 3 with L-Histidine..... 129

Figure 4.1 P21-RUNX2-8R-FITC loaded MPs characterization. MPs were fabricated using PLGA (50:50), loaded with P21-RUNX2-8R-FITC (0.5%

(w/w)), and mixed with PBS 0.1% (w/w) and L-Histidine 25% (w/w). (A) SEM analyses for MPs (scale bars represent 100μm on left image, and 10μm on right image). (B) Summary of size characterization and corresponding loading efficiencies (n = 3). 146

Figure 4.2 In vitro release profiles of P21-RUNX2-8R-FITC from PLGA MPs (pH 7.4 at 37 ºC). MPs were fabricated using PLGA (50:50), loaded with P21-RUNX2-8R-FITC (0.5% (w/w)), and mixed with PBS 0.1% (w/w) and L-Histidine 25% (w/w). Protein release was quantified using Micro BCA assay kit (A) Relative cumulative protein release. (B) Cumulative protein quantity. Error bars indicate SD (n = 3). 148

Figure 4.3 Transduction activity of the released P21-RUNX2-8R-FITC. PLGA MPs were prepared using S/O/W method, loaded with P21-RUNX2-8R-FITC (0.5% (w/w)). Transduction activity of the released protein was assessed using hMSC in monolayer. Representative fluorescence microscopy images of the hMSCs treated with the sampled P21-RUNX2-8R-FITC (Scale bar represents 100μm). 151

Figure 4.4 Relative transduction activity of the released P21-RUNX2-8R-FITC. PLGA MPs were prepared using S/O/W method, loaded with P21-RUNX2-8R-FITC (0.5% (w/w)). Transduction activity of the released protein was assessed using hMSC in monolayer. (A) Flow cytometry histograms showing cellular uptake of P21-RUNX2-8R-FITC on hMSCs. The red histograms are the P21-RUNX2-8R-FITC samples, while the black histograms are the experimental control. (B) Relative transduction activity of released P21-RUNX2-8R-FITC. Protein activity was compared to the experiment control. Error bars indicate SD (n = 3). 152

Figure 4.5 Relative transfection activity of the released P21-RUNX2-8R-FITC. PLGA MPs were prepared using S/O/W method, loaded with P21-RUNX2-8R-FITC (0.5% (w/w)). (A) Schematic showing the experimental procedure. (B) Transcriptional activity of the released P21-RUNX2-8R-FITC measured using luciferase reporter gene assay. Error bars indicate SD (n = 3). 153

Figure 4.6 Cell attachment and proliferation on scaffolds. (A) Schematic of scaffolds fabrication and cell attachment on scaffolds. (B) Number of viable hMSCs measured by the Prestoblue metabolic activity on day 3, 6 and 9 post-seeding. (C) SEM images of scaffolds without cells (scale bar as indicated). (D) SEM images of cell-seeded scaffolds 3 days post-seeding (scale bar as indicated). Right images are for scaffolds cut in half to show internal morphology (scale bar as indicated). 157

Figure 4.7 Cells differentiation on scaffolds. ALP expression after week 1 for hMSCs seeded on scaffolds in osteo-permissive and osteo-inductive media (DAB). Blank MPs represents cell seeded scaffold containing blank MPs cultured in osteo-permissive media. Loaded MPs represents cell-seeded scaffolds containing P21-RUNX2-8R-loaded MPs cultured in osteo-permissive media. DAB media represents cell seeded scaffolds containing blank MPs cultured in osteo-inductive media (DAB). ** is $P< 0.01$. 160

Figure 4.8 Cells differentiation on scaffolds. Osteocalcin staining at week 2 samples (scale bar as indicated). Blank MPs represents cell seeded scaffold containing blank MPs cultured in osteo-permissive media. Loaded MPs represents cell-seeded scaffolds containing P21-RUNX2-8R-loaded MPs cultured in osteo-permissive media. DAB media represents cell seeded scaffolds containing blank MPs cultured in osteo-inductive media (DAB). 161

Figure 4.9 Cells differentiation on scaffolds. Von Kossa-stained samples at week 3, calcified deposits are indicated by white arrows (scale bar is 1mm). Blank MPs represents cell seeded scaffold containing blank MPs cultured in osteo-permissive media. Loaded MPs represents cell-seeded scaffolds containing P21-RUNX2-8R-loaded MPs cultured in osteo-permissive media. DAB media represents cell seeded scaffolds containing blank MPs cultured in osteo-inductive media (DAB). 162

Figure 4.10 Gene expression analysis on scaffolds at week 1 and 2. Blank MPs represents cell-seeded scaffold containing blank MPs, cultured in osteo-permissive media. Loaded MPs represents cell-seeded scaffolds containing P21-RUNX2-8R loaded MPs, cultured in osteo-permissive media. DAB represents cell-seeded scaffolds containing blank MPs, cultured in osteo-inductive media. RNA was extracted from cells at week 1 (A) and week 3 (B) and gene expression analysis was performed. The results were plotted based on expression fold change to non-induced hMSCs on blank scaffold. Statistical analysis was performed using two-way ANOVA in comparison with the non-transduced hMSCs, α=0.05. Error bars indicate SD. 164

Figure 4.11 SEM images of scaffolds at day 21. SEM images of scaffolds with and without cells cultured in growth media for 21 days. No cells represents scaffold prepared from blank MPs without cells kept in osteo-permissive media. Blank MPs represents cell-seeded scaffold containing blank MPs cultured in osteo-permissive media. Loaded MPs represents cell-seeded scaffolds containing P21-RUNX2-8R loaded MPs cultured in osteo-permissive media. DAB media represents cell seeded scaffolds containing blank MPs cultured in

osteo-inductive media. Right images are for scaffolds cut in half to show internal morphology. 166

Figure 4.12 Microstructural analysis of scaffolds. Micro-CT images for scaffolds at different conditions. Scaffolds were treated with osmium tetroxide prior to scan. (A) Non seeded scaffold prepared from blank MPs placed in cell culture media at day 1 (left) and day 21 (right) (B) cell-seeded scaffold prepared from blank MPs cultured in osteo-permissive media for 1 day (left) and merged cells and scaffold showing cell distribution (right) cells are in blue. (C) Cell seeded scaffold prepared from blank MPs cultured in osteo-permissive media for 21 days (left image) and merged cells and scaffold showing cell distribution (right). (D) Cell seeded scaffold prepared from P21-RUNX2-8R loaded MPs cultured in osteo-permissive media for 21 days (left image) and merged cells and scaffold showing cell distribution (right). (E) Cell seeded scaffold prepared with blank MPs cultured in osteo-inductive media for 21 days (left image) and merged cells and scaffold showing cell distribution (right). Scale bar is 1mm. 167

Figure 4.13 3D printing formula optimisation using various ratios and concentrations of PF-127. Dissection microscope images (A) PLGA/PEG: PF127 15% (1:1.2 ratio). (B) PLGA/PEG: PF127 15% (1:1.3 ratio). (C) PLGA/PEG: PF127 18% (1:1.5 ratio). Scale bar represents 1mm. Images taken from G Bruce CDT report. 169

Figure 4.14 Complex structure printing using the optimised formula (PLGA/PEG with PF-127 18% 1:1.5 ratio). L5 vertebra printed structure (A) left and right parts before sintering. (B) After sintering for 2 hours at 37°C. Printed vertebrae length is 4cm. Images taken from G Bruce CDT report. 170

Figure 4.15 Tri-acetin effect on the scaffolds structure. Various concentrations of tri-acetin (0%, 0.5%, 1%, 2.5% and 5%) were mixed with PLGA/PEG and sintered for various periods (30minutes, 60 minutes and 120 minutes. (A) Sintered for 30 minutes at 37°C. (B) Sintered for 60 minutes at 37°C. (C) Sintered for 120 minutes at 37°C. Scale bar as indicated. 172

Figure 4.16 Effect of carrier quantity on scaffolds. Scaffolds were mixed with various concentrations and quantities of tri-acetin. (A) SEM evaluation of scaffolds. PLGA/PEG was mixed with 2.5% (v/v) tri-acetin and 18% (w/v) Pluronic in 1:0.6 ratio (left). with 2.5% (v/v) tri-acetin and 18% (w/v) Pluronic in 1:1.5 ratio (middle). with 1% (v/v) tri-acetin and 18% (w/v) Pluronic in 1:1.5 ratio (right). (B) Mechanical evaluation of scaffolds. Error bars indicate SD (n = 3). * is $p < 0.05$. ** is $p < 0.01$. 174

Figure 4.17 Effect of washing on scaffold properties. PLGA/PEG mixed with 1% tri acetin and 18% pluronic (1:1.5 ratio). Scaffolds were sintered at 37°C for 30 minutes. Scaffolds were then washed with PBS at 4°C (left), 37°C (middle) or 4°C then at 37°C (right). 176

Figure 4.18 Scaffolds disintegration upon washing and cells proliferation. Various quantities of cells (1M, o.5M 0.25M 0.1M and 0.05M) were mixed with 60uL of 1% tri-acetin (v/v), 18% pluronic (w/v) solution and added to 40mg PLGA/PEG forming a paste at room temperature. The paste was then loaded into Teflon mould to produce cylindrical scaffolds (6mm X 3mm). The scaffolds were then sintered at 37°C for 30 minutes. The scaffolds were then washed in PBS at 4°C for 45 minutes and then transferred to 24 well plate and immersed in 1 ml media and incubated at 37°C for the entire study. (A) Microscope images for scaffolds after sintering and after washing showing intact scaffolds (scale bar

represents 1mm). (B) PrestoBlue cell viability at different time points for the cultured scaffolds. Error bars indicate SD (n = 3). 178

Figure 4.19 3D printed scaffold using PLGA/PEG particles mixed with Pluronic (18%) and tri-acetin (1%) in 1:1.5 ratio (PLGA/PEG : carrier). Scaffold was sintered at 37°C for 30 minutes after printing. 180

Figure 4.20 Holding time evaluation study. PLGA/PEG was mixed with 1% (v/v) tri-acetin and 18% (w/v) pluronic solution at 4°C. The mixture was then placed at the syringe at 25°C then printed (A). The mixture at they syringe was then held at 25°C for 30 minutes and then printed (B). PLGA/PEG mixture was loaded to the syringe at 25°C and left for 45 minutes then printed (C)..... 180

Figure 4.21 Bio-printing and cells proliferation on 3D printed scaffolds. PLGA/PEG particles were mixed with Pluronic 18% - Treacetin 1% solution in 1:1.5 ratio. The solution was mixed with cells (10^6 per ml). The mixture was loaded to the printing syringe and printed at 25°C. After sintering at 37°C for 30 minutes and washing in cold PBS at 4°C, scaffolds were then cultured in media for 7 days. Cells proliferation was evaluated. (A) PrestoBlue cell viability at different time points for the cultured scaffolds. Error bars indicate SD (n = 3). (B) Toluidine blue stain at day 7. Scale bar is represents 1mm. 182

List of Tables

Table 1.1 Synthetic polymers classes and examples..... 25

Table 1. 2 Scaffolds materials used for tissue engineering application..... 35

Table 3.1 Blank MPs surface charge at various pH conditions (3, 5 & 7). 90

Table 3.2 P21-mR-8R, mR, P21 & 8R theoretical molecular weights, isoelectric points and charge at various pH values 90

Table 4.1 List of carriers (concentration and ratio) used to prepare scaffolds. Scaffolds were sintered at 37°C..... 140

Chapter I: Introduction

1. Introduction

Elderly people have an increasing incidence of bone fracture complications. The number of hip and knee replacement procedures in 2010 in US alone was around 7 million cases [1]. When bone damage is larger than the normal repair mechanisms can handle (critical size defect), synthetic fillers or grafts are required. Grafting materials are categorised based on the source; autograft, allograft and synthetic materials. Accordingly, the need for synthetic fillers, which can be compatible with patients, is increasing [2].

Tissue engineering aims for the renewal or replacement of tissue functions lost through disease or trauma [3], The aim of tissue engineering is to generate new tissues from cells seeded onto scaffolds [4, 5]. These scaffolds can be employed to deliver therapeutic factors essential for the regeneration process. Tissue engineering utilises cell, biological factors and scaffolds to restore functions of lost tissues [6, 7].

In this thesis an injectable scaffold was utilised to incorporate transcription factor (RUNX2) loaded microparticles essential for osteogenesis, the injectable scaffold will serve as a template for the seeded cells. The essential tissue engineering components; scaffolds, biological factor and cells were employed for this purpose.

1.1. Bone physiology and structure

Bone is a complex tissue supporting framework of the body, characterized by its rigidity and hardness. It protects the vital organs, controls calcium homeostasis, acts as a reservoir of growth factors and also takes part in acid–base balance [8, 9].

Bone can be divided into two components, based on the structure; the cortical bone and the cancellous bone. Cortical bone characterised by its density and hardness, also, it surrounds the marrow space. Alternatively, the cancellous bone is more lightweight and porous and consists of a network of random fine plates of lamellar bone called trabeculae that are separated by interconnecting pores (Figure 1.1) [8, 10, 11].

The structure of bone is composed of inorganic component (99% hydroxyapatite) and organic component (90% collagen) [8, 9].

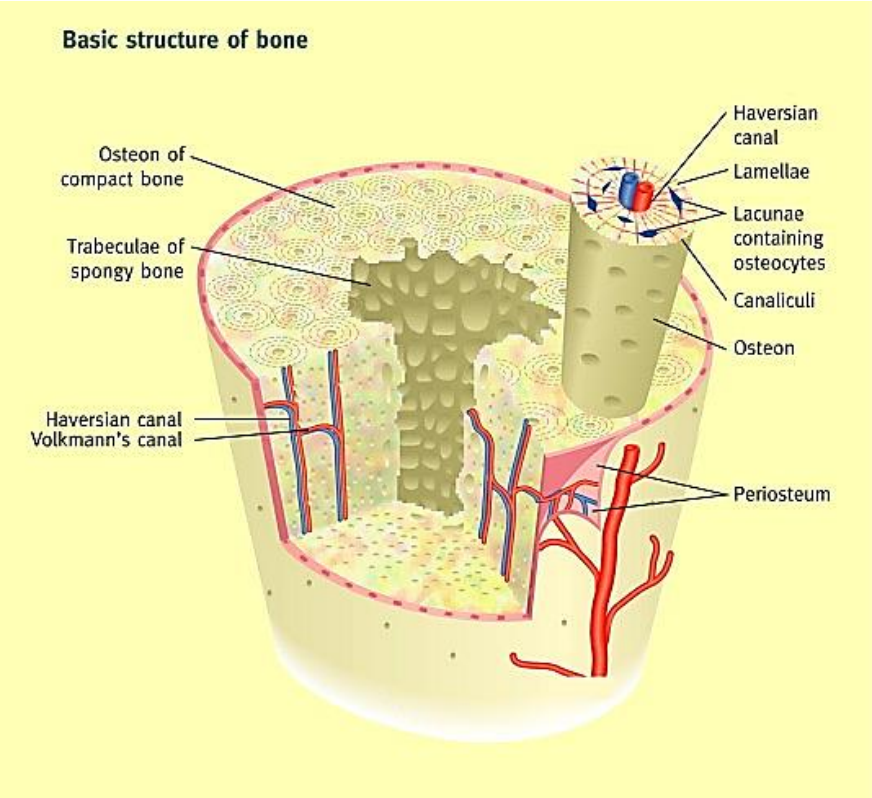


Figure 1.1 Basic structure of bone. The cortical or compact bone structure is shown at the circumference with the more porous cancellous or spongy bone structure within the centre of the bone. [11]

1.2. Bone development and growth

Bone has a number of inherent cell types which play an important role in bone development and maintenance.

Osteoblasts (bone forming cells) are mononuclear cells. These cells are derived from mesenchymal stem cells. The main role of these cells is the synthesis and mineralisation of osteoid. They usually found below the bone matrix which they secrete. Osteoblast cells may become osteocytes once trapped inside the mineralised matrix, or they may undergo apoptosis [11, 12].

Osteoclasts (bone resorption) are large multinucleated cells derived from the monocyte/macrophage lineage. The role of these cells is mainly during the bone resorption. It helps in local degradation of the bone matrix.

Osteocytes are terminally differentiated, star shaped cells derived from osteoblasts entrapped within the bone matrix. They form the largest component of the bone, and they exceed the osteoblasts in number [11, 12].

Osteogenesis is the process of new bone formation by osteoblast cells. The formation of normal and healthy bone is carried out by two important routs:

1. Intramembranous osteogenesis characterized by laying down of bone into the connective tissue (mesenchyme) resulting in the formation of bones.

2. Endochondral osteogenesis where a cartilage model acts as a precursor.

Three basic steps involved in osteogenesis are:

- Synthesis of extracellular organic matrix (osteoid).
- Matrix mineralization leading to the formation of bone.
- Re-modelling of bone by the process of resorption and reformation.

1.3.Bone repair

Depending on biomechanical properties, fractures can be divided into two main types.

Primary bone healing: there is absolute stability (no motion between fracture surfaces under functional load).

Secondary bone healing: at this healing type, movement at the fracture site is required. There are four main stages of bone healing that occurs sequentially (haematoma, inflammation, repair and remodelling) figure 1.2 summarises the stages [13].

Haematoma: Blood cells accumulate in tissues at the injury site. A blood clot of insoluble fibrin is formed, which called haematoma. Bone ends at the fracture site are destroyed by osteoclasts.

Inflammation: the formed clot provides a framework for the influx of various migrating cells (e.g. neutrophils, platelets). These cells release various cytokines (such as transforming growth factor-β). Endothelial cells undergo mitosis to form capillaries and, together with fibroblasts, granulation tissue is formed. Primary healing occurs via granulation tissue, which tolerates high strains. Osteoclasts start to resorb the dead bone ends and phagocytes remove other necrotic tissue.

Repair: at this stage, soft callous formation occurs which refers to the cartilaginous phase that form at the fracture gap which then differentiates into hard callus. The process whereby soft callus is replaced by hard callus is called endochondral ossification. The chondrocytes become hypertrophic, calcify and die, allowing angiogenesis to occur, and osteoblasts lay down woven bone on the collagen framework left by the chondrocytes.

Remodelling: osteoblasts and osteoclasts deposit and remove bone until the normal shape is restored.

1.4. Clinical interventions for non-union bone Fracture

In some cases, normal physiological mechanisms fail to fulfil the needed outcome, which requires clinical intervention. Hypertrophic non-union fractures (sufficient callus formed but without union) are treated with rigid immobilisation. Atrophic non-union fractures (where little or no callus formed) have other treatment options. Bone graft is one of the used treatment [14].

Bone grafts can be of various types: Autograft, allograft, or synthetic. Each have their own advantages and disadvantages.

Autograft: bone grafts involve processing the patient's own bone. Autografts are currently considered the clinical gold standard. The best grafting success rates have been achieved with vascularised autografts [15]. This method avoids issues of tissue rejection. However, there is a limited supply of bone [16, 17].

Allograft: bone is obtained from a donor and can be fresh or freeze dried. Bone banks specialise in preparing these grafts. The risks associated with this process are pathogenic infection and immune rejection.

Synthetic implants: various types of synthetic components are used in orthopaedic surgeries. These can be grouped into two categories: ceramics and polymers. Ceramics include glass ceramics [18, 19], calcium sulphate [20] and calcium phosphate [21]. Polymeric implants are another option. Available commercial product is HEALOS® (DePuy Synthes).

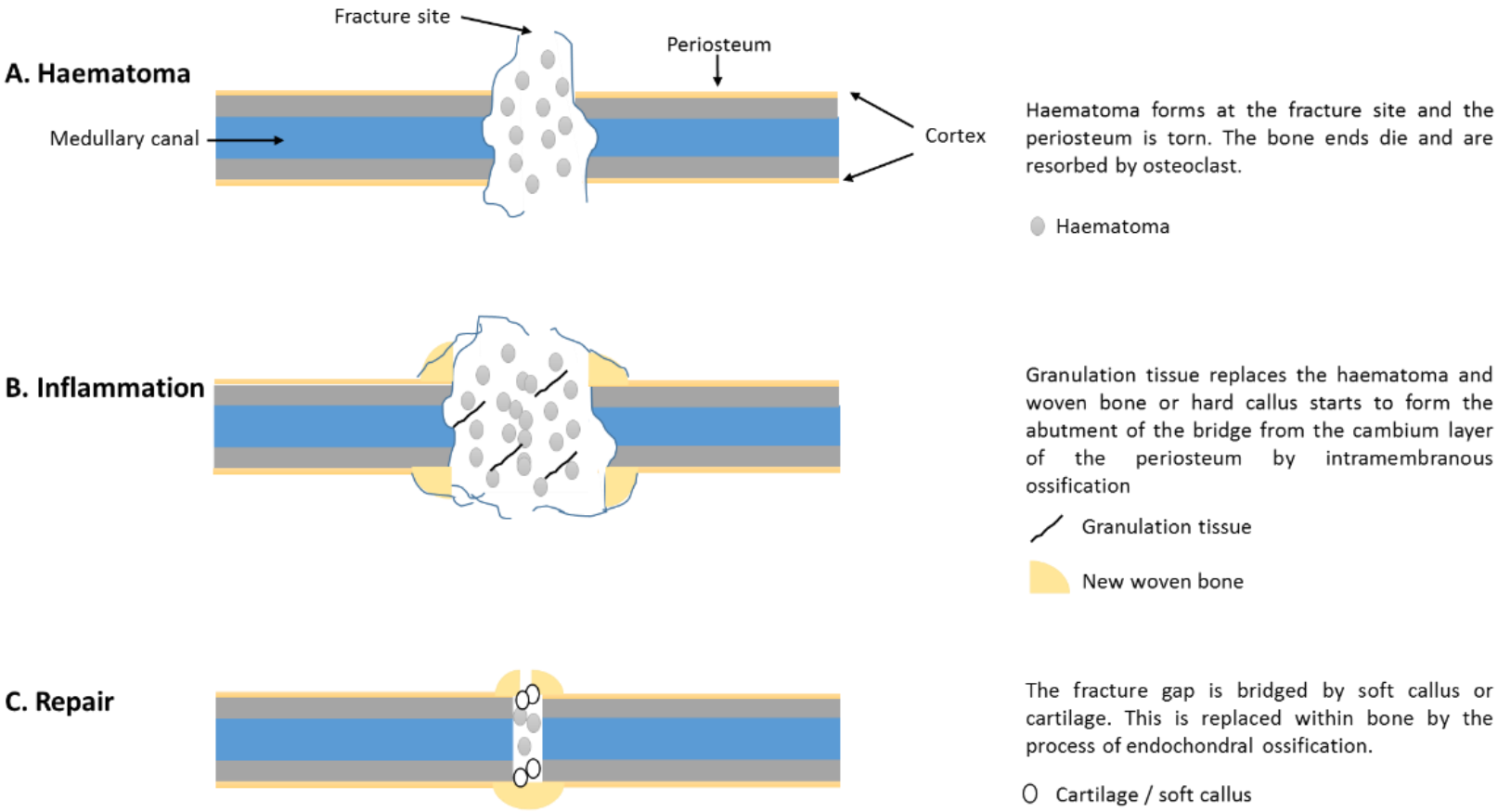


Figure 1.2 Schematic showing the stages of normal bone fracture repair. Secondary fracture healing: bridging of a fracture by external callus. Adopted from Jahagirdar et. al. [13]

HEALOS® consists of cross-linked collagen coated with hydroxyapetite. These implants lack the required functions to encourage tissue integration and self-repair. Methods are currently under investigation that impart bio-functionality onto these materials [22, 23].

Autografts, the clinical gold standard have good efficacy but limited availability, allograft may cause infection. There is an increasing need for a synthetic materials of unlimited supply and functional characteristics.

The aim in conducting this research was to develop a synthetic scaffold, that can be moulded in any shape, and provide the needed biological molecules to initiate osteogenesis.

Therapeutic molecules (such as growth factors) can be utilised to provide the needed functionalities [24, 25]. Scaffolds can be utilised to provide a template for cells, as well as supply the needed therapeutic molecules [24]. The combination of scaffolds component, cells and therapeutic molecules can be used for localised and targeted bone regeneration therapies [25].

The upcoming sections will summarise and discuss the materials used for synthetic scaffolds as well as the therapeutic molecules (and their delivery mechanisms) to regenerate bone.

1.5. Growth factors for bone regeneration

Autografts are considered effective way for bone regeneration as they contain the necessary signalling molecules [26]. These molecules are osteo-conductive (process of bone growth on a surface) scaffold, growth factors needed for osteo-induction (process of osteogenesis induction and stimulation of cells to develop into pre-osteoblasts) and cells with osteogenic potential. These signalling molecules are not available in synthetic implants, however, can be added to the scaffold material.

Bone Morphogenetic Proteins (BMPs) are a group of signalling molecules that belongs to the Transforming Growth Factor-β (TGF-β) superfamily of proteins [27-30]. BMPs were initially known for their ability to induce bone formation. BMPs are important in embryogenesis, and also in maintenance of adult tissue homeostasis [27, 28].

More than 15 known BMPs are structurally related and can be further categorized into subgroups based on amino acid or nucleotide similarity [27]. BMP 2, 4, 6, 7, and 9 are commonly referred to as the osteogenic BMPs, based on their potent bone-inducing activity [27, 31].

FDA has approved two recombinant human bone morphogenetic protein (rhBMP) carrier systems for clinical use; OP-1 (Stryker ®) which delivers BMP-7 and InFUSE^{TM} (Medtronic) which delivers BMP-2. These systems are collagen carrier based and deliver a supra-physiological concentrations of growth factor.

BMP-2 is the most researched osteo-inductive protein and InFUSE is indicated for various uses; such as tibial fractures, oral maxillofacial bone and spinal fusion [32, 33]. However, with more use of BMP-2, an increasing side effect

profiles had been reported [27-29]. This includes postoperative inflammation, ectopic bone formation, osteoclast-mediated bone resorption, and inappropriate adipogenesis [28, 29].

In 2008, the FDA issued a public health notification of 'Life-threatening Complications Associated with Recombinant Human Bone Morphogenetic Protein in Cervical Spine.'

1.5.1. BMP-2 signalling pathway

BMP-2 induces osteoblast differentiation via SMAD 1/5 proteins which are intracellular proteins that transduce extracellular signals from ligand binding at the cell membrane to the nucleus where they activate gene transcription (Figure 1.3). Initiation of the BMP-2 signalling pathway occurs at the cell membrane by the binding of BMP-2 to a BMP type II receptor resulting in the phosphorylation and activation of the BMP type I receptor. This in turn, transmit the signal by phosphorylating a family of proteins known as SMAD proteins. These proteins transduce extracellular signals from ligand binding to the nucleus where gene transcription is activated. The type I receptor will firstly phosphorylate the receptor-regulated SMADs (R-SMADs) which then bind the coSMAD SMAD4. [27, 30, 34].

R-SMAD/coSMAD complexes accumulate in the nucleus where they act as transcription factors and participate in the regulation of target gene expression. This complex may cooperate with RUNX2 or function alone to induce the expression of osteogenesis related genes and then regulate the osteogenic differentiation at the transcriptional level [27, 30, 34].

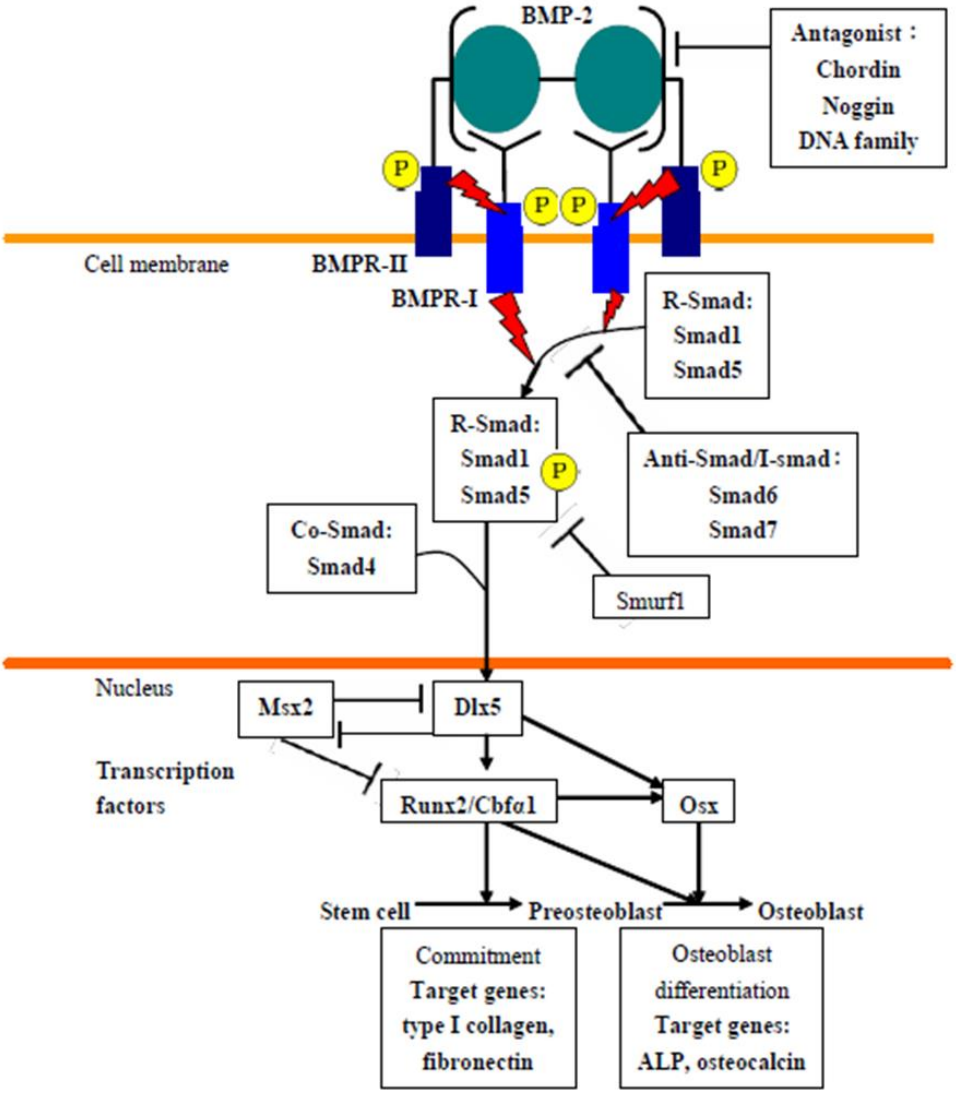


Figure 1.3 The main components of the SMAD 1/5 signalling pathways of BMP-2 in osteogen(P)s. Indicates phosphorylation. Phosphorylation steps are highlighted by [ ][27].

1.6. Transcription factor (RUNX2)

The major transcription factor regulating osteoblast commitment and osteogenic differentiation of mesenchymal stem cells is RUNX2, also named Cbfa1 [35-37]. Activation of RUNX2 in human bone marrow (BM) mesenchymal stem cells induces the expression of specific osteoblastic markers such as alkaline phosphatase (ALP), and osteocalcin (OC) during osteoblast maturation [38]. RUNX2 belongs to RUNX family which composed of three genes, RUNX1/Cbfa2 RUNX2/Cbfa1, and RUNX3/Cbfa3. All three genes contain a runt domain, which is the DNA-binding domain [35, 36].

RUNX2 is first detected in pre-osteoblasts, and the expression is increased initially at the immature osteoblasts, but the expression decreases upon osteoblast maturation. RUNX2 is the earliest transcription factor needed for identification of the osteoblast lineage, while Sp7 and canonical Wnt-signaling further direct the fate of mesenchymal cells to osteoblasts [35, 36, 39-41]. Interestingly, in differentiated osteoblasts, RUNX2 needs to be suppressed in order to form mature bone [42, 43]. Therefore RUNX2 activity is clearly required to trigger the initial osteogenic gene regulatory network and direct the bone developmental program.

Accordingly, and in order to direct cells differentiation selectively to the osteoblast lineage and to avoid using BMP-2, many groups have studied delivering RUNX2 to control osteogenesis. However, since RUNX2 has relatively high molecular weight (~56kDa), delivery vector is needed to deliver RUNX2 into the cells. Zhao et. al. studied the delivery of RUNX2 to Marrow stromal cells (MSCs) using adenoviral vectors [44]. Matrix mineralisation as well as calcium deposition were assessed against control samples. The results

showed cells differentiation into osteoblast lineage in response to RUNX2 transduction. It was concluded that *RUNX2* gene therapy enhances the osteogenic activity of MSCs [44].

Zheng et. al. investigated the effect of RUNX2 on bone formation [45]. Adenoviral vector carrying mouse *RUNX2* gene to transduce primary cultured bone marrow stromal cells (MSCs) was used. It was found that transduced MSCs produced RUNX2 protein and differentiated into osteoblast-like cells. The transduced MSCs had increased alkaline phosphatase activity, increased expression of osteocalcin, osteopontin and bone sialoprotein, and increased matrix mineralization. The study concluded that RUNX2 can induce osteoblast differentiation and bone formation both in vitro and in vivo [45].

Another study by Byers et. al. investigated *RUNX2* gene delivery using retroviral vector to bone marrow stromal cells [46]. The modified cells were combined into three dimensional polymeric scaffolds to create tissue-engineered constructs. RUNX2 transduced cells showed osteoblastic differentiation and mineralization. The study concluded that RUNX2 overexpression enhanced mineralization and the transduced cells can be integrated with three dimensional scaffold structures [46].

The mentioned gene delivery approaches focus on overexpression of osteogenic factors to induce osteoblastic differentiation and matrix mineralization. However, the unregulated production of osteo-inductive molecules may result in abnormal bone formation and tumorigenesis [47]. To address these limitations, Gersbach et. al. described a retroviral system to deliver the RUNX2 transcription factor under control of hydro-tetracyline inducible system. Osteoblastic gene expression, alkaline phosphatase activity, and matrix mineralization were

evaluated. Moreover, engineered cells were seeded onto collagen scaffolds and implanted intramuscularly in the limbs of syngeneic mice. The results showed successful regulation of osteoblast differentiation [47].

It can be seen that the mentioned approaches are utilising viral vectors to deliver *RUNX2* gene [45-47]. Two main limitations are associated with this approach, the use of gene to program cells, which needs to be switched off [48-50] and the risks associated with viral vectors [51-53].

The driving force of the work presented in this thesis was to be able to deliver RUNX2, eliminating the need for BMP-2, and to use safe delivery vectors instead of the currently used viral vectors.

RUNX2 contains a nuclear localization signal domain that directs nuclear localization, however, RUNX2 does not get endocytosed [54, 55]. This limits the use of RUNX2 unless it is combined with a delivery tool, to facilitate endocytosis.

Various delivery systems have been reported, Um et. al. summarised them in their review article [56]. The main reported methods are viral- and lipid-mediated transfection systems. However, these methods have been reported to be inappropriate for therapies due to virus-based safety risks and low efficiency in vivo, respectively [57-60].

In order to remove the need for *RUNX2* gene delivery, it was suggested to deliver RUNX2 as recombinant protein. Delivery of proteins has been considered as the safest and most useful application in therapeutic application of stem cells [50], because proteins can regulate gene expression transiently without any genomic alteration.

Since the discovery of Cell Penetrating Peptides (CPPs), several techniques have been reported to deliver various molecules such as oligonucleotides, small molecules, siRNA, nanoparticles, peptides and proteins [61-63]. Ravindran et. al. have reported successful delivery of RUNX2 protein using cell penetrating peptide [54]. A novel fusion peptides were developed in our group (lead by Dr. James Dixon) called GET peptides, the aim was to utilise these peptides to deliver RUNX2 to induce hMSCs differentiation. An overview of this technology is presented in the upcoming section.

1.7. Glycosaminoglycan Enhanced Transduction (GET) Peptides

The previously mentioned transfection methods (viral, and lipid delivery) have some drawbacks, such as low efficiency and high toxicity. An alternative strategy to deliver cargos intracellularly was needed.

In 1988, the HIV TAT trans-activating factor was discovered [64-66]. TAT was the first discovery of a new type of molecular vectors, which can enhance the delivery of cargos, called cell-penetrating peptides (CPPs).

Cell-penetrating peptides are class of various peptides; usually consist of 5–30 amino acids. This type of peptides can cross the cellular membrane, by endocytosis. Due to their ability in crossing the cellular membrane, CPPs can be used for different applications [67]. CPPs were used as vectors for siRNA [68] nucleotides, small molecules, and proteins [69, 70]. Moreover, CPPs were used to carry a functional peptide, and can incorporate a functional motif [71, 72].

CPPs may have different amino acid contents and 3D structure. CPPs have different degrees of hydrophobicity and polarity; this can be seen with different examples of cationic, anionic, and neutral CPPs. The various structures of CPPs

can result in different levels of cellular uptake. Also, the type of cargo carried by a CPP will affect the mode and levels of uptake [73].

The exact mechanism of cellular uptake of CPPs was not clear, various debates were reported [66, 67, 74-76]. However, endocytosis-mediated uptake is assumed to be the main pathway through which CPPs are internalized within membranes [66, 77, 78], specifically, lipid raft–dependent micropinocytosis [76, 79].

The main limitation related to CPPs protein delivery mediated via endocytosis is the entrapment of the internalized cargo in the cytoplasm within endosomes. This prevents the release of the cargo and exposes it to degradation in lysosome [77]. Eventually, this will require high starting concentration of CPPs to bypass entrapment inside endosomes [77, 80] and this may expose the cells to toxic dose.

Tissue engineering group at University Of Nottingham (lead by Dr. James Dixon) has developed a novel cellular delivery system to overcome the delivery limitations using CPPs. This novel system is a series of fusion proteins that binds a membrane docking peptides to heparin sulphate glycosaminoglycans (GAGs) with cell penetrating peptide [81].

Heparan sulphate (HS) is a proteoglycan commonly present on cell surfaces which plays an important role in the extracellular matrix regulating a variety of biological processes [82]. For this reason, P21, a heparin binding domain (HBD) that is comprised of a short 21 peptide residue (KRKKKGKGLGKKRDPCLRKYK) was used to enhance cell binding.

The GAG-binding peptide (arginine) was added to stimulate cell interaction and the CPP functions for high efficiency membrane transduction [81].

This technology provides combination of cell-targeting and cell-penetrating potentials and allows the delivery of therapeutic proteins to different cell-types. Functional quantities of various protein cargos, such as fluorescent proteins, transcription factors and enzymes, were successfully delivered using this proposed technology [81]. An example for delivery of Red Fluorescent Protein is shown in figure 1.4. This figure was printed from Dixon et. al. research [81] This technology will be utilised in this research to deliver the transcription factor RUNX2.

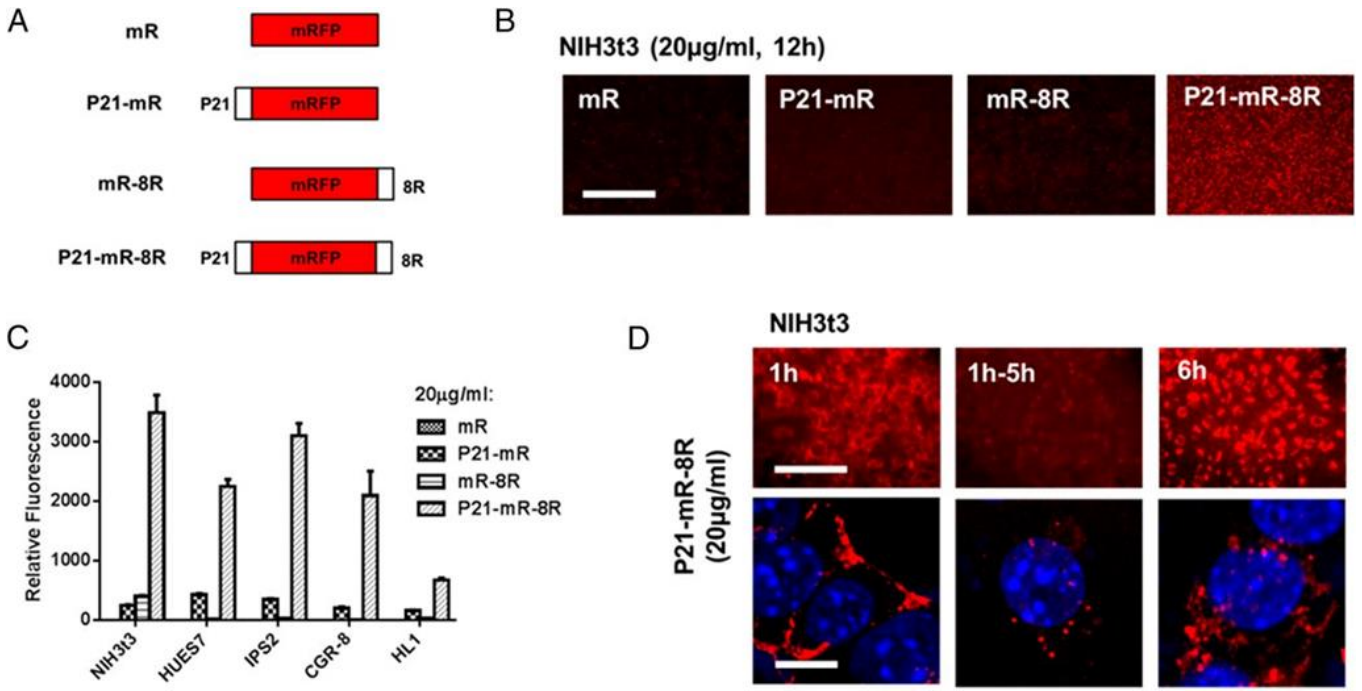


Figure 1.4 Printed from Dixon et. al. [81]. P21 improves PTD-mediated cellular uptake.

(*A*) Schematic of the proteins created after screening domains that improve efficiency of protein delivery to cells. P21-mR is mRFP with an *N*-terminal fusion of the P21 domain of HB-EGF. P21-mR-8R is mRFP with N-terminal fusion of P21 and C-terminal fusion of 8R. (*B*) Fluorescence microscopy images of NIH3t3 cells treated with proteins (20 μg/mL) for 12 h in standard media conditions. (Scale bar, 100 μm.) (*C*) P21-mR-8R is efficiently taken into hESCs and mESCs (HUES7 and CGR-8, respectively) and hiPSCs (IPS2) and mouse cardiomyocyte cell line HL1. Flow cytometry analyses of the mR-8R inefficiently delivered cell lines treated with proteins mR-8R (20 μg/mL) for 12 h. (*D*) P21-mR-8R initially strongly interacts with cell membranes and progressively is taken up and localized perinuclearly. Fluorescence (*Top*) and confocal laser scanning microscopy (*Bottom*) images of NIH3t3 cells treated with P21-mR-8R (20 μg/mL) for 1 h, 1 h with washes and a further 5 h incubation (in serum-free media), or 6 h treatment. Cells were pre-incubated for 1 h in serum-free media and transduced for the desired time in serum-free media. (Scale bars, top, 50 μm; bottom, 10 μm). [81].

1.7.1. RUNX2 delivery using GET peptides

It was previously shown that CPPs can be used to deliver RUNX2 protein [54]. Accordingly, it was suggested to study the combination of RUNX2 protein with the previously mentioned GET peptides (section 1.7).

A study was done in our group (Tissue Engineering group – University of Nottingham) investigated the effect of GET-RUNX2 delivery on hMSCs differentiation [55].

P21-RUNX2-8R cDNA was synthesised and cloned into the pGEX6-P1 expression vector and expressed proteins in BL21 (DE3) pLysS Escherichia coli. The synthesised protein was transduced to hMSCs, dose, dose frequency, as well as cell viability were first evaluated before studying cells differentiation were evaluated. Figure 1.5 shows the evaluation results (figure was printed from Thigarajan et. al. [55]).

The results showed that the cells commit to osteoblast lineage in response to P21-RUNX2-8R treatment. The best response was at dose of 60μg supplied in two equal doses (30μg each). Moreover, BMP-2 and Dexamethasone were used as positive controls to compare to P21-RUNX2-8R effect. The results showed comparable cells behaviour [55].

Based on these findings, and in order to achieve the needed dose of P21-RUNX2-8R when cells seeded on scaffolds, for the purpose of bone tissue engineering, polymeric microparticles will be employed to release P21-RUNX2-8R.

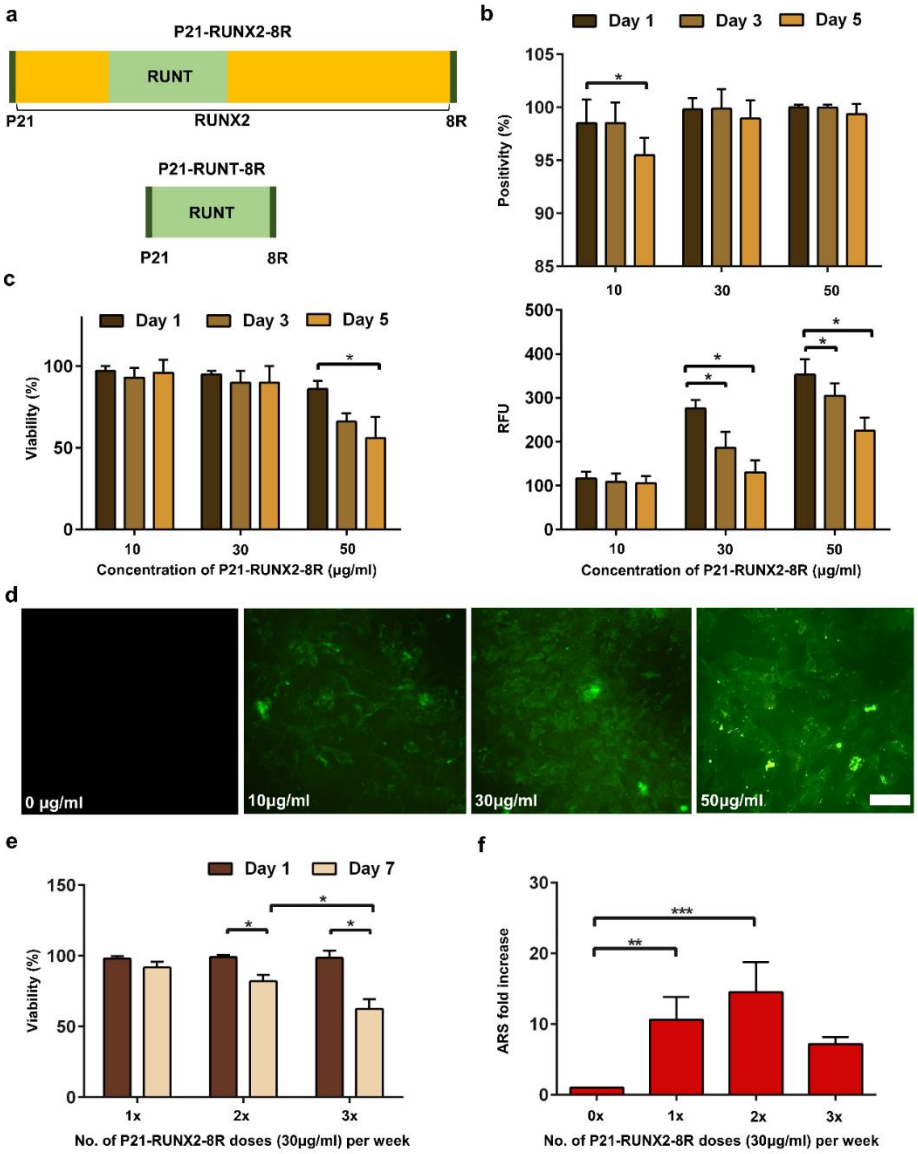


Figure 1.5 Printed from Thiagarajen et. al. [55]. P21-RUNX2-8R delivery induce osteogenesis. (A) Design of the osteogenic constructs. P21-RUNX2-8R is a RUNX2 transcription factor with an N-terminal fusion of P21 and a C-terminal fusion of 8R. P21-RUNT-8R contains only the DNA binding domain, RUNT, sandwiched between P21 and 8R. (B) To assess the delivery of the fusion peptide, the proteins were labelled with FITC and delivered at different concentrations overnight. Flow cytometry analysis of percentage positivity and relative fluorescence unit (RFU) of hMSCs treated with different concentrations of P21-RUNX2-8R-FITC (10, 30, 50 µg/ml) overnight. Statistical significance was determined using the Holm-Sidak method, α=0.05. (C) Viability of hMSCs measured using trypan blue at day 1 and 7 after overnight treatment with 30

μg/ml of P21-RUNX2-8R. 30 μg/ml of P21-RUNX2-8R was used as the optimal concentration on further experiments. Statistical significance determined using the Holm-Sidak method, with alpha=5.000%. (D) Fluorescence microscopy images of hMSCs treated with 10, 30 and 50 μg/ml P21-RUNX2-8R-FITC overnight. As the concentration increases, fluorescence intensity of P21-RUNX2-8R-FITC inside hMSCs increases. Scale bar is 50 μm. (E) For the first week, hMSCs were treated overnight with P21-RUNX2-8R (30 μg/ml) every other night (3x), every three days (2x) or treated only once (1x). Viability of hMSCs measured using trypan blue at day 1 and 7 after overnight treatment with 30 μg/ml of P21-RUNX2-8R once, twice and thrice per week. Statistical significance determined using the Holm-Sidak method, with alpha=5.000%. (F) Treated hMSCs were cultured in osteo-permissive medium for three weeks, stained with Alizarin Red S (ARS) for matrix mineralization and quantified using a microplate reader. 30 μg/ml of P21-RUNX2-8R treated twice during the first week was identified as the optimal dose and the same conditions were used in the subsequent assays. Statistical significance was determined using one way ANOVA. Error bars indicate standard deviation (SD).

1.8. Therapeutic molecules delivery from microparticles

In vivo, therapeutic proteins can be delivered by subcutaneous and intramuscular administration, or intravenous infusion. However, most proteins possess short biological half-lives in bodily fluids which means that frequent injection regimens at high dosages are required for sustained effect. Moreover, systemic delivery by nature does not allow targeted or localised delivery of proteins, meaning off-target effects and significant amounts of the administered therapy is miss-targeted. In order to overcome these limitations, biodegradable polymers have been used to control the release of therapeutic proteins locally at the disease site. These controlled release approaches can be powerful as they extend the duration of activity, overcoming the need for frequent administration, and also implantation at the therapeutic site allows localized delivery to the tissue of interest [83-87].

Controlled delivery devices can provide the flexibility to optimise the system based on the needed drug release rate; for example, providing a continuous rate of delivery or fluctuating release. Second, controlled release devices can be used to protect drugs from being destroyed in the body; such as proteins. Moreover, controlled release systems can enhance patient compliance by having less frequently administered doses [87, 88].

Biodegradable polymeric microparticles are one of the common types for the controlled release delivery devices [87, 89]. Polymeric microparticles have many advantages; they can be used to encapsulate different types of drugs, including small molecules, proteins and nucleic acids. Polymeric microparticles are easily administered by syringe; they can provide high bioavailability. Moreover, they can sustain the release for longer periods [87, 89]. Disadvantages

of microparticles include limitations of large-scale manufacturing and loss of drug activity during fabrication [87, 88].

1.8.1. Polymers used for controlled drug release systems

Many polymers can be used for controlled delivery applications; however, in order to facilitate their study, polymers have been classified into groups with common properties, of the polymers, within the group.

Polymers are categorised into the two major types; natural polymers and synthetic polymers. Synthetic polymers can be classified into biodegradable polymers and non-biodegradable polymers [90-95].

A- Natural polymer:

1. Protein-based polymer: albumin, collagen, gelatine.

2. Polysaccharides: alginate, chitosan, agarose, hyaluronic acid, cellulose, starch.

B- Synthetic polymers

The below table summarizes the types of synthetic polymers.

Table 1.1 Synthetic polymers classes and examples.

Material	**Class**	**Example**
Biodegradable polymers	Polyester	Poly lactic acid, poly glycolic acid, poly lactide-co-glycolide (PLGA), poly hydroxyl butyrate, polyester, polycaprolactone.
	Polyanhydride	Poly adepic acid, poly sebacic acid.
	Polyamides	Poly amino acid, poly imino carbonate.
	Phosphorous based polymer	Polyphosphates, poly phosphonates.
	Others	Poly cyanoacrylates, poly urethanes, etc.
Non-biodegradable polymers	Cellulose based	Carboxy methyl cellulose, ethyl cellulose, cellulose acetate hydroxyl propyl methyl cellulose.
	Silicons	Polydimethyl siloxane, colloidal silica, polymethacrylate, polymethyl methacrylate.
	Others	Poly vinyl pyrolidine, Ethyl vinyl acetate, Poloxamine etc.

Microbial contamination, batch to batch variation and uncontrolled rate of hydration are the main disadvantages of natural derived polymers [96]. On the other hand, synthetic polymers can overcome these disadvantages and they are preferred to be used in formulation. Moreover, biodegradable polymers can provide localized and sustained delivery of drug, with an expected release rate [89].

1.8.2. PLGA use in controlled drug release systems

PLGA properties make it an attractive polymer to be used for drug delivery applications. PLGA biocompatibility, biodegradability, and flexible erosion times make it of interest to use in controlled delivery systems. Moreover, PLGA has flexible mechanical properties and is FDA approved polymer [97].

For the development of controlled delivery systems for small molecules, proteins, DNA, peptides and RNA, PLGA has been widely studied in both commercial and research use [98-100].

Polyester PLGA is a copolymer of poly lactic acid (PLA) and poly glycolic acid (PGA). Poly lactic acid contains asymmetric α-carbon which is described as the D or L form. The enantiomeric forms of the polymer PLA are poly D-lactic acid (PDLA) and poly L-lactic acid (PLLA). PLGA is generally an acronym for poly D,L-lactic-co-glycolic acid where D- and L- lactic acid forms are in equal ratio [97].

1.8.3. Physico-chemical characteristics of PLGA

The physicochemical properties of optically active PDLA and PLLA are nearly the same. PLA can be either highly crystalline (PLLA) or highly amorphous (PDLA). PGA doesn't have any methyl side group, and have crystalline structure. Figure 1.6 shows the PLGA structure.

PLGA is soluble in various solvents such as tetrahydofuran, chlorinated solvents, ethyl acetate and acetone [89, 101]. PLGA biodegrades by hydrolysis of its ester linkages.

Methyl side group in PLA component is making it more hydrophobic. Accordingly, the polymer that has more lactide content is considered more hydrophobic (or less hydrophilic). As a result, the lactide rich polymer absorbs less water and degrades more slowly [97].

1.8.4. Factors Affecting Polymer Degradation

Several factors can affect the degradation behaviour of PLGA polymer. The polymer composition plays an important role in determining degradation rate. Increasing the glycolic acid content will facilitate the polymer weight loss. PLGA 50:50 (PLA/PGA) has a faster degradation than PLGA 65:35. This might be attributed to the degradation of glycolic acid proportion associated with higher hydrophilicity. In addition, PLGA 65:35 shows faster degradation than PLGA 75:25 and PLGA 75:25 than PLGA 85:15 [102-104]. The degradation of the polymer, and consequently, drug release rate, can be controlled by the quantity of glycolic acid.

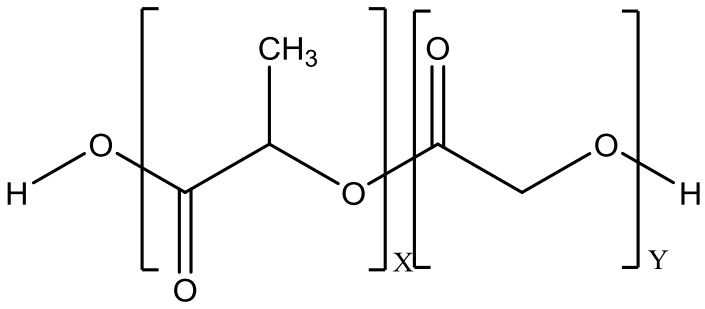


Figure 1.6 Chemical Structure of PLGA (x is the repeat of lactic acid units and y is repeat of glycolic acid units).

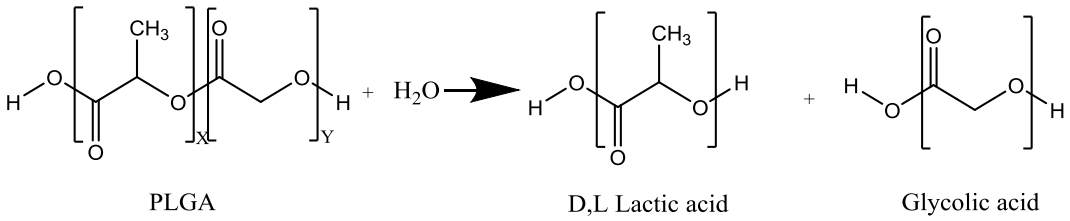


Figure 1.7 Hydrolysis of PLGA

Another factor affecting the degradation rate is the polymer average molecular weight (Mw). Lower degradation rates can be achieved with higher molecular weight polymers [105]. The polymer chain size is influencing the molecular weight. Increasing the polymer chain length will results in higher molecular weight polymer which will results in longer degradation time, compared to the small polymer chains. There is an exception in the PLLA polymer, where longer chains will degraded faster, due to lower degree of crystallinity with the higher molecular weight [105, 106].

The ratio of surface area to volume is another important factor for polymer degradation rate. Higher surface area ratio will result in higher degradation rate. Higher surface are to volume ratio has faster release profile [107-109].

1.8.5. Microparticle fabrication techniques

Various fabrication techniques are available to create polymeric microparticles, such as emulsion techniques, spray drying, supercritical CO_2 and microfluidic and solvent exchange [110-112].

Spray drying is a common method to fabricate microparticles. The polymer solution is placed in a chamber through an atomiser where it is rapidly dried by a hot gas [111]. The cost of spray drying equipment is a limiting factor to use it for microparticles production.

Microfluidic and solvent exchange techniques have resulted in the manufacture of polymer microparticles of uniform size [112], however, these techniques are slow to produce feasible yield [113].

The most common method to fabricate polymeric microparticles is using a variety of emulsion techniques and these will be discussed in the coming Section.

1.8.5.1. The Principle of Emulsion Formation

An emulsion is formed as a result of mixing two immiscible liquids (e.g. oil and water) together. The emulsion is formed by dispersing one liquid in the other in the form of drops (figure 1.8). The emulsions can be either oil in water (O/W) or water in oil (W/O). A stabilizer has to be used to maintain the stability of the emulsion as when mixing stops, the drops may coalesce and the two phases may separate and the emulsion may collapse. The stabilizers are usually in form of surfactants that form a film at the interface of the droplet and resist coalescence. The stability of an emulsion is dependent on interfacial viscosity, electric charge on drops, droplet size and concentration, and viscosity of the continuous phase. Walstra did a review of the principles of emulsion formation [114].

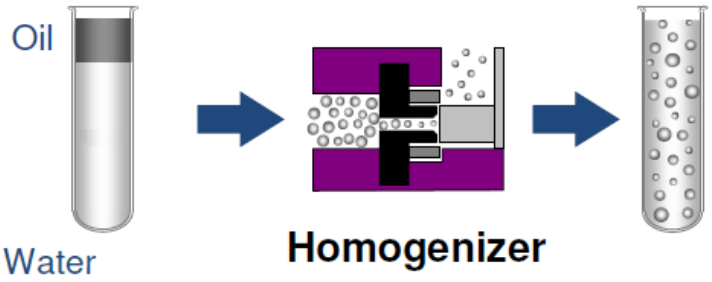


Figure 1.8 The principle of oil in water emulsion [115]

1.8.5.2. Microparticles Manufacture by Emulsion and Solvent Evaporation

The principle of emulsion formation has been exploited to manufacture drug encapsulated polymeric microparticles for use in drug delivery applications. The work presented here will focus primarily on encapsulation of proteins as these have complex structures which are directly related to their function and thus pose challenges to avoid denaturation and loss of bioactivity during the encapsulation process. There are two major methods developed to encapsulate proteins into polymer microparticles, solid-in-oil-in-water (S/O/W) emulsion and water-in-oil-in-water emulsion (W/O/W) [116-120]. The W/O/W method of microparticles production is widely used and involves dissolving the required drug or protein in a small volume of water then creating a primary water-in-oil emulsion by homogenising the protein solution with a solution of the required polymer in an organic solvent such as dichloromethane. The primary emulsion is then transferred into another aqueous solution comprising of an emulsion stabiliser such as polyvinyl alcohol where it is homogenised for a second time. The organic solvent must then be removed by solvent extraction or evaporation to leave protein loaded microparticles (figure 1.9).

Proteins tend to adsorb at water/organic solvent interfaces and this is thought to destroy the delicate conformation of proteins and to affect various physico-chemical transformations leading to protein destabilization reactions [121, 122]. Therefore the S/O/W method which maintains proteins in their solid state and only subjects them to one oil water interface would therefore seem more appropriate to maintain protein function. A novel method of protein micronisation with polyethylene glycol (PEG) by lyophilisation was suggested by Morita to improve protein encapsulation and stability [116].

Although the double emulsion is simple, it has a number of variables which will affect the resulting microparticles. Without proper control of the method, the microparticles will have a wide distribution of the size and variable protein content [123]. The challenge would be to optimise a reproducible and robust fabrication protocol to produce microparticles in defined size range with feasible entrapment efficiency without loss of biological activity of the entrapped molecule.

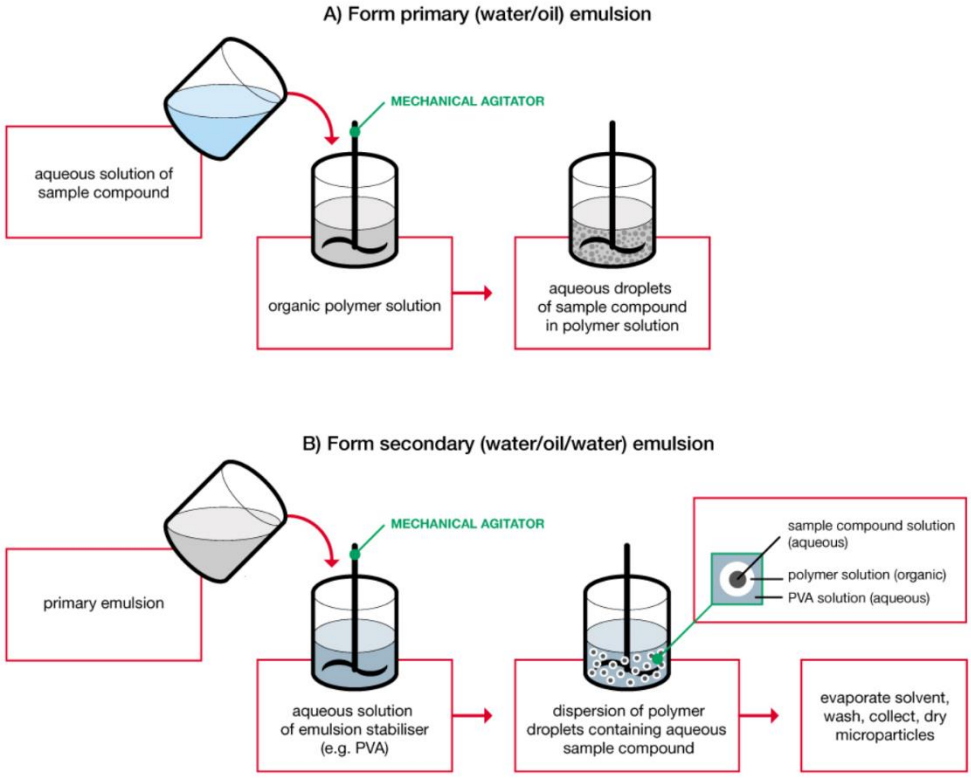


Figure 1.9 Schematic showing the water-in-oil-in-water double emulsion method of polymer microparticles manufacture [120].

1.8.6. Factors affecting protein stability during MPs fabrication

During MPs fabrication, many factors can affect protein stability, such as protein instability at the water – organic interface using double emulsion methods such as water-in-oil-in-water (W/O/W) [121], protein–polymer interaction [124], and local acidity created within degrading polymer matrix [125-127].

Several approaches have been developed to protect protein activity during MPs fabrication, such as adding excipients to the inner aqueous phase or removing the need for the primary aqueous phase [128-131]. Excipients (such as Cyclodextrin and PEG [86, 129-131]) can be added to compete with the therapeutic protein for exposure at the water-organic interface. A study by Morita et al [132] suspended dry protein particles in the organic solvent with the aid of PEG, which removes the primary water–organic interface, and is termed solid-in-oil-in-water (S/O/W) emulsion.

In order to overcome local acidity limitation, many groups studied pH neutralization in the PLGA microenvironment [86, 133-135]. Various low soluble basic salts were studied, such as magnesium hydroxide [135] and Poly-L-Histidine coupled with PEG [86]. The use of these excipients resulted in neutralized acidic microenvironment within the PLGA MPs system. Other issues can arise if the therapeutic proteins interacts with the polymer used [86]. Protein–polymer interactions can occur through hydrogen bonding, and through hydrophobic or electrostatic interactions [86]. Furthermore, proteins may interact with the degradation products of the polymer; PLGA degrades through an acid-catalysed hydrolysis and produces carboxylic acid molecules which can interact with cationic molecules. Electrostatic and hydrophobic interactions are also common factors for protein–polymer complexation [136-138].

1.9. Scaffolds for bone regeneration applications

A scaffold is a temporary framework used to fill and support cells in the repair of large structures. Bio-absorbable scaffolds are temporary replacement structures that preserve tissue, and provide template to the cells during repair process [139, 140]. Scaffolds can be fabricated from inorganic, synthetic and naturally sourced materials as an alternative to grafting strategies [141].

Scaffolds were developed to serve as an adhesive structure for the implanted cells, enhances cell growth, and allow the retention of differentiated cell functions. In order to do this function appropriately, scaffolds design should meet certain criteria: (1) surface properties: it should allow cell adhesion to allow cell growth; (2) It should be biocompatible and biodegradable; (3) Porosity should be suitable for scaffold function; (4) The materials should be reproducible and process-able [142].

The utilisation of scaffolds as a template for cells and delivery device for biological factors has showed enhanced *in vivo* tissue engineering [143]. However, the cells have to be able to form 3D tissue structure of full viability and with homogenous cell phenotype [144].

1.9.1. Scaffold Materials

The main function of scaffolds is to provide support in the development of tissue constructs; these scaffolds have a defined shape at room temperature. Also, they can be utilised in helping tissue restoration by temporary filling of a defect site, or temporary replacement of the tissue. Hydrogels are swollen materials which composed of highly hydrated polymeric chains [145]. Solid and hydrogel scaffolds are derived from natural polymers such as collagen, or synthetic

polymers such as poly (α-hydroxyacids), or inorganic materials such as tricalcium phosphate. Table 1.2 summarizes examples of some scaffold materials used for various tissue engineering applications.

Table 1. 2 Scaffolds materials used for tissue engineering application

Materials	Types	Advantages/disadvantages
Natural Polymers	Chitosan, Chitin, Collagen, Gelatin, Hyaluronic acid, alginate, Agarose	**Advantages:** Biocompatible, biodegradable. **Disadvantages**: Poor mechanical strengths, disease transfer, processability.
Inorganic Materials	Calcium orthophosphate cements; porous coralline; ceramics; Hydroxypaptite; titanium; bioactive glass, β-tricalcium phosphate; Ceramics	**Advantages:** good mechanical Strength, biocompatible. **Disadvantages**: difficult to mould into different shapes and Forms.
Synthetic Polymers	Poly (lactic acid); Poly (glycolide); Poly (lactide – co- glycolide); Poly(lactic acid-co-ethylene glycol); Poly (propylene fumarate); Polycaprolactone; Polyhydroxyalkanoates; Poly(glycerol sebacate); Pluronic F127.	**Advantages:** design flexibility, tailored biodegradability. **Disadvantages**: solvents are required for processing. Poor cell adhesion. Acidic microenvironment upon degradation.

1.9.1.1. Natural Polymers

Natural polymers used to create scaffolds include collagen [146], chitosan [147], alginate [148] . They are biocompatible and biodegradable. However, the poor control of degradation rate and limited mechanical properties are the two main disadvantages for using naturally derived polymers in tissue engineering [149].

1.9.1.2. Inorganic Materials

It includes ceramics, like calcium phosphate (e.g. hydroxyapatite (HAP), and tricalcium phosphate (TCP)). Another inorganic components are metals and bioglass. HAP is commonly used because it is the main component of bone and it is been used clinically since the 1980s [150]. HAP has the ability to fuse directly with bone since its chemical nature is similar to that of bone. HAP is brittle, unless mixed with other materials, moreover, HAP blocks are difficult to mould into bone defects.

1.9.1.3. Synthetic Polymers

The main biodegradable synthetic polymers include polyfumarates, polycarbonates, polycaprolactone, polyesters, polyanhydrides and polyorthoesters [151]. Polyesters such as poly(glycolic acid) (PGA), poly (lactic acid) (PLA) and their copolymer of poly[lactic-co-(glycolic acid)] (PLGA), are widely used as they have gained the approval of US Food and Drug Administration for certain human clinical use, such as surgical sutures.

A novel polymeric scaffold formulation has been developed in Tissue Engineering Group at University of Nottingham. This formulation undergoes thermo-responsive sintering under physiological conditions to form solid

scaffolds [152-154]. The particles in this formulation are composed of a blend of PLGA and poly(ethylene glycol) (PEG). The PEG component acts to lower the glass transition of the mixture to be around the body temperature (i.e. 37°C) [154]. These particles can be suspended in an aqueous carrier to form a paste for use as an injectable defect filler. When the temperature of the paste is raised to 37°C the particles soften and form adhesion bridges to one another. The presence of the carrier then allows the hydrophilic PEG component to leach out. This causes the polymer and thus the particle-to-particle adhesion bridges to re-solidify.

1.9.2. Injection of the Scaffold

The traditional tissue engineering model is based on a matrix that can be used as filling material for the defect and a host for cells and a delivery system for therapeutic agents. Injectable materials is promising for various tissue engineering applications as they have superior advantages over pre-fabricated scaffolds [155].

Injectable delivery systems for RUNX2 could provide a less harm method for repair of bone defects, minimizing invasive surgery. Injectable scaffolds provide the flexibility to fill the space in which they are placed and will fill irregular shape defects. Clinical indications might include nonunion fractures, or delayed union of bone which may cause serious complications in fracture treatment, and large defects associated with bone tumor resection [155, 156].

1.9.2.1. Injectable Scaffold Requirements

Choosing a material for tissue engineering applications requires the material to have certain characteristics. Essentially, the material must be biocompatible.

Moreover, the degradation products (for biodegradable materials) need to be biocompatible, as well as any material leachable molecules [156]. Another important parameter needs to be considered is the scaffold porosity. Spaces within the scaffold structure are necessary to permit tissue growth and transportation of nutrients waste products [24]. Another essential factors that have to be taken into consideration are the mechanical properties and the degradation rate of the scaffold. For example, if a scaffold will be used as a tissue carrier, it must have enough mechanical strength to support the tissue, especially at the beginning of the development [156].The scaffold degradation rate is critical. Ideal degradation rate would be matching new tissue formation, a quicker degradation rate is needed sometimes, especially to allow the release of bioactive agents, other applications need a slower degradation rate which can keep its structural and mechanical characteristics for longer periods of time [156].

Injectable scaffolds have been thoroughly studied for applications in bone regeneration. Multiple factors play important roles in bone formation; such as macromonomer concentration, localized release of therapeutic agents within the injectable matrix [24].

Bone formation can be stimulated by controlled release of biological factors used in the scaffolds. For example, the release of osteo-inductive factors from PEG hydrogels was shown to be dependent on the macromonomer concentration and quantity of the degradable chains in the polymer [157].

1.9.3. 3D printing of scaffolds for bone tissue engineering

3D printing, is used to create complex three-dimensional scaffolds by building up layers of polymer using a 3D printer [158, 159]. It involves precise deposition of the polymeric material which can be further sintered via various techniques (i.e. temperature, chemical and laser cross linking). 3D printing allows fabrication of scaffolds with very complex structures and irregular shapes which are difficult to mould. Utilising 3D printing technique allows the treatment of the scaffolds before being introduced to the body, such as seeding and growing cells. Different materials (such as PLGA and ceramic) were printed with optimized scaffolds characteristics such as porosity and mechanical strength [158, 160, 161].

3D printing is a scaffold manufacturing technique where a nozzle extrusion system can be used to fabricate thermally or chemically treated materials [162]. The materials are deposited in a layer-by-layer fashion, where each layer may contain a combination of different materials. A key feature of 3D printing systems is that they can print cell-laden gels, with other polymeric materials such as PCL, to produce functional scaffolds [163]. The printer has a pneumatic pressurized system to extrude the material from the ink cartridges.

A recent study from our group showed that we can 3D print PLGA based polymeric scaffolds with optimised mechanical properties [158]. The material's properties as well as sintering mechanism will be discussed in chapter 4.

1.10. Thesis Aims

This introduction has highlighted the need to deliver safe therapeutic molecules to help in bone regeneration. Utilising GET peptide, transcription factor (RUNX2) can be delivered to control osteogenesis. This transcription factor has to be delivered at defined dose and time intervals. Polymeric microparticles will be used to deliver GET-RUNX2 molecule to the needed site at the needed time. Scaffolds, which serve as a template for both the loaded microparticles and the cells, are usually used in bone regeneration. Polymeric scaffolds will be used, in this work, to evaluate stem cells osteogenesis in response to released GET-RUNX2. The ability to 3D print the scaffold material will provide advantage to the technology, providing complex structures and irregular shapes.

The goal of the work presented here is to create polymeric scaffolds to deliver selected transcription factors in a controlled manner with the potential to serve as injectable biomaterials for skeletal repair.

The aims of the following results chapters are as follows:

- Chapter 2: GET peptide loaded PLGA MPs
    - Develop a protocol to create PLGA microparticles with controllable size and morphology, ideally MPs to be below 50μm, to allow 3D printing.
    - Encapsulate of GET-tagged protein within PLGA MPS with high efficiency.
    - Investigate the effect of the fabrication process on encapsulated GET peptide.
    - Optimise the fabrication parameters to have biologically active encapsulated GET peptide.

- Chapter 3: Optimisation of the release profile matching the RUNX2 therapeutic dose and test the activity of the released GET peptide
    - Characterise the release profile from the fabricated MPs.
    - Optimise the release profile to match the needed therapeutic dose.
    - Test the activity of the released GET tagged protein.
    - Investigate the effect of the release process on biological activity of GET peptide.
    - Investigate potential stabilisation approaches for the released GET peptide, if needed.
- Chapter 4: Evaluate mesenchymal stem cells differentiation in response to released GET-RUNX2
    - Translate the technology from model protein delivery to GET-RUNX2 delivery.
    - Determine that biological activity of GET-RUNX2 is retained post release.
    - Scaffolds fabrication using thermosensitive particles and GET-RUNX2 loaded microparticles.
    - Study the effect of the released GET-RUNX2 on stem cells osteogenesis.
    - Develop a technique using 3D printer to provide complex structures of scaffolds to be used as defect fillers.

Chapter II:

Development of a method to fabricate GET-protein loaded PLGA microparticles

2. Development of a method to fabricate GET-protein loaded PLGA microparticles

2.1. Introduction

Biodegradable polymeric microparticles (MPs) have been used for many years as drug delivery devices and in the field of tissue engineering as 3D scaffolds for tissue support. They have been utilised to provide alternatives for bone graft. However, there still a need for an efficient tissue-engineered substitute that can provide suitable environment for successful new tissue regeneration.

MPs can be utilised to serve as biological factors delivery devices to help in tissue regeneration. Various methods have been developed to create MPs; such as solvent evaporation, phase separation and spray drying. Dan Cho et al. summarised them in their review article about MPs fabrication methods [164]. The emulsion method is considered inexpensive and easy to use for MP fabrication. However, there are number of factors which can affect the resultant MPs. This may include size distribution and the encapsulation efficiency of the loaded molecule which will be reflected on the efficiency of the system.

Many emulsion methods can be utilised to produce microparticles, depending on the characteristics of the molecule to be encapsulated. Water in Oil in Water (W/O/W), Solid in Oil in Water (S/O/W) and Water in Oil (W/O) or Oil in Water (O/W) were all studied as methods for microparticles fabrication [116, 165, 166]. Amongst these methods, W/O/W and S/O/W were considered in this work to encapsulate GET tagged molecules within PLGA MPs. Generally, these two methods have similar procedure. They mainly consist of three phases; protein encapsulation phase, microparticles formation phase and microparticles drying. At each phase, there are certain parameters affecting the produced microparticles

and the stability of the encapsulated molecule. In order to validate a method for PLGA MPs fabrication, both methods were extensively investigated. Figure 2.1 summarises the potential factors affecting the MP morphology and stability of the encapsulated protein.

There is a need to have a robust microparticles fabrication method that is reproducible and maintain the activity of the encapsulated protein during MP formation. Moreover, the microparticles should be able to release the encapsulated protein at the right dose (time and quantity) without loss of protein activity over time.

There are many parameters affecting protein stability during MP fabrication, such as shear force, organic solvent, surfactants and surface tension. The limiting factor, to choose a suitable method, is the encapsulated protein. The balance between all the parameters can provide the needed MP characteristics and maintain the activity of the protein.

Several approaches have been developed to protect protein activity during MP fabrication, such as adding excipients to the inner aqueous phase or removing the need for the primary aqueous phase [128-131]. Excipients (such as Cyclodextrin and PEG [86, 129-131]) can be added to compete with the therapeutic protein for exposure at the water-organic interface. A study by Morita et al. [116] suspended dry protein particles in the organic solvent with the aid of PEG, which removes the primary water–organic.

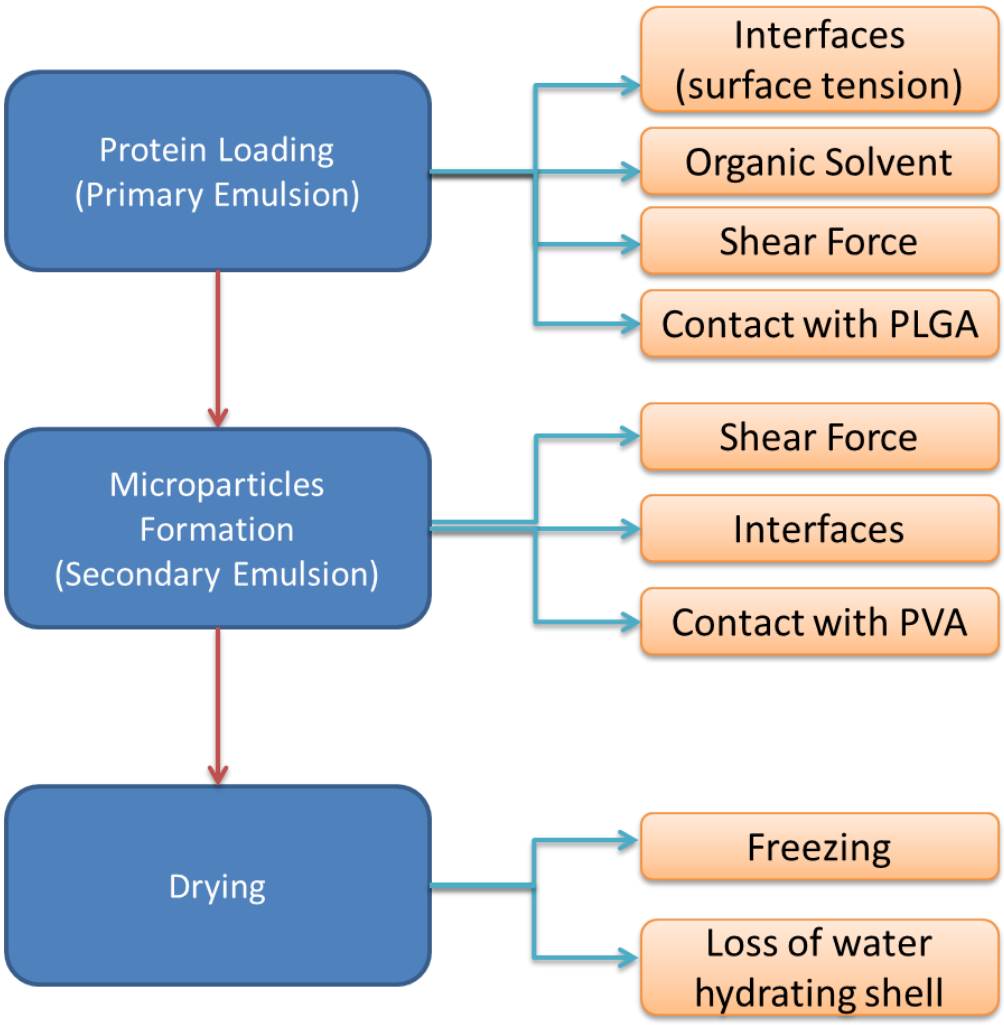


Figure 2.1 Phases of MP formation using W/O/W and S/O/W methods and factors affecting MP morphology and possible factors affecting protein stability during MP fabrication. Adopted from van de Weert wt al. *[167]*.

Proteins have different characteristics (physically and chemically) which suggests that a MP fabrication method suitable for a certain protein is not necessary to be suitable for another protein. Method validation has to be done for each protein to ensure compatibility of the used method and the protein, to provide the needed MP characteristics.

The work presented in this thesis is aiming to have a robust delivery system for GET peptide [81] tagged with various therapeutic molecules. The encapsulated molecules will have two parts; GET peptide (to enhance cellular uptake) and therapeutic agent. In order to have a robust MP fabrication method, the encapsulated molecule should maintain the activity of both GET peptide and therapeutic activity.

Therefore, in order to understand the effect of fabrication method on GET peptide, they were tagged with a self-reporter model protein Red Fluorescent Protein (mRFP). The activity of the molecule (P21-mR-8R) can be evaluated directly by testing its transduction activity. P21-mR-8R was used during the methods investigation and validation.

2.1.1. Aims

The main aims for this chapter were to thoroughly investigate the double emulsion methods (W/O/W and S/O/W) and identify the parameters affecting the GET peptide stability during MP fabrication. Also, the concerns were to identify the parameters affecting MPs morphology and try to balance between them to have a reproducible method to fabricate spherical MPs with identified size ranges and maintain the GET peptide activity during fabrication stages.

2.2.Materials and methods

2.2.1. Expression and purification of P21-mR-8R

P21-mR-8R was expressed as recombinant protein as previously described by Dixon et al. [81]. cDNA for mRFP1 (mR) was provided as a kind gift from Dr. R. Y. Tsien (University of California, USA). 8R and P21 were synthesized by de novo (Eurofins MWG Operon).cDNAs were cloned into the pGEX6-P1 expression vector (Novagen) to create in-frame fusions and expressed proteins in BL21 (DE3) pLysS Escherichia coli (Novagen). Exponentially growing LB cultures (OD600 = 0.4) were shaken at 220rpm at 37˚C and then induced using 0.5mM Isopropyl β-D-1-thiogalactopyranoside (IPTG) and shaken for 48 hours at 25˚C. bacterial pellets were then lysed and sonicated (10 amplitudes, 30 second , 5 times) in extraction buffer (50 mM Tris, pH 7.5, 150 mM NaCl, 1 mM EDTA containing 1mM DTT, 0.2 mg/ml lysozyme, and 1X protease inhibitor cocktail). Insoluble protein was retrieved using the Rapid GST inclusion body solubilisation and renaturation kit (AKR-110; Cell Biolabs, Inc., San Diego, CA). Recombinant proteins were purified by affinity chromatography using Glutathione-Sepharose resin (GE Healthcare). GST-tags were removed and eluted from resin by PreScission^{TM} Protease cleavage (GE healthcare) in cleavage buffer (50 mM Tris-HCI pH 7.0, 150 mM NaCl, 1 mM EDTA and 1 mM DTT).

Protein concentration was determined using a BCA-based protein assay (BioRad) with absorbance measured at 595nm using recombinant mR as a standard. Protein purity was checked through SDS-PAGE gel electrophoresis.

2.2.2. Microparticles fabrication using S/O/W

Poly (D,L-lactide-co-glycolide, (PLGA) LA:GA ratio: 50:50; Mw 52 kDa, Evonik Industries, USA) MPs were formed using solid-inoil- in-water (S/O/W) emulsion as previously described by Morita et al. [116], with some modifications. Briefly, 1 mg of P21-mR-8R, was mixed with 0.5 mg PEG 6000 (Sigma-Aldrich, UK) and freeze dried overnight (this ratio was reported to produce protein-PEG particles of less than 5μm [116]). Blank MPs were prepared by freeze drying 0.5 mg PEG 6000 only. PLGA was dissolved in dichloromethane (DCM, Fisher, UK) (200 mg of PLGA was dissolved in 1.5 ml DCM) and then added to the freeze dried powder. The solution was then mixed by vortexing. 4 ml of 0.25% (w/v) methylcellulose (Sigma-Aldrich, UK) solution was then added to the mixture and vortexed again. The resultant emulsion was then poured into 400 ml of distilled water; and the resultant (S/O/W) emulsion was left stirring for 3 h to allow DCM evaporation. The hardened MPs were then collected by centrifugation and washed three times by distilled water (DW). The obtained MPs were then freeze dried for 24 h. Figure 2.2 summarises the S/O/W fabrication method.

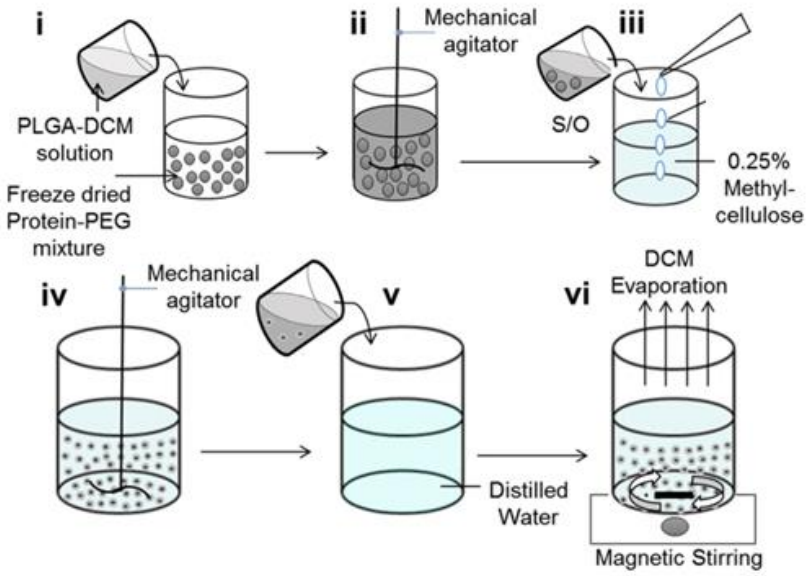


Figure 2.2 Schematic showing the solid-in-oil-in-water emulsion method of PLGA MPs manufacturing.

2.2.3. Microparticles fabrication using W/O/W

This method was adapted from the method previously mentioned by Bible et al. [120]. PVA solution (0.3% (w/v)) was prepared by adding 3 g of PVA to 1 litre of distilled water and stirred overnight. The PVA solution was then filtered through a 0.2 μm filter. 200mg PLGA (LA:GA ratio: 50:50; Mw 52 kDa, Evonik Industries, USA) was weighed into a PTFE jar and 1.5ml of DCM was then added. 1mg protein of protein solution was then added to the PLGA/DCM (100 μl of distilled water was used to prepare blank microparticles). The mixture was then homogenised using the Silverson L5M at 4,000 rpm for 2 minutes. This emulsion was then transferred to 40 ml of 0.3% (w/v) PVA and further homogenised at 9,000 rpm for 2 minutes to produce a secondary emulsion. The solution was then stirred to allow the solvent to evaporate. The hardened MPs were then collected by centrifugation and washed three times by distilled water (DW). The obtained MPs were then freeze dried for 24 h.

2.2.4. Microparticles characterisation

2.2.4.1. Microparticles sizing: laser diffraction

The mean MP diameter and size distribution were measured using a Coulter LS230 particle size analyser (Beckman, UK). MPs were suspended in HPLC grade water, under stirring conditions. Size distribution data was collected after achieving an obscuration value of 8–12%. Three different batches for each condition were analysed. The results represent average of these batches ± SD.

2.2.4.2. Microparticles imaging: scanning electron microscope

A thin layer of MPs were placed onto an adhesive stub and gold coated using a SCD030 gold sputter coater (Balzers Union Ltd., Lichtenstein), for five minutes at 30 mA. The morphology of the MPs was assessed by scanning electron microscopy (SEM), using a JEOL 6060L imaging system (JEOL Ltd., Hertfordshire, UK) with the accelerating voltage set to 10 kV.

2.2.4.3. Measurement of entrapment efficiency

Measurement of protein content in the MPs was conducted as previously described [168, 169] (modified from a technique proposed by Sah [170] and Morita et al. [171]). 10 mg of PLGA MPs were added to 750 µl DMSO and shaken at room temperature for one hour; 2150 µl of 0.02% (w/v) SDS in 0.2 M NaOH was then added and incubated for one hour at room temperature. The Micro BCA protein assay kit was used to measure the total protein content and compared against a freshly generated standard curve of P21-mR-8R. 150 µL sample volume was mixed with 150 µL µ-BCA working reagent and incubated at 37ºC for 2 h. Absorbance at 562 nm was then measured using a plate reader (Infinite M200, Tecan UK Ltd.).

2.2.5. Protein extraction from PLGA microparticles by acetone precipitation

Protein transduction activity was evaluated after the manufacturing process of PLGA MPs. This was done to test the effect of PLGA MPs manufacturing process on protein activity. Known quantity of MPs were vortexed with cold acetone and incubated for 1 h at -20ºC. The solution was then centrifuged at

12,000g for 10 min. The acetone was then removed, and the pellet was allowed to dry from the remaining acetone. Growth media was then added to the protein pellet. The protein activity was evaluated by adding the protein to plated NIH 3t3 cells, as mentioned in Section 2.3.7.

2.2.6. Cell Culture

NIH3T3 mouse fibroblast cells were maintained in Growth Media (GM; DMEM with 10% (v/v) foetal calf serum (FCS; Sigma) media supplemented with 2 mM L-glutamine, 100 units/ml penicillin and 100 lg/ml streptomycin). Cells were maintained in a humidified tissue-culture incubator at 37ºC and with 5% CO2 atmosphere.

2.2.7. GET peptide transduction activity

Protein transduction activity was evaluated using pre-plated NIH 3t3 cells. Briefly, $1X10^5$ cells/well (in 24-well plates) were plated and attached for 4 h, culture media was then replaced with the media containing P21-mR-8R protein samples. After 18 h, cells were washed with PBS, trypsinized and fixed in 4% (w/v) PFA for flow cytometry analysis. Transduction activity term will be referred to as indication of the protein biological activity and ability of internalisation within cells.

2.2.8. Flow cytometry and microscopy

Fixed cells were analysed on a Beckman Coulter Astrios EQ Flow Cytometer using green laser (561 nm). (20,000 cells; gated on live cells by forward/side scatter). Mean fluorescence was used for statistical analyses with background from un-transduced cells subtracted and values were then calculated in ratio to the experimental control. For microscopy, cells were imaged with fluorescence microscope using a TRITC filter (Leica DM IRB).

2.3.Results

2.3.1. Microparticles fabrication using W/O/W and S/O/W methods

2.3.1.1. Protein synthesis and characterisation

The synthesised GET peptide protein (P21-mR-8R) (Figure 2.3A) was collected and ran through SDS-PAGE gel electrophoresis to confirm the size and purity. Figure 2.3B shows representative sample of the prepared P21-mR-8R. the protein molecular weight is expected to be , as previously shown by [172].

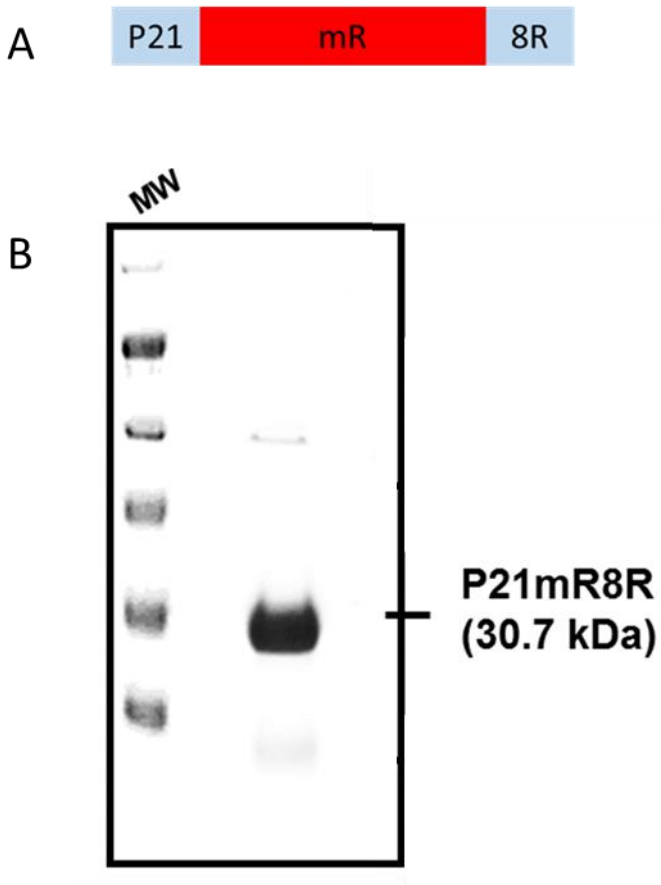


Figure 2.3 Schematic of P21-mR-8R structure (A). P21-mR-8R characterisation through SDS-PAGE gel electrophoresis (B). Protein sample was ran through against ladder to confirm molecular weight.

2.3.1.2. Microparticles size

Initially, blank MPs were fabricated in order to investigate the effect of fabrication method (for both W/O/W and S/O/W) on the resultant MP size. Three batches were fabricated for each method. Size distribution was then assessed using laser diffraction. As it is previously mentioned (section 2.2.2), S/O/W was adopted to remove the homogeniser use, and instead vortexer will be used to create emulsion (this will be discussed later).

The size distribution profiles showed that using the homogeniser, we can achieve small MPs (~30μm), and narrow size distribution profile (W/O/W fabrication method) (figure 2.4). On the other hand, S/O/W method resulted in larger MP size (~45μm) and wider distribution profile (figure 2.4). Taking into consideration that in S/O/W method, vortexer was used to create emulsion (compared to 9000rpm homogeniser in W/O/W), this gives advantage to encapsulate delicate molecules which are sensitive to shear force.

It is know that the difference in surfactant viscosity can influence the fabricated MPs size [173-175]. MPs fabricated using S/O/W method have diameter comparable to the MPs fabricated following W/O/W method although no homogenisation was used. Accordingly, viscosity of both surfactants (0.3% PVA and 0.25% methylcellulose) was studied (figure 2.4). It was shown that viscosity of 0.25% methylcellulose is 50 times higher than 0.3% PVA, which supports that methylcellulose is preventing droplets from fusion, resulting in relatively small diameter MPs.

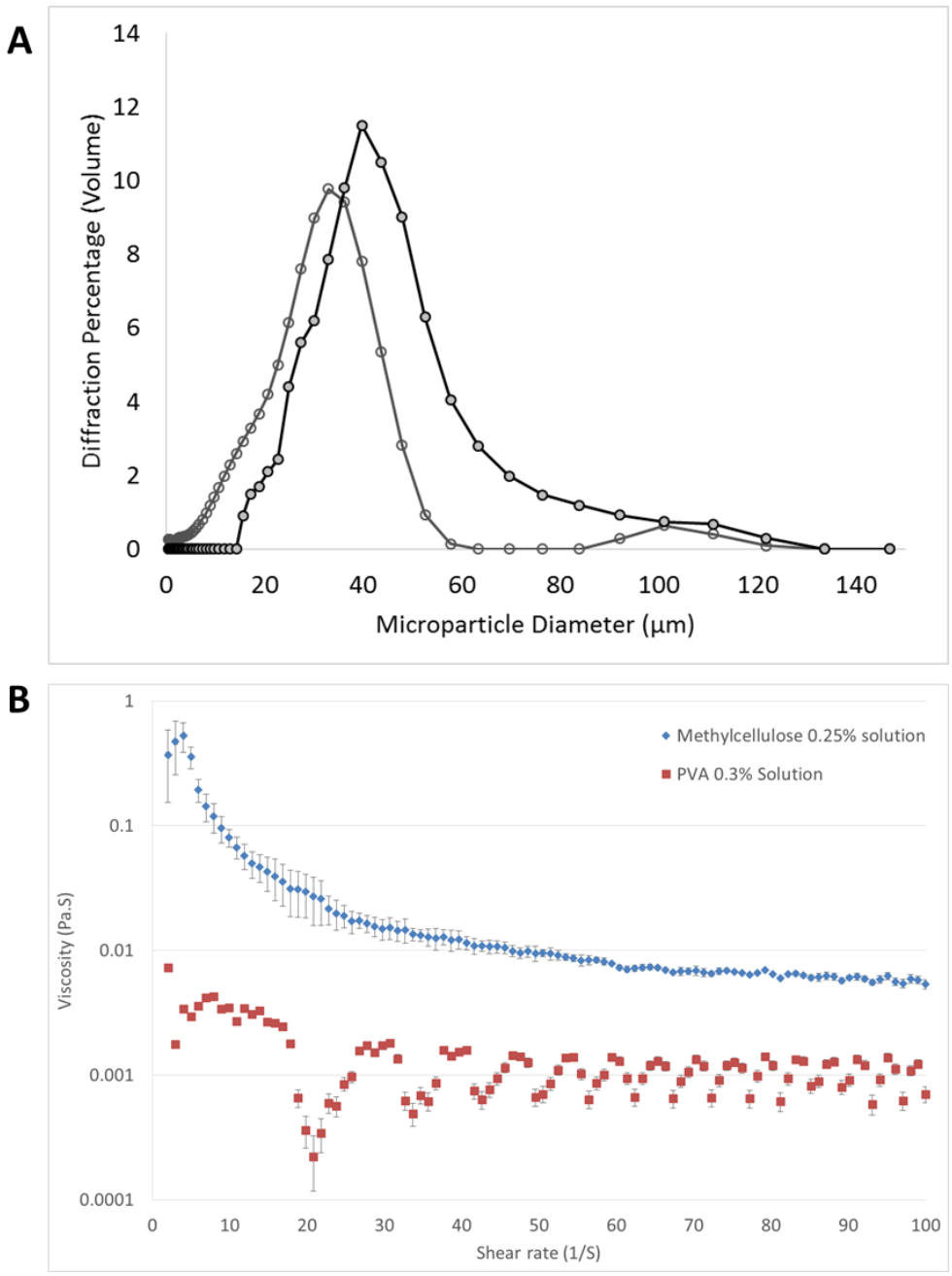


Figure 2.4 (A) MP size distribution comparing MPs manufactured by W/O/W (grey line) and S/O/W (black line). The mean MP size for the W/O/W batch was 31.9± 4.3 µm and for the S/O/W batch 42.5 ± 2.5 µm. (B) 0.25% methylcellulose solution and 0.3% PVA solution viscosity measured at various shear rates at 25°C. Error bars indicate SD (n = 3).

2.3.1.3. Entrapment efficiency

Microparticles were fabricated using the two previously described methods; W/O/W and S/O/W. The microparticles were loaded with P21-mR-8R (self-reporter protein mR tagged with GET peptide P21 and 8R) (Figure 2.5). The loading quantity was 0.5% (w/w) for both methods. The average entrapment efficiency for MPs prepared using W/O/W method was 87.3% (±1.4). On the other hand, the MPs prepared using S/O/W showed lower entrapment efficiency (compared to W/O/W method) with average efficiency of 73.2% (±7.6%). In both methods, the entrapment efficiency is considered feasible for MPs fabrication, however, W/O/W can be considered superior to S/O/W method.

The loaded microparticles size was assessed using laser diffraction method, and compared to blank MPs. No significant size difference could be detected between blank and loaded MPs in both studied fabrication methods, with slight increase in diameter for the loaded MPs compared to the blank MPs (40.3µm vs 31.9µm for the W/O/W MPs and 44.2µm vs 42.5 µm for the S/O/W MPs). Figure 2.5 summarises the size distribution profile.

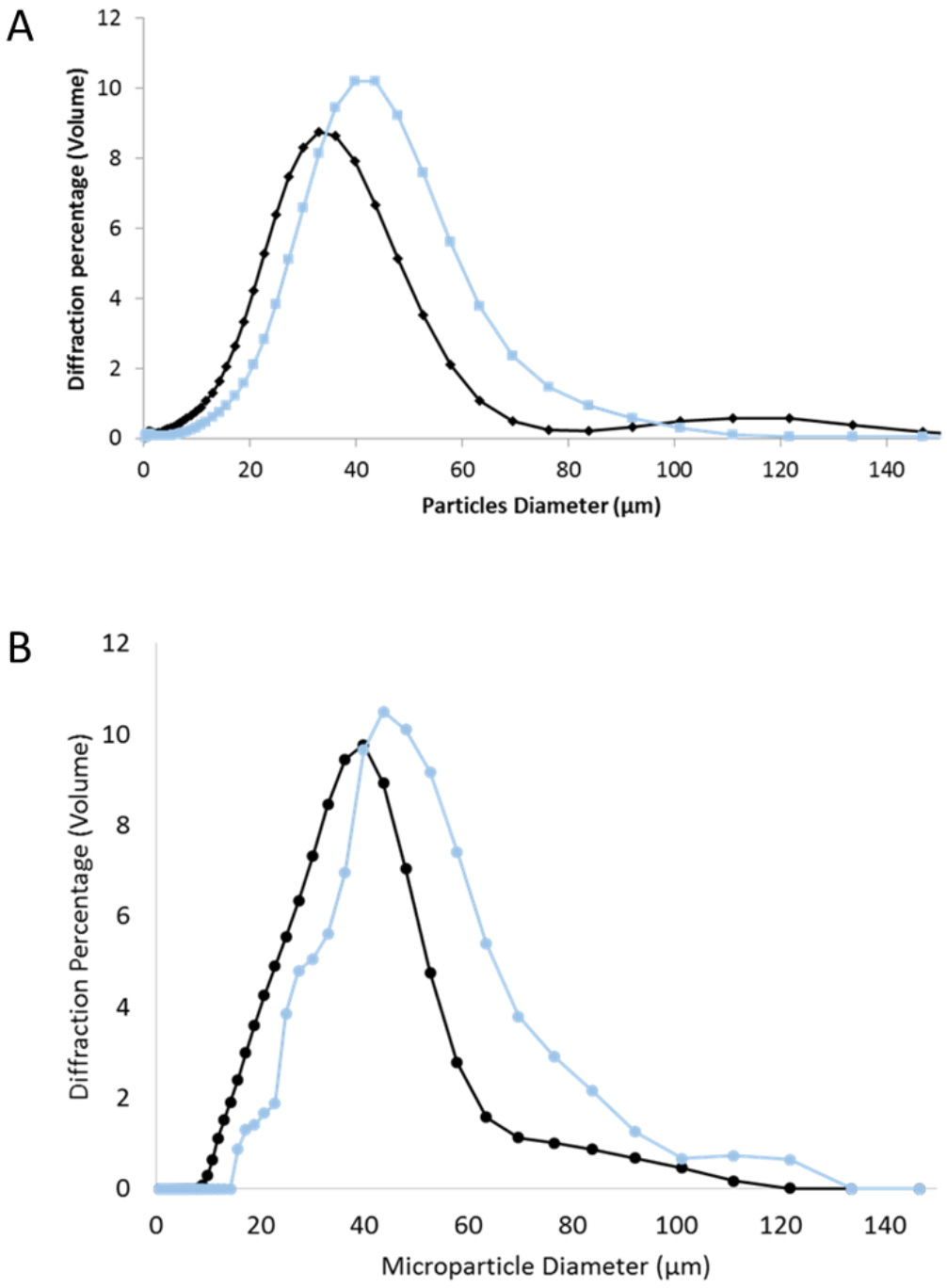


Figure 2.5 Size distribution of MPs manufactured by W/O/W (A) and by S/O/W (B). Black line is blank MPs and blue line is P21-mR-8R loaded MPs (0.5% w/w).

2.3.1.4. Microparticles morphology

The two methods of MP fabrication were investigated (W/O/W and S/O/W). It was important to ensure that the resultant MPs have spherical morphology indicating that a stable emulsion had been formed, and to determine whether there were any surface pores on the MPs which may affect the outcome of future protein release studies. Accordingly, blank and loaded MPs were imaged using SEM.

Figure 2.6 shows the morphology of the blank MPs fabricated by the two methods. In both methods, SEM showed very few surface pores and exhibit a smooth surface for blank MPs. On the other hand, loaded MPs prepared using W/O/W showed some pores on the surface (figure 2.7), which may be attributed to the salt content of the protein solution. Although protein de-saltation was done, the pores still there. A study was done to compare MPs porosity with different buffers (ammonium bicarbonate, PBS and tris-buffer), ammonium bicarbonate showed the lowest porosity among the buffers. No further optimisation was done at this stage as the fabrication method was dropped later. Loaded MPs prepared using S/O/W method showed smooth spherical surface with no pores (figure 2.7).

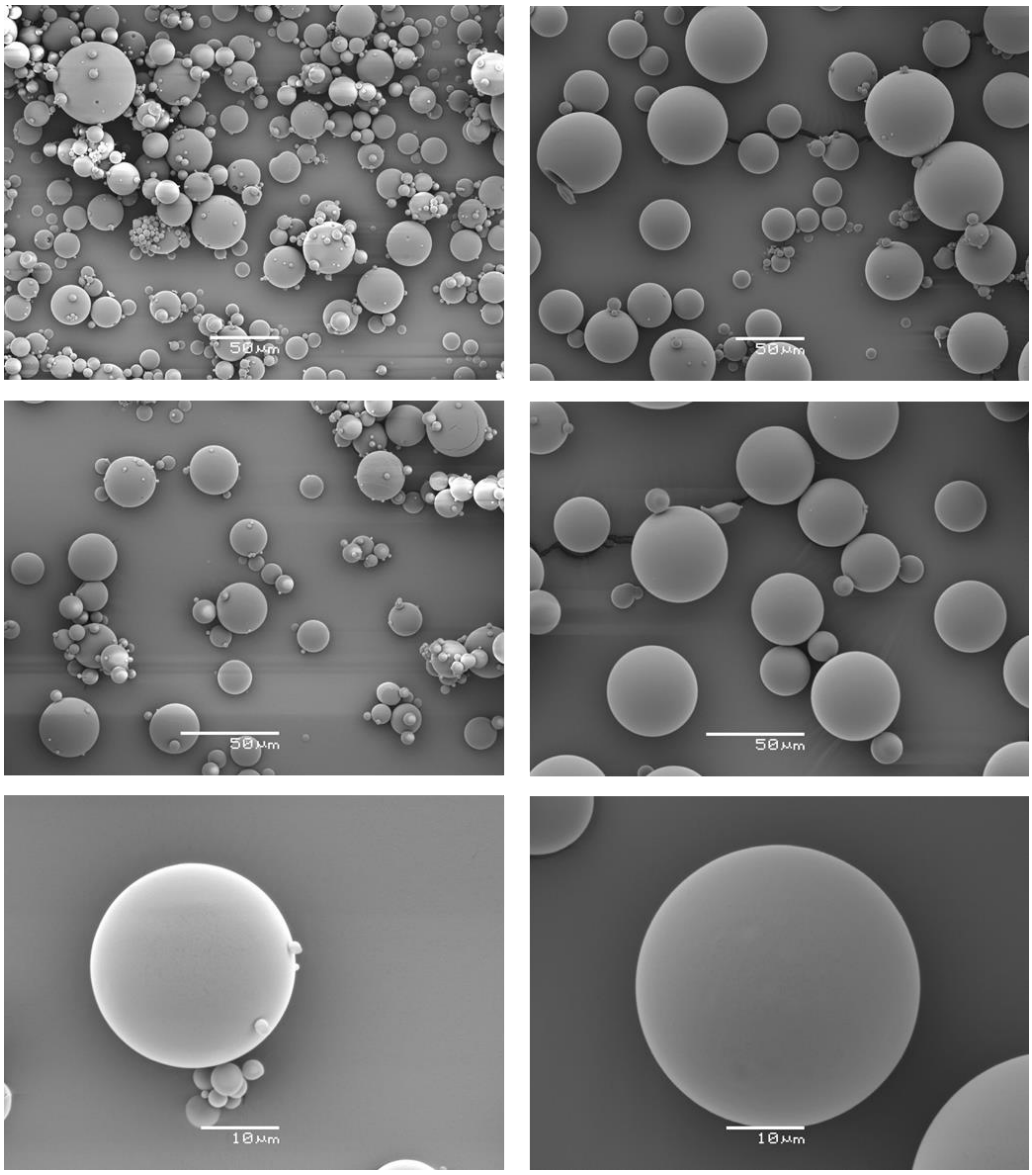


Figure 2.6 Scanning electron images comparing blank PLGA MPs manufactured by the W/O/W emulsion method (left) and the S/O/W emulsion method (right). Scale bars are as indicated.

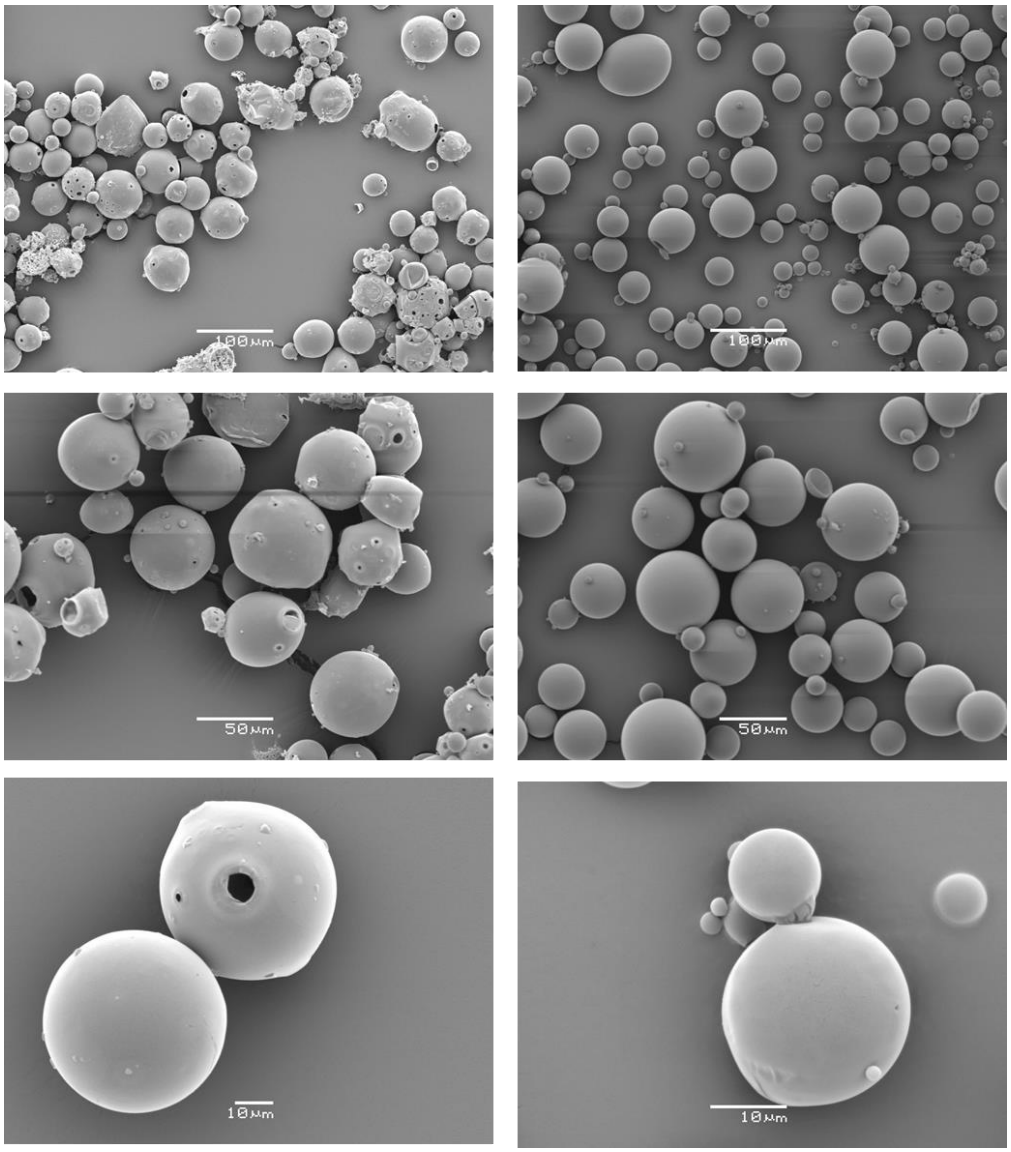


Figure 2.7 Scanning electron images comparing P21-mR-8R loaded PLGA MPs manufactured by the W/O/W emulsion method (left) and the S/O/W emulsion method (right). Scale bars are as indicated.

2.3.2. Protein activity upon extraction from microparticles produced by W/O/W and S/O/W

The main aim for the work presented in this chapter was to develop a PLGA microparticles fabrication method that does not affect protein activity upon encapsulation inside the MPs. After showing that we were able to fabricate PLGA MPs using two different methods, and load GET peptide (tagged with a self-reporter protein) with high efficiency, it was critical to show that the encapsulated protein still have the activity.

In order to validate protein activity after encapsulation inside PLGA MPs (prepared using the two mentioned methods; W/O/W and S/O/W), the GET peptide tagged protein (P21-mR-8R) was extracted from PLGA MPs using cold acetone extraction method, after that, the protein was quantified and the activity was tested on plated NIH 3t3 cells. Protein activity was compared to fresh non encapsulated protein (diluted to the same concentration).

Incubated cells were then evaluated for transduction by fluorescence microscopy and flow cytometry analyses.

Fluorescent microscopy showed significant GET protein internalization for samples extracted from MPs prepared using S/O/W, with relative transduction activity of 89.9 % (±3.3%) (Figure 2.8). On the other hand, samples extracted from MPs prepared using W/O/W showed limited protein internalization and relative transduction activity of 24.5% (±3.9%) (Figure 2.8).

It was a very important finding that the protein lost its transduction activity upon encapsulation inside PLGA MPs using W/O/W, but not the S/O/W. The W/O/W method exposes the protein to a water-organic interface and high shear stress to create emulsion, which can be considered harsh for GET peptide. On the hand,

protein was exposed to organic solvent (DCM) and PLGA polymer in both fabrication methods, however, the protein maintained its activity for MPs prepared using S/O/W, it was thought that it is less likely that DCM or PLGA polymer would affect the protein activity, at least during encapsulation,

Accordingly, GET peptide stability upon exposure to shear stress was studied, to understand their behaviour upon encapsulation using W/O/W.

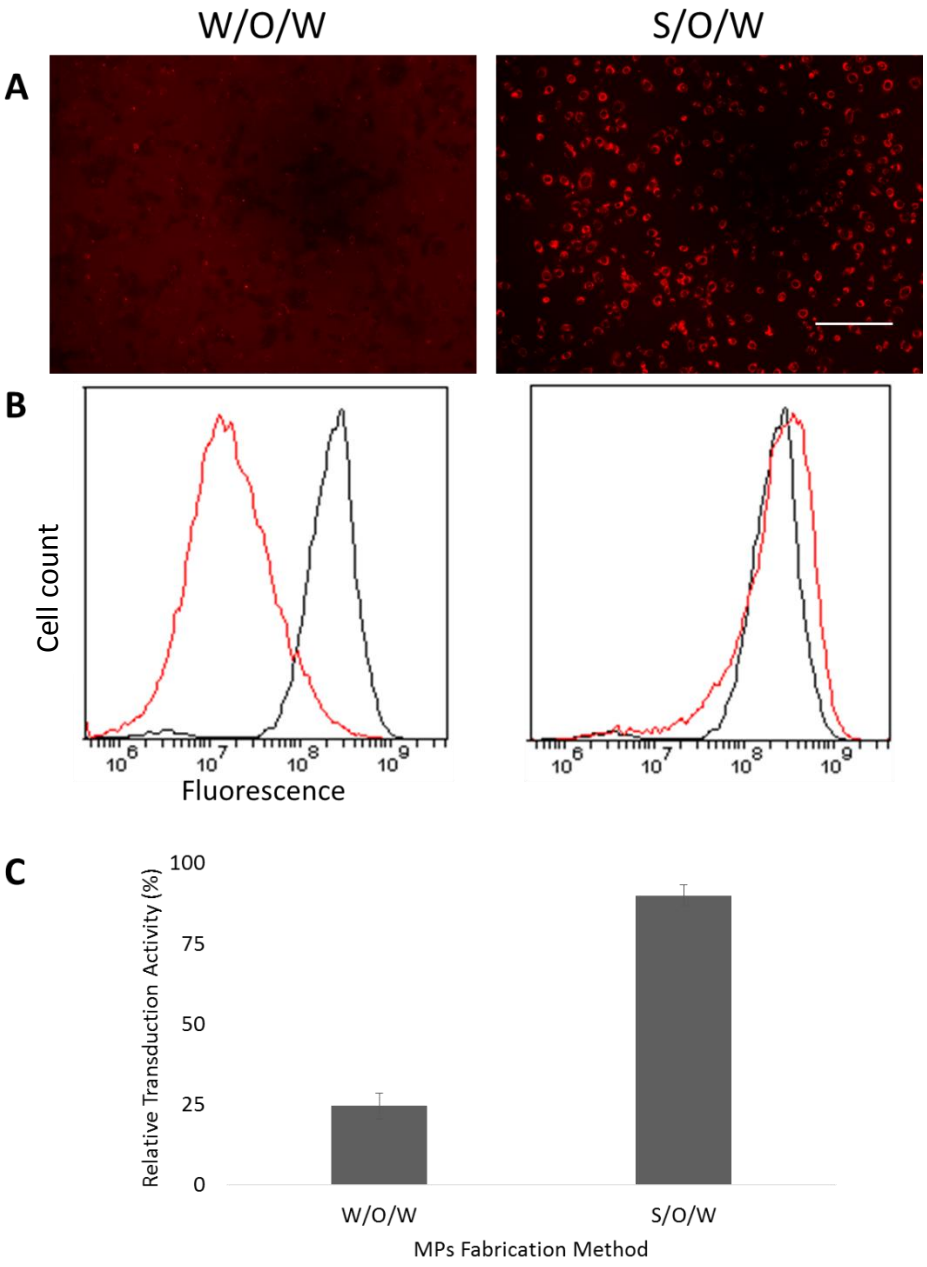


Figure 2.8 P21-mR-8R activity after extraction from PLGA MPs prepared using W/O/W and S/O/W methods. Protein was quantified and added to pre-plated NIH3t3 cells. Protein transduction activity was evaluated. (A) Fluorescence microscopy images of the NIH3t3 cells treated with the sampled P21-mR-8R (Scale bar 10 μm). (B) Flow cytometry histograms showing cellular uptake of P21-mR-8R after application of the samples to NIH3t3 cells. The red histograms are the P21-mR-8R samples, while the black histograms are the experimental control. (C) Relative biological activity of the sampled P21-mR-8R. Protein transduction activity was compared to the experiment control. Error bars indicate SD (n = 3).

2.3.3. Protein stability at shear stress

In order to assess GET tagged protein stability upon exposure to homogenisation, protein solution samples were exposed to various homogenization speeds (2000 rpm, 4000 rpm and 9000 rpm), mimicking the PLGA MPs fabrication conditions (for W/O/W method). After that, the protein was incubated with plated NIH3t3 cells to evaluate its transduction activity. Incubated cells were then evaluated for transduction by fluorescence microscopy and flow cytometry analyses. Protein samples were compared to non-homogenized protein.

Fluorescent microscopy showed significant GET protein internalization for samples homogenized at 2000rpm with relative transduction activity of 90.9% (±7.5%) (Figure 2.9). On the other hand, samples homogenized at 4000rpm and 9000rpm showed very low GET protein internalisation, with relative transduction activity of 10.4% (±1.6%) and 13.1% (±5.2%) respectively (Figure 2.9). This finding demonstrates that the protein is losing its activity upon exposure to high shear force (i.e. above 2000 rpm homogenization speed) which may justify loss of activity for P21-mR-8R encapsulated inside PLGA MPs using W/O/W method. Inactivation due to shear force has been reported in literature before [167, 176]. The suggested approaches to protect protein were to reduce homogenization time, minimize exposure to shear or use other homogenization method [167].

In order to confirm that homogenization is affecting protein activity upon encapsulation, PLGA MPs were prepared using W/O/W but without application of any homogenization force, the emulsions were created by low vortexing speed, to minimise harsh conditions. The PLGA MPs were then characterised

and GET protein was then extracted from them, and the transduction activity was evaluated as previously mentioned (Figure 2.10).

Interestingly, fluorescent microscopy showed significant GET protein internalization with relative transduction activity of 87.0% (±12.8%) (Figure 2.10). This finding demonstrates that the homogenization is affecting GET peptide activity and W/O/W method in its current procedure cannot be used to encapsulate GET peptide.

The current results suggested that the GET peptide part (P21 and 8R) is affected by homogenisation as the fluorescent part of the protein (mR) could be detected upon protein quantification (using fluorometric analysis), however once applied on cells, no transduction activity could be noticed. No further characterisation was carried out (i.e. check if GET peptide were detached from mR protein or lost their functions) as the fabrication method dropped at this stage.

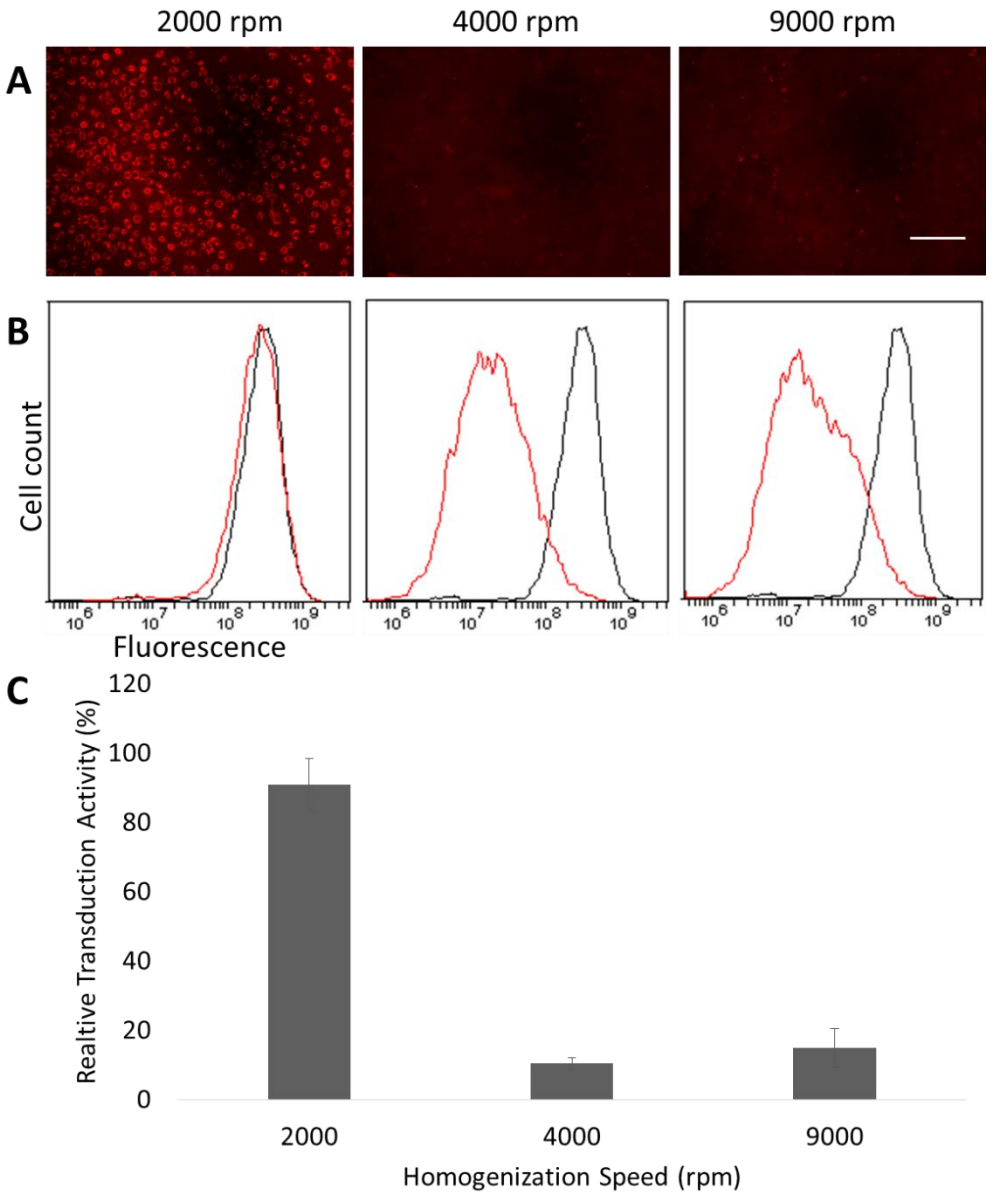


Figure 2.9 P21-mR-8R activity upon exposure to various homogenisation speeds. P21-mR-8R was then added to pre-plated NIH3t3 cells. P21-mR-8R transduction activity was evaluated. (A) Fluorescence microscopy images of the NIH3t3 cells treated with the sampled P21-mR-8R (Scale bar 10µm). (B) Flow cytometry histograms showing cellular uptake of P21-mR-8R after application of the samples to NIH3t3 cells. The red histograms are the P21-mR-8R samples, while the black histograms are the experimental control. (C) Relative biological activity of the sampled P21-mR-8R. Protein transduction activity was compared to the experiment control. Error bars indicate SD (n = 3).

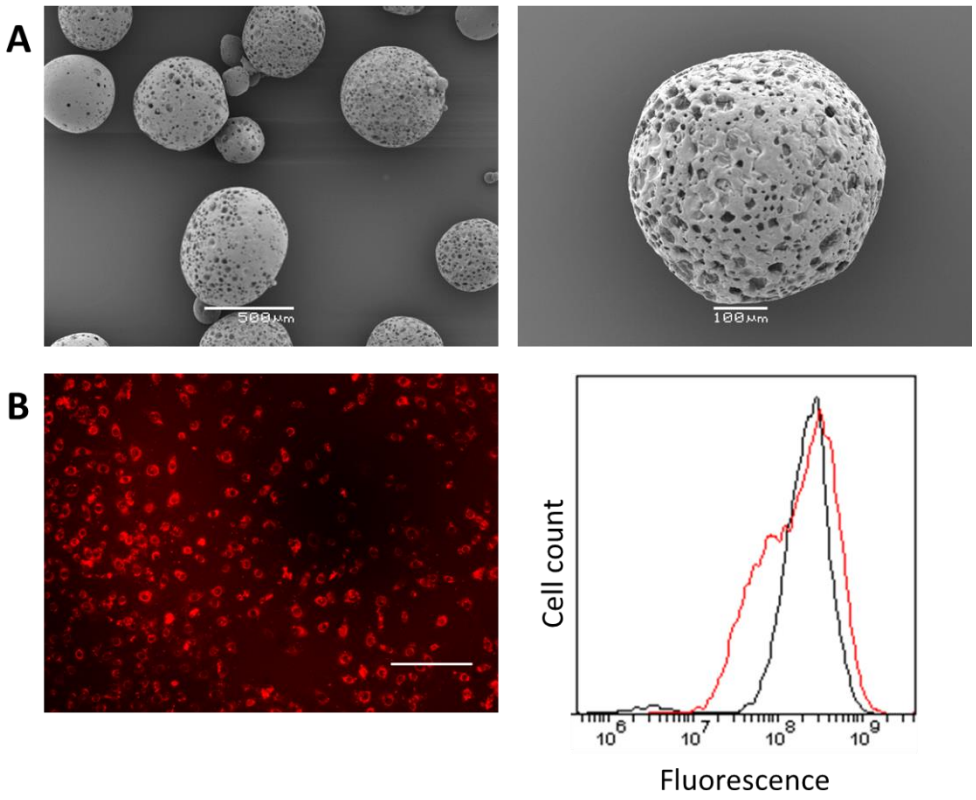


Figure 2.10 PLGA MPs characterisation upon preparation using W/O/W method without homogenisation and activity of P21-mR-8R extracted from these microparticles. (A) SEM analyses for prepared MPs (scale bars as indicated). (B) Fluorescence microscopy images of the NIH3t3 cells treated with the sampled P21-mR-8R (Scale bar 10 μm) (Left) and flow cytometry histograms showing cellular uptake of P21-mR-8R after application of the samples to NIH3t3 cells (right). The red histograms are the P21-mR-8R samples, while the black histograms are the experimental control.

2.4. Discussion

PLGA MPs were prepared using two fabrication methods, W/O/W and S/O/W. Homogeniser was used to create emulsion for the MPs prepared using W/O/W, on the other hand, vortexing (low shear stress) was used to create MPs using S/O/W. Interestingly, the resultant MPs (fabricated using both methods) showed similar size distribution range, although high homogenisation speed were used for the W/O/W method, but not in the S/O/W method. This can be attributed to the different excipient (surfactant) used in the two mentioned methods. Polyvinyl Alcohol (PVA) was used as surfactant in the W/O/W while methylcellulose was used in the S/O/W method. It was shown that surfactant type can influence the produced particle size [173-175]. Difference in viscosity between methylcellulose solution and PVA solution can justify getting small MPs size (figure 2.4). The high viscosity may prevent droplets from fusion or aggregates. Another advantage of the S/O/W method was having smooth surface of the MPs, without pores, compared to MPs obtained from W/O/W. encapsulating the protein in the solid form helped removing the salt leach from the MPs (which help creating pores on the surface). On the other hand, MPs prepare using W/O/W showed smaller MPs size (compared to the MPs prepare using S/O/W method), which can be of superior advantage to match the needed release profile for RUNX2 (i.e. fast release within 7 days).

Protein encapsulation efficiency was comparable between the two followed methods, with feasible values (i.e. above 70.0%). The limiting factor to choose a fabrication method will be the characteristics of the encapsulated protein and it's stability during the applied fabrication process.

Upon protein extraction from the fabricated PLGA MPs, the activity of the protein was tested. It was important to extract the protein from the MPs rather than release it, to study the effect of the fabrication method on the protein activity eliminating the effect of the release environment on the protein (i.e. acidic microclimate upon PLGA degradation).

After testing the transduction activity of the extracted protein, it was concluded that the homogenisation is affecting the GET peptide activity, this was confirmed by homogenising the protein solution itself (eliminating the effect of PLGA, DCM and PVA) at various speeds. It was clearly shown that increasing the homogenisation speed will result in inactive GET peptide. Further confirmation was done by preparing P21-mR-8R loaded PLGA MPs following W/O/W but without application of homogenisation. The extracted protein showed transduction activity comparable to the experimental control, confirming the homogenisation effect on the GET peptide. Homogenisation was previously reported to affect protein activity [167, 177-179], it can be attribute to either GET peptide degradation or detachment from the reporter protein. The MPs prepared using W/O/W method without application of homogenisation showed active protein, however, the MPs size is considered a limitation to proceed with this method as the aim is to prepare MPs in the size of below 50μm to allow 3D printing.

A robust method to prepare GET peptide loaded PLGA MPs was optimised using S/O/W approach. GET peptide activity post encapsulation was shown to be comparable to fresh samples, indicating GET peptide stability throughout the fabrication process. The prepared MPs can be used for further studies.

2.5. Conclusions

This Chapter has highlighted two methods to create PLGA MPs; W/O/W and S/O/W. These two methods were evaluated for MPs size distribution, morphology and protein entrapment efficiency. Moreover, the potential manufacturing parameters that may affect the GET peptide activity upon encapsulation in PLGA MPs were tested.

High encapsulation efficiency was achieved in both described methods. Smaller MPs size could be achieved using W/O/W, which is beneficial to our targeted release profile, however, upon validating GET protein activity after encapsulation, it was clear that shear stress is affecting protein activity and homogenizer can't be used to create PLGA MPs. Accordingly, the adopted S/O/W fabrication method was preferred to prepare GET protein encapsulated PLGA MPs.

The aim of this chapter was to develop a robust method to fabricate PLGA MPs, without affecting GET protein activity, which can be used for further studies and applications. The S/O/W MPs fabrication technique will be used to make MPs for future studies to determine the release profile over time and optimise the formulation in attempt to tailor the release profile to match the needed therapeutic dose for the transcription factor RUNX2.

Chapter III:

Control of Protein Delivery and Bioactivity Assessment of Released GET peptide

3. Control of protein delivery and bioactivity assessment of released GET peptide

3.1. Introduction

The previous chapter described the development and optimisation of a process to produce PLGA microparticles (MPs) in defined size ranges. In addition, the MPs were successfully loaded with GET peptide (tagged with a reporter protein). Moreover, some of the potential causes of GET peptide degradation resulting from entrapment into MPs were studied. One of the main causes is the shear force (i.e. homogenisation) present during emulsification. The process was optimised to specifically address this. This included optimisation of a fabrication method without need of high shear force (i.e. applying minimum vortexing agitation for emulsification). Moreover, in order to remove the risk of GET peptide denaturation at water-organic interface, protein was encapsulated in the solid form, utilising a solid in oil in water emulsion method.

This chapter will utilise the developed MPs manufacturing method to study the release profile of GET peptide from the fabricated PLGA MPs utilising in-vitro release assays and attempt to accelerate the protein release from the microparticles, matching the needed dose for a therapeutic molecule (RUNX2) that will be used later in this work.

It was previously shown that protein release from PLGA is a tri-phasic profile [180]. This involves two mechanisms; diffusion and erosion. The three phases can be defined as an initial burst release followed by a lag phase and then a second phase of release. In the burst and lag phase, protein release is mainly due to diffusion through a network of water filled channels. The burst is caused by the rapid diffusion of surface and near surface protein. The lag phase continues

until erosion of the polymer matrix by hydrolysis occurs releasing more of the entrapped protein from the structure.

Polymer type, loading quantity, size and porosity of the microparticles are highlighted as main roles affecting release mechanisms [181]. A study investigated altering MP fabrication procedures to modify internal morphology to change the release kinetics was done by Mao et. al. [182].

The strategy proposed in this chapter, to accelerate GET peptide release, was to make porous PLGA MPs by incorporating a porogen (such as PBS) at the point of MP fabrication. PBS was previously shown to produce porous microparticles [183] and pore size can be modulated through an additional EtOH - NaOH treatment.

Encapsulated GET peptide will be exposed to physiological temperature and, once the polymer hydrates, will be exposed to water and a pH drop [86, 184]. At this stage the protein is more susceptible to hydrolysis or degradation due to acidic conditions. Moreover, as the pH continues to drop, the risk of interaction between the negatively charged carboxylic acid (resulting from PLGA degradation) and the positively charged GET peptide is increasing. In order to validate the robustness of PLGA MPs as a delivery system of GET peptide, the activity of GET peptide post-release has to be guaranteed.

In order to overcome local acidity limitation, many groups studied pH neutralization in the PLGA microenvironment [86, 133-135]. Various low soluble basic salts were studied, such as magnesium hydroxide [135] and Poly-L-Histidine coupled with PEG [86]. The use of these excipients resulted in neutralized acidic microenvironment within the PLGA MPs system. Proteins may interact with the degradation products of the polymer; PLGA degrades

through an acid-catalysed hydrolysis and produces carboxylic acid molecules which can interact with cationic molecules. Electrostatic and hydrophobic interactions are also common factors for protein–polymer complexation [136-138].

Assessment of GET peptide activity post release was carried out using a fluorescently labelled GET peptide (red fluorescent protein; mR). Evaluation involved releasing P21-mR-8R in-vitro (in cell culture media) and collect the supernatant and quantify it, then measure the cellular uptake of the released P21-mR-8R and compare it to equivalent fresh quantities.

3.1.1. Aims

The purpose of the work presented in this chapter was to modulate the release profile of GET peptide to match the required does for the potential transcription factor to be used (RUNX2). Also, it was essential to test if the released GET peptide were active, and if not active, attempt to understand the mechanism of loss of activity and find a suitable stabilisation approach for GET peptide, post release.

3.2. Materials and Methods

3.2.1. Porous PLGA microparticles preparation using S/O/W method

Poly (D,L-lactide-co-glycolide, (PLGA) LA:GA ratio: 50:50; Mw 52 kDa, Evonik Industries, USA) MPs were formed using solid-in oil-in-water (S/O/W) emulsion as previously mentioned. Briefly, 1 mg of P21-mR-8R, was mixed with 0.5 mg PEG 6000 (Sigma-Aldrich, UK) and freeze dried overnight. For MPs containing L-Histidine, 0.25 mg L-Histidine (Sigma-Aldrich, UK) was mixed with the P21-mR-8R–PEG solution and then freeze dried. Blank MPs were prepared by freeze drying 0.5 mg PEG 6000 only. PLGA was dissolved in dichloromethane (DCM, Fisher, UK) (200 mg of PLGA was dissolved in 1.5 ml DCM) was added to the freeze dried powder. The solution was then mixed by vortexing. For MPs prepared with phosphate buffered saline (PBS), 200 µL PBS (Gibco, UK) was added to the solution and vortexed to produce homogenous emulsion. 4 ml of 0.25% (w/v) methylcellulose (Sigma-Aldrich, UK) solution was then added to the mixture and vortexed again. The resultant emulsion was then poured into 400 ml of distilled water; and the resultant (S/O/W) emulsion was left stirring for 3 h to allow DCM evaporation. The hardened MPs were then collected by centrifugation and washed three times by distilled water (DW). The obtained MPs were then freeze dried for 24 h.

3.2.2. MP characterization: Size, charge and morphology

A thin layer of MPs were placed onto an adhesive stub and gold coated using a SCD030 gold sputter coater (Balzers Union Ltd., Lichtenstein), for five minutes at 30 mA. The morphology of the MPs was assessed by scanning electron

microscopy (SEM), using a JEOL 6060L imaging system (JEOL Ltd., Hertfordshire, UK) with the accelerating voltage set to 10 kV.

The mean MP diameter and size distribution were measured using a Coulter LS230 particle size analyser (Beckman, UK). MPs were suspended in HPLC grade water, under stirring conditions. Size distribution data was collected after achieving an obscuration value of 8–12%.

The zeta potential of the MPs was measured using NanoZS instrument (Malvern, UK) in PBS buffer of various pH values (3, 5 & 7).

3.2.3. Protein release from PLGA microparticles prepared using S/O/W

Known quantity of MPs were re-suspended in 1 ml Growth media (GM) or HBSS. Samples were rocked on a 3D shaker (Gyrotwister, Fisher Scientific UK Ltd) at 5 rpm in a humidified incubator at 37°C. At defined time points, samples were centrifuged and the supernatant was removed from the MPs and replaced with fresh GM or HBSS. The supernatants were assayed for GET and total protein content using fluorometric analysis for mRFP1 (excitation: 584 nm; emission: 620 nm; GM samples) and mBCA assay kit (HBSS samples). Released protein contents were compared against freshly generated standard curve of P21-mR-8R.

3.2.4. Cell culture

NIH3T3 mouse fibroblast cells were maintained in Growth Media (GM; DMEM with 10% (v/v) foetal calf serum (FCS; Sigma) media supplemented with 2 mM L-glutamine, 100 units/ml penicillin and 100 µg/ml streptomycin). Cells were maintained in a humidified tissue-culture incubator at 37°C and with 5% CO2 atmosphere.

3.2.5. GET peptide stability at various pH conditions

GET peptide stability in different pH conditions was evaluated. The pH of cell culture media was adjusted (pH 3, 5 & 7) using one of the following solutions; 1 M lactic acid, 1 M glycolic acid, 1 M acetic acid, 1 M phosphoric acid, 1 M hydrochloric acid and 1 M sulfuric acid. 200 μg/ml P21-mR-8R (with or without L-Histidine; 200 μg/ml) solution was prepared and incubated at 37°C. At defined time-points, samples were taken and diluted 1:10 in fresh cell culture media to neutralize the sample to pH 7.2. Protein was then transduced into cells by addition to pre-plated NIH3t3 cells.

3.2.6. GET peptide transduction activity assessment

Protein transduction activity was evaluated using pre-plated NIH 3t3 cells. Briefly, 1 X 10^5 cells/well (in 24-well plates) were plated and attached for 4 h, culture media was then replaced with the media containing P21-mR-8R protein (protein released from MPs or protein samples from stability test). After 18 h, cells were washed with PBS, trypsinized and fixed in 4% (w/v) PFA for flow cytometry analysis. Transduction activity term will be referred to as indication of the protein biological activity and ability of internalisation within cells.

3.2.7. GET peptide interaction with blank PLGA microparticles

Known quantity of P21-mR-8R was mixed with blank PLGA MPs, for 30 min at 37°C in 1 ml PBS. The solution was centrifuged (10,000g for 10 min) and the free P21-mR-8R quantity in the supernatant was measured using fluorometric analysis for mRFP1 (excitation: 584 nm; emission: 620 nm).

3.2.8. GET peptide interaction with PLGA degradation product

GET peptide interaction with PLGA degradation products was tested by suspending blank PLGA MPs in media for one week at 37°C. The solution was centrifuged (10,000g for 10 min) to collect PLGA degradation products. The supernatant was mixed with P21-mR-8R and different quantities of L-Histidine (P21-mR-8R: L-Histidine ratios were 1:0, 1:0.1, 1:0.25, 1:0.5 & 1:1). Protein was then transduced into cells by addition to pre-plated NIH3t3 cells.

3.2.9. Flow cytometry and Microscopy

Fixed cells were analysed on a Beckman Coulter Astrios EQ Flow Cytometer using green laser (561 nm). (20,000 cells; gated on live cells by forward/side scatter). Mean fluorescence was used for statistical analyses with background from un-transduced cells subtracted and values were then calculated in ratio to the experimental control. For microscopy, cells were imaged with fluorescence microscope using a TRITC filter (Leica DM IRB).

3.2.10. Statistical analysis

Statistical analysis was carried out using GraphPad Prism (version 6). The statistical significance was determined using one way ANOVA with Sidak post hoc test. Results were considered significant at $p < 0.05$, mean values are given plus or minus the standard deviation (SD).

3.3. Results and Discussion

3.3.1. Protein release from PLGA microparticles prepared using S/O/W

The previous chapter described a method to fabricate PLGA microparticles (S/O/W) with high encapsulation efficiency. The results showed that the encapsulated protein didn't lose the activity during the fabrication process. The mentioned method was used to produce P21-mR-8R loaded PLGA microparticles to examine the release profile. The aim was to release all the protein quantity in 7 days (as required for delivery of RUNX2). Accordingly, release study for P21-mR-8R was carried out. The study was done for 21 days, to ensure complete release. Microparticles characterisation and release study profile are shown in figures 3.1 and 3.2 respectively.

The microparticles showed spherical structure with smooth, non-porous surface. The mean diameter of these MPs was 45.2 ± 9.7 μm, with average loading efficiency of 73.2 ± 7.6%. Protein release was quantified by two methods, biochemically using μBCA assay (spectrophotometry) and intensity of the released mRFP1 fluorescence (fluorometry). MPs showed initial burst release (around 20% ± 4.2 of total loaded) within the first day, with no further detectable protein was released even with a further 21 days of incubation. It is known that after burst release, the protein release depends on the hydrophobic PLGA degradation rate [185]. Another study was performed and showed that the release will continue after day 21 [169]. However, in this project, all the quantity of GET peptide needed to be released in the first week, as the requirement of RUNX2 dose.

Since the needed release profile could not be achieved with the current formula, further formulation optimisation was needed.

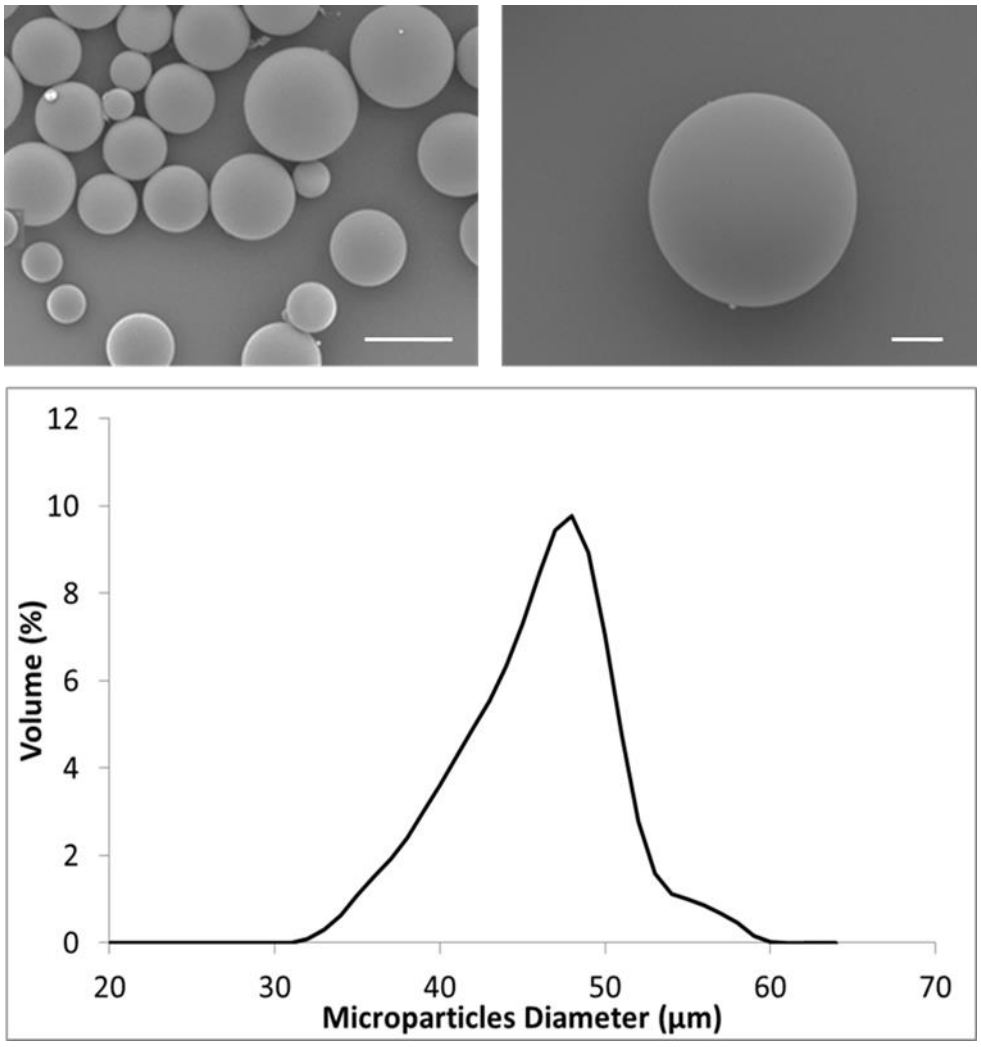


Figure 3.1 MP characterization; SEM and size analyses. MPs were loaded with P21-mR-8R (0.5% (w/w)). SEM analyses for MPs (scale bars represent 50 µm on left image, and 10 µm on right image). Representative size distribution, average of three different loaded PLGA microparticles batches (n=3).

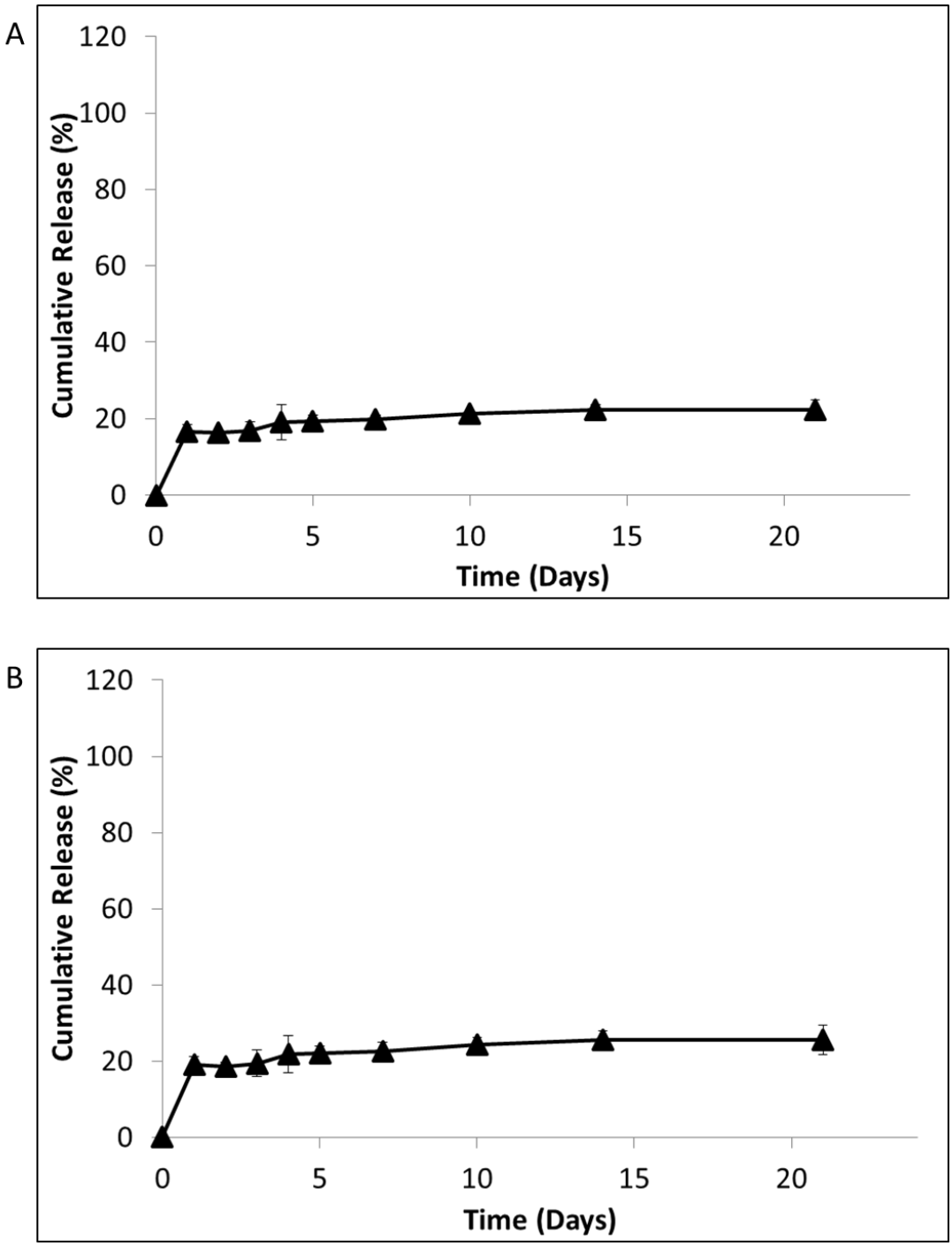


Figure 3.2 In vitro release profiles of P21-mR-8R from PLGA MPs (pH 7.4 at 37°C) MPs were prepared using S/O/W method loaded with P21-mR-8R (0.5% (w/w)). (A) Protein was quantified using Micro BCA assay kit. (B) Protein was quantified using fluorescence intensity. Error bars indicate SD (n = 3).

3.3.2. Acceleration of protein release using porous PLGA microparticles

It was shown that the size and porosity of the microparticles are the main parameters in release mechanisms [181, 186]. Accordingly, changing microparticles porosity was considered to enhance release profile.

PBS is known to be used for porous microparticles fabrication [183]. PBS work as a porogen, which is expected to increase MPs porosity and generate channels within and on the surface of the MPs.

MPs were fabricated with addition of PBS to the primary emulsion, the microparticles morphology, size and encapsulation efficiency were studied and compared to the formulation without PBS. Additionally, the release profile was evaluated.

Spherical structure of microparticles, with some pores on the surface, could be achieved. Pores were seen on most of the fabricated particles using SEM imaging. The prepared MPs diameter was 41.5µm (±10.5), comparable to the non-porous MPs (45.2µm ±9.7) (Figure 3.3). Encapsulation efficiency remained feasible (around 65%) and compared to the previous formulation (73.2% vs. 65.7%). The release profile of the developed formulation was then studied and compared to the previously achieved one (Figure 3.4).

The release profile obtained from MPs with PBS-created pores showed similar burst release (on day 1, 18% ± 3.7) but this level was retained producing a continuous protein release over 5–7 day period. More than 90% ± 7.9, cumulative release, could be achieved after 10 days, after which little further protein was released (Figure 3.4). This finding shows that we have a process to encapsulate GET peptide with high loading efficiency and a formulation that releases the peptides gradually over 10 days' time, matching the needed dose.

The use of porous MPs for protein release has been used previously [187], however it is suggested that the release is dependent on the protein diffusion from MPs rather than bulk PLGA MPs degradation.

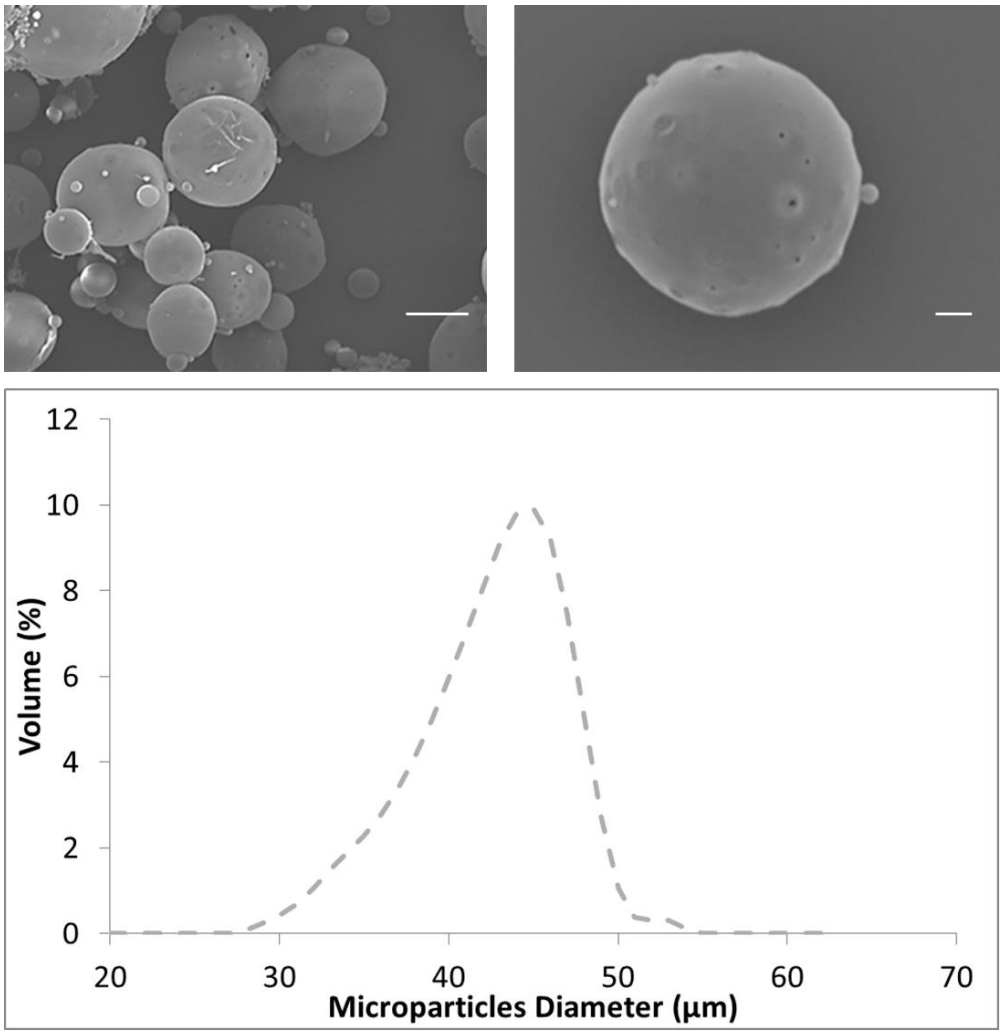


Figure 3.3 MP characterization; SEM and size analyses. MPs were prepared with addition of 200µL PBS to the primary emulsion. MPs were loaded with P21-mR-8R (0.5% (w/w)). SEM analyses for MPs (scale bars represent 50 µm on left image, and 10 µm on right image). Representative size distribution, average of three different loaded PLGA microparticles batches (n=3).

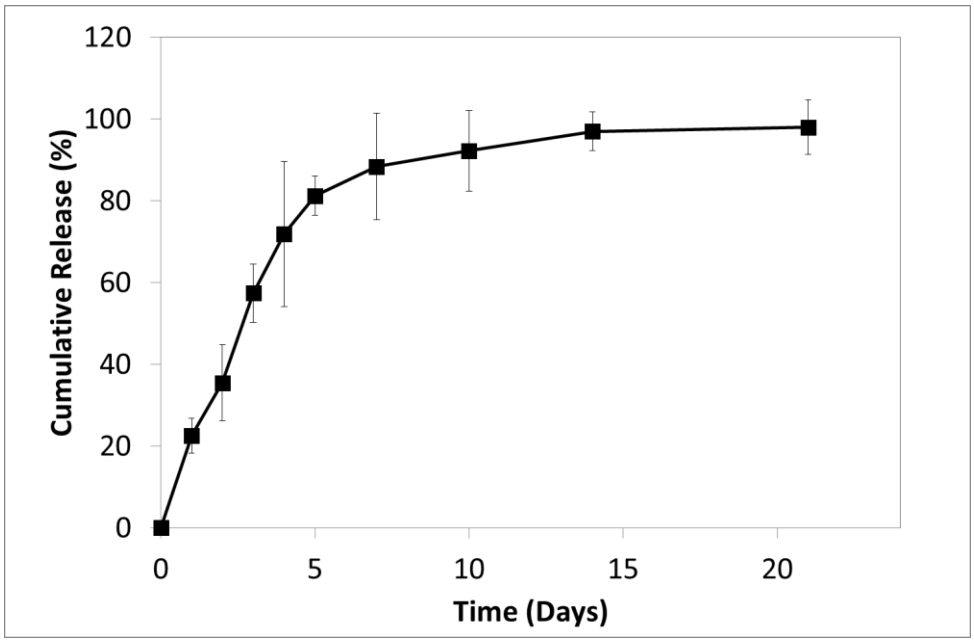


Figure 3.4 In vitro release profiles of P21-mR-8R from PLGA MPs (pH 7.4 at 37°C) MPs were prepared with addition of 200µL PBS to the primary emulsion. MPs were loaded with P21-mR-8R (0.5% (w/w)). Protein was quantified using Micro BCA assay kit. Error bars indicate SD (n = 3).

3.3.3. Released GET peptide transduction activity assessment

Efficient release of GET peptide was achieved utilising S/O/W method to fabricate PLGA porous-MPs, and the required release profile could be obtained. The aim was at this point to show that we have active GET peptide post release. The work in previous chapter demonstrated active GET peptide upon encapsulation, and here the effect of release conditions on GET peptide activity will be studied.

The released GET peptide transduction activity evaluated by comparing released P21-mR-8R to non-encapsulated controls. Released GET-protein (from porous PLGAPBS MPs) was collected over the 7 day time course and was incubated with NIH3t3 cells to assess internalization and transduction ability. Importantly transduction activity was compared to non-encapsulated controls diluted to the same final concentration. Incubated cells were then evaluated for transduction by fluorescence microscopy and flow cytometry analyses.

Fluorescent microscopy showed significant GET protein internalization for samples released from PLGA-PBS MPs in the first day (Figure 3.5). Flow cytometry results showed that the protein released at the first day has a relative transduction activity of 85% ± 12.3 (Figure 3.6). However, GET-protein released from these MPs (PLGA-PBS) showed gradual loss of protein transduction activity with relative transduction activity below 35% ± 4.7 at day 7 (Figure 3.6). Overall, activity of the fully released GET-protein over the 7 days is therefore significantly inhibited (with only 35% ± 4.7 activity could be achieved towards the end of the release profile).

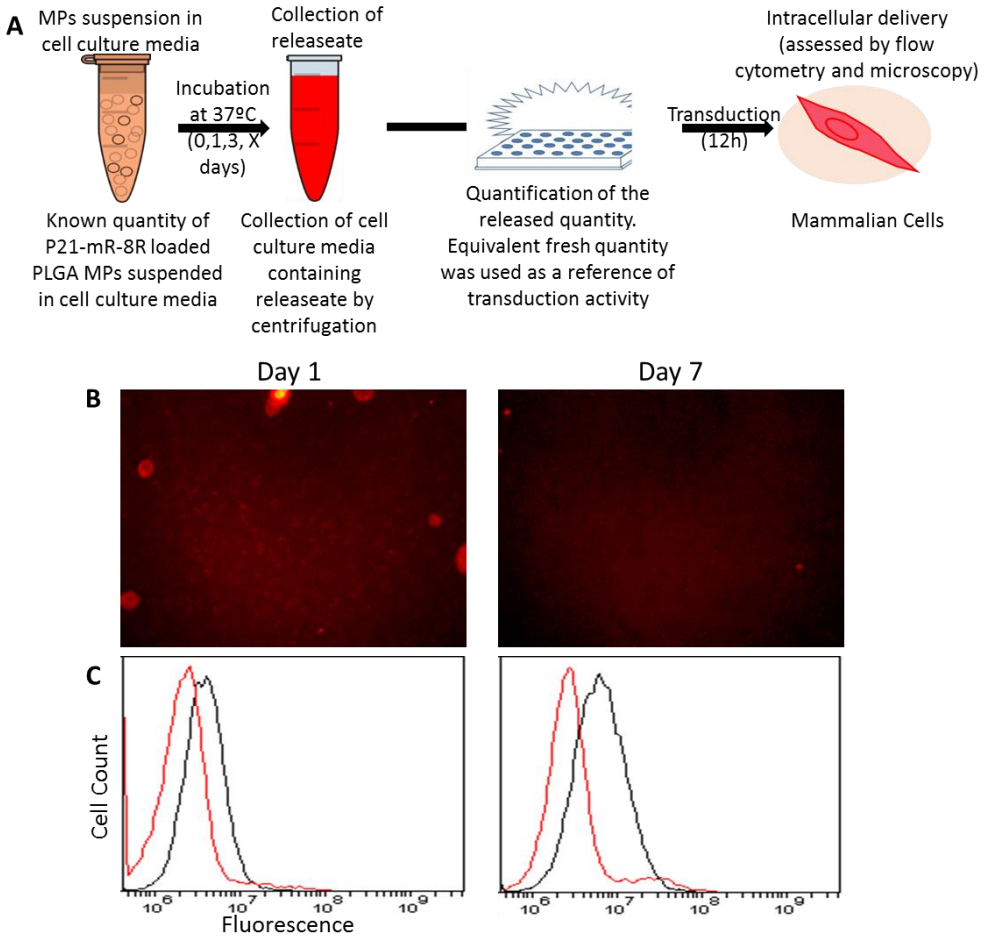


Figure 3.5 Transduction activity of the released P21-mR-8R. MPs were prepared using S/O/W method and loaded with P21-mR-8R (0.5% (w/w)), mixed with PBS. Transduction activity of the released protein was assessed by addition to plated NIH3t3 cells. (A) Schematic showing the sampling of the released protein and quantification. (B) Fluorescence microscopy images of the NIH3t3 cells treated with the sampled P21-mR-8R (Scale bar 10 µm). (C)Flow cytometry histograms showing cellular uptake of P21-mR-8R after application of the samples to NIH3t3 cells. The red histograms are the P21-mR-8R samples, while the black histograms are the experimental control.

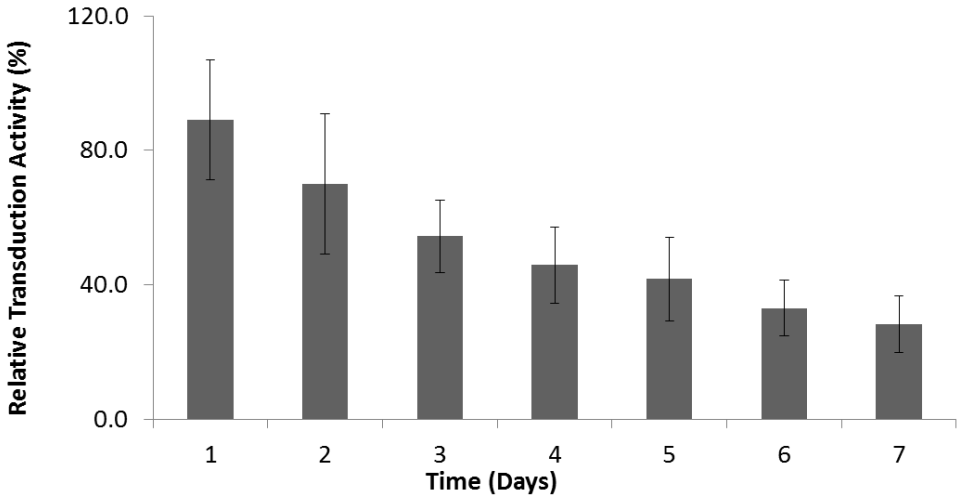


Figure 3.6 Relative biological activity of the sampled P21-mR-8R. GET Protein transduction activity was compared to the experiment control. Error bars indicate SD (n = 3).

3.3.4. Building a hypothesis for GET peptide loss of activity

The released protein could be detected using fluorometric analysis, which suggests that the fluorescent part of the protein (mR) was intact but the GET peptide, enhancing the protein internalization in the cells, were no longer functional. This may be attributed to protein hydrolysis (i.e. detachment of the GET peptide (P21 & 8R) from the fluorescent part (mR)), or interaction between the negatively charged PLGA (or it's degradation product) with the positively charged GET peptide [86, 133-138, 186], which would prevent the interaction between GET peptide and cell membrane heparan sulfate.

This inhibitory phenomenon would restrict the use of GET-protein in this controlled release system and it was needed to further understand the loss of activity mechanism and to optimize the delivery system formula to improve the relative transduction activity of GET protein post release.

3.3.5. Validation of GET peptide loss of activity hypothesis

Loss of protein activity during release can be due to possible interaction between the molecule and PLGA material, it's degradation products, or protein instability in low pH values [86]. Accordingly, and in order to understand the loss of GET peptide activity mechanism, the mentioned possibilities were studied.

3.3.5.1. GET peptide interaction with blank PLGA microparticles

PLGA MPs are negatively charged [188]. In order to confirm this, blank PLGA MP charged was measured at various pH values (3, 5 & 7). The results showed that the PLGA MPs are negatively charged at all studied pH values (Table 3.1). As GET peptide are positively charged [81] (the calculated isoelectric point (pI)

for P21 and 8R is 10.9 and 12.9 respectively (Table 3.2) it is expected that P21-mR-8R interacts with the negatively charged PLGA MPs. In order to evaluate the interaction between the GET peptide and PLGA MPs, direct interaction between P21-mR-8R and PLGA MPs was assessed in a pulldown assay. P21-mR-8R was mixed with various quantities of blank PLGA MPs. After incubation, MPs were removed by centrifugation and the loss of soluble P21-mR-8R (binding to PLGA) was assessed by fluorometry. This assay was designed to determine if there was any direct interaction of P21-mR-8R with intact PLGA polymer. The results demonstrated that at neutral pH less P21-mR-8R protein remains free in the supernatant with increasing MPs quantities (i.e. only 20% of the protein quantity could be detected when mixed with 25 mg of PLGA MPs) indicating that the P21-mR-8R interacts with PLGA polymer in the MPs (Figure 3.7). Many interaction types can be associated in P21-mR-8R binding to PLGA MPs, but the main type to control the interaction, in presence of positively charged peptides, is electrostatic interaction [189]. Hydrophobic interaction might be affecting the adsorption of P21-mR-8R on the surface of PLGA MPs due to the fact that the PLGA is hydrophobic. However this interaction was considered negligible [136, 138, 189].

Table 3.1 Blank MPs surface charge at various pH conditions (3, 5 & 7).

pH	ZP (mV) Average (±SD)
3.0	- 15.6 (1.3)
5.0	-7.9 (1.0)
7.0	-1.0 (0.4)

Table 3.2 P21-mR-8R, mR, P21 & 8R theoretical molecular weights, isoelectric points and charge at various pH values

Peptide	Molecular Weight (kDa)	Isoelectric point (pI)	Charge at various pH										
			3.0	3.5	4.0	4.5	5.0	5.5	6.0	6.5	7.0	7.5	8.0
mR	26.6	5.7	36.1	33.1	26.6	16.4	7.3	2.3	-0.3	-2.2	-3.8	-4.9	-5.7
P21	2.5	10.9	12.5	12.2	11.8	11.5	11.2	11.1	11	11	10.9	10.6	10.2
8R	1.3	12.9	8.6	8.3	8.1	8	8	8	8	8	7.9	7.8	7.5
P21mR8R	30.7	9.6	56.1	53	46.3	35.8	26.5	21.3	18.7	16.7	15.1	14	13

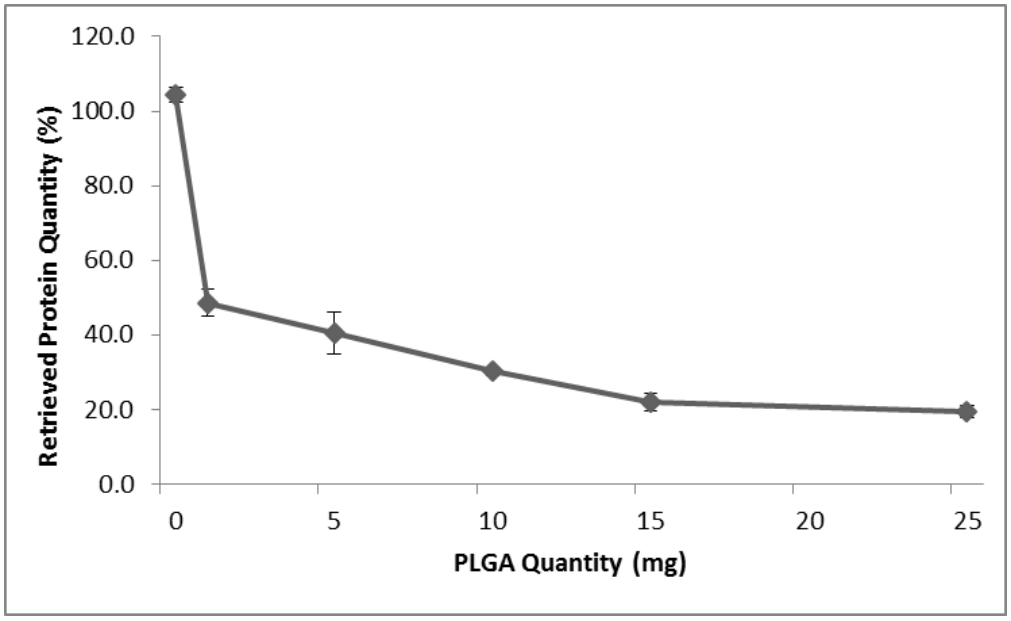


Figure 3.7 GET peptide interaction with blank PLGA MPs at pH 7.4 PLGA MPs were suspended in solution and P21-mR-8R was then added, the solution was then centrifuged and the P21-mR-8R quantity in the supernatant was measured. Error bars indicate SD (n = 3).

It was shown that P21-mR-8R is interacting with PLGA MPs at neutral pH, however, as PLGA degrades it releases lactic and glycolic acid molecules (carboxylic acid containing molecules) which decrease the pH. It's been hypothesized that the interaction between P21-mR-8R and PLGA will be affected by the presence of carboxyl groups. The pull down assay was repeated at lower pH value (~ pH 3) where the pH was adjusted using acetic acid (to create carboxylic acid rich environment). Interestingly, at pH 3, all the protein remained in the supernatant, and there was no significant interaction with the PLGA MPs (Figure 3.8). This was unexpected as it's been hypothesized that in a low pH microenvironment (which would be similar to that generated in hydrolysing PLGA during the release process) that P21-mR-8R would still interact with PLGA polymers, as the results suggested that the PLGA will be negatively charged at this pH (Table 3.1). This observation was important, demonstrating that P21-mR-8R can directly interact with PLGA, but that this can be disrupted by the presence of carboxylic acid. We therefore conclude that P21-mR-8R can interact with both PLGA directly (most likely electrostatically) and also with carboxylic groups (which can disrupt the PLGA interaction).

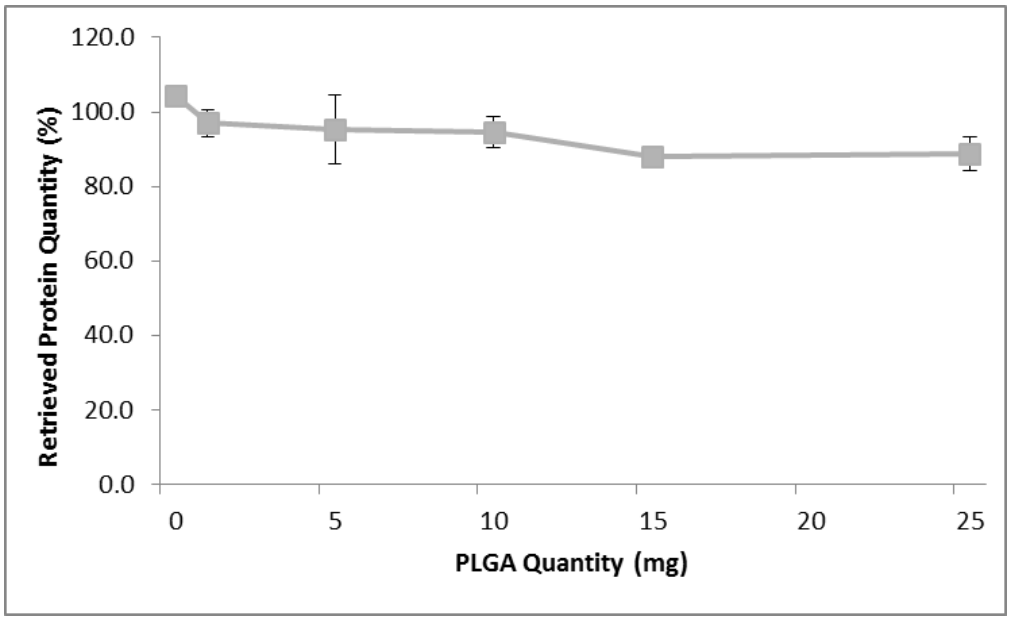


Figure 3.8 GET peptide interaction with blank PLGA MPs at pH 3. PLGA MPs were suspended in solution of pH 3 and P21-mR-8R was then added, the solution was then centrifuged and the P21-mR-8R quantity in the supernatant was measured. Error bars indicate SD (n = 3).

3.3.5.2. GET peptide activity in presence of PLGA degradation products

It's been identified that the controlled release (i.e. PLGA degradation) as the inhibitory process on GET transduction activity. The aim was to assess any possible interaction between the GET peptide and the PLGA degradation products and its impact on GET peptide transduction activity. When PLGA degrades by hydrolysis, it releases carboxyl group containing molecules which may interfere with GET transduction activity. Accordingly, the GET peptide activity in presence of PLGA degradation products, collected from PLGA degradation in media, was studied. The pH of the media upon GET peptide addition was 6.0 ± 0.2. Fluorescence microscopy showed that there was very low transduction activity for P21-mR-8R added to cells with degraded PLGA supernatants (Figure 3.9), flow cytometry showing a relative transduction activity of 34% ± 8.9. This data therefore confirms that during controlled release, PLGA degradation products will have an inhibitory effect of GET protein transduction activity.

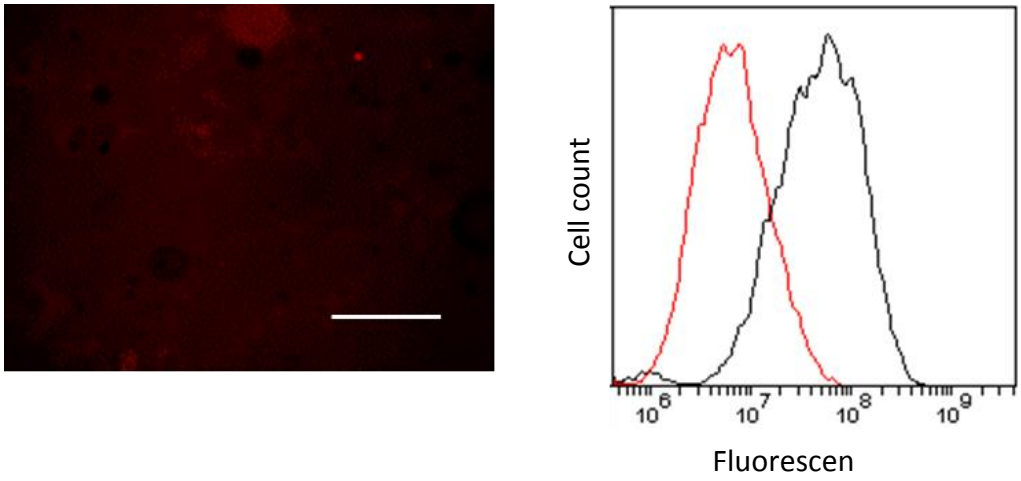


Figure 3.9 Effect of PLGA degradants containing media on GET peptide stability. Blank PLGA MPs were left to degrade in media, after that P21-mR-8R was mixed with the media. Protein was then transduced into cells by addition to plated NIH3t3 cells. Fluorescence microscopy images of the NIH3t3 cells treated with the sampled P21-mR-8R (left) (Scale bar 10μm) and flow cytometry histograms showing cellular uptake of P21-mR-8R after application of the samples to NIH3t3 cells (right). The red histograms represent P21-mR-8R samples while black histograms are the experiment control.

3.3.5.3. GET peptide stability in various pH conditions simulating PLGA MP Microenvironment

3.3.5.3.1. GET peptide activity in presence of carboxylic acid groups

In order to fully understand the mechanism by which GET protein transduction activity is inhibited post-release, it was aimed to model the conditions experienced by the P21-mR-8R protein inside the MPs without the fabrication. During protein release the degrading PLGA is hydrolysed, releasing glycolic and lactic acid (carboxyl group containing molecules) into the microenvironment and it is progressively acidified. It has been previously shown that the pH microclimate within PLGA MPs can be very acidic (pH ~2) [86, 125]. To test the effect of such acid groups and the overall pH have on retention of GET-transduction activity, P21-mR-8R was incubated in cell culture media of various pH values (3, 5 & 7), pH adjusted using either 1 M lactic acid, 1 M glycolic acid or 1 M acetic acid solutions. After incubation, samples were neutralized by dilution and protein transduction activity was evaluated, using NIH 3t3 cells (fluorescence microscopy and flow cytometry). The neutralization process is important as all proteins were transduced into cells at the same neutral pH (pH 7.2), therefore this directly assesses the effect of pH during the incubation, with transduction as a readout of functionality. Protein storage, sampling and transduction into cells were done as diagrammed in Figure 3.10. Fluorescence microscopy showed significant protein internalization, for samples stored at pH 3, at day 1 compared to controls, however, protein transduction was undetectable for day 7 samples. This can be seen in samples of all studied solutions; lactic acid, glycolic acid and acetic acid. Flow cytometry results confirmed a loss in

transduction for day 7 samples (Figures 3.11, 3.12 and 3.13), and gradual loss of relative transduction activity over the time-points, reaching values below 30% at day 7. Interestingly, fluorescent microscopy showed protein transduction for samples stored at pH 5 & 7 at all studied time points. For pH 5, flow cytometry results confirmed this with relative transduction activity above 80% of non-treated controls at all studied time points. For pH 7, flow cytometry results showed minimal decrease in relative transduction activity with values of 60% at all studied time points. Importantly both pH 5 and 7 data shows high levels of activity is retained, even with extended storage (7 days). This is unlike activity seen at pH 3 samples which is progressively decreased until very low levels are left at day 7 (~ 25%). Therefore high concentration carboxylic acid inhibits the activity of GET transduction over time. Importantly this is not due to stability of the protein as fluorescence of the P21-mR-8R was not affected by these conditions.

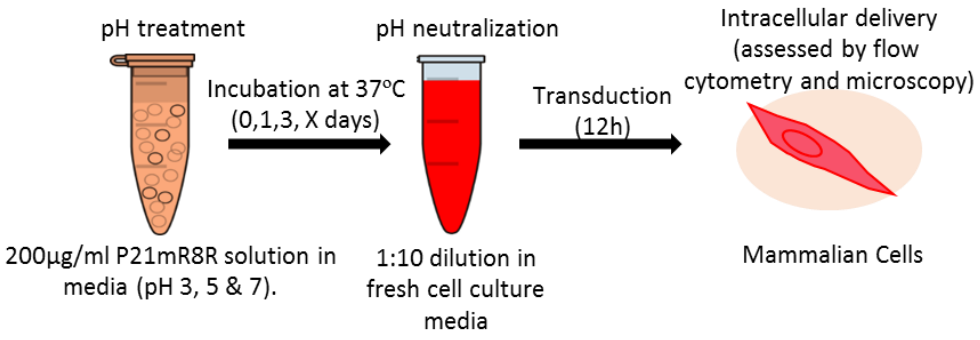


Figure 3.10 Schematic of the protein storage and sampling, 200µg/ml P21-mR-8R solution prepared with various pH values (3, 5 &7) and stored at 37ºC. A sample was taken from each solution, at defined time points, and diluted 1:10 in fresh cell culture media. Protein was then transduced into cells by addition to plated NIH3t3 cells.

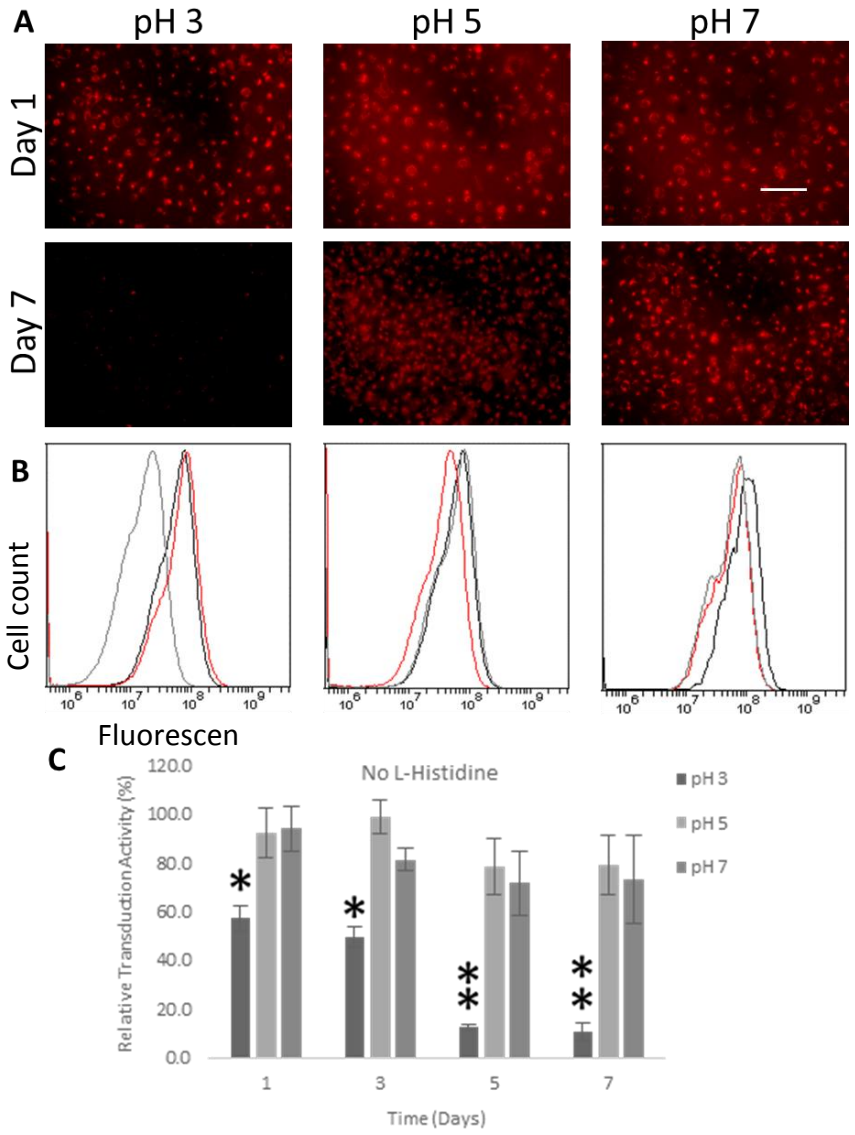


Figure 3.11 GET-peptide stability at various pH values mimicking the PLGA Microenvironment. P21-mR-8R stability in cell culture media of various pH values (3, 5 & 7), pH was adjusted using 1M **lactic acid** solution Protein sample was transduced into cells by addition to plated NIH3t3 cells. (A) Fluorescence microscopy images of the NIH3t3 cells treated with the protein samples (Scale bar 10µm). (B) Flow cytometry histograms showing cellular uptake of P21-mR-8R after application of the samples to NIH3t3 cells. The red histograms represent P21-mR-8R samples taken at day 1, while the grey histograms represent day 7 samples, black histograms are the experiment control. (C) Relative transduction activity of the samples. Protein transduction activity was compared to the experiment control. Error bars indicate SD (n = 3). * is $p<0.05$, ** is $p<0.01$.

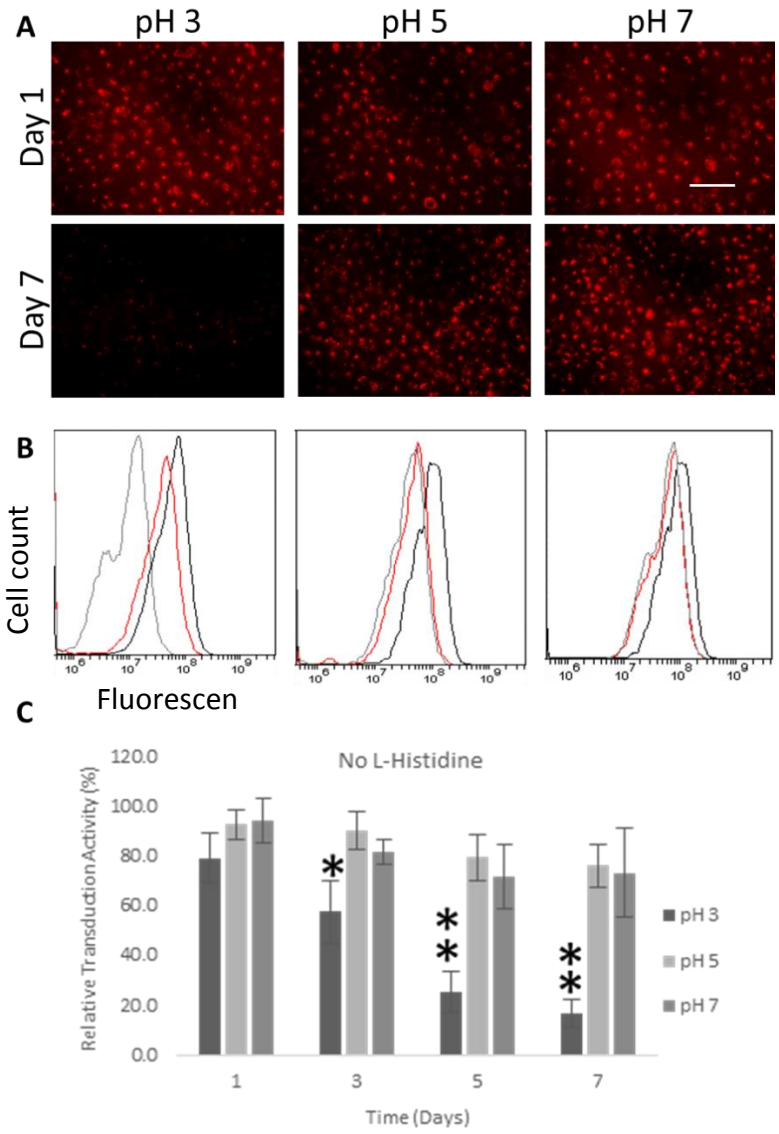


Figure 3.12 GET-peptide stability at various pH values mimicking the PLGA Microenvironment. P21-mR-8R stability in cell culture media of various pH values (3, 5 & 7), pH was adjusted using 1M **glycolic acid** solution Protein sample was transduced into cells by addition to plated NIH3t3 cells. (A) Fluorescence microscopy images of the NIH3t3 cells treated with the protein samples (Scale bar 10µm). (B) Flow cytometry histograms showing cellular uptake of P21-mR-8R after application of the samples to NIH3t3 cells. The red histograms represent P21-mR-8R samples taken at day 1, while the grey histograms represent day 7 samples, black histograms are the experiment control. (C) Relative transduction activity of the samples. Protein transduction activity was compared to the experiment control. Error bars indicate SD (n = 3). * is $p<0.05$, ** is $p<0.01$.

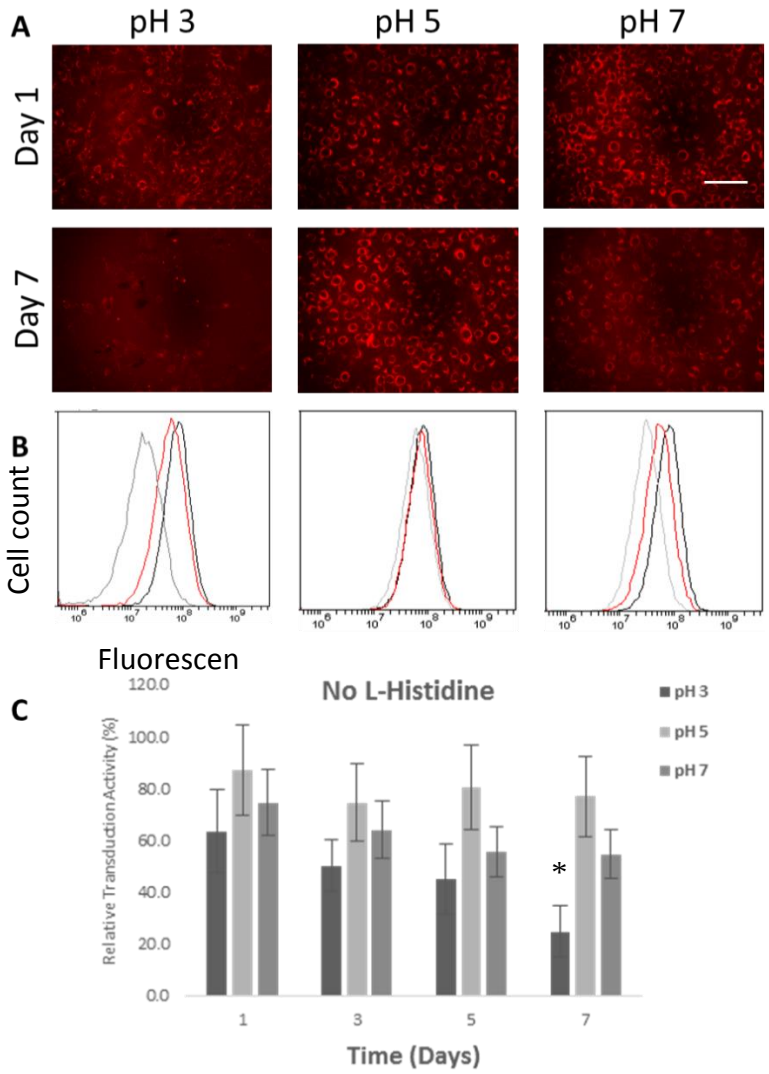


Figure 3.13 GET-peptide stability at various pH values mimicking the PLGA Microenvironment. P21-mR-8R stability in cell culture media of various pH values (3, 5 & 7), pH was adjusted using 1M **acetic acid** solution Protein sample was transduced into cells by addition to plated NIH3t3 cells. (A) Fluorescence microscopy images of the NIH3t3 cells treated with the protein samples (Scale bar 10μm). (B) Flow cytometry histograms showing cellular uptake of P21-mR-8R after application of the samples to NIH3t3 cells. The red histograms represent P21-mR-8R samples taken at day 1, while the grey histograms represent day 7 samples, black histograms are the experiment control. (C) Relative transduction activity of the samples. Protein transduction activity was compared to the experiment control. Error bars indicate SD (n = 3). * is $p<0.05$.

3.3.5.3.2. GET peptide activity is inhibited in presence of other acidic groups

In order the study the GET peptide stability in presence of other acidic groups (i.e. strong acids), GET peptide were incubated, for 7 days, in media of various pH values (3, 5 & 7), the pH was adjusted using different solutions, 1M phosphoric acid (weak acid), 1M hydrochloric acid (HCl) (strong acid), or 1M sulfuric acid (strong acid). This will indicate the stability of GET peptides in various acidic groups and suggest degradation mechanism (i.e. chemical degradation or electrostatic interaction). The collected samples were then applied to plated NIH 3t3 cells and cellular uptake of GET peptide was evaluated using fluorescence microscopy and flow cytometry. Fluorescence microscopy showed significant protein internalisation, for samples stored at pH 3, at day 1, for samples stored in media containing phosphoric acid. However, protein transduction was undetectable for day 7 samples. Flow cytometry results confirmed a loss in transduction for day 7 samples, and gradual loss of relative transduction activity over the time-points, reaching values below 20% at day 7 (Figure 3.14). Interestingly, fluorescent microscopy showed protein transduction for samples stored at pH 5 & 7 at all studied time points. Flow cytometry results confirmed this with relative transduction activity above 80% of non-treated controls at all studied time points. This behaviour is comparable to the previous obtained results using lactic, glycolic and acetic acid. On the other hand, fluorescent microscopy for samples stored at pH 3 media containing strong acids (hydrochloric or sulfuric acid) showed major loss of GET peptide activity from day 1, with relative transduction activity below 40% (figure 3.15 and 3.16). Samples stored at pH 5 & 7 showed minimal loss of activity with relative transduction activity above 60% in all studied time points.

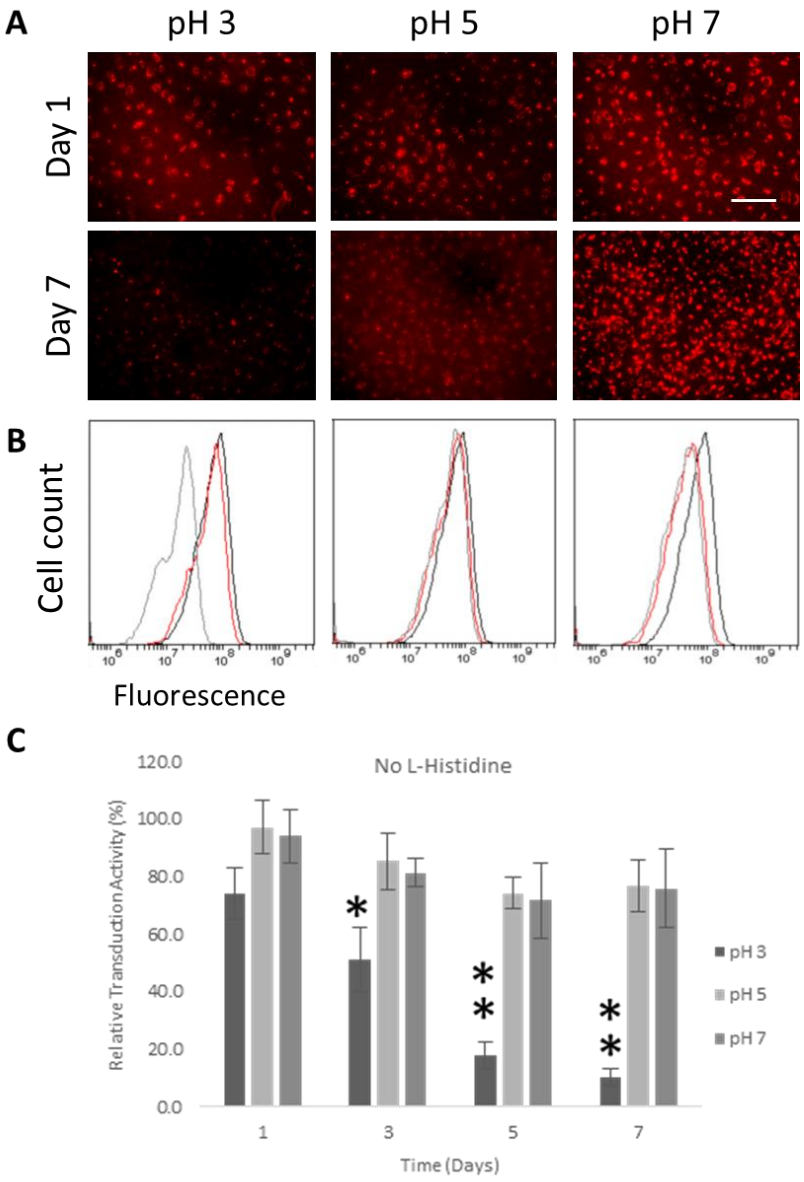


Figure 3.14 P21-mR-8R stability in cell culture media of various pH values (3, 5 & 7). pH was adjusted using 1M **phosphoric acid** solution. (A) Fluorescence microscopy images of the NIH3t3 cells treated with the samples contain P21-mR-8R (Scale bar 10μm). (B) Flow cytometry histograms showing cellular uptake of P21-mR-8R after application of the samples to NIH3t3 cells. The red histograms represent P21-mR-8R samples taken at day 1, while the grey histograms represent day 7 samples, black histograms are the experiment control. (C) Relative biological activity of the P21-mR-8R. Protein transduction activity was compared to the experiment control. Error bars indicate SD (n = 3). * is $p<0.05$, ** is $p<0.01$.

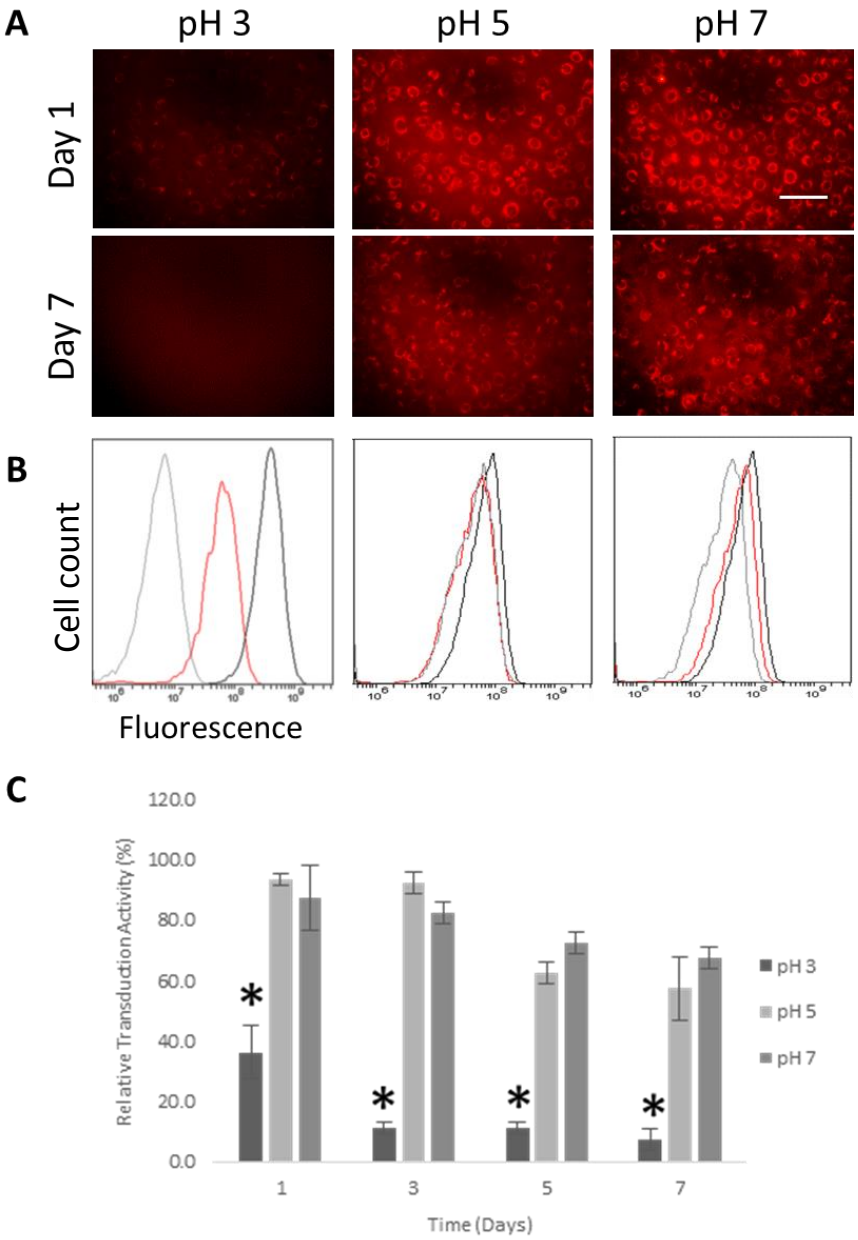


Figure 3.15 P21-mR-8R stability in cell culture media of various pH values (3, 5 & 7). pH was adjusted using 1M **hydrochloric acid** solution. (A) Fluorescence microscopy images of the NIH3t3 cells treated with the samples contain P21-mR-8R (Scale bar 10μm). (B) Flow cytometry histograms showing cellular uptake of P21-mR-8R after application of the samples to NIH3t3 cells. The red histograms represent P21-mR-8R samples taken at day 1, while the grey histograms represent day 7 samples, black histograms are the experiment control. (C) Relative biological activity of the P21-mR-8R. Protein transduction activity was compared to the experiment control. Error bars indicate SD (n = 3). * is $p<0.05$.

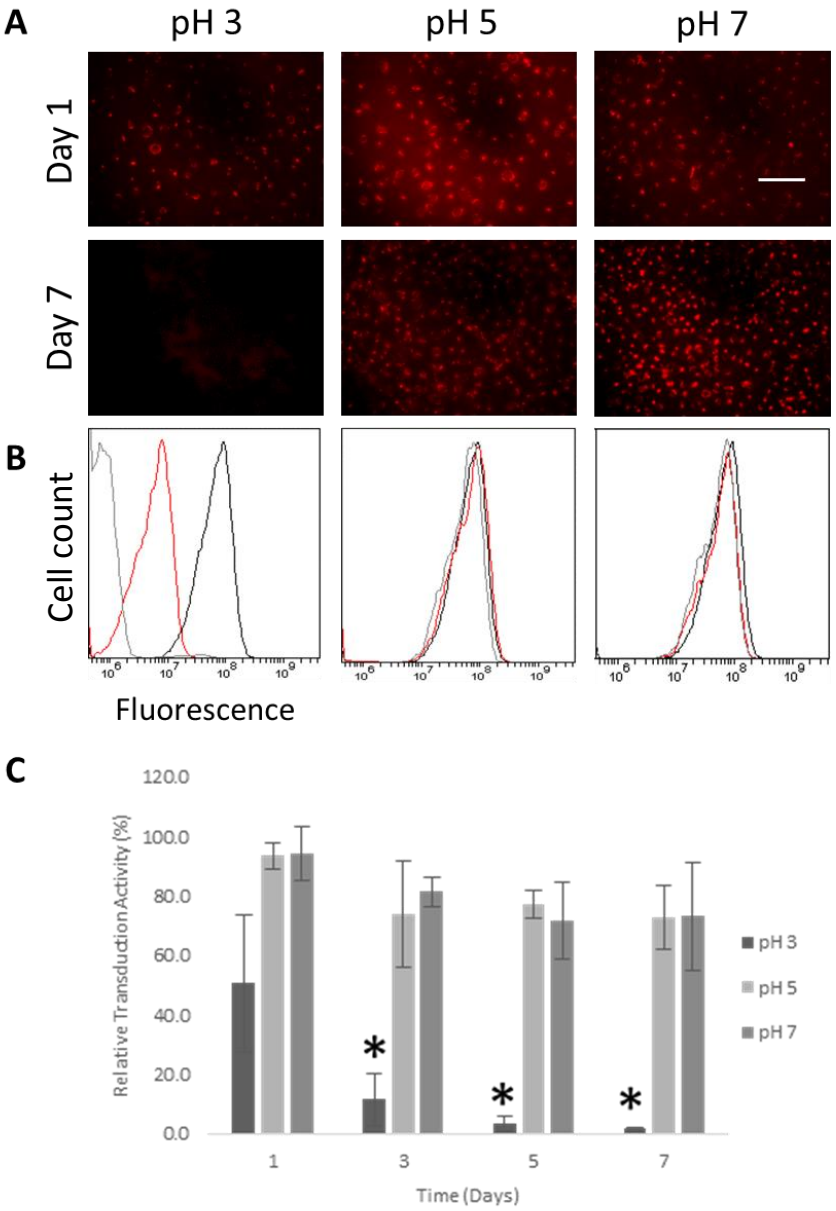


Figure 3.16 P21-mR-8R stability in cell culture media of various pH values (3, 5 & 7). pH was adjusted using 1M **sulfuric acid** solution. (A) Fluorescence microscopy images of the NIH3t3 cells treated with the samples contain P21-mR-8R (Scale bar 10µm). (B) Flow cytometry histograms showing cellular uptake of P21-mR-8R after application of the samples to NIH3t3 cells. The red histograms represent P21-mR-8R samples taken at day 1, while the grey histograms represent day 7 samples, black histograms are the experiment control. (C) Relative biological activity of the P21-mR-8R. Protein transduction activity was compared to the experiment control. Error bars indicate SD (n = 3). * is $p<0.05$.

3.3.6. Building a hypothesis for protein inactivation and stabilisation approach of GET peptide using L-histidine

Low pH usually develops in PLGA MPs as a result of accumulation of acidic degradants [86, 135, 186]. From the performed simulation studies, a highly acidic environment (~ pH 3) was needed to inactivate the protein transduction activity. The results suggested that the negatively charged carboxylic acid groups, which results from PLGA degradation, will interact with the positively charged GET peptide, preventing them from binding to the cell membrane and consequently preventing protein internalization.

Since GET peptide activity is compromised in presence of carboxylic acid group, the intended approach is to scavenge this group by adding a molecule that will compete with the protein in interaction with carboxylic acid. GET peptide are positively charged, and it is expected that they will interact with the negatively charged molecules. L-Histidine is positively charged amino acid at pH ~6. L-Histidine is expected to compete with the P21-mR-8R in interacting with the carboxylic group. Consequently, to test whether the L-Histidine could enhance GET peptide activity at low pH, the pH simulation study was repeated, in presence of L-Histidine. L-Histidine was added in quantities that will not affect the solution pH. Various pH conditions were studied (3, 5 & 7) with L-Histidine, and the same protein behaviour was noticed, which suggests that the L-Histidine works at low pH only, due to its charge, and the presence of L-Histidine along with the protein, at higher pH, will not alter its activity.

3.3.7. Validation of L-Histidine stabilisation approach

In order to validate the above mentioned hypothesis about L-Histidine capability of stabilising GET peptide in presence of PLGA (and its degradation products), it was important to test all the previously studied parameter in presence of L-Histidine and compare the findings.

3.3.7.1. GET peptide interaction with blank PLGA microparticles in presence of L-Histidine

It was shown that GET peptide interact with the negatively charged PLAGA MPs at neutral pH, and at low pH the GET peptide interacted with the carboxylic groups and remained in the supernatant. Accordingly, addition of L-Histidine to both pH conditions was tested. It was expected that L-Histidine will disrupt GET peptide interaction with carboxylic groups.

Applying the same conditions in presence of L-Histidine resulted in GET peptide interaction with MPs at neutral pH (Figure 3.17), with only 20% of the protein quantity could be detected, which is expected as the L-Histidine is not positively charged at this pH. Interestingly, at pH 3, the positively charged L-Histidine appeared to act as a scavenger for the carboxyl groups from the added carboxyl groups and P21-mR-8R retained its ability to interact with the negatively charged PLGA MPs. Therefore, it was conclude that P21-mR-8R can interact with both PLGA directly (most likely electrostatically) and also with carboxylic groups (which can disrupt the PLGA interaction). By using L-Histidine we could retain P21-mR-8R/PLGA interaction, most likely through a sequestering of free carboxylic acid groups by positively charged L-Histidine (Figure 3.17).

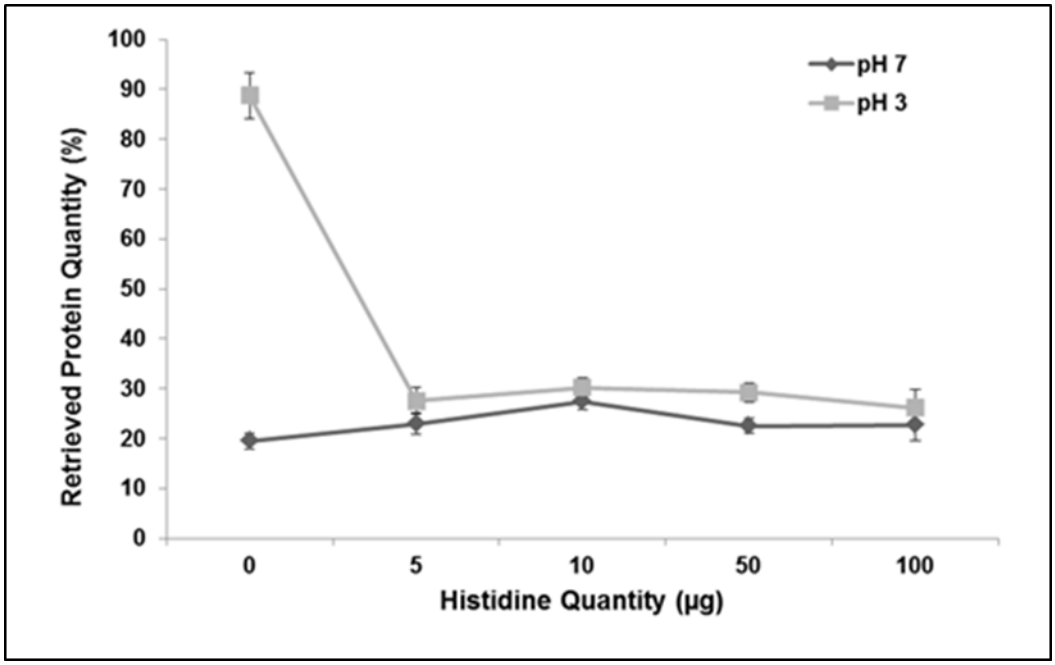


Figure 3.17 GET peptide interaction with 25mg PLGA MPs at various pH conditions in presence of different L-Histidine quantities. PLGA MPs were suspended in solution of different pH values and P21-mR-8R with L-Histidine was then added, the solution was then centrifuged and the P21-mR-8R quantity in the supernatant was measured. Error bars indicate SD (n = 3).

3.3.7.2. GET peptide activity in presence of PLGA degradation products in presence of L-Histidine

The previous results showed that PLGA degradation product is inhibiting GET peptide activity, in order to assess L-Histidine effect on GET-PLGA degradation product interaction, the experiment was repeated with various quantities of L-Histidine being incorporated with P21-mR-8R (Figure 3.18). Addition of L-Histidine resulted in enhanced transduction activity, as the L-Histidine is expected to interact with the carboxylic group containing PLGA degradants.

Samples of 1:0.1 ratio (P21-mR-8R:LHistidine) showed enhanced transduction activity, compared to samples with no L-Histidine (Figure 3.18), however, only 55% ± 4.3 transduction activity could be achieved. For samples prepared with addition of L-Histidine >25% of the P21-mR-8R quantity, fluorescent microscopy and flow cytometry results showed comparable protein transduction activity at all time points, with relative transduction activity above 80% could be achieved. This clearly demonstrates the role of L-Histidine in maintaining the activity of GET peptide in presence of PLGA degradation products. A schematic showing L-Histidine proposed mechanism is shown in figure 3.32 (page 130).

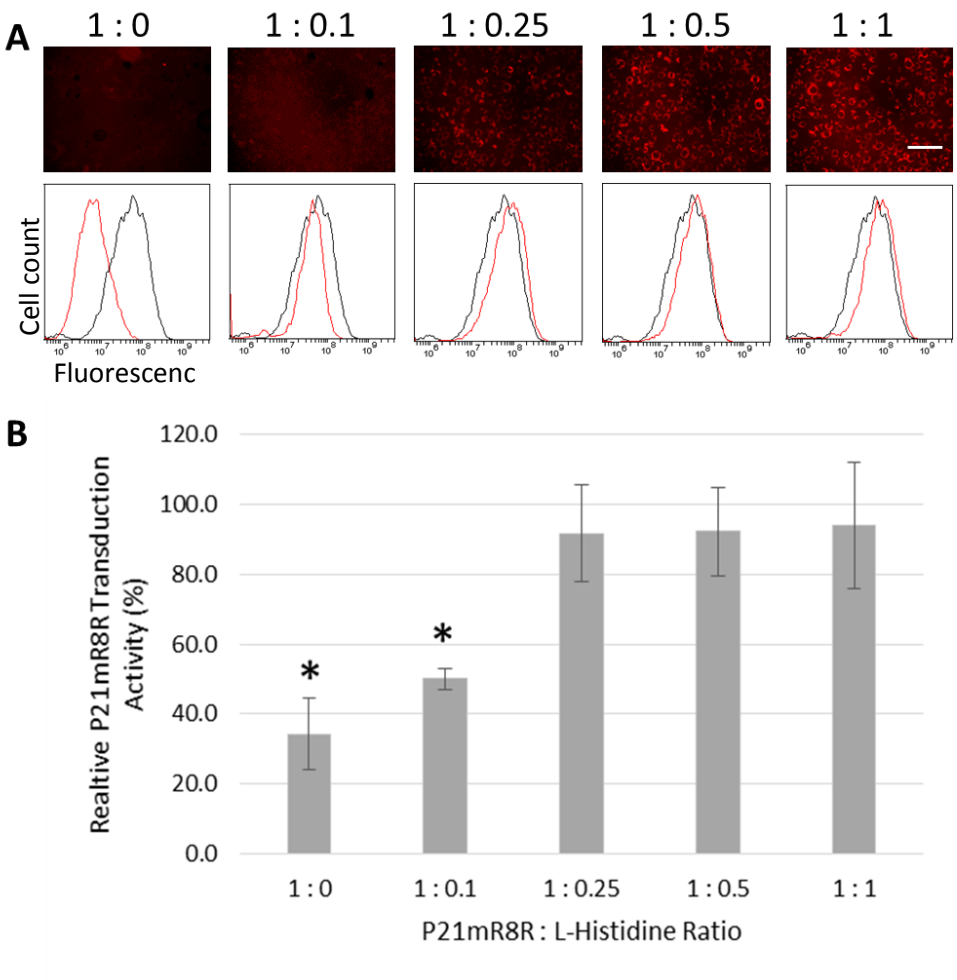


Figure 3.18 Effect of L-Histidine on GET peptide stability in media contains PLGA degradation product. Blank PLGA MPs were left to degrade in media, after that P21-mR-8R was mixed with the media and different quantities of L-Histidine. Protein was then transduced into cells by addition to plated NIH3t3 cells. (A) Fluorescence microscopy images of the NIH3t3 cells treated with the sampled P21-mR-8R (Scale bar 10μm) and flow cytometry histograms showing cellular uptake of P21-mR-8R after application of the samples to NIH3t3 cells. The red histograms represent P21-mR-8R samples while black histograms are the experiment control. (B) Relative transduction activity of the sampled P21-mR-8R. Protein transduction activity was compared to the experiment control. Error bars indicate SD (n = 3). * is $p<0.05$.

3.3.7.3. GET peptide activity at various pH conditions in presence of L-Histidine

3.3.7.3.1. GET peptide activity in presence of carboxylic acid groups and L-Histidine

To determine if L-Histidine could promote GET-protein transduction in high carboxylic acid/low pH as for MP-released protein, the simulation experiments were repeated in presence of L-Histidine. As before, protein was stored in cell culture media of various pH values (3, 5 & 7); adjusted using either 1 M lactic acid, 1 M glycolic acid or 1 M acetic acid. Unlike P21-mR-8R alone, L-Histidine (200 µg/ml) containing samples (fluorescence microscopy and flow cytometry analyses) did not lose P21-mR-8R transduction activity for all the studied pH conditions including those at pH 3 (Figures 3.19, 3.20 and 3.21). Protein relative transduction activity was above 60% for all the studied conditions and therefore it was clear that the presence of L-Histidine during incubation prevented the loss of GET transduction activity.

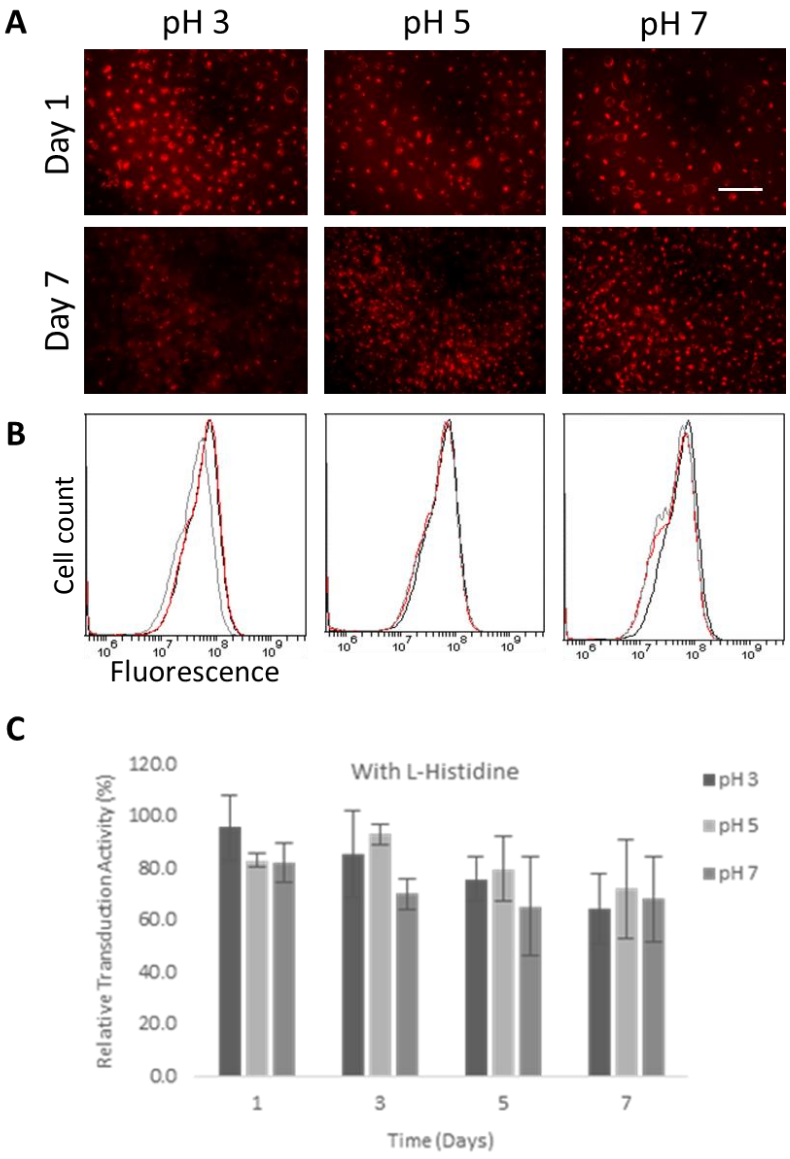


Figure 3.19 GET-peptide stability at various pH values mimicking the PLGA Microenvironment. P21-mR-8R with L-Histidine stability in cell culture media of various pH values (3, 5 & 7), pH was adjusted using 1M **lactic acid** solution Protein sample was transduced into cells by addition to plated NIH3t3 cells. (A) Fluorescence microscopy images of the NIH3t3 cells treated with the protein samples (Scale bar 10μm). (B) Flow cytometry histograms showing cellular uptake of P21-mR-8R after application of the samples to NIH3t3 cells. The red histograms represent P21-mR-8R samples taken at day 1, while the grey histograms represent day 7 samples, black histograms are the experiment control. (C) Relative transduction activity of the samples. Protein transduction activity was compared to the experiment control. Error bars indicate SD (n = 3).

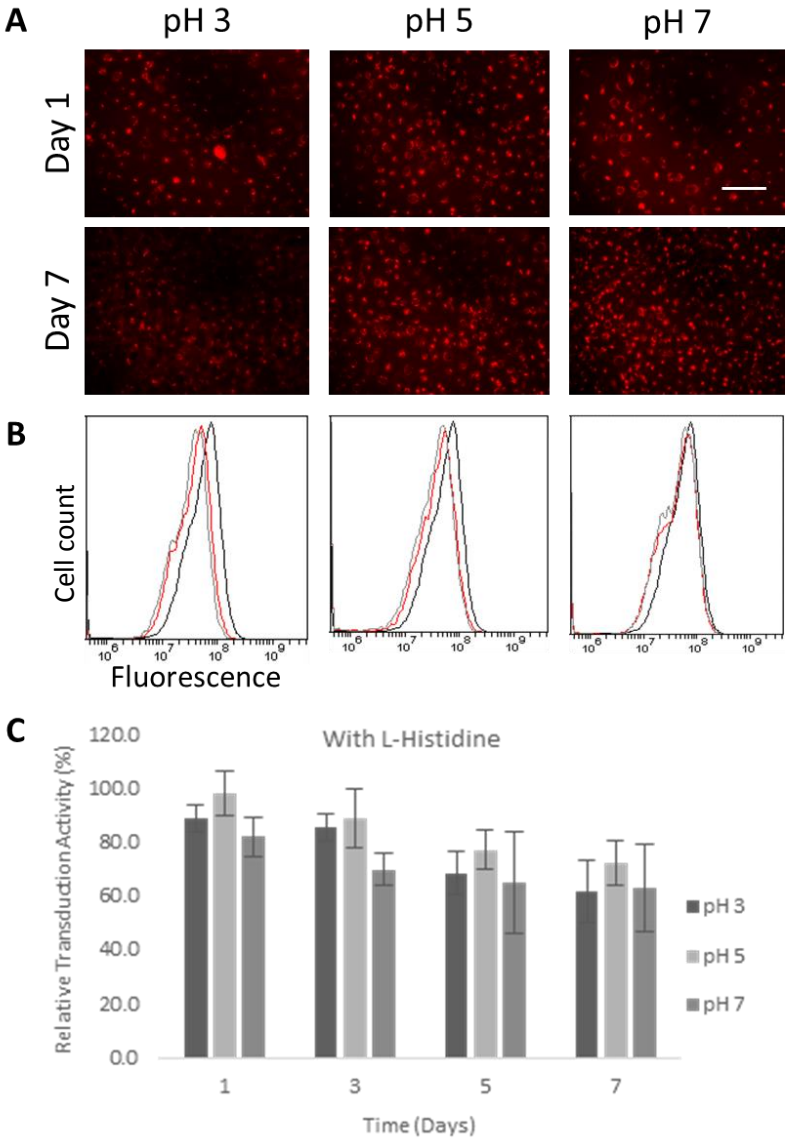


Figure 3.20 GET-peptide stability at various pH values mimicking the PLGA Microenvironment. P21-mR-8R with L-Histidine stability in cell culture media of various pH values (3, 5 & 7), pH was adjusted using 1M **glycolic acid** solution Protein sample was transduced into cells by addition to plated NIH3t3 cells. (A) Fluorescence microscopy images of the NIH3t3 cells treated with the protein samples (Scale bar 10µm). (B) Flow cytometry histograms showing cellular uptake of P21-mR-8R after application of the samples to NIH3t3 cells. The red histograms represent P21-mR-8R samples taken at day 1, while the grey histograms represent day 7 samples, black histograms are the experiment control. (C) Relative transduction activity of the samples. Protein transduction activity was compared to the experiment control. Error bars indicate SD (n = 3).

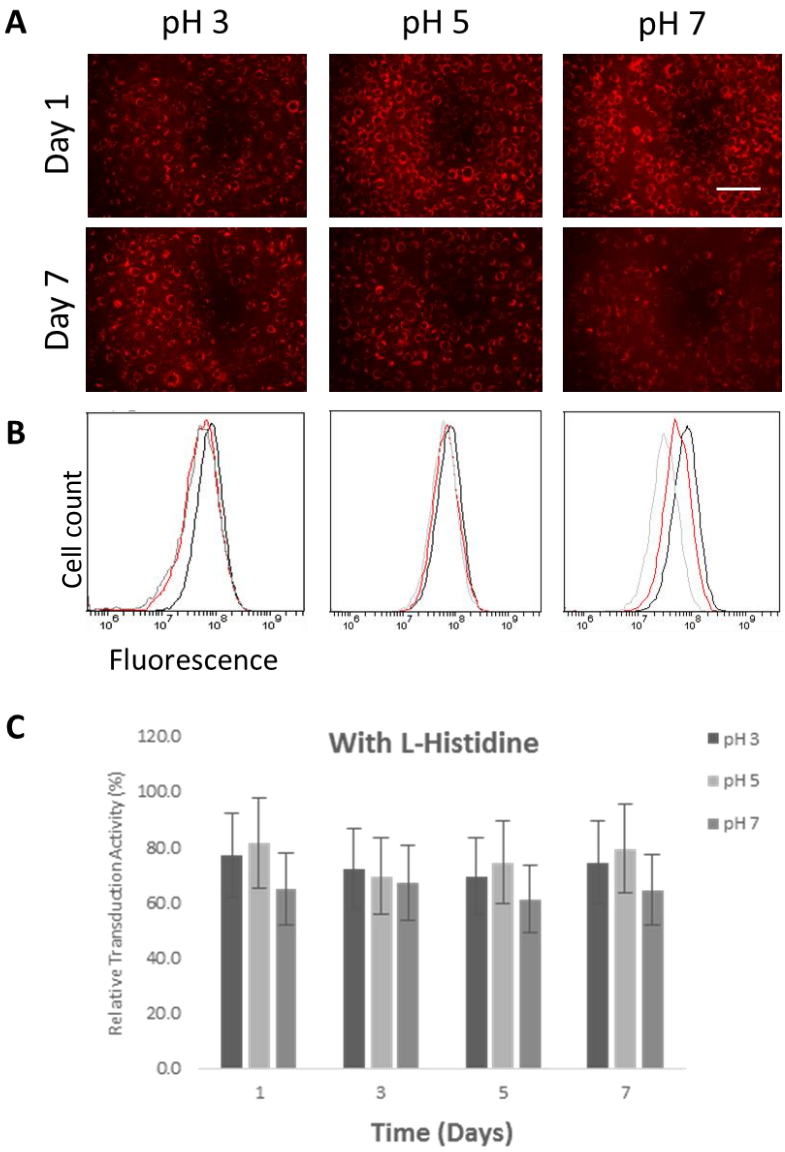


Figure 3.21 GET-peptide stability at various pH values mimicking the PLGA Microenvironment. P21-mR-8R with L-Histidine stability in cell culture media of various pH values (3, 5 & 7), pH was adjusted using 1M **acetic acid** solution Protein sample was transduced into cells by addition to plated NIH3t3 cells. (A) Fluorescence microscopy images of the NIH3t3 cells treated with the protein samples (Scale bar 10μm). (B) Flow cytometry histograms showing cellular uptake of P21-mR-8R after application of the samples to NIH3t3 cells. The red histograms represent P21-mR-8R samples taken at day 1, while the grey histograms represent day 7 samples, black histograms are the experiment control. (C) Relative transduction activity of the samples. Protein transduction activity was compared to the experiment control. Error bars indicate SD (n = 3).

3.3.7.3.2. L-Histidine protect GET peptide in presence of weak acid but not strong acid

To determine if L-Histidine could promote GET-protein transduction in presence of various acidic groups, pH incubation experiments were repeated in the presence of L-Histidine. As before, protein was stored in cell culture media of various pH values (3, 5 & 7); adjusted using either 1M phosphoric acid, 1M hydrochloric acid (HCl), or 1M sulfuric acid.

In presence of phosphoric acid (weak acid) L-Histidine (200µg/ml) containing samples (fluorescence microscopy and flow cytometry analyses) showed comparable P21-mR-8R transduction activity for all the studied pH conditions including those at pH 3 (Figure 3.22). Protein relative transduction activity was above 60% for all the studied conditions and therefore it was clear that the presence of L-Histidine during incubation prevented the loss of GET transduction activity. On the other hand, L-Histidine did not protect GET peptide at pH 3 in presence of strong acids (HCl or sulfuric acid), with relative transduction activity below 40% from day 1 (Figure 3.23 and Figure 3.24).

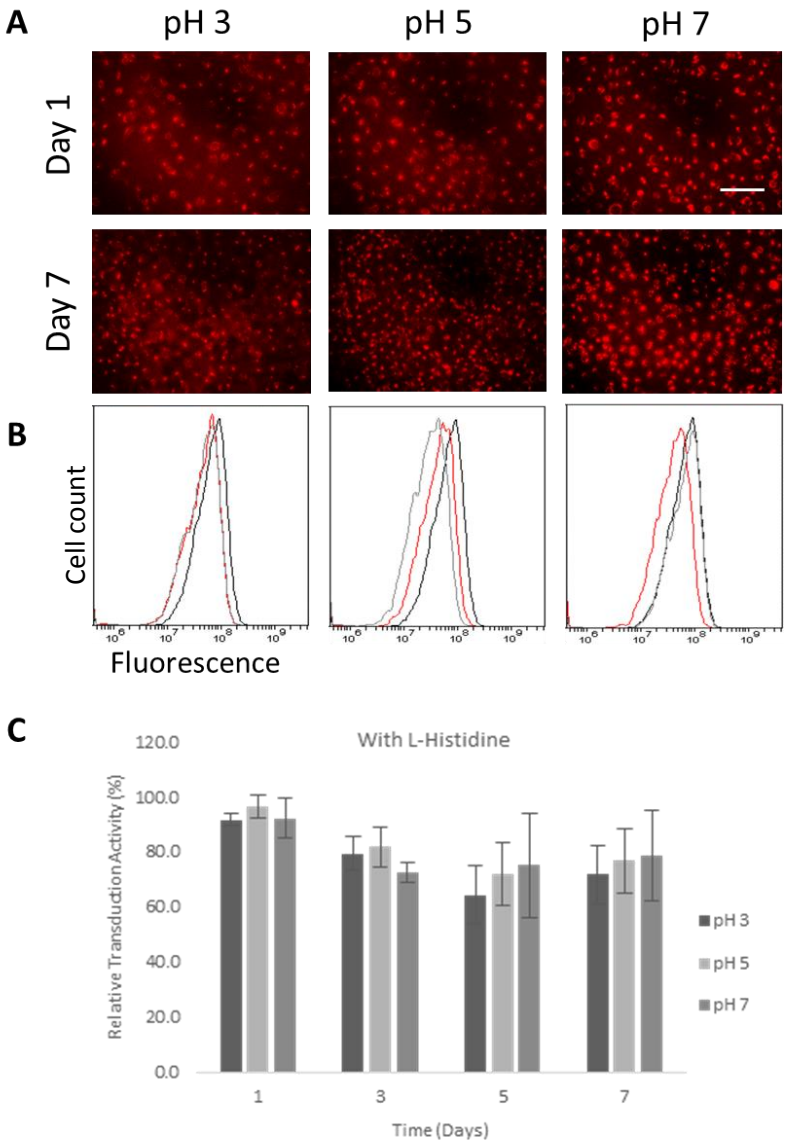


Figure 3.22 GET-peptide stability at various pH values mimicking the PLGA Microenvironment. P21-mR-8R with L-Histidine stability in cell culture media of various pH values (3, 5 & 7), pH was adjusted using 1M **phosphoric acid** solution Protein sample was transduced into cells by addition to plated NIH3t3 cells. (A) Fluorescence microscopy images of the NIH3t3 cells treated with the protein samples (Scale bar 10μm). (B) Flow cytometry histograms showing cellular uptake of P21-mR-8R after application of the samples to NIH3t3 cells. The red histograms represent P21-mR-8R samples taken at day 1, while the grey histograms represent day 7 samples, black histograms are the experiment control. (C) Relative transduction activity of the samples. Protein transduction activity was compared to the experiment control. Error bars indicate SD (n = 3).

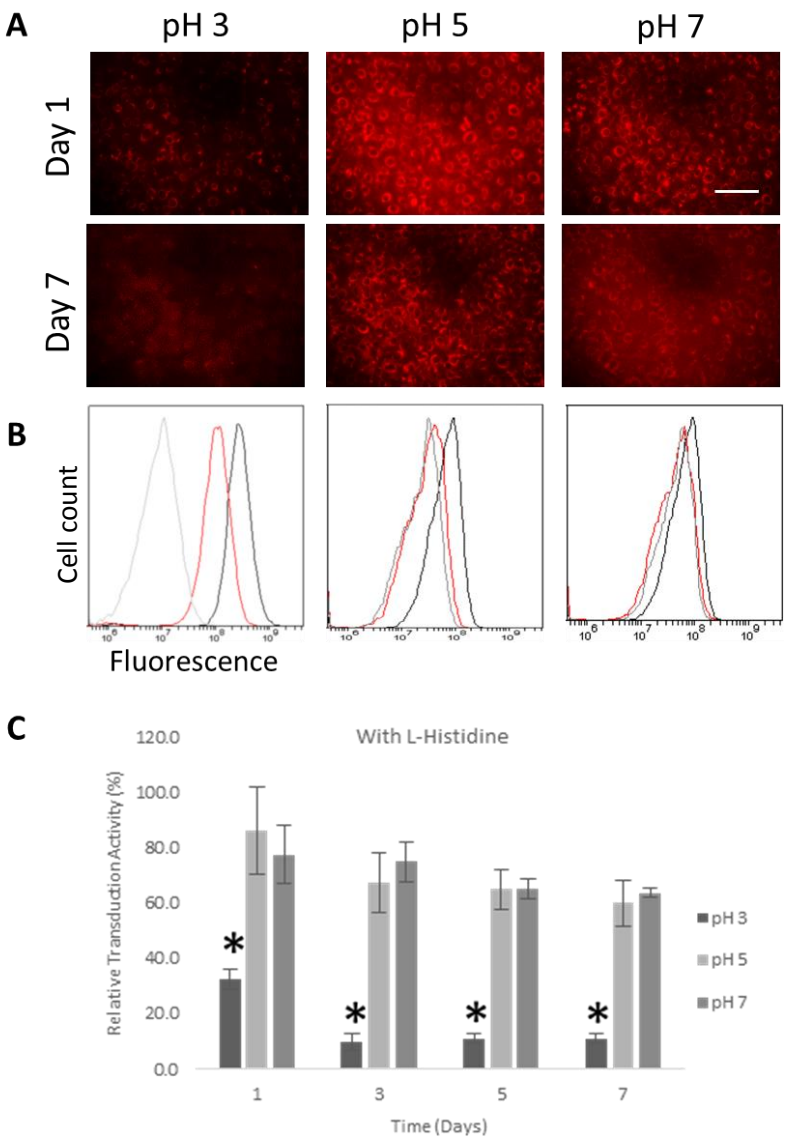


Figure 3.23 GET-peptide stability at various pH values mimicking the PLGA Microenvironment. P21-mR-8R with L-Histidine stability in cell culture media of various pH values (3, 5 & 7), pH was adjusted using 1M **hydrochloric acid** solution Protein sample was transduced into cells by addition to plated NIH3t3 cells. (A) Fluorescence microscopy images of the NIH3t3 cells treated with the protein samples (Scale bar 10μm). (B) Flow cytometry histograms showing cellular uptake of P21-mR-8R after application of the samples to NIH3t3 cells. The red histograms represent P21-mR-8R samples taken at day 1, while the grey histograms represent day 7 samples, black histograms are the experiment control. (C) Relative transduction activity of the samples. Protein transduction activity was compared to the experiment control. Error bars indicate SD (n = 3). * is $p<0.05$.

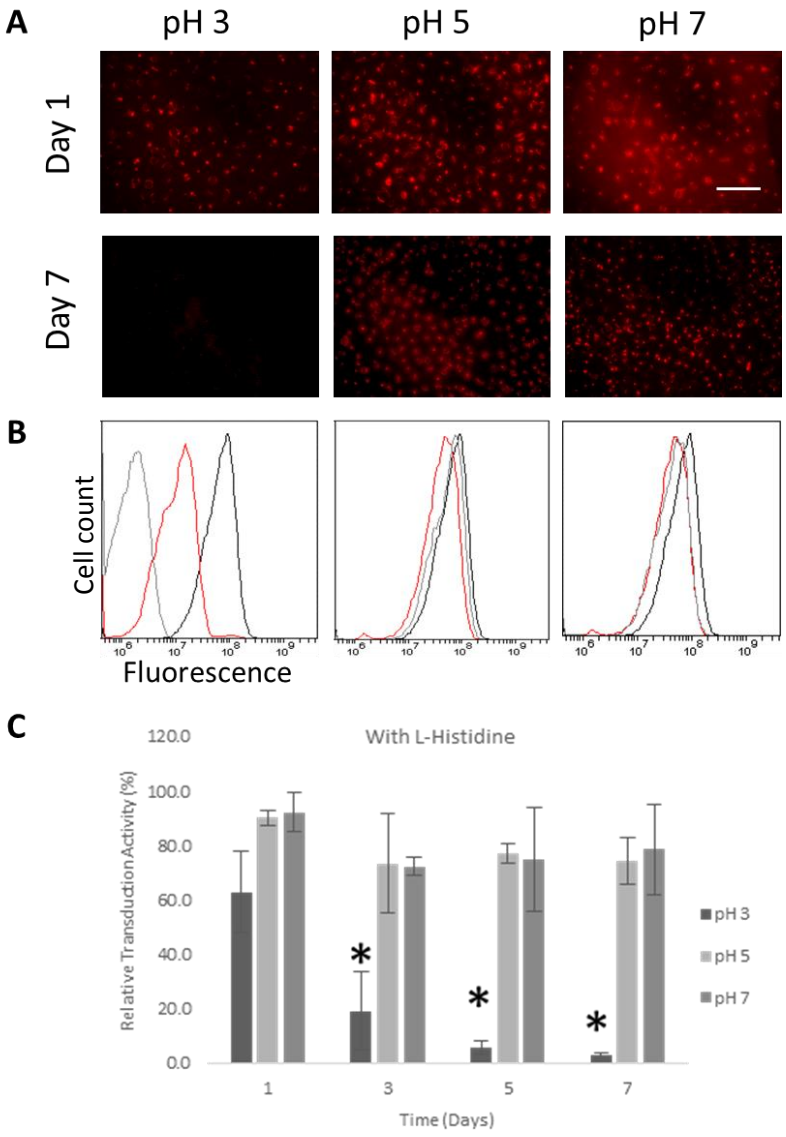


Figure 3.24 GET-peptide stability at various pH values mimicking the PLGA Microenvironment. P21-mR-8R with L-Histidine stability in cell culture media of various pH values (3, 5 & 7), pH was adjusted using 1M **sulfuric acid** solution Protein sample was transduced into cells by addition to plated NIH3t3 cells. (A) Fluorescence microscopy images of the NIH3t3 cells treated with the protein samples (Scale bar 10μm). (B) Flow cytometry histograms showing cellular uptake of P21-mR-8R after application of the samples to NIH3t3 cells. The red histograms represent P21-mR-8R samples taken at day 1, while the grey histograms represent day 7 samples, black histograms are the experiment control. (C) Relative transduction activity of the samples. Protein transduction activity was compared to the experiment control. Error bars indicate SD (n = 3). * is $p<0.05$.

3.3.8. L-Histidine does not neutralize carboxyl group acidity

In order to clarify why L-Histidine has such profound effect on carboxyl acid-mediated inhibition of GET transduction, we determined if the addition of L-Histidine could neutralize the acidity of the carboxyl acid-containing media. The pH of the media after addition of L-Histidine (200µg/ml) was measured in the three studied pH conditions (3, 5 & 7). The pH found to be the same, with no significant change (Figure 3.25). Also, to confirm the quantities of L-Histidine required to neutralize the pH we employed, we performed a back titration with L-Histidine. Our titration showed that the molar ratio of 1:5 between the acetic acid and L-Histidine is required for neutrality. Accordingly, it is very unlikely that the L-Histidine is neutralizing the pH conditions in our system, but will work as a scavenger competing with PLGA degradation products for GET peptide interaction.

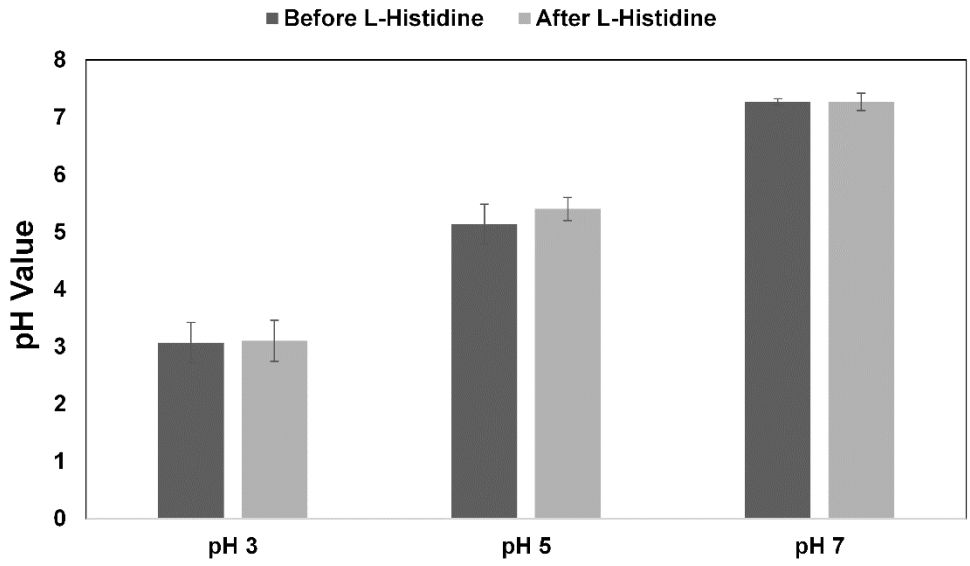


Figure 3.25 pH values for media before and after addition of L-Histidine (200µg/ml). pH was initially adjusted using 1M acetic acid solution. Error bars indicate SD (n = 3).

3.3.9. Co-incubation with L-Histidine is required to prevent inhibition of GET transduction by carboxylic acid

In order to assess if the mechanism of L-Histidine was during incubation, or could be manifest by its addition post-incubation, pH incubation experiments were repeated. After samples were taken and diluted, 20µg L-Histidine was added and transduction activity tested. Fluorescent microscopy showed no protein transduction in the cells incubated at pH 3 with or without addition of L-Histidine post-incubation. Flow cytometry confirmed that L-Histidine addition had no effect unless it was present throughout the pH incubation, with relative transduction activity around ~20%. It is therefore likely that L-Histidine prevents P21-mR-8R/carboxylic acid interaction or pH-dependent inhibition of transduction which is a gradual process over the 7 days experiment.

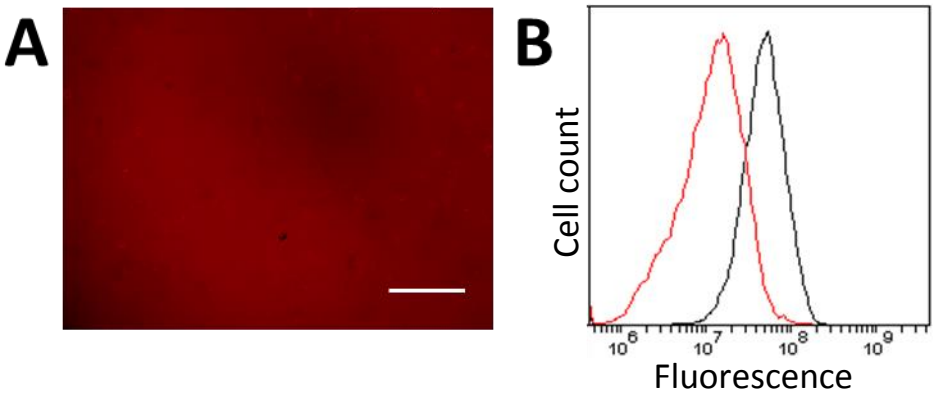


Figure 3.26 Effect of L-Histidine on P21-mR-8R stability upon storage in cell culture media of pH 3, adjusted using 1M acetic acid solution. 200µg/ml P21-mR-8R solution of pH 3 was prepared and stored at 37ºC for 7 days. A sample was taken from the solution, after 7 days, and diluted 1:10 in fresh cell culture media, producing a P21-mR-8R solution of 20µg/ml. 20µg of L-Histidine was then added to the solution. Protein was then transduced into cells by addition to plated NIH3t3 cells. (A) Fluorescence microscopy images of the NIH3t3 cells treated with the sampled P21-mR-8R (Scale bar 10µm). (B) Flow cytometry histograms showing cellular uptake of P21-mR-8R after application of the sample to NIH3t3 cells. The red histograms represent P21-mR-8R sample, black histogram is the experiment control.

3.3.10. L-Histidine dose is important to preserve GET transduction

The previous analyses employed one concentration (200 µg/ml) of L-Histidine to negate the negative effect of carboxylic acid on GET peptide transduction. Next the dose requirement for this activity was assessed. P21-mR-8R (200 µg/ml) with different quantities of L-Histidine (0–200 µg/ml) was incubated at pH 3 in acetic acid adjusted cell culture media. Fluorescence microscopy and flow cytometry demonstrated gradual loss of protein transduction activity for samples with no L-Histidine. Samples containing 20 µg/ml L-Histidine showed enhanced transduction activity, compared to samples with no L-Histidine, however, only 50% transduction activity could be achieved after 3 days (Figure 3.27). For samples prepared with addition of >50 µg/ml of L-Histidine, fluorescent microscopy and flow cytometry results showed comparable protein transduction activity at all time points, with relative transduction activity above 60% could be achieved in all time points (Figure 3.27). Therefore 50 µg/ml L-Histidine was sufficient to mediate the maximum effect to negate the inhibitory effect of carboxylic acid. This represents 25% of the P21-mR-8R quantity.

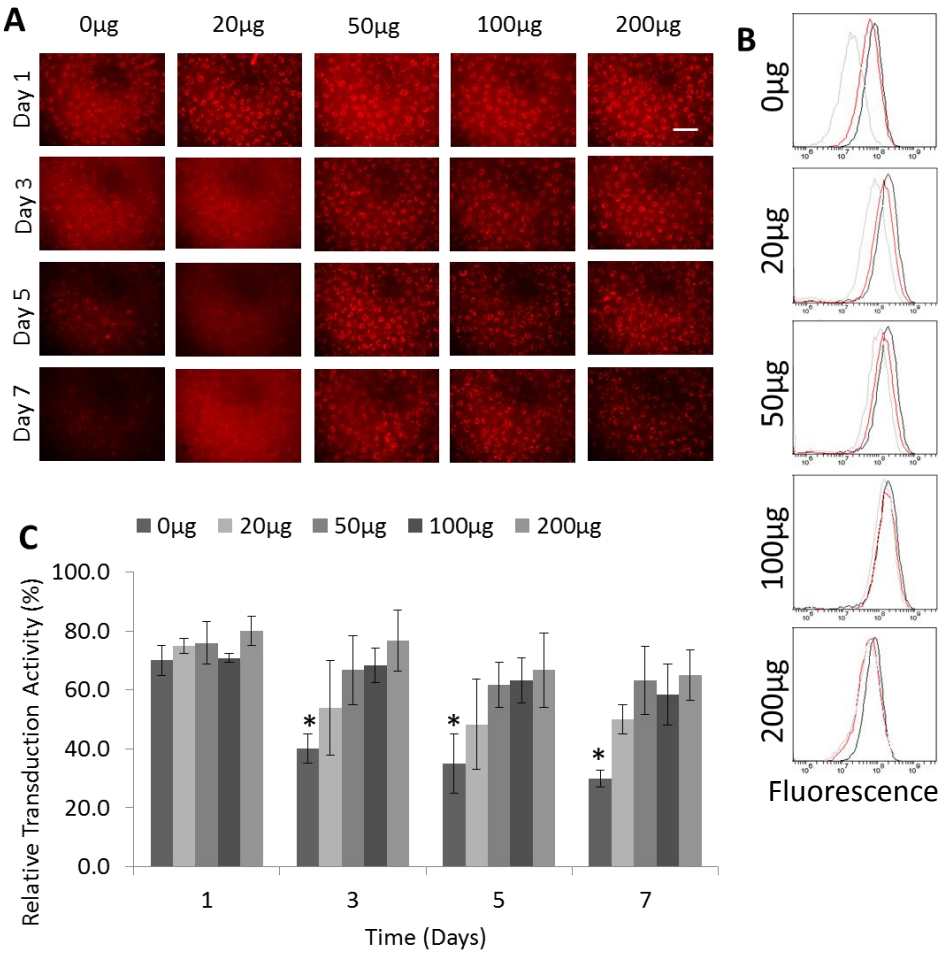


Figure 3.27 Dose of L-Histidine required to promote GET-peptide activity. Effect of different quantities of L-Histidine on P21-mR-8R stability upon storage in cell culture media of pH 3 (pH was adjusted using 1M acetic acid solution). 200µg/ml P21-mR-8R solution was prepared with various quantities L-Histidine (0 – 200µg) and stored at 37ºC. A sample was taken from each solution, at defined time points, and diluted 1:10 in fresh cell culture media. Protein was then transduced into cells by addition to plated NIH3t3 cells. (A) Fluorescence microscopy images of the NIH3t3 cells treated with the sampled P21-mR-8R (Scale bar 10µm). (B) Flow cytometry histograms showing cellular uptake of P21-mR-8R after application of the samples to NIH3t3 cells. The red histograms represent P21-mR-8R samples taken at day 1, while the grey histograms represent day 7 samples, black histograms are the experiment control. (C) Relative transduction activity of the sampled P21-mR-8R. Protein transduction activity was compared to the experiment control. Error bars indicate SD (n = 3). * is $p<0.05$.

3.3.11. Co-encapsulation of L-Histidine during fabrication of porous PLGA MPs

In the light of the above findings, porous PLGA MPs containing L-Histidine (25% w/w in respect to protein quantity) were fabricated. L-Histidine MPs prepared with addition of PBS, have the average diameter and loading efficiency of 42.3 ± 9.1 mm and 67.4 ± 6.3% respectively. Using SEM and particle sizing, we were able to determine that incorporation of L-Histidine did not affect the morphology, size and the loading efficiency of MPs, as shown in the representative SEM images, size distribution and loading efficiency results (Figure 3.28). This demonstration was important as we showed it is possible to add excipients (such as L-Histidine) directly to the formulation without affecting MP physical properties.

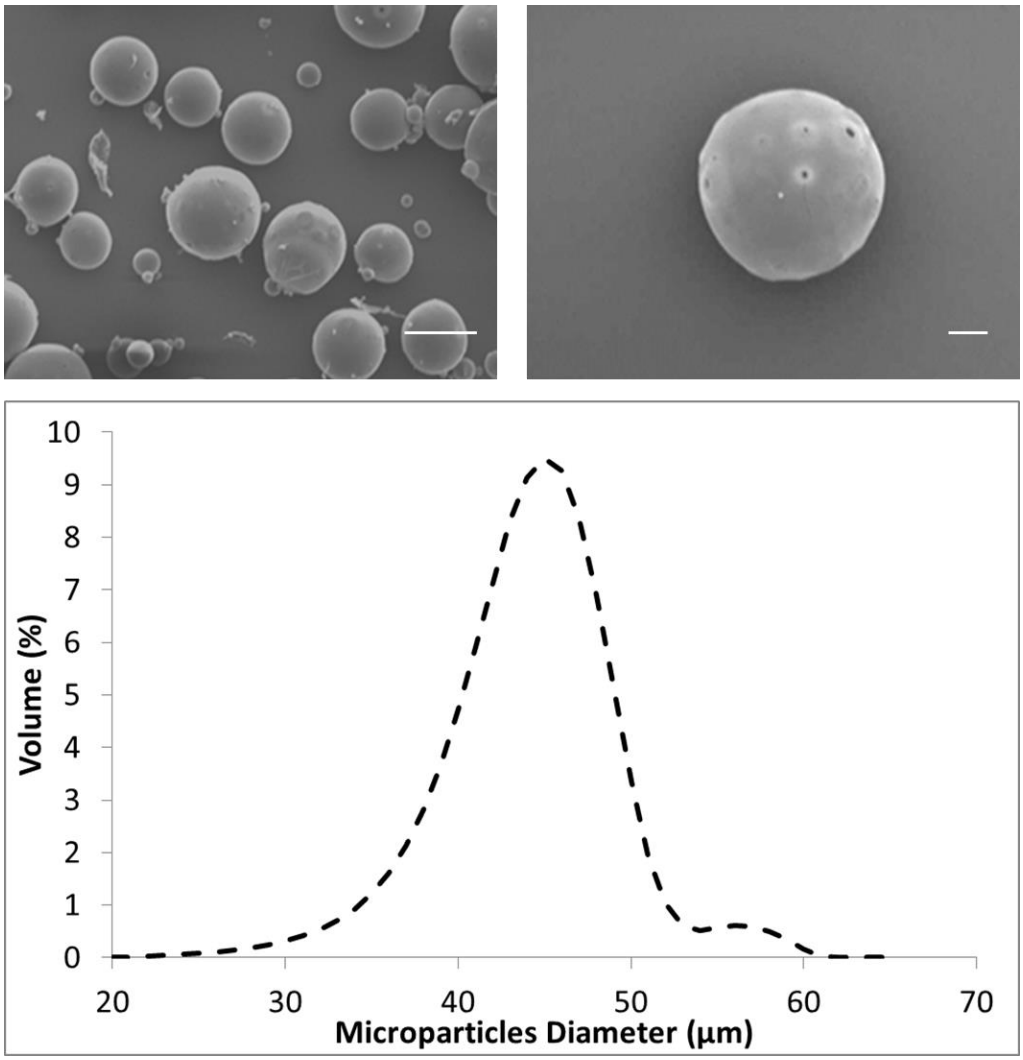


Figure 3.28 MP characterization; SEM and size analyses. MPs were prepared with addition of 200µL PBS to the primary emulsion. MPs were loaded with P21-mR-8R (0.5% (w/w)) mixed with L-Histidine (25% (w/w)). SEM analyses for MPs (scale bars represent 50 µm on left image, and 10 µm on right image). Representative size distribution, average of three different loaded PLGA microparticles batches (n=3).

3.3.12. L-Histidine has no effect on sustained release of GET proteins from porous MPs

To confirm that the same release kinetics are retained with incorporation of L-Histidine, analyses of P21-mR-8R release over time was repeated. Incorporation of L-Histidine to the formulation (PLGA-PBS-Histidine) did not change the release profile significantly (Figure 3.29), MPs showed gradual and continuous release similar to plain porous-MPs (PLGA-PBS), with 83% ± 9.8 cumulative release, after 10 days.

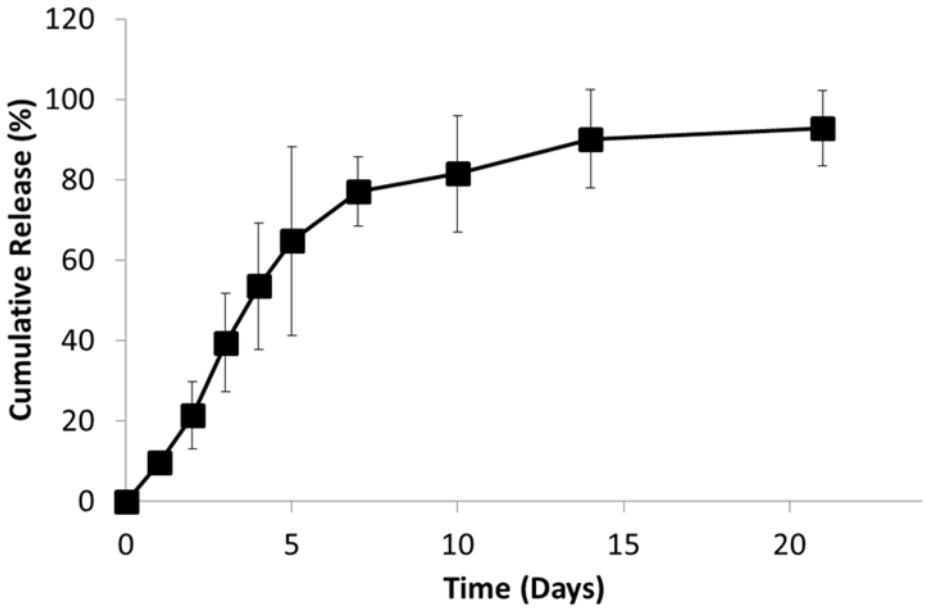


Figure 3.29 In vitro release profiles of P21-mR-8R from porous PLGA MPs (pH 7.4 at 37°C) MPs were prepared using S/O/W method loaded with P21-mR-8R (0.5% (w/w)) mixed with L-Histidine (25% (w/w)). Protein was quantified using Micro BCA assay kit. Error bars indicate SD (n = 3).

3.3.13. Released GET peptide transduction activity assessment

Whether the addition of L-Histidine to MPs can improve the transduction activity of the released GET protein (PLGA-PBS-L-Histidine formulations) was assessed. Flow cytometry results showed that the protein released at the first day has a relative transduction activity above 85% ± 8.6, similar to that of PLGA-PBS MPs (Figure 3.30). However, GET-protein released from PLGA-PBS-Histidine MPs retained its relative transduction activity above 80% on all studied time points (Figure 3.31).

This observation clearly demonstrates that L-Histidine addition to porous-PLGA MPs significantly prevents the loss of GET transduction activity during protein release. As it is studied and showed in the previous sections, L-Histidine is expected to act as a scavenger, minimising the interaction between GET peptide and negatively charged carboxylic acid containing molecules, resulting from PLGA degradation.

A schematic showing the mechanism of P21-mR-8R loss of activity upon release from PLGA MPs and the proposed mechanism of L-Histidine stabilising effect is shown in figure 3.32.

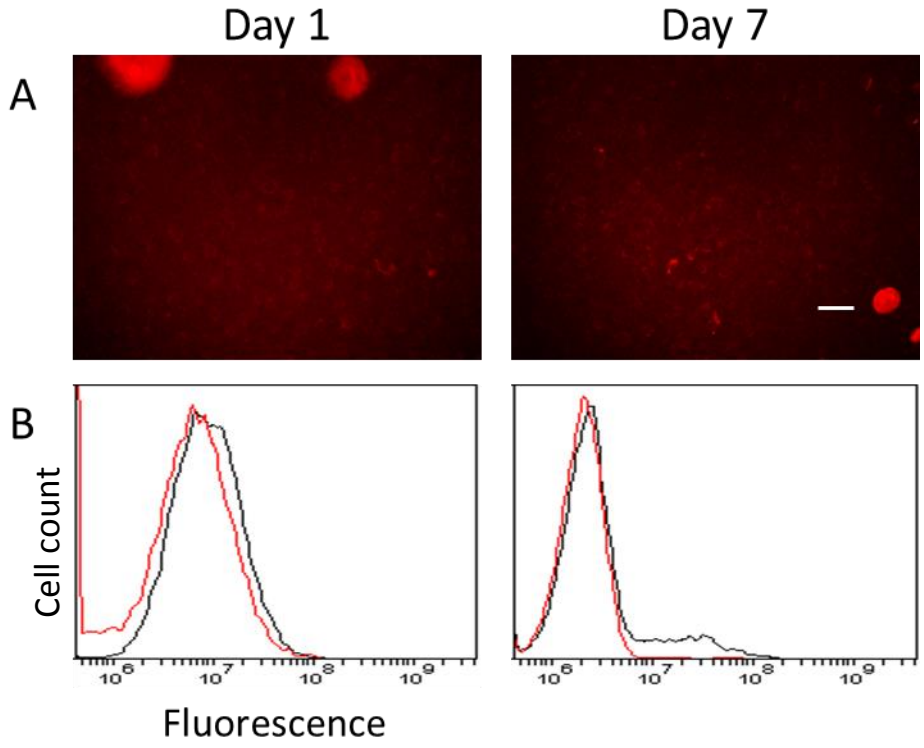


Figure 3.30 Transduction activity of the released P21-mR-8R. Porous MPs were prepared using S/O/W method and loaded with P21-mR-8R (0.5% (w/w)) mixed with L-Histidine (0.25% (w/w)). Transduction activity of the released protein was assessed by addition to plated NIH3t3 cells. (A) Fluorescence microscopy images of the NIH3t3 cells treated with the sampled P21-mR-8R (Scale bar 10 µm). (B) Flow cytometry histograms showing cellular uptake of P21-mR-8R after application of the samples to NIH3t3 cells. The red histograms are the P21-mR-8R samples, while the black histograms are the experimental control.

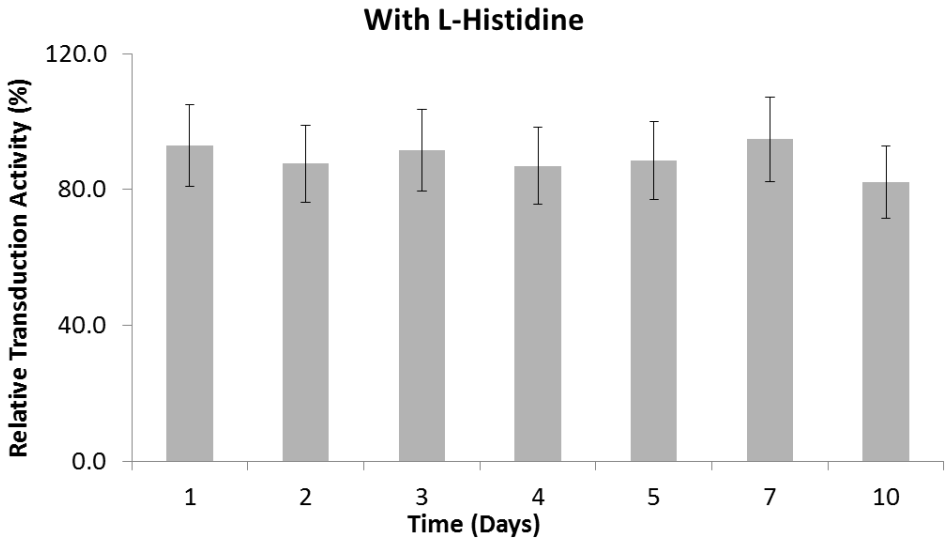


Figure 3.31 Relative biological activity of P21-mR-8R released from PLGA MPs prepared using S/O/W (0.5% w/w) and containing L-Histidine (25% w/w). GET Protein transduction activity was compared to the experiment control. Error bars indicate SD (n = 3).

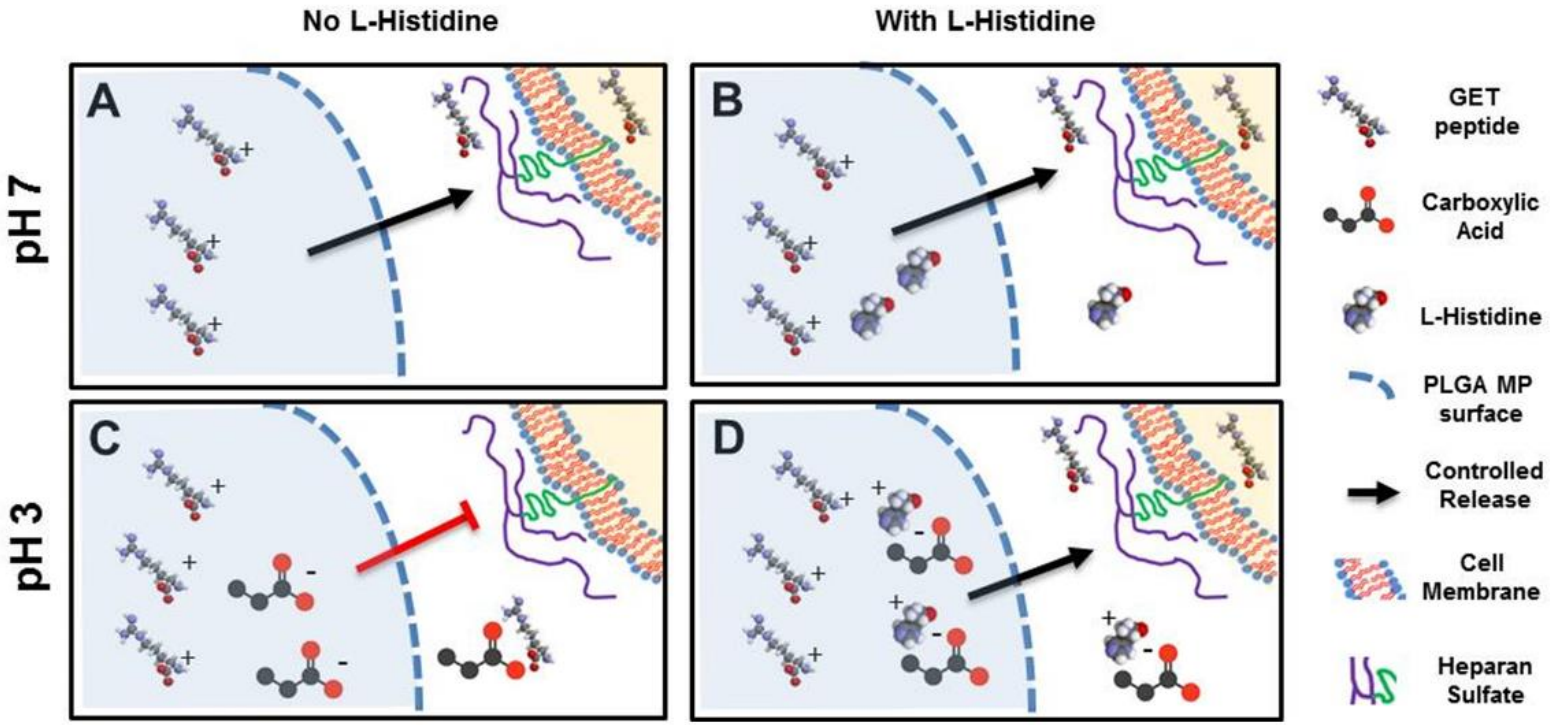


Figure 3.32 Schematic for hypothesis of GET peptide interaction with Carboxyl groups and L-Histidine. Interaction between GET peptide released from MPs and cells in presence of carboxyl groups resulted from PLGA degradation, with and without L-Histidine. (A) pH 7 without L-Histidine. (B) pH 7 with L-Histidine. (C) pH 3 without L-Histidine. (D) pH 3 with L-Histidine.

3.4. Conclusions

The work presented in this chapter evaluated the release profile and activity of the GET peptide (tagged with fluorescent protein) released from PLGA MPs fabricated using S/O/W method.

The release was very low, with 20% of the protein released in the first day, and no further release detected up to 21 days. The PLGA MPs fabrication was modulated to produce porous MPs, using PBS as a porogen in the primary emulsion phase. The produced MPs had some pores on the surface on the MPs without significant influence on the encapsulation efficiency. The release profile was modulated to match the required dose; releasing the contents in the first 7 days. Upon activity evaluation of the released GET peptide conducted, gradual loss of activity was noticed, which later on correlated to the degradation of the PLGA MPs and formation of local acidic environment. L-Histidine was used as a stabilizer to maintain the GET system activity during release from MPs.

Incorporation of L-Histidine in PLGA MPs did not change the protein release profile. The presence of L-Histidine in the MPs enhanced the protein stability in acidic conditions caused by degradation of PLGA. The maintenance of the protein stability by incorporating L-Histidine in PLGA MPs is enough evidence supporting that the GET peptide are interacting with acidic degradation products of the PLGA and the addition of L-Histidine is a successful strategy. The work in the coming chapter will utilise this delivery system to deliver RUNX2 to control cells differentiation.

It was noted that in some conditions, the protein showed higher stability (in presence of L-Histidine) at pH 3 and pH 5 compared to pH 7. This may indicate the suitable storage condition for the protein (i.e. pH 5), however, further studies need to be conducted in future.

Chapter IV:

Development of Injectable Bone System to Study the Effect of GET peptide Loaded Microparticles on Bone Regeneration

4. Development of Injectable Bone system to Study the Effect of GET Peptide Loaded Microparticles on Bone Regeneration

4.1. Introduction

After the development of a controlled release system for GET peptide, the plan was to replace the self-reporter protein (mRFP) with a therapeutic molecule RUNX2. The manufacturing, formulation and release profiles of the PLGA MP detailed in the first two results chapters in this thesis will be utilised for this purpose.

Osteogenic transcription factor, RUNX2 (also called Core-binding factor alpha, CBFa1) is essential for osteoblast commitment, differentiation, matrix production, and mineralization during bone formation [190]. RUNX2 regulates downstream genes that determine the osteoblast phenotype and controls the expression of osteogenic marker genes such as *ALP, OP, OSX, COL1A1* (*type-I collagen), BSP*, and *OCN* [42, 191-193] in response to physiological signals [194]. A recent study performed in our group showed that GET-RUNX2 molecule can be used to direct hMSCs osteogenesis [55], removing the need to use pleiotropic compounds (such as dexamethasone), or growth-factors (such as BMP2) which may trigger unwanted off-target cellular responses, however, this transcription factor needs to be supplied at specific dose over a period of time [55]. The reported dose (i.e. 60μg in the first week) will be used in the controlled release system to overcome the need for repeated administration of RUNX2.

In order to supply a therapeutic molecule locally and to provide a host for cells, scaffolds are usually used [24]. The combination of biomaterials (scaffolds component), cells and therapeutic molecules can be used for localised and targeted regeneration therapies [25].

A novel polymer scaffold formulation has been developed in our group. This formulation undergoes thermo-responsive sintering under physiological conditions to form solid scaffolds [152-154]. The particles in this formulation are composed of a blend of PLGA and poly(ethylene glycol) (PEG). The PEG component acts to lower the glass transition of the mixture to be around the body temperature (i.e. 37°C) [154]. These particles can be suspended in an aqueous carrier to form a paste for use as an injectable defect filler. When the temperature of the paste is raised to 37°C the particles soften and form adhesion bridges to one another. The presence of the carrier then allows the hydrophilic PEG component to leach out. This causes the polymer and thus the particle-to-particle adhesion bridges to re-solidify.

A solid scaffold is formed with mechanical properties which are comparable to those of cancellous bone [152-154]. The mild processing conditions used for the fabrication of these PLGA/PEG scaffolds allow cells to be suspended in the carrier and then be retained and proliferate within the fully-formed scaffolds [153]. Moreover, loaded PLGA MPs can be mixed with the PLGA/PEG particles to allow localised and controlled release of therapeutic molecules.

Various bone structures can be found in the body, for example, mastoid bone is highly porous (above 80% porosity [195]) and have large pore size. On the other hand, the vertebrate have very complex structures and fine details that is hard to mould. In order to provide various scaffolds structures, matching the actual bone properties, it was suggested that 3D printer can be used to provide complex structures with high accuracy. Developing a 3D printable formula can provide solutions to have this variability in structures.

Bio-printing usually starts by having images for the needed structure (CT scan or MRI), then design the structure to be printed based on these images, the material and cells to be printed is then selected [196, 197]

For a material to be printable, some characteristics have to fulfilled, such as; Viscosity, gelation method and rheological properties [158, 196, 197]. Previously, carboxymethyl cellulose (CMC) and pluronic F-127 (PF-127) were used to facilitate PLGA/PEG printing [158]. However, minimal cell viability results were shown in presence of CMC. The aim for the work presented in this chapter was to demonstrate printing of PLGA/PEG with PF-127 and study cell viability and proliferation.

4.1.1. Aims

The aims of this chapter were to:

- Encapsulate GET-RUNX2 molecule in PLGA MPs using the developed formulation and fabrication process.
- Characterise the MPs and evaluate the released GET-RUNX2 activity.
- Formulate scaffolds using PLGAE/PEG thermos-responsive particles with PLGA GET-RUNX2 loaded MPs.
- Seed hMSCs on the prepared scaffolds and evaluate cells proliferation.
- Evaluate seeded hMSCs differentiation in response to released GET-RUNX2 molecule.
- Utilise 3D printing technology to provide complex scaffolds structure and evaluate the need to use potential viscosity enhancer compounds.
- Study the cells proliferation on the printed scaffolds and evaluate the bio-printing feasibility.

4.2.Materials and Methods

4.2.1. Protein synthesis and FITC tagging

CPP (eight arginine, 8R) and heparin binding domain; HBD (P21), which compose the Glycosaminoglycan – binding enhanced transduction (GET) system were tagged with RUNX2 producing P21-RUNX2-8R protein. GET-RUNX2 was expressed and purified from *Escherichia coli* using GST affinity purification as previously described [198].

For protein tracking, P21-RUNX2-8R was tagged with FITC using NHS-Fluorescein as per manufacturers protocol (Thermo Scientific) at a 1:50 protein: label molar ratio and purified/buffer exchanged to PBS using Bio-Spin P-6 spin columns (Bio-Rad).

4.2.2. PLGA Microparticles fabrication

Poly (D,L-lactide-co-glycolide, (PLGA) LA:GA ratio: 50:50; Mw 52 kDa, Evonik Industries, USA) MPs were formed using solid-in-oil- in-water (S/O/W) emulsion as previously described [132, 199]. Briefly, 1 mg of P21-RUNX2-8R, was mixed with 0.5 mg PEG 6000 (Sigma-Aldrich, UK) and 0.25mg L-Histidine (Sigma-Aldrich, UK) and freeze dried overnight. Blank MPs were prepared by freeze drying 0.5 mg PEG 6000 only. PLGA was dissolved in dichloromethane (DCM, Fisher, UK) (200 mg of PLGA was dissolved in 1.5 ml DCM) and added to the freeze dried powder. The solution was then mixed by vortexing. Phosphate buffered saline (PBS), 200µl PBS (Gibco, UK) was added to the solution and vortexed to produce homogenous emulsion. 4ml of 0.25% (w/v) methylcellulose (Sigma-Aldrich, UK) solution was then added to the mixture and vortexed again. The resultant emulsion was then poured into 400 ml of distilled water; and the resultant (S/O/W) emulsion was left stirring for 3 h to allow DCM evaporation.

The hardened MPs were then collected by centrifugation and washed three times by distilled water (DW). The obtained MPs were then freeze dried for 24h.

4.2.3. MP characterization: size and morphology

A thin layer of MPs were placed onto an adhesive stub and gold coated using a SCD030 gold sputter coater (Balzers Union Ltd., Lichtenstein), for five minutes at 30 mA. The morphology of the MPs was assessed by scanning electron microscopy (SEM), using a JEOL 6060L imaging system (JEOL Ltd., Hertfordshire, UK) with the accelerating voltage set to 10 kV.

The mean MP diameter and size distribution were measured using a Coulter LS230 particle size analyser (Beckman, UK). MPs were suspended in HPLC grade water, under stirring conditions. Size distribution data was collected after achieving an obscuration value of 8–12%.

4.2.4. MP characterization: Determination of protein loading (loading efficiency)

Measurement of protein content in the MPs was conducted as previously described [168, 169, 199]. 10 mg of PLGA MPs were added to 750µl DMSO and shaken until completely dissolved; 2150µl of 0.02% (w/v) SDS in 0.2 M NaOH was then added and incubated at room temperature until clear solution is obtained. The Micro BCA protein assay kit was used to measure the total protein content and compared against a freshly generated standard curve of P21-RUNX2-8R. 150µL sample volume was mixed with 150µL µ-BCA working reagent and incubated at 37 ºC for 2 h. Absorbance at 562 nm was then measured using a plate reader (Infinite M200, Tecan UK Ltd.).

4.2.5. MP characterization: P21-RUNX2-8R release

MPs were suspended in 1 ml Growth media (GM) or HBSS. Samples were rocked on a 3D shaker (Gyrotwister, Fisher Scientific UK Ltd) at 5 rpm in a humidified incubator at 37 ºC. At defined time points, samples were centrifuged and the supernatant was removed from the MPs and replaced with fresh GM or HBSS. The supernatants were assayed for protein content using µBCA assay kit (HBSS samples). Released protein contents were compared against freshly generated standard curve of P21-RUNX2-8R.

4.2.6. Cell culture

Human Mesenchymal Stem Cells (hMSCs) were purchased from Lonza (21 year old male donor) and were maintained in growth medium (Lonza) in 5% (v/v) CO2 humidified incubator at 37ºC. hMSCs were sub-cultured at 80% confluence preventing spontaneous differentiation and contact inhibition of growth. hMSCs were used between passage 4 and 6 for all experiments.

4.2.7. GET peptide transduction activity

40,000 cells/well (in 24-well plates) were seeded; incubated for 6 hours for attachment. Culture media was then replaced with the media containing the released P21-RUNX2-8R-FITC protein (protein released from MPs). After overnight transduction, cells were washed with PBS, trypsinized with Trypsin-EDTA (Lonza) and fixed in 4% (w/v) PFA (Sigma) for flow cytometry. Transduction activity term will be referred to as indication of the protein biological activity and ability of internalisation within cells.

4.2.8. Luciferase reporter assay

Cells were transfected with firefly luciferase reporter (kindly gifted by Dr Haijun Zhang, Indiana University) mOG2-Luc along with the internal control, Renilla luciferase reporter pRL-TK as previously described [200]. hMSCs were transduced with the P21-RUNX2-8R proteins released from MPs (Section 4.2.5) before & after transfection. As a positive control to compare the promoter activity, hMSCs were transfected with pSIN-RUNX2 plasmid DNA (1 μg) (as described in Dixon et. al) [201] using Lipofectamine 2000 (Invitrogen) and analysed the luciferase activity. Fresh P21-RUNX2-8R equivalent to the quantity of protein released from MPs was transduced into another samples to compare the activity of the released protein vs fresh protein sample of the same concentration. Relative luciferase activities were measured using dual luciferase assay kit (Promega).

4.2.9. Flow cytometry and microscopy

Fixed cells were analysed on a Beckman Coulter Astrios EQ Flow Cytometer using 488 laser. (20,000 cells; gated on live cells by forward/side scatter). Mean fluorescence was used for statistical analyses with background from un-transduced cells subtracted and values were then calculated in ratio to the experimental control. For fluorescence imaging, cells were imaged with fluorescence microscope using a TRITC filter (Leica DM IRB).

4.2.10. PLGA/PEG particle production

Particles were fabricated from blends of poly(DL-lactic acid-co-glycolic acid) (PLGA) 85:15 53 kDa (Lakeshore Biomaterials, USA) and poly(ethylene glycol) 400 (PEG) (Sigma Aldrich) as previously described by Dhillon et al. [152, 202].

Briefly, a mixture of 93.5%:6.5% PLGA:PEG (w/v) was blended at 80–90°C, mixed and allowed to cool. Cooled polymer was ground into particles and sieved to obtain the 50–100 μm size fraction.

The resultant particles were mixed with different carriers of different concentrations and ratios for paste formation or 3D printing. Table 4.1 summarises the used carriers, concentrations and ratios. The paste was left to sinter at 37°C to allow scaffolds formation.

Table 4.1 List of carriers (concentration and ratio) used to prepare scaffolds. Scaffolds were sintered at 37°C.

Carrier	Concentration (%) v/v	Ratio (PLGA/PEG : Carrier)
PBS	-	1 : 0.6
TriAcetin	0.5, 1, 2.5 & 5	1 : 0.6
Pluronic	18	1: 1.5
Pluronic - Triacetin	18 – 2.5 18 – 1	1:0.6 1:1.5

4.2.11. Scaffold preparation

Scaffolds were prepared in PTFE moulds producing cylindrical scaffolds of 3 mm length and 6 mm diameter. PLGA/PEG particles were mixed with P21-RUNX2-8R loaded MPs (or blank MPs for blank scaffolds). The mixture was then mixed with PBS at a ratio of 1:0.6 (mixture: PBS). The paste was packed into the mould which was placed at 37°C for 2 hours to allow scaffold formation.

4.2.12. Cell seeding on scaffolds

50,000 cell in 20μL suspension was seeded per scaffold. The scaffolds were incubated for 1 hour at 37ºC, to allow attachment, prior to addition of 1ml media to each well.

4.2.13. Osteogenesis assay

DMEM: F12 media (Life technologies) supplemented with 10% (v/v) fetal bovine serum, 2mM L-glutamine, 100 units/ml penicillin and 100 µg/ml streptomycin (Sigma) was used as the basal media for osteogenic media. 50,000 cells per scaffold (containing blank MPs or P21-RUNX2-8R loaded MPs) were seeded and cultured for four weeks depending on the experiment with appropriate media. 50 µg/ml L-Ascorbic acid 2-phosphate sesquimagnesium salt hydrate (Sigma) and 10 mM β glycerophosphate disodium salt pentahydrate (Acros organics) were added to the basal media for osteo-permissive medium. To make osteo-inductive media, 100 nM Dexamethasone (Sigma) was added to the osteo-permissive medium. Cells were cultured for three to four weeks for complete osteogenesis. Medium was changed every other day.

4.2.14. Cell viability assay

The PrestoBlue cell viability assay (Invitrogen Life Sciences, UK) was performed on day 3, 6 and 9 post-seeding on three scaffolds per time point. Each scaffold was submerged in 900µl of media, and 100µl of Prestoblue was added to each well. The scaffolds were then incubated at 37ºC for 2 hours. Three 100µl media samples were taken from each well and were read on Tecan plate reader with the excitation wavelength set to 560 nm and the emission wavelength set at 590 nm. The results were then compared with standard curve to calculate number of cells.

4.2.15. Alkaline phosphatase (ALP) assay

The expression of ALP was measured at day 7 using a SigmaFAST pNPP kit. Scaffolds were transferred to new 24 well plate and pNPP solution, made to

manufacturer's guidelines, was added (500µl) to the wells and incubated at 37ºC for 45 minutes. Absorbance at 405 nm was then measured (three readings per well) using Tecan plate reader.

4.2.16. Osteocalcin immunostaining

After 14 days, scaffolds were rinsed with PBS, fixed in 4% (w/v) PFA (Sigma) in deionized water for 20 min, stained with antibody osteocalcin (OCN) (Millipore; 1:200), detected with secondary antibody Alexa Fluor 546 (Abcam) and viewed using Leica TCS SPE confocal Macroscopy.

4.2.17. Von kossa staining

After 21 days, scaffolds were washed three times with deionized water and fixed with 4% (w/v) PFA and washed three times with deionised water. Scaffolds were incubated with 1% silver nitrate solution (sigma) under exposure to UV light for 60 minutes. Scaffolds were then washed with deionized water 3 times and then with 2.5% sodium thiosulfate solution (Sigma) for 3 times. Scaffolds were then washed again three times with deionized water. Mineralized nodules were visualized as black spots using Nikon SMZ1500 dissection microscope.

4.2.18. Gene Expression analysis

The scaffolds with hMSCs were homogenised with RLT buffer (RNAeasy kit) using a hand-held homogenizer and total RNA was extracted using QIAShredder (Qiagen) and RNAeasy kit (Qiagen) according to the manufacturer's instructions. RNA samples were treated with DNase I (Invitrogen), quantified using a NanoDrop 1000 spectrophotometer (Thermo-Fisher). Osteogenic genes (RUNX2 – Hs00231692_m; OSX/SP7 – Hs00541729_m1; OPN –

Hs00959010_m1) were determined relative to ACTB according to the TaqMan gene expression assay protocol (Applied Biosystems/ Life Technologies). TaqMan primers and probes were from Applied Biosystems. All TaqMan PCR reactions were performed in triplicates with three biological repeats.

4.2.19. µCT

Samples were analysed using Skyscan 1172 (Skyscan, Belgium) desktop x-ray CT scanner with a pixel resolution of 12.2 µm, x-ray source current 800 µA and voltage 50 kV. Samples were mounted vertically and rotated thorough 360°. Captured images were then reconstructed using the NRecon software (Skyscan, Belgium). The construct was then analysed with 3D histomorphometric using the CTAn software by thresholding the sample lower grey 20 upper grey 150. For the reconstruction of the cell-seeded samples, cells were stained with osmium tetroxide and the previous method was used to distinguish the cells from the 3D pictures. The thresholds for the cells were lower grey 155 and upper grey 255. Materialise 3-matic software (version 9) was used for images overlay.

4.2.20. 3D printing of PLGA/PEG composites

The RegenHU 3D Discovery (Switzerland) was used for 3D printing with Huber Pilot ONE temperature controller (Switzerland). PLGA/PEG particles (50 – 100 µm) were mixed by spatula with different carriers at 4°C before being transferred into a syringe. The syringe was then placed into the printer and allowed to equilibrate with the printing temperature. During printing, the pressure was manually adjusted (1-3 bar) to ensure adequate flow of material through the 20 gauge (0.61mm) tapered syringe tip (adhesive dispensing Ltd. UK). The print speed varied between 20 and 60 mm/s. BioCAD software (RegenHU) was used

to design the lattice structure to be printed. Dissection microscope Nikon SMZ1500 was used to image the printed structures.

4.2.21. Statistical analysis

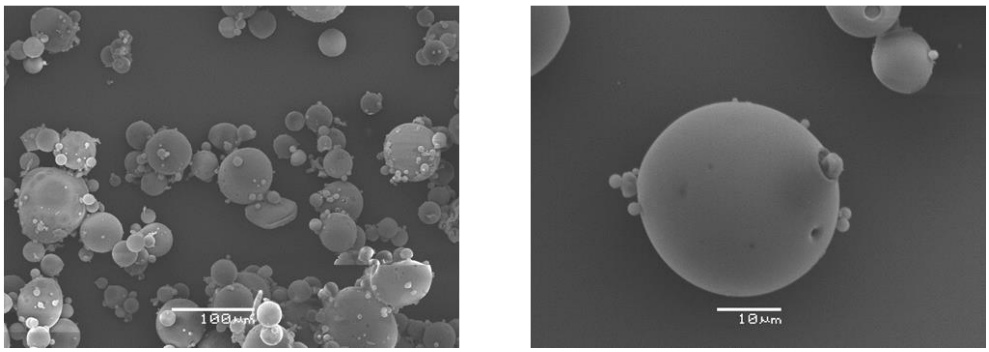
Statistical analysis was carried out using GraphPad Prism (version 7). The statistical significance was determined using one way ANOVA with Holm-Sidak post hoc test for ALP study. Results were considered significant at $p < 0.05$, mean values are given plus or minus the standard deviation (SD).

4.3. Results

4.3.1. RUNX2-GET peptide loaded PLGA microparticles characterisation: morphology, size & entrapment efficiency

PLGA MPs were fabricated using an optimized S/O/W emulsion process and encapsulated a GET-tagged RUNX2 protein (P21-RUNX2-8R-FITC). PBS was added to the formulation to accelerate the protein release. L-Histidine was added to protect GET peptide during release, as previously shown. MPs prepared using the S/O/W method showed spherical structure with smooth and porous surface due to the addition of PBS (Figure 4.1). The mean diameter of these MPs was 36.5 ± 7.2 μm, with average loading efficiency of 58.4 ± 7.0% (Figure 4.1). P21-RUNX2-8R loaded MPs average diameter was comparable to these loaded with P21-mR-8R (36.5μm ±7.2 vs 42.3μm ±9.1 respectively), they were both in the same targeted size range (30 - 50μm). Moreover, encapsulation efficiency was feasible and comparable to the previously shown using P21-mR-8R (58.4% vs 67.4%). This finding demonstrates that the developed S/O/W fabrication method is robust and can give microparticles in the same size range with workable encapsulation efficiency.

A



B

Microparticles Formulation	Size (µm) mean ± SD	Loading efficiency (%) mean ± SD
PLGA-PBS-Histidine	36.5 (7.2)	58.4 (7.0)

Figure 4.1 P21-RUNX2-8R-FITC loaded MPs characterization. MPs were fabricated using PLGA (50:50), loaded with P21-RUNX2-8R-FITC (0.5% (w/w)), and mixed with PBS 0.1% (w/w) and L-Histidine 25% (w/w). (A) SEM analyses for MPs (scale bars represent 100µm on left image, and 10µm on right image). (B) Summary of size characterization and corresponding loading efficiencies (n = 3).

4.3.2. RUNX2-GET peptide release from PLGA microparticle

The needed dose was previously mentioned by Thiagarajan et. al. [55], 60µg of P21-RUNX2-8R is needed to be delivered in the first week, in two doses. P21-RUNX2-8R release profile was optimised (using PBS to make MPs porous to accelerate the release and using the MPs in this size range to increase the surface area of release) to have release quantities matching the dose need of RUNX2 to initiate differentiation.

The release profile showed comparable P21-RUNX2-8R quantities (i.e. 30µg in the burst release phase and another 30ug over 5 days) (Figure 4.2) moreover, this represents more than 90% of the protein loaded in MPs, which guarantees that minimal quantities protein will be released after the first week. This is necessary as RUNX2 is needed predominantly during the early stages of osteogenesis and overexpression of RUNX2 during the late stages delays matrix mineralization [203].

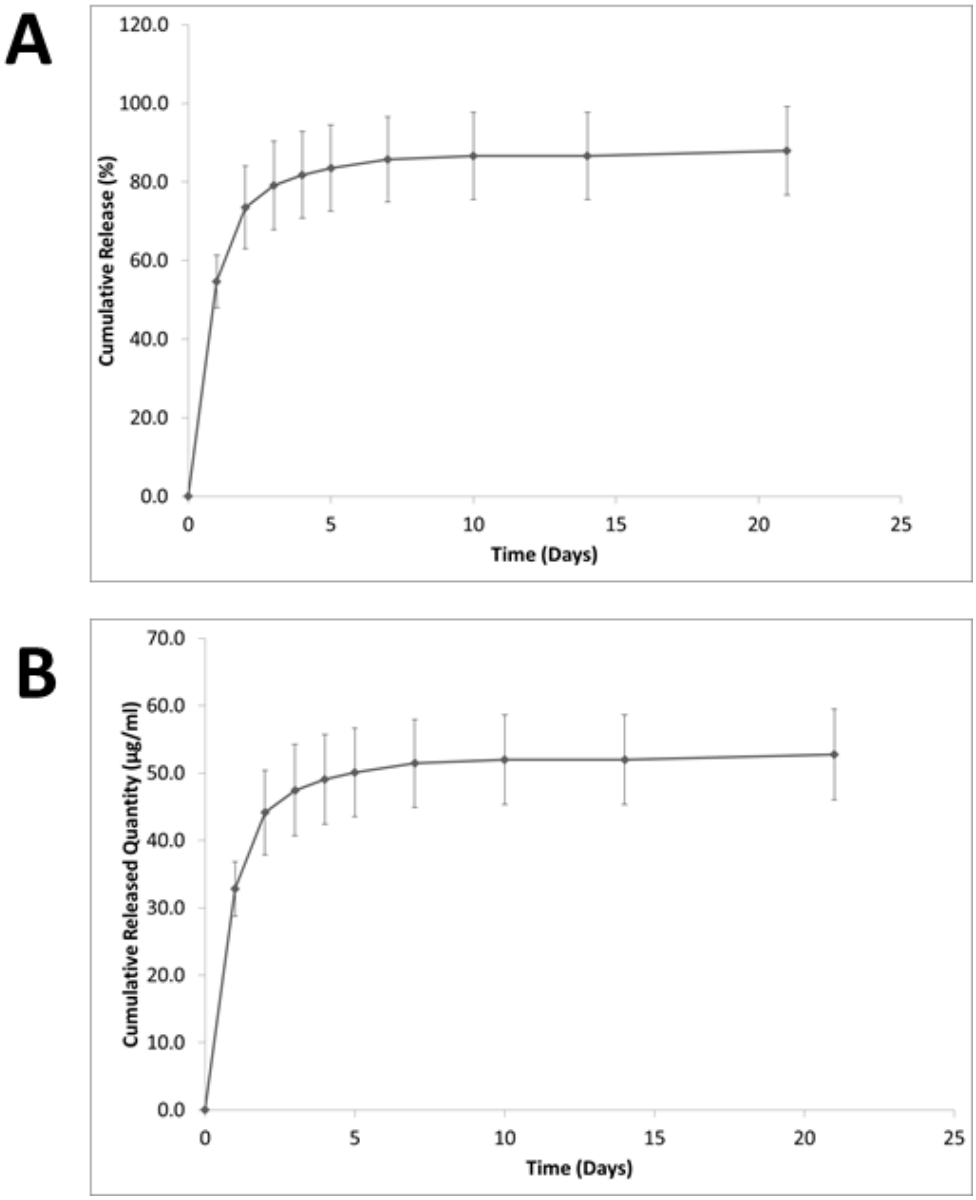


Figure 4.2 In vitro release profiles of P21-RUNX2-8R-FITC from PLGA MPs (pH 7.4 at 37 ºC). MPs were fabricated using PLGA (50:50), loaded with P21-RUNX2-8R-FITC (0.5% (w/w)), and mixed with PBS 0.1% (w/w) and L-Histidine 25% (w/w). Protein release was quantified using Micro BCA assay kit (A) Relative cumulative protein release. (B) Cumulative protein quantity. Error bars indicate SD (n = 3).

4.3.3. Biological activity evaluation of the released GET-RUNX2 using hMSC

After showing efficient release of P21-RUNX2-8R in the required dose over identified period using the fabricated PLGA MPs, it was crucial to show that the released protein retained the biological activity (both GET peptide and RUNX2). PLGA MPs were fabricated to maintain the biological activity of GET peptide by incorporation of L-Histidine encapsulated with P21-RUNX2-8R. The L-Histidine is needed to maintain the activity of GET peptide upon increased acidity in the microenvironment, as shown in the previous chapter. The biological activity of the protein was confirmed by comparing the released P21-RUNX2-8R-FITC to non-encapsulated controls. Released P21-RUNX2-8R-FITC was collected over the 7 day time course and was incubated with plated hMSCs to assess internalization, transduction and transcriptional ability. Importantly the released samples activity was compared to non-encapsulated controls diluted to the same final concentration. Incubated cells were then evaluated for transduction by fluorescence microscopy and flow cytometry analyses (Figure 4.3 and 4.4).

Fluorescent microscopy showed significant GET protein internalization for the collected samples released from PLGA MPs (Figure 4.3). Flow cytometry results showed high transduction activity with relative transduction activity above 70% for all the studied samples (Figure 4.4). Therefore it was clear that the released protein retained their transduction activity throughout out the release period.

In order to study the transcriptional activity of the released P21-RUNX2-8R, the immediate transcriptional activation of RUNX2-responsive luciferase reporters containing the transcriptional responsive sequence from the OSTEOCALCIN (OCN) promoter was tested. This test was previously mentioned by Thiagarajen et. al [55]. The activity of the released P21-RUNX2-8R samples were compared with non-encapsulated P21-RUNX2-8R.

We observed that the released P21-RUNX2-8R induces mOG2-Luc reporter expression to a magnitude comparable to the fresh P21-RUNX2-8R (Figure 4.5) (i.e. 1.57 (±0.51) fold verses 2.2 (±0.21) fold respectively). These findings indicate that the released P21-RUNX2-8R retained its transduction and transcriptional activity upon delivery from PLGA MPs.

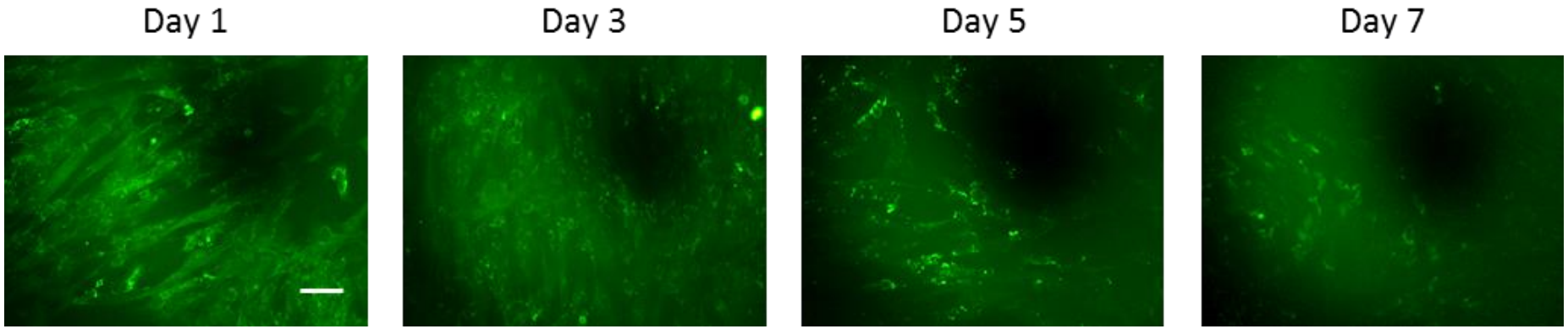


Figure 4.3 Transduction activity of the released P21-RUNX2-8R-FITC. PLGA MPs were prepared using S/O/W method, loaded with P21-RUNX2-8R-FITC (0.5% (w/w)). Transduction activity of the released protein was assessed using hMSC in monolayer. Representative fluorescence microscopy images of the hMSCs treated with the sampled P21-RUNX2-8R-FITC (Scale bar represents 100μm).

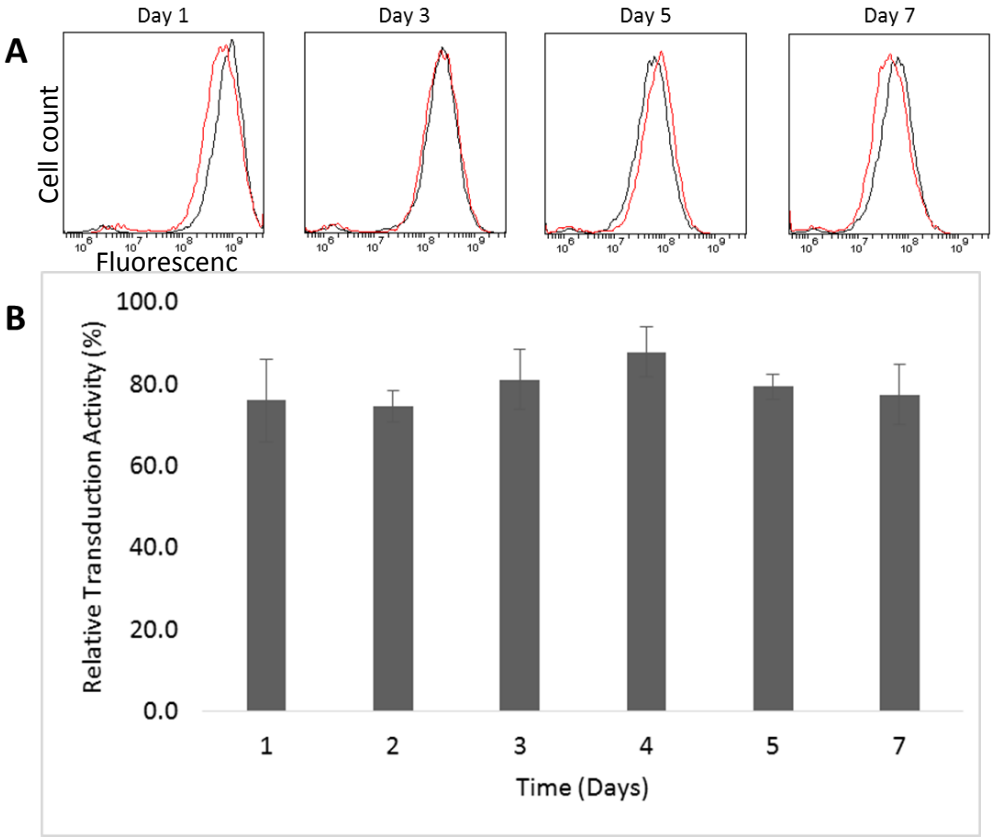


Figure 4.4 Relative transduction activity of the released P21-RUNX2-8R-FITC. PLGA MPs were prepared using S/O/W method, loaded with P21-RUNX2-8R-FITC (0.5% (w/w)). Transduction activity of the released protein was assessed using hMSC in monolayer. (A) Flow cytometry histograms showing cellular uptake of P21-RUNX2-8R-FITC on hMSCs. The red histograms are the P21-RUNX2-8R-FITC samples, while the black histograms are the experimental control. (B) Relative transduction activity of released P21-RUNX2-8R-FITC. Protein activity was compared to the experiment control. Error bars indicate SD (n = 3).

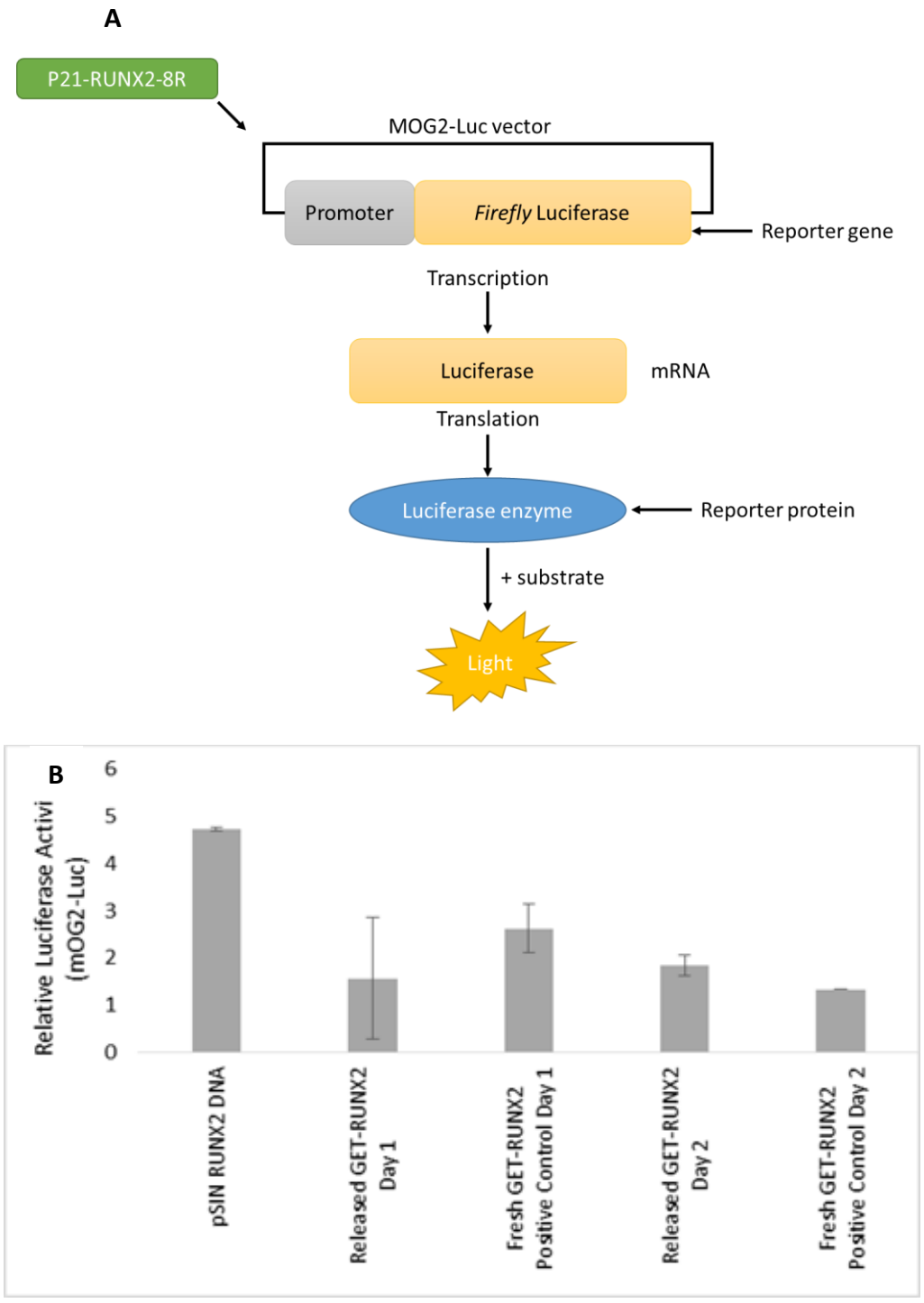


Figure 4.5 Relative transfection activity of the released P21-RUNX2-8R-FITC. PLGA MPs were prepared using S/O/W method, loaded with P21-RUNX2-8R-FITC (0.5% (w/w)). (A) Schematic showing the experimental procedure. (B) Transcriptional activity of the released P21-RUNX2-8R-FITC measured using luciferase reporter gene assay. Error bars indicate SD (n = 3).

The challenging issues in controlled release system are encapsulating and releasing biologically active molecules [125, 126]. We have previously shown that GET peptide activity is compromised in presence of carboxylic acid group produced upon PLGA degradation. The use of L-Histidine was shown to maintain the activity of GET peptide upon release. Consequently, L-Histidine was added to the formulation with the encapsulated P21-RUNX2-8R. In order to validate the biological activity for P21-RUNX2-8R post release, the activity of the released protein was tested. The results showed that the released P21-RUNX2-8R has activity comparable to the experimental controls, confirming our previous findings and validating our delivery system for targeted delivery of therapeutic molecules.

4.3.4. Injectable bone scaffolds formation and characterisation: cell attachment and proliferation

In order to have a vehicle for cells and MPs, and in order to have a localised delivery of P21-RUNX2-8R, scaffolds were prepared aiming to incorporate the fabricated MPs and seed the cells on them. The previously developed temperature sensitive scaffold (composed from PLGA/PEG) was used [152-154]. This system allows incorporation of PLGA MP with the PLGA/PEG particles that will sinter at 37°C, while at room temperature will form a paste once mixed with carrier. PLGA/PEG temperature sensitive particles were prepared as shown in figure 4.6. PLGA MPs were mixed with the PLGA/PEG material before the sintering, the material was then loaded into PTFE mould creating a cylindrical shape scaffold (3mm x 6mm).

After scaffolds sintering, hMSCs were seeded on the scaffolds for attachment. PrestoBlue was performed on days 3, 6 & 9 to check cells proliferation on scaffolds. The results showed that the scaffold is conducive for cell proliferation (i.e. the cell number increased from around 40,000 at day 3 to around 65,000 at day 9) (figure 4.6). SEM images showed a different morphology for cell-seeded scaffolds (compared to non-seeded scaffold) with cells covering the scaffolds with no pores on the surface (figure 4.6).

Scaffolds were formed by mixing thermo-sensitive PLGA/PEG particles with PLGA MPs, PBS was used to create a paste like material and packed in a PTFE mould and left for 2 hours at 37ºC for sintering. This technology was previously described by Dhillon et al. [152-154, 204]. The ability to paste the scaffold at a defect site can offer improved clinical application when compared to metallic implants.

PLGA/PEG scaffolds have potential to be used *in vivo*, the ability of hMSCs to grow on the scaffolds *in vitro* was assessed. The results showed attachment and proliferation of hMSCs on the scaffolds over a 9-day period, demonstrating the potential for cells to proliferate on the scaffolds, which has implications for their successful use for bone repair *in vivo*.

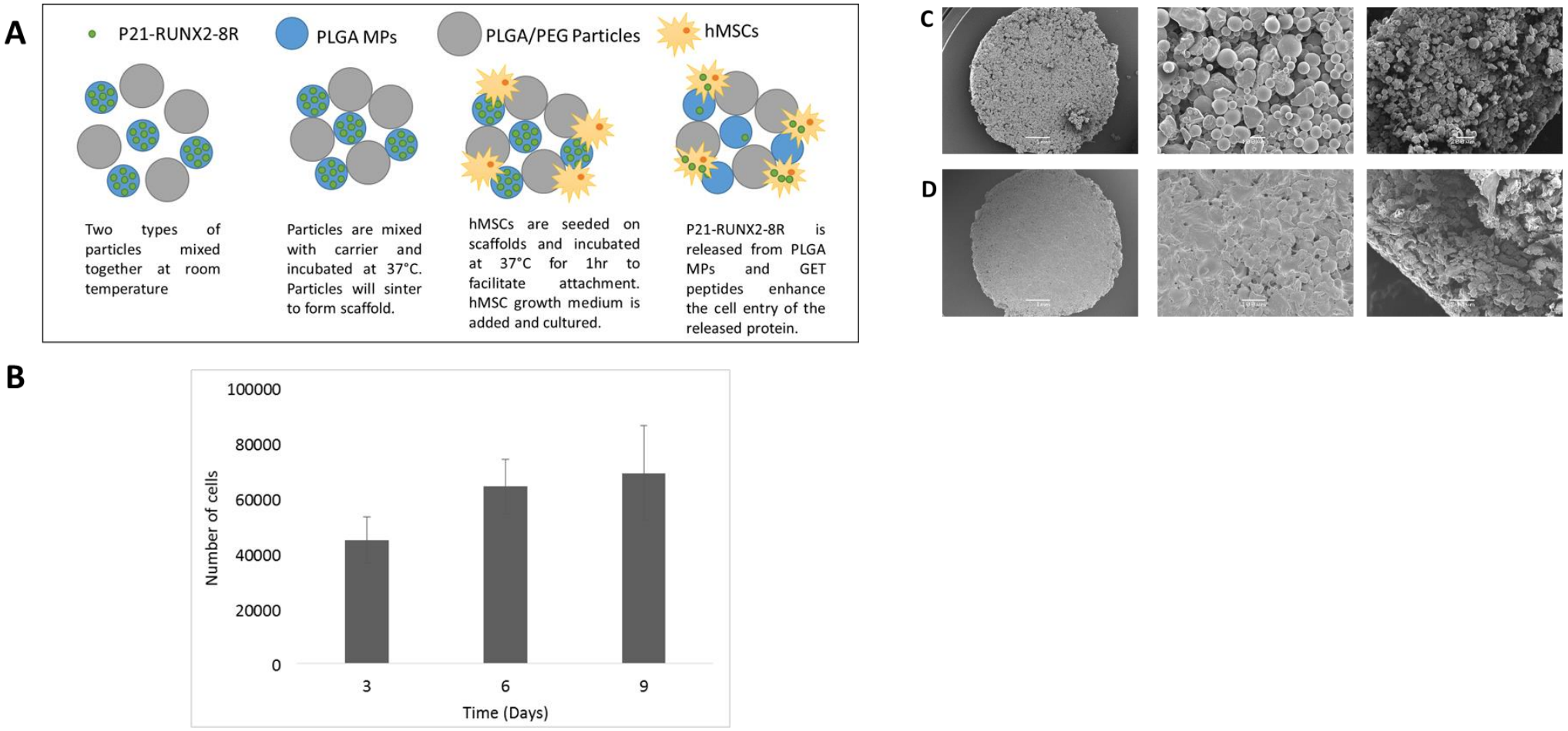


Figure 4.6 Cell attachment and proliferation on scaffolds. (A) Schematic of scaffolds fabrication and cell attachment on scaffolds. (B) Number of viable hMSCs measured by the Prestoblue metabolic activity on day 3, 6 and 9 post-seeding. (C) SEM images of scaffolds without cells (scale bar as indicated). (D) SEM images of cell-seeded scaffolds 3 days post-seeding (scale bar as indicated). Right images are for scaffolds cut in half to show internal morphology (scale bar as indicated).

4.3.5. Cell differentiation on injectable bone scaffolds containing RUNX2-GET peptide loaded PLGA microparticles

To prove that these scaffolds can template the cells and loaded MPs, a cell differentiation study was performed. For hMSC osteogenic differentiation *in vitro*, ascorbic acid and β-glycerophosphate (AB) are essential for final stages of bone nodule formation by promoting collagen matrix production and providing inorganic phosphate for mineralization, respectively. In order to test the effect of P21-RUNX2-8R bone differentiation, this media condition termed 'osteo-permissive' was used during the differentiation study. hMSCs were seeded on scaffolds containing either P21-RUNX2-8R loaded MPs or blank MPs. Osteo-inductive media containing 100nM Dexamethasone (along with ascorbic acid and β-glycerophosphate) was used as a positive control along with scaffolds containing blank MPs. Differentiation was assessed at different stages by the following tests, ALP quantification and gene expression at week 1, Osteocalcin staining and gene expression at week 2, and von kossa staining at week 3.

4.3.5.1. ALP quantification

Alkaline phosphatase (ALP), which is responsible for the mineralization of the extracellular matrix (ECM) [205, 206], is usually used to describe osteogenic differentiation progression [205-207]. ALP expression levels were evaluated as an early differentiation marker. ALP assay was performed on three types of scaffolds; blank scaffold in osteo-permissive media, blank scaffold in osteo-inductive media (DAB) and P21-RUNX2-8R loaded scaffold in osteo-permissive media. The ALP expression, as measured by absorbance at 405 nm, was comparable between P21-RUNX2-8R loaded scaffolds and the scaffolds

cultured in osteo-inductive media and significantly higher than the blank scaffolds cultured in osteo-permissive media (figure 4.7). This finding proved that P21-RUNX2-8R released from PLGA MPs could elicit a biological response on the surrounding cells.

4.3.5.2. Osteocalcin staining

Osteocalcin (OCN) is a bone-specific protein synthesized by osteoblasts and its expression can confirm full osteogenic commitment before progression towards bone nodule formation [207-209]. Accordingly, OCN expression was tested at day 14. The previously mentioned scaffolds were stained for OCN. The results were comparable for scaffolds seeded in osteo-inductive media and scaffolds containing P21-RUNX2-8R loaded MPs, on the other hand there was no evidence of OCN formation in blank scaffold seeded in osteo-permissive media (figure 4.8).

4.3.5.3. Von Kossa staining

Mineralisation was tested using von kossa staining utilising silver nitrate at day 21. Bone nodules were spotted in scaffolds seeded in osteo-inductive media and scaffolds containing P21-RUNX2-8R loaded microparticles. This former confirms that P21-RUNX2-8R can stimulate osteogenic differentiation on hMSCs seeded on scaffolds.

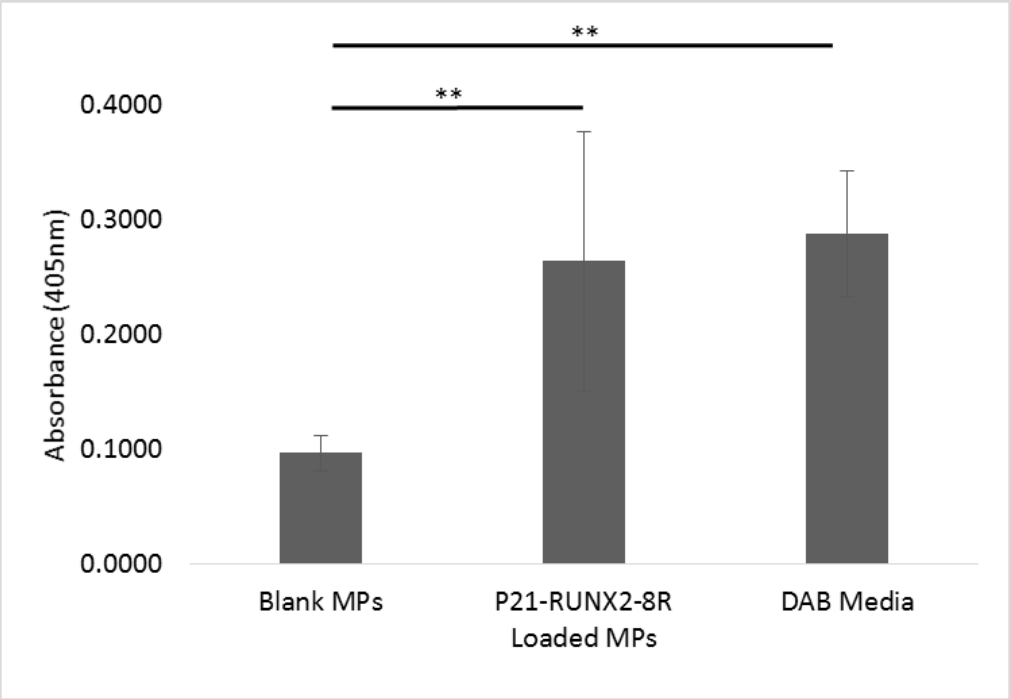


Figure 4.7 Cell differentiation on scaffolds. ALP expression after week 1 for hMSCs seeded on scaffolds in osteo-permissive and osteo-inductive media (DAB). Blank MPs represents cell seeded scaffold containing blank MPs cultured in osteo-permissive media. Loaded MPs represents cell-seeded scaffolds containing P21-RUNX2-8R-loaded MPs cultured in osteo-permissive media. DAB media represents cell seeded scaffolds containing blank MPs cultured in osteo-inductive media (DAB). ** is $P < 0.01$.

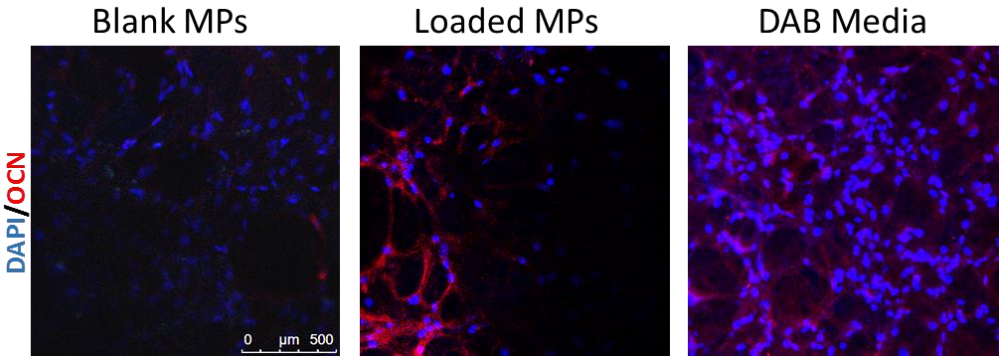


Figure 4.8 Cell differentiation on scaffolds. Osteocalcin staining at week 2 samples (scale bar as indicated). Blank MPs represents cell seeded scaffold containing blank MPs cultured in osteo-permissive media. Loaded MPs represents cell-seeded scaffolds containing P21-RUNX2-8R-loaded MPs cultured in osteo-permissive media. DAB media represents cell seeded scaffolds containing blank MPs cultured in osteo-inductive media (DAB).

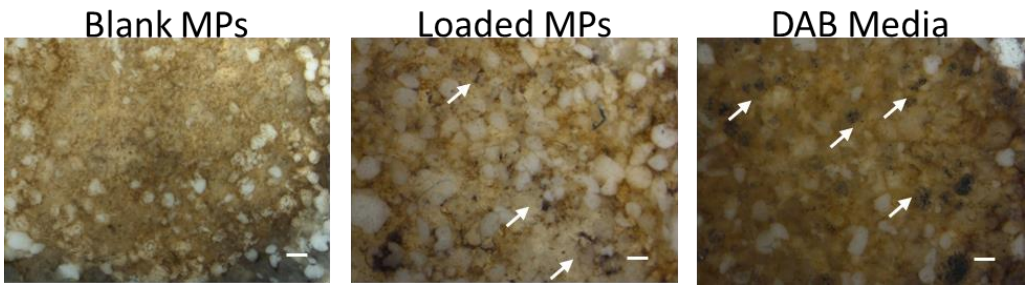


Figure 4.9 Cell differentiation on scaffolds. Von Kossa-stained samples at week 3, calcified deposits are indicated by white arrows (scale bar is 1mm). Blank MPs represents cell seeded scaffold containing blank MPs cultured in osteo-permissive media. Loaded MPs represents cell-seeded scaffolds containing P21-RUNX2-8R-loaded MPs cultured in osteo-permissive media. DAB media represents cell seeded scaffolds containing blank MPs cultured in osteo-inductive media (DAB).

4.3.5.4. Gene expression (qPCR)

Finally, we studied the molecular effects of RUNX2 loaded MPs on early and late osteogenic genes in hMSCs. Significant activation of osteogenic genes can be observed in RUNX2 loaded cells in both week 1 and 2. As expected, RUNX2 loaded MPs released active P21-RUNX2-8R which induced endogenous *RUNX2* expression in hMSCs after week 1 (Figure 4.10). *OSTERIX (OSX)*, one of the prime target gene for RUNX2 is significantly activated (8.2 fold over non-induced control; $p<0.05$) in week 1 of RUNX2 loaded hMSCs (Figure 4.10). Expression of these two genes in RUNX2-loaded MP cells were similar to cells cultured on scaffolds in osteo-inductive medium (positive control). *OSTEOPONTIN (OPN)*, a notable bone matrix protein [210] however was lower in RUNX2-loaded MP cells in comparison to positive control cells. This might be due to the continuing release of RUNX2 which is delaying the terminal differentiation of the hMSCs in comparison to the positive control.

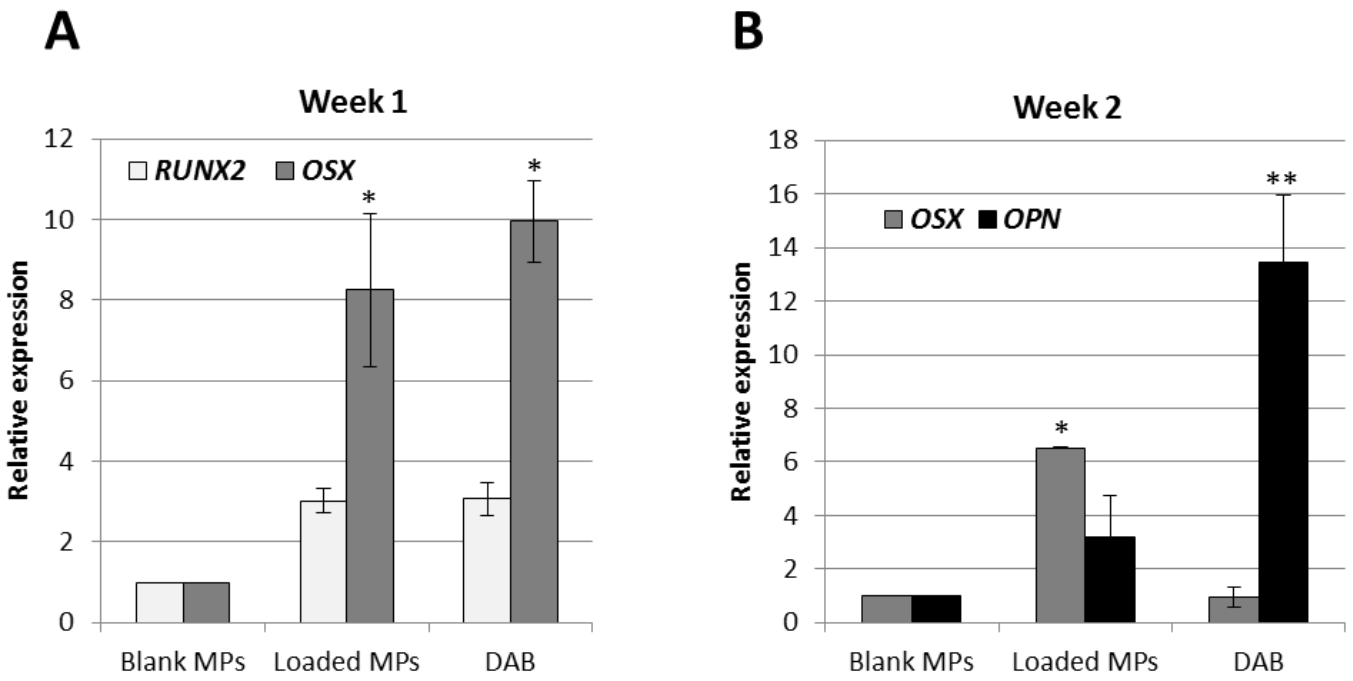


Figure 4.10 Gene expression analysis on scaffolds at week 1 and 2. Blank MPs represents cell-seeded scaffold containing blank MPs, cultured in osteo-permissive media. Loaded MPs represents cell-seeded scaffolds containing P21-RUNX2-8R loaded MPs, cultured in osteo-permissive media. DAB represents cell-seeded scaffolds containing blank MPs, cultured in osteo-inductive media. RNA was extracted from cells at week 1 (A) and week 3 (B) and gene expression analysis was performed. The results were plotted based on expression fold change to non-induced hMSCs on blank scaffold. Statistical analysis was performed using two-way ANOVA in comparison with the non-transduced hMSCs, α=0.05. Error bars indicate SD.

4.3.6. Scaffold characterisation: SEM and Micro-CT

SEM evaluation of scaffolds was done at day 21. Non-seeded scaffolds (kept in media for 21 days) was tested to evaluate polymer degradation. The cell seeded scaffolds showed less porosity as the cells were covering the surface. The cells were seen to grow on the surface, as shown in the scaffolds cut in half, this can be attributed to low porosity of the prepared scaffolds. The media used (osteo-permissive or osteo-inductive) did not have an impact on cell morphology, as in both cases the cells covered the scaffolds with no noticeable difference (figure 4.11).

The microstructure evaluation of scaffolds (using micro-CT) showed comparable results between all scaffolds. The cell distribution was mainly on the surface of the scaffolds, with little cells within the scaffold structure, this may be due to low porosity of the scaffolds (figure 4.12).

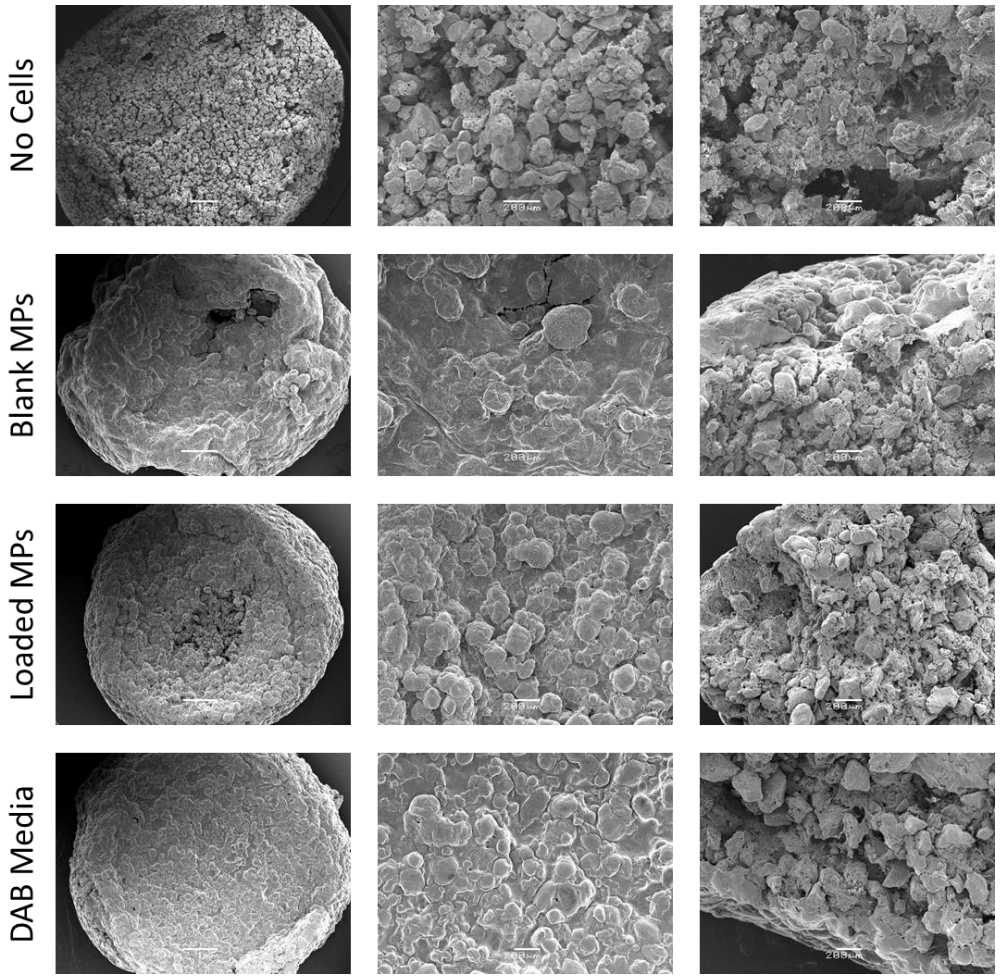


Figure 4.11 SEM images of scaffolds at day 21. SEM images of scaffolds with and without cells cultured in growth media for 21 days. No cells represents scaffold prepared from blank MPs without cells kept in osteo-permissive media. Blank MPs represents cell-seeded scaffold containing blank MPs cultured in osteo-permissive media. Loaded MPs represents cell-seeded scaffolds containing P21-RUNX2-8R loaded MPs cultured in osteo-permissive media. DAB media represents cell seeded scaffolds containing blank MPs cultured in osteo-inductive media. Right images are for scaffolds cut in half to show internal morphology.

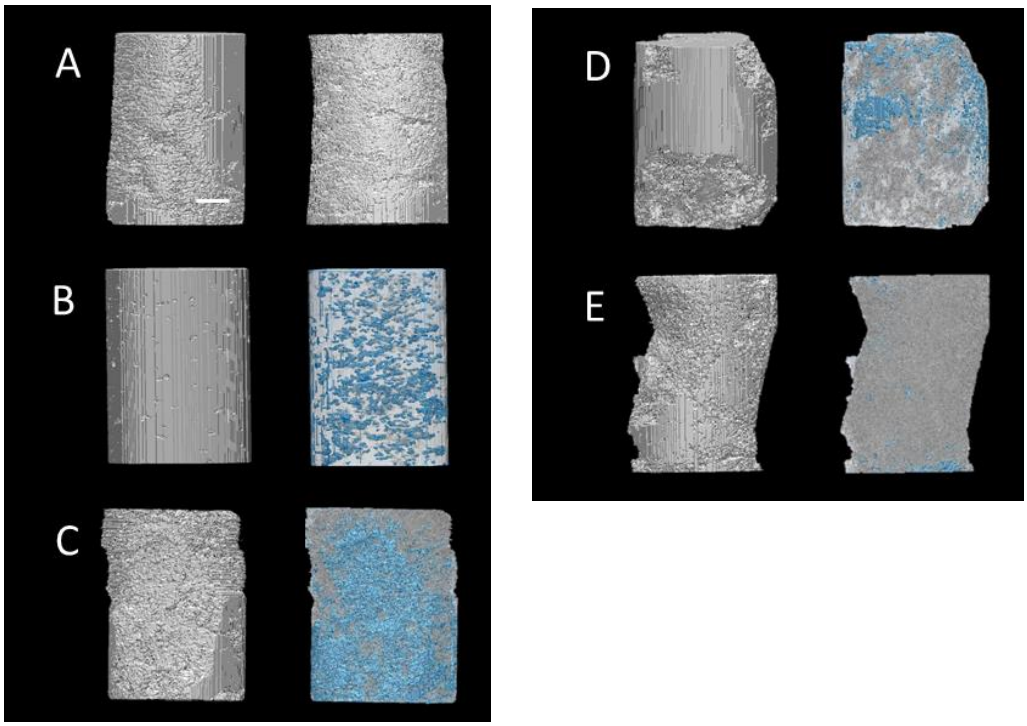


Figure 4.12 Microstructural analysis of scaffolds. Micro-CT images for scaffolds at different conditions. Scaffolds were treated with osmium tetroxide prior to scan. (A) Non seeded scaffold prepared from blank MPs placed in cell culture media at day 1 (left) and day 21 (right) (B) cell-seeded scaffold prepared from blank MPs cultured in osteo-permissive media for 1 day (left) and merged cells and scaffold showing cell distribution (right) cells are in blue. (C) Cell seeded scaffold prepared from blank MPs cultured in osteo-permissive media for 21 days (left image) and merged cells and scaffold showing cell distribution (right). (D) Cell seeded scaffold prepared from P21-RUNX2-8R loaded MPs cultured in osteo-permissive media for 21 days (left image) and merged cells and scaffold showing cell distribution (right). (E) Cell seeded scaffold prepared with blank MPs cultured in osteo-inductive media for 21 days (left image) and merged cells and scaffold showing cell distribution (right). Scale bar is 1mm.

4.3.7. PF-127 concentration and quantity affects the printing quality

PF-127 is FDA approved ploxamer [211]. It is a triblock copolymer of poly (ethyleneoxide)/poly (propyleneoxide)/poly (ethyleneoxide) [211-213]. PF-127 has thermo-reversible gelation properties and it has been widely used as cell carrier and for various 3D printing applications [211-214]. At certain concentrations, aqueous PF-127 solutions gel at physiological temperatures [211].

In order to make the scaffold formula printable, it has to have certain viscosity [196, 197] that allow continuous flow of the material through the printing needle. In order to achieve the needed viscosity, Pluronic F-127 (PF-127) was mixed with the PLGA/PEG particles.

The work presented in this section was done with Gordon Bruce, a CDT student, did his first year rotation in University of Nottingham, Regenerative Medicine and Cellular Therapies department. Gordon worked on studying the addition of PF-127 to the PLGA/PEG particles to make printable. This section summarises what was done in this regard.

Viscosity for various concentrations of PF-127 at different temperatures were studied. It was concluded that suitable PF-127 concentration for printing should be between 15 – 20 % (w/v). The temperature was fixed at 25°C. PF-127 will be gel at this temperature and suitable for printing. Figure 4.13 summarises the used concentrations and ratios for printing. It was clear that the suitable printing concertation is 18% (w/v) and in 1:1.5 ratio (PLGA/PEG particles : PF-127).

The optimised formula was used to print a complex structure to demonstrate the printability of the PLGA/PEG particles, when mixed with PF-127. Figure 4.14 shows L5 vertebrate printed structure.

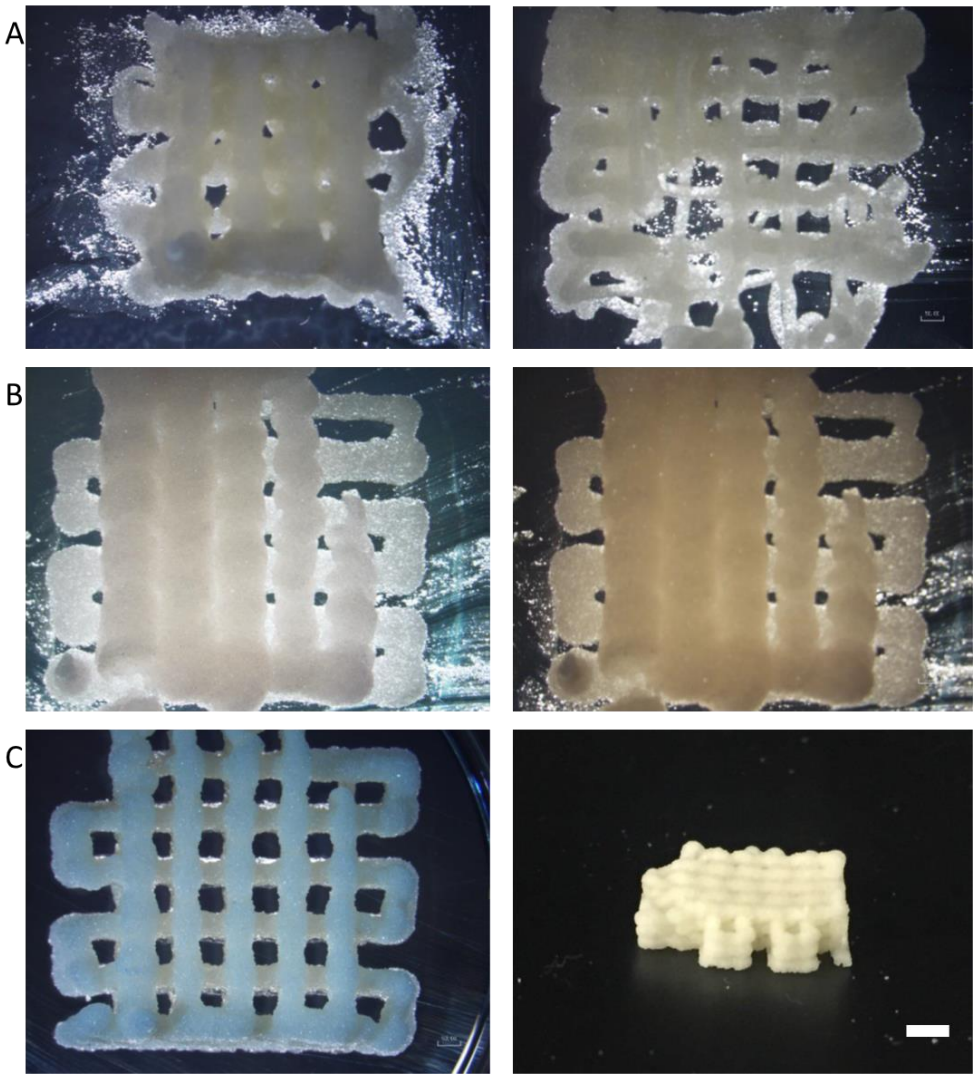


Figure 4.13 3D printing formula optimisation using various ratios and concentrations of PF-127. Dissection microscope images (A) PLGA/PEG: PF127 15% (1:1.2 ratio). (B) PLGA/PEG: PF127 15% (1:1.3 ratio). (C) PLGA/PEG: PF127 18% (1:1.5 ratio). Scale bar represents 1mm. Images taken from G Bruce CDT report.

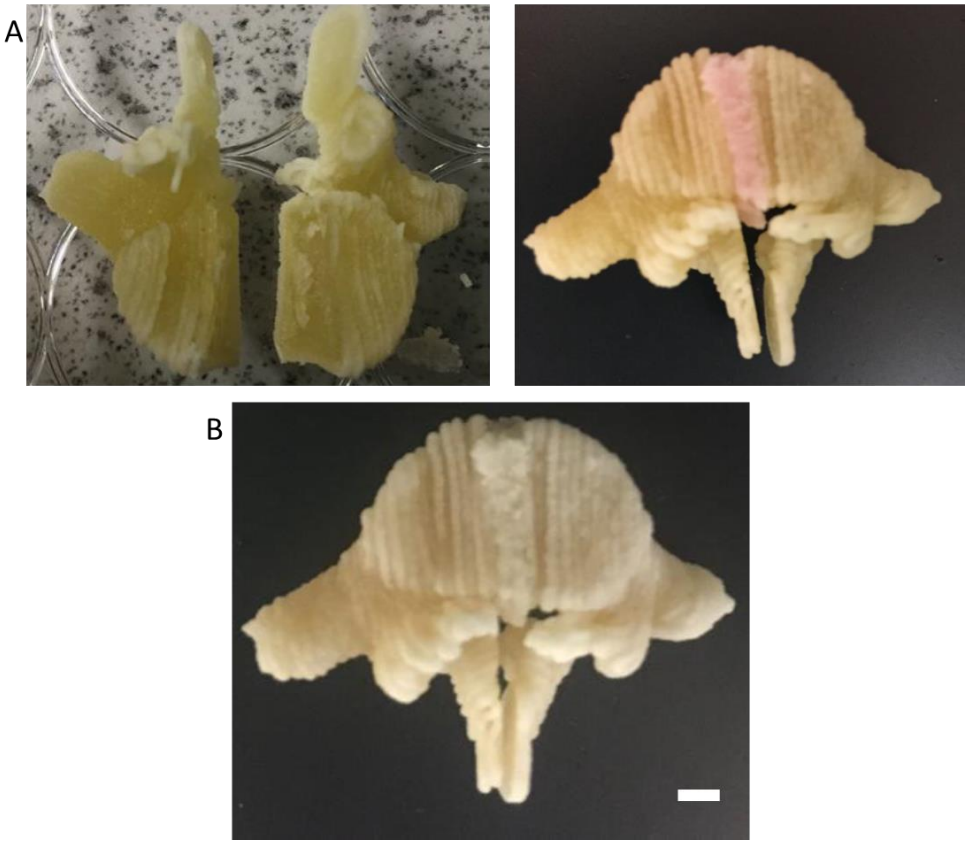


Figure 4.14 Complex structure printing using the optimised formula (PLGA/PEG with PF-127 18% 1:1.5 ratio). L5 vertebra printed structure (A) left and right parts before sintering. (B) After sintering for 2 hours at 37°C. Printed vertebrae length is 4cm. Scale bar represents 1mm. Images taken from G Bruce CDT report.

4.3.8. Tri-acetin can be used to accelerate scaffolds sintering

After optimising the formula to be printable, using Pluronic F-127, it was suggested that the sintering process and time needs to be shortened. Shortening the sintering time will help in decreasing the time of cell exposure to pluronic, which help maintain cell viability.

The current sintering process includes incubating the scaffold (with cells) at 37°C for two hours, which will be affecting cell viability (if bio-printing is needed). By decreasing the sintering time, it was suggested that more cells will be viable.

Accordingly, tri-acetin, which is used as a plasticiser [215, 216], was studied to accelerate the sintering process.

In order to determine the effect of tri-acetin on sintering process, various concentrations of tri-acetin were studied over time. The studied concentrations were 0%, 0.5%, 1%, 2.5% and 5% and the studied incubation times were 30 minutes, 60 minutes and 120 minutes at 37°C. To evaluate the sintering properties, scaffolds morphology (by SEM) was tested. It can be seen that the scaffolds morphology starts to change after 30 minutes of incubation at 37°C if 2.5% tri-acetin (or more) were added to the scaffolds. The concept of PLGA/PEG injectable bone is that the PLGA/PEG particles will to fuse together upon exposure at 37°C, this process is gradually happening. However, upon addition of tri-acetin (2.5% or 5%), the particles start to fuse together after 30 minutes (figure 4.15). It can be seen that the particles morphology with 2.5% after 30 minutes is comparable to the scaffolds without tri-acetin after 120 minutes (figure 4.15). Addition of 5% tri-acetin resulted in instant hardening of the scaffold, and it was difficult to mould the PLGA/PEG into the mould (figure 4.14 A).

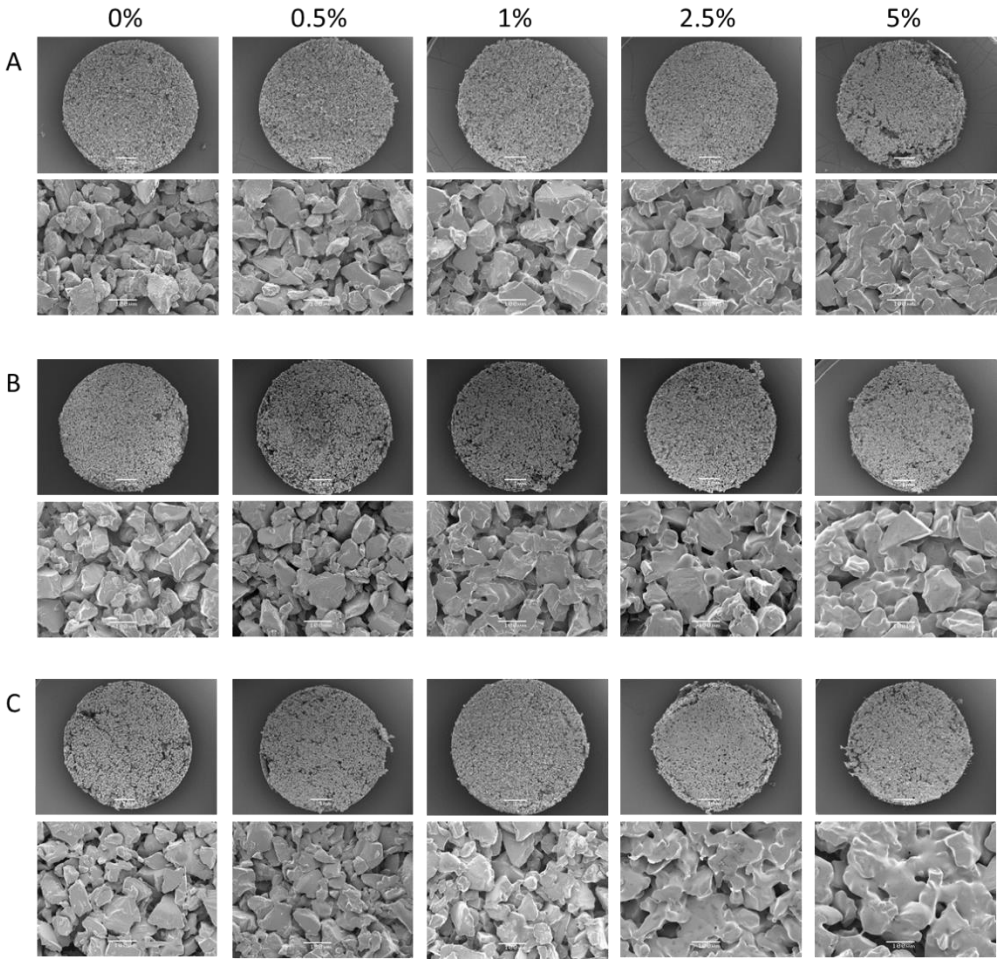


Figure 4.15 Tri-acetin effect on the scaffold structure. Various concentrations of tri-acetin (0%, 0.5%, 1%, 2.5% and 5%) were mixed with PLGA/PEG and sintered for various periods (30minutes, 60 minutes and 120 minutes. (A) Sintered for 30 minutes at 37°C. (B) Sintered for 60 minutes at 37°C. (C) Sintered for 120 minutes at 37°C. Scale bar as indicated.

4.3.9. Mixing pluronic and tri-acetin to enhance printing and sintering properties

After demonstrating that with pluronic the PLGA/PEG particles can be printed and showing that the addition of tri-acetin can accelerate the sintering of the scaffold, it was important to study the effect of mixing the two components together and evaluate the scaffolds structure.

The used pluronic concertation was 18% and mixed with the PLGA/Peg particles in 1.5 : 1 ratio (PF-127 : PLGA/PE particles), on the other hand, the used ratio to prepare scaffolds with tri-acetin was 1:0.6 (PLGA/PEG particles : PBS with tri-acetin). It was critical to stick to the same concentration and ratio of pluronic as it showed successful printing. Accordingly, it was thought to decrease the concentration of tri-acetin and use larger volume (i.e. 60µL of 1% tri-acetin instead of 24µL of 2.5% per 40mg scaffold). By simple calculation 24µl of 2.5% tri-acetin contains 0.6µL tri-acetin and 60µL of 1% tri-actin contains 0.6µL tri-actin. Using these quantities will keep the ratio between PLGA/PEG particles and tr-acetin quantity exactly the same.

Accordingly, scaffolds were prepare with pluronic (18%) and tri-acetin in different concentrations (2.5% and 1%) and mixed in various ratios (1:0.6 and 1:1.5 PLGA/PEG to carrier). The scaffolds morphology was comparable in scaffolds prepared with pluronic (18%) and triacetin 2.5% (1:0.6 ratio) and scaffolds prepare with pluronic (18%) and triacetin 1% (1:1.5 ratio). On the other hand, scaffolds prepared with pluronic (18%) and tri-acetin (2.5%) in 1:1.5 ratio were overloaded with tri-actin (figure 4.16). mechanical strength was comparable in the two previously mentioned scaffolds and significantly higher than the scaffolds prepared with pluronic (18%) and tri-acetin (2.5%) in 1:1.5 ratio.

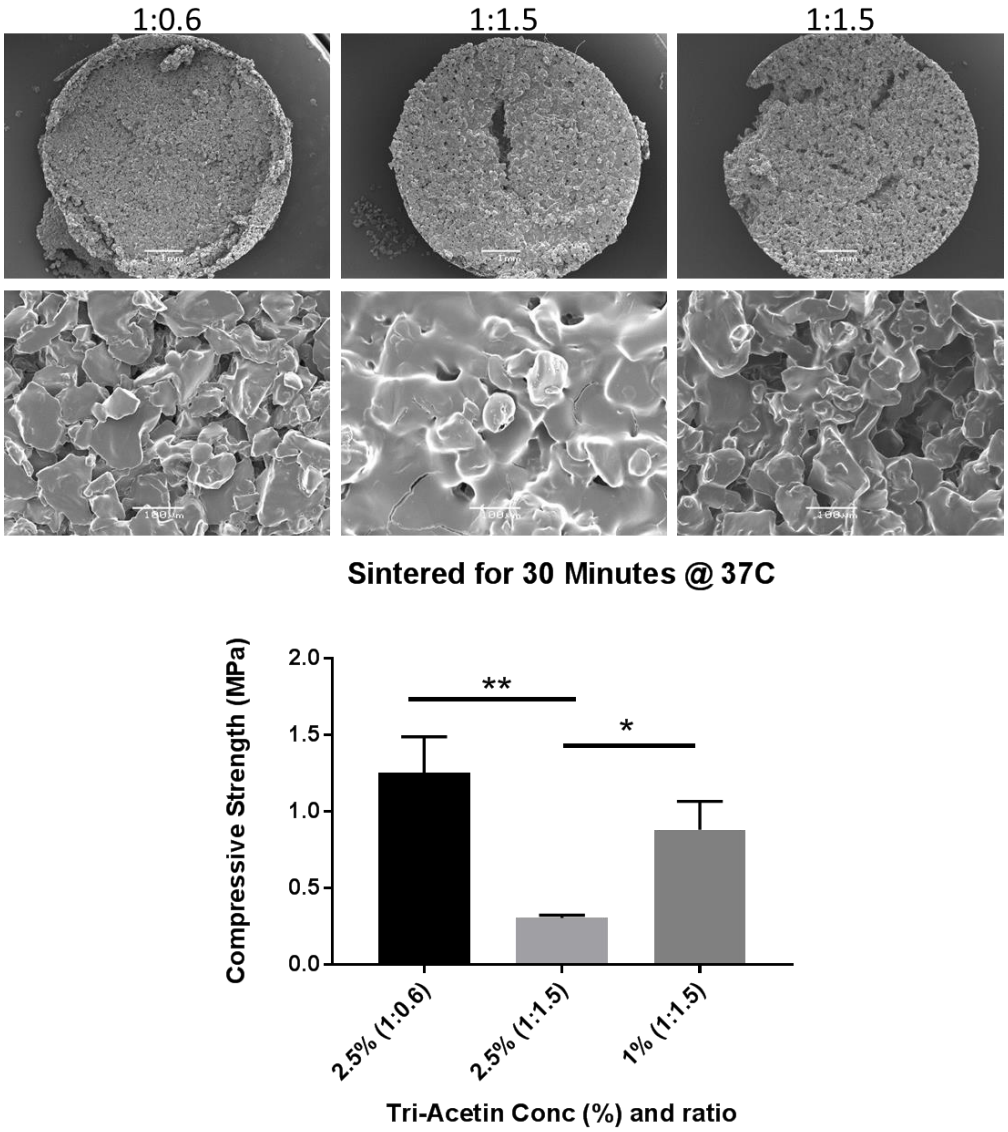


Figure 4.16 Effect of carrier quantity on scaffolds. Scaffolds were mixed with various concentrations and quantities of tri-acetin. (A) SEM evaluation of scaffolds. PLGA/PEG was mixed with 2.5% (v/v) tri-acetin and 18% (w/v) Pluronic in 1:0.6 ratio (left). with 2.5% (v/v) tri-acetin and 18% (w/v) Pluronic in 1:1.5 ratio (middle). with 1% (v/v) tri-acetin and 18% (w/v) Pluronic in 1:1.5 ratio (right). (B) Mechanical evaluation of scaffolds. Error bars indicate SD (n = 3). * is $p < 0.05$. ** is $p < 0.01$.

4.3.10. Scaffold washing post-sintering

After sintering the scaffolds, it will be cultured in media and incubated at 37°C. At this temperature, PF-127 was reported to form unstable gel when immersed in culture media [211] and it was shown that it affects cell viability at these conditions [212]. Accordingly, it was suggested that PF-127 to be removed after scaffolds sintering. However, it has to be removed at temperatures low enough to be liquid rather than a gel.

Accordingly, scaffolds were washed in PBS at 4°C for 45 minutes after sintering, as a control another scaffold was washed at 37°C for 45 minutes and to evaluate the washing efficiency, after washing a scaffold at 4°C it was placed in PBS at 37°C for 30 minutes. It was thought that if the washing process was not efficient at 4°C, the remaining PF-127 will gel at 37°C and the scaffolds will swell. Scaffolds morphology was evaluated using SEM.

The scaffolds washed at 4°C showed smooth structure with no swelling (figure 4.17), on the other hand, the scaffold washed at 37°C showed swollen structure with PF-127 adsorbed on the surface of the particles (figure 4.17). The scaffold washed at 4°C then 37°C showed comparable structure to the scaffold washed at 37°C indicated efficient removal of PF-127 (figure 4.17).

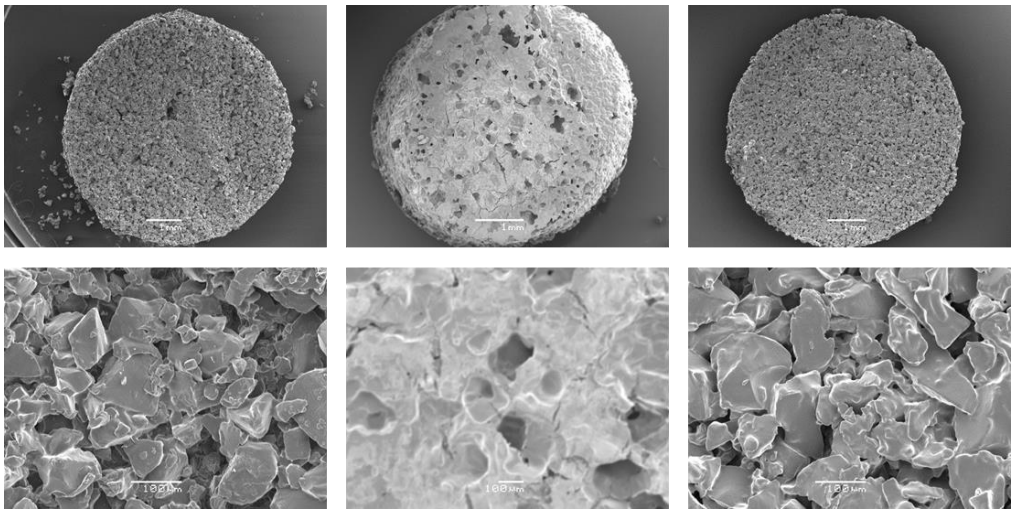


Figure 4.17 Effect of washing on scaffold properties. PLGA/PEG mixed with 1% tri acetin and 18% pluronic (1:1.5 ratio). Scaffolds were sintered at 37°C for 30 minutes. Scaffolds were then washed with PBS at 4°C (left), 37°C (middle) or 4°C then at 37°C (right).

4.3.11. Cell proliferation on scaffolds

After optimising the formulation and introducing pluronic and tri-acetin to enhance the viscosity and accelerate sintering process, it was important to determine the cell density that will be used for printing and to study the effect of the whole process on cells viability and proliferation.

Accordingly, various cell densities were studied and cell proliferation was tested. The scaffolds were prepared by mixing ihMSCs with PLGA/PEG particles. The used carrier was 18% PF-127 and 1% tri-acetin mixed in 1:1.5 ratio (PLGA/PEG : carrier).

The tested cell densities were (0.05Million (M), 0.1M, 0.25M, 0.5M and 1M per scaffold). After mixing the cells, the paste was loaded into PTFE moulds and sintered at 37°C for 30 minutes. The scaffolds were then washed in PBS at 4°C for 45 minutes.

Scaffolds disintegration was evaluated before and after wash by taking microscope images. The results showed the scaffolds were intact before washing in PBS at 4°C (after sintering) and after washing (figure 4.18), indicating that the sintering time was enough for the scaffolds to maintain the structure and also that pluronic removal is not affecting the scaffolds structure and integrity.

After that, scaffolds were cultured in growth media and incubated at 37°C. PrestoBlue® cell viability test was done on the scaffolds to test cell proliferation (figure 4.18). As expected, the results showed that the more cells we start with, the more cells will attach to the scaffolds. The cells were proliferating with time demonstrating viable cells on the scaffolds.

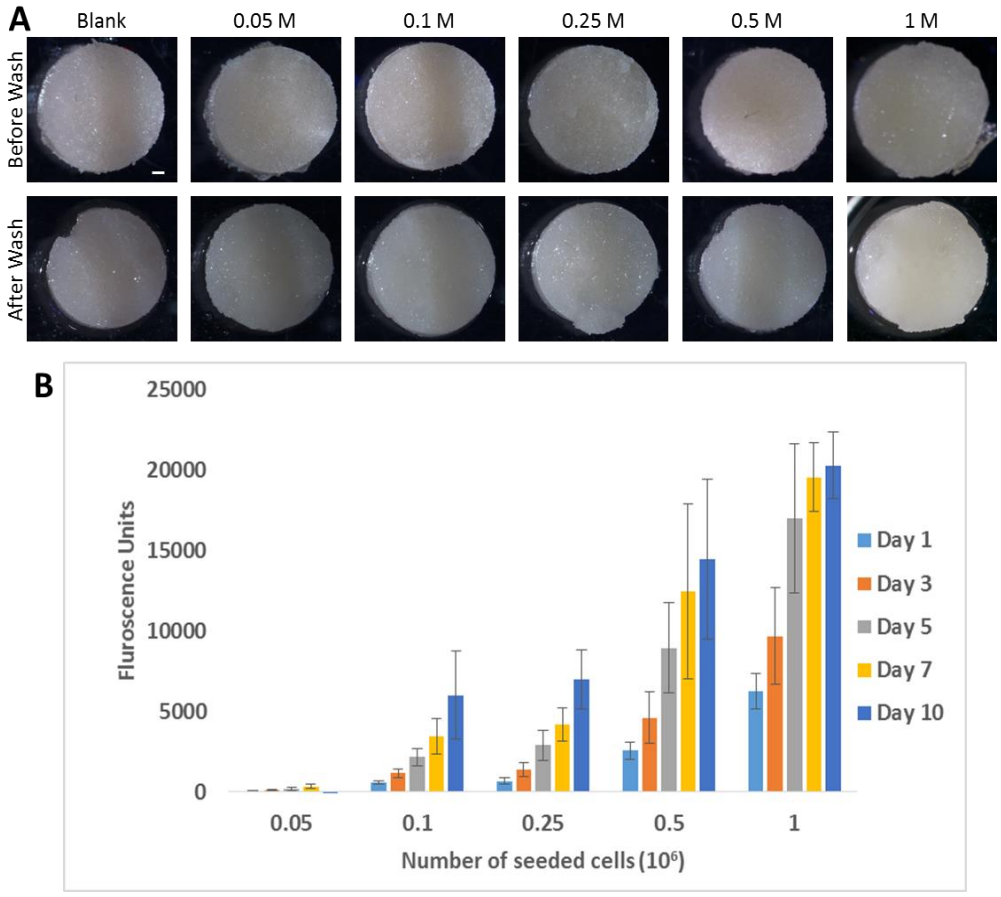


Figure 4.18 Scaffold disintegration upon washing and cells proliferation. Various quantities of cells (1M, o.5M 0.25M 0.1M and 0.05M) were mixed with 60uL of 1% tri-acetin (v/v), 18% pluronic (w/v) solution and added to 40mg PLGA/PEG forming a paste at room temperature. The paste was then loaded into Teflon mould to produce cylindrical scaffolds (6mm X 3mm). The scaffolds were then sintered at 37°C for 30 minutes. The scaffolds were then washed in PBS at 4°C for 45 minutes and then transferred to 24 well plate and immersed in 1 ml media and incubated at 37°C for the entire study. (A) Microscope images for scaffolds after sintering and after washing showing intact scaffolds (scale bar represents 1mm). (B) PrestoBlue cell viability at different time points for the cultured scaffolds. Error bars indicate SD (n = 3).

4.3.12. 3D printing of injectable bone mixed with pluronic and tri-acetin

After demonstrating that the pluronic and tri-acetin can be mixed to enhance scaffolds characteristics, it was important to show that the previous printing approach can be reproduced in presence of tri-acetin. Accordingly, printing was repeated with tri-acetin included in the formula.

The printed structure was reproducible, showing comparable structure (to the previously reported in figure 4.13), demonstrating successful addition of tri-acetin without affecting printing characteristics (viscosity and gelation) (figure 4.19).

Since there will be time between preparing the material, loading it into the printing syringe and printing process itself, it was suggested to study the time frame allowed without affecting mixture properties.

Accordingly, after mixing the material with the carrier and loading it to the printing syringe (at 25°C), a holding time study was done, by leaving the material in the syringe at 25C for various time points. The printability of the material was studied by printing similar structures at various time points and compare the morphology of these structures (figure 4.20).

It can be seen that by increasing the holding time, the printed strands were thicker. It worth mentioning that the pressure used for printing structures (after 30 minutes and 45 minutes) had to be increased since the material was sticking inside the syringe and higher pressure was needed to print it. Higher pressure may justify the thicker strands achieved (figure 4.20).

This finding indicates that the printing time window is within 30 minutes of material mixing and loading to the syringe.

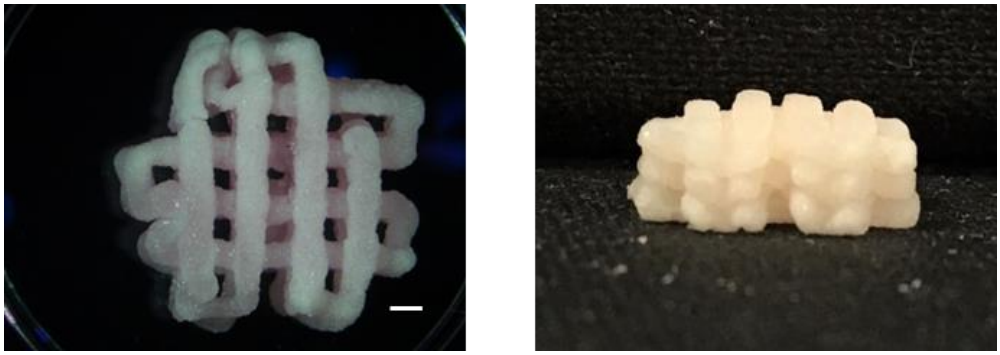


Figure 4.19 3D printed scaffold using PLGA/PEG particles mixed with Pluronic (18%) and tri-acetin (1%) in 1:1.5 ratio (PLGA/PEG : carrier). Scaffold was sintered at 37°C for 30 minutes after printing. Scale bar represents 1mm.

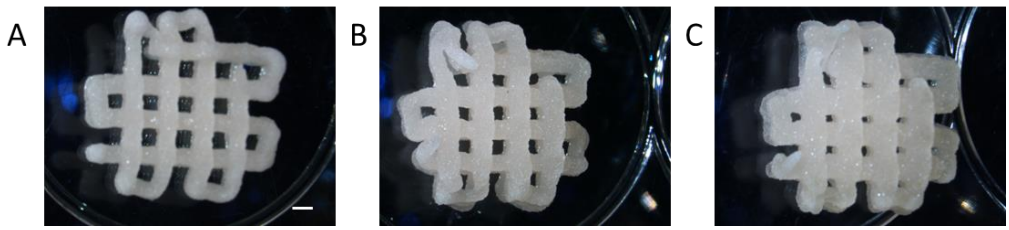


Figure 4.20 Holding time evaluation study. PLGA/PEG was mixed with 1% (v/v) tri-acetin and 18% (w/v) pluronic solution at 4°C. The mixture was then placed at the syringe at 25°C then printed (A). The mixture at they syringe was then held at 25°C for 30 minutes and then printed (B). PLGA/PEG mixture was loaded to the syringe at 25°C and left for 45 minutes then printed (C). Scale bar represents 1mm.

4.3.13. Bio-printing and assessment of cell viability

The main aim presented in the section was to be able to provide complex structures of polymeric bone scaffolds that can be used for various applications. However, it was suggested that bio-printing can be demonstrated as well, which may help for future applications to load all the components together.

Accordingly, cells were mixed with the carrier (18% PF-127 and 1% tri-acetin) with final density of 10M/ml and mixed with PLGA/PEG particles in 1:1.5 ratio at 4°C. The mixture was then loaded to the printing syringe and heated to 25°C. The mixture was then printed, and sintered at 37C for 30 minutes. The sintered scaffolds were then washed in cold PBS for 45 minutes and then cultured in media for 7 days.

In order to test cell proliferation, PrestoBlue® cell viability test was done on days 1, 3, 5 and 7 (figure 4.21). In addition toluidine blue stain was done on day 7 to visualise cells on scaffolds (figure 4.21).

Cells were proliferating with time, indicating successful bio-printing of scaffolds and robustness of the process, although number of cells could not be estimated, but were enough to proliferate with time (figure 4.21). Toluidine blue stain showed distribution of the cells along the strand, as well as within the strand, shown by cross sectional images of scaffold (figure 4.21), scaffolds were physically cut and stained to show cell proliferation within scaffold structure.

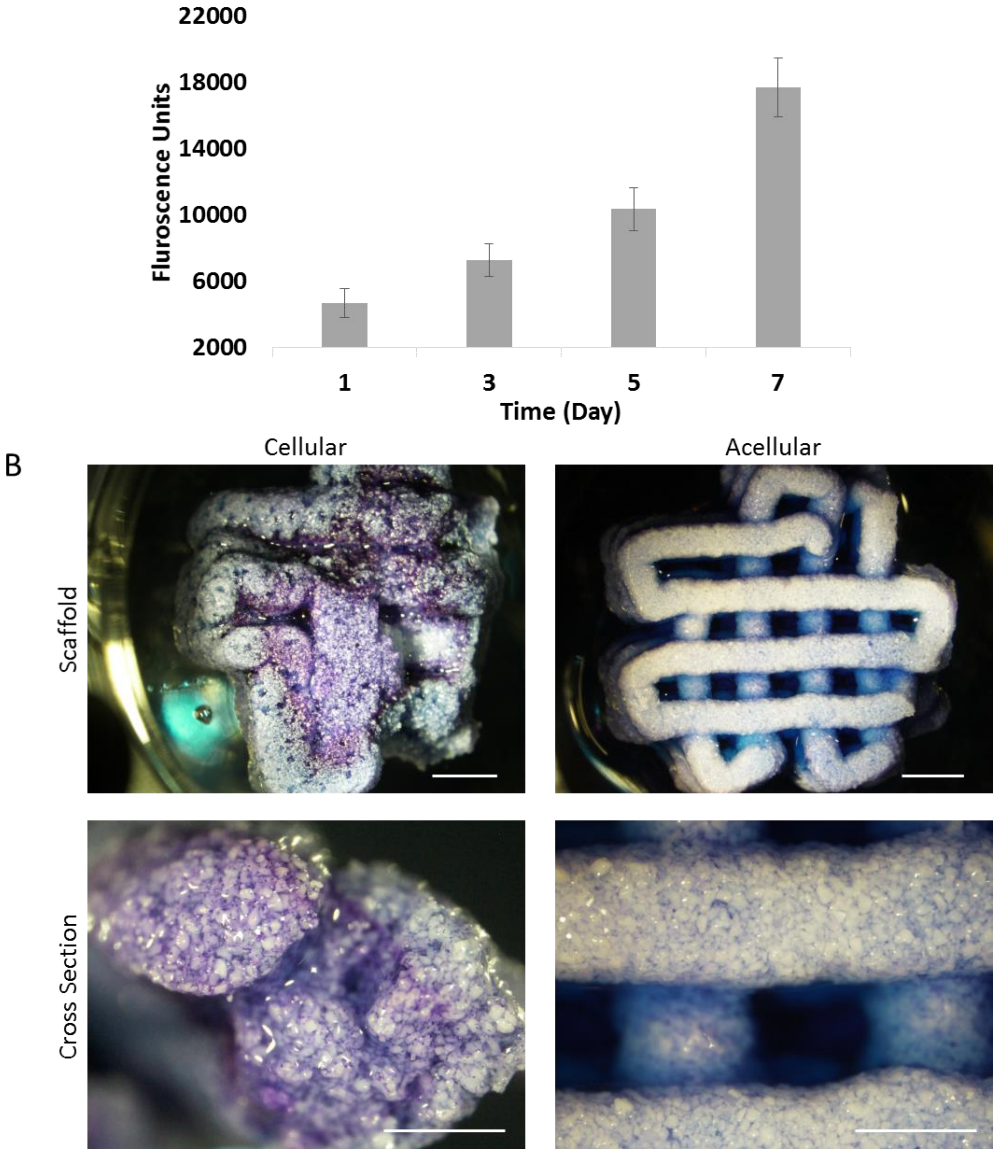


Figure 4.21 Bio-printing and cell proliferation on 3D printed scaffolds. PLGA/PEG particles were mixed with Pluronic 18% - Treacetin 1% solution in 1:1.5 ratio. The solution was mixed with cells (10^6 per ml). The mixture was loaded to the printing syringe and printed at 25°C. After sintering at 37°C for 30 minutes and washing in cold PBS at 4°C, scaffolds were then cultured in media for 7 days. Cells proliferation was evaluated. (A) PrestoBlue cell viability at different time points for the cultured scaffolds. Error bars indicate SD (n = 3). (B) Toluidine blue stain at day 7. Scale bar is represents 1mm.

4.4. Discussion

Microparticles and scaffolds have been used extensively for the delivery of growth factors and drug molecules [217-219]. Several studies have demonstrated successful tissue regeneration with the delivery of a growth factor from polymeric carriers [220-222]. The incorporation of these molecules into scaffolds have been shown to further promote stem cells growth and differentiation [223-225].

The work presented in this chapter focused on controlled release delivery of transcription factor (RUNX2). RUNX2 was utilised to direct hMSCs osteogenesis, removing the need to use pleiotropic compounds (such as dexamethasone), or growth-factors (such as BMP2) which may trigger unwanted off-target cellular responses. Combining RUNX2 loaded MPs with scaffolds material will take the benefit of using polymeric scaffolds for tissue regeneration as well as reduce the disadvantages associated with the use of growth factors or hormones. The results described here represent induction of osteogenic differentiation of hMSCs by the controlled release of GET-RUNX2 from PLGA MPs based scaffolds.

The advantage of controlled release is that the cells will be continuously exposed to the therapeutic molecule (RUNX2) and protecting the molecule from hydrolysis or denaturation. On top of that, controlled release system will avoid multiple administration of the therapeutic molecule avoiding multiple injections for the patient once applied inside the body.

GET-RUNX2 was encapsulated into PLGA microparticles with high efficiency (~58%). The release was accelerated, to achieve optimal dose (i.e. 60μg of RUNX2 over the first week of the study), using PBS as shown in the previous

chapter. PBS works as a porogen which will create channels within and on the surface of the microparticles[183]. Porous MPs have been previously prepared to accelerate release of various therapeutic molecules depending on diffusion from microparticles [226-229]. Activity of released GET-RUNX2 was validated for both; GET peptide (transduction) and RUNX2 (transfection). The activity was comparable to fresh equivalent quantities of GET-RUNX2 demonstrating efficiency of the delivery system as well as validation of the stabilisation approach followed in the development of the delivery system (i.e. addition of L-Histidine).

GET-RUNX2 loaded MPs have been successfully fabricated and mixed with PLGA/PEG temperature sensitive particles to provide a polymer based scaffolds. hMSCs were seeded on the scaffolds fabricated from PLGA MPs mixed with PLGA/PEG particles. Scaffolds were fabricated either from GET-RUNX2 loaded MPs or blank MPs. For differentiation study, scaffolds were cultured in media containing ascorbic acid and β-glycerophosphate with or without Dexamethasone.

Dexamethasone (a synthetic member of the glucocorticoid class of steroid hormones) was used as a positive control to compare the effect of RUNX2 on cells differentiation. The ability of Dexamethasone for osteoblast differentiation from stem cells has been reported extensively. It is believed that it plays a major role in promoting the differentiation of stem cells [230-232].

Ascorbic acid is required for use in the synthesis of collagen (a major component of bone) and cell proliferation [233]. β-glycerophosphate is an organic phosphate added to induce mineralization of the collagen matrix through calcium phosphate deposition. Scaffolds containing GET-RUNX2 loaded MPs were cultured on

media containing ascorbic acid and β-glycerophosphate, while the positive control blank MPs were used to fabricate scaffolds and 100nM Dexamethasone was added to the media along with ascorbic acid and β-glycerophosphate.

Increased alkaline phosphatase (ALP) expression usually used to describe osteogenic differentiation progression [205-207]. The scaffolds exposed to RUNX2 showed 3 folds increase in the expression levels of ALP (compared to scaffolds not exposed to RUNX2) (figure 4.7), moreover, this level of expression was comparable to scaffolds cultured in Dexamethasone, which indicates the efficiency of RUNX2 delivery in initiating osteogenic differentiation.

Tissue mineralization is a necessary precursor for bone tissue formation. Bone tissue is known by bone nodules which occur by secretion of ECM and osteocalcin which is important for deposition of calcium phosphate crystals within the matrix by osteoblasts [234-236].

Staining for osteocalcin showed an increased synthesis of osteocalcin (figure 4.8). Increased production is an indication of committal towards osteogenic differentiation [236]. The distribution of bone nodules indicated the successful induction of osteogenesis (figure 4.9).

These findings, in 3D structures, are comparable to the previously reported 2D differentiation findings [55]. The use of P21-RUNX2-8R loaded MPs will help in targeted stem cells reprograming. This strategy of delivering specific factors for promoting bone formation also helps in preventing undesirable, undirected differentiation, off-target or systemic side-effects. It was demonstrated that the GET peptide promoted TF delivery thereby directing the differentiation towards a desired lineage.

RUNX2 transcription factor delivery was previously mentioned by Gersbach et. al. [47]. Retrovirus was utilised to deliver RUNX2 transcription factor to osteogenesis, moreover, RUNX2 expression was regulated by anhydrotetracyline concentration in cell culture media. The developed delivery system (in this thesis) overcome the risk associated with the use of viral vectors (i.e. infection) as well as eliminates the need to regulate RUNX2 expression since the controlled release system will provide the needed dose at the needed time. Other studies have utilised *RUNX2* gene delivery, their strategy as well as their results were discussed earlier in this thesis (section 1.6) [45-47].

PLGA scaffolds were used, in combination of biological factors, to induce osteogenesis, Kim et. al. developed PLGA scaffolds releasing ascorbate-2-phosphate and dexamethasone to induce mesenchymal stem cells osteogenesis [237]. Mineralisation was significantly higher in these scaffolds compared to control scaffolds.

Zhang et. al. developed a PLGA and hydroxyapatite scaffolds coated with BMP-2 and insulin-like growth factor 1 (IGF-1) [238]. Alkaline phosphatase (ALP) activity, expression of osteogenesis-related genes and the mineralization capacity of MC3T3-E1 cells were increased by the incorporation of BMP-2 and IGF-1.

Kim TH et. al. fabricated polycaprolactone/PLGA scaffolds with a heparin-dopamine (Hep-DOPA) conjugate for controlled release of bone morphogenic protein-2 (BMP-2). The results showed that (MG-63) cells grown on these scaffolds had significantly enhanced ALP activity and calcium deposition compared to controls [239].

The previously mentioned approaches to induce osteogenesis on cell seeded scaffolds followed the use of growth factor (BMP-2) or steroid (dexamethasone), although both reported to have pleiotropic effects [240, 241]. The use of RUNX2 eliminates the need to use these compounds and the utilisation of GET peptide technology removed the need to use viral vectors for cellular transduction.

The development of controlled release delivery system was superior to the previously mentioned approaches of delivering therapeutic molecules, such as surface coating or mixing with scaffold material.

Following the successful fabrication of PLGA/PEG scaffolds containing P21-RUNX2-8R loaded MPs and successful programming of seeded hMSCs towards osteogenesis, it was planned to modulate the PLGA/PEG formula to be 3D printable to provide various scaffold structures with modified properties.

Pluronic (F-127) was utilised here to enhance printability of PLGA/PEG particles. PF-127 has temperature sensitive gelation properties [212, 214] which allows mixing the components together in the liquid state (i.e. ~ 4°C), to provide homogeneous mixture, then print this structure in the gel state at higher temperatures (i.e. ~ 25°C).

The gelation properties were found to be dependent on the concentration of the PF-127, which was previously reported [212, 214]. The quantity of PF-127 along with concentration showed various printing resolution and accurcy (figure 4.13). the suitable printing conditions were found to be 18% PF-127 mixed in 1:1.5 ratio (PLGA/PEG particles : PF-127) mixed at 4°C and printing temperature of 25°C.

Shortening the sintering time was important to minimise the work time of scaffolds preparation, which can give more applications for the injectable bone,

if needed in emergency cases. Tri-acetin was used for this purpose. Tri-acetin is an external plasticiser which is previously used as plasticiser for PLA [215, 216, 242]. No full characterisation of tri-acetin effect on PLGA/PEG properties was done at this stage, however extensive characterisation is needed for better understanding of the mechanism.

The use of tri-acetin could reduce the sintering time to 30 minutes (instead of 120 minutes) which enhances the feasibility of the printing process as well as the time efficiency. Moreover, tri-acetin didn't affect the printing parameters developed previously, maintaining the same PF-127 concentration and quantity to be used (figure 4.20).

Since cells were previously reported not to proliferate well in presence of PF-127, and the structure was reported to be less stable [211, 212], it was suggested to remove the PF-127 after sintering. PF-127 will be liquid at low temperature and it will leach out of the scaffold without destroying the structure, it was suggested to wash out PF-127 in cold PBS (at 4°C). 45 minutes found to be effective for PF-127 removal (figure 4.17).

Although it was suggested to 3D print the complex structure and then seed the cells on the printed structure, it was worth studying the bio-printing process, which will provide more homogenous cells distribution (compared to seeding process). Accordingly, feasibility of cells proliferation on both moulded and printed scaffolds was evaluated (figures 4.18 and 4.20). Cells found to proliferate on the fabricated scaffolds, however, estimation of number of cells remained alive after the process was difficult and a suitable approach need to be followed.

4.5. Conclusions

The work presented in this chapter evaluated the encapsulation of GET-RUNX2 molecule within PLGA MPs fabricated using the previously developed S/O/W method.

The release profile was developed matching the needed therapeutic dose of RUNX2 to induce osteogenesis. The activity of the released GET-RUNX2 was evaluated. The transduction and transfection activities were retained with values above 70% (compared to controls).

hMSCs attachment and proliferation on PLGA/PEG scaffolds was evaluated. The cells were proliferating indicating compatibility with the scaffold material.

The stem cells seeded on the scaffold can then be induced towards osteogenesis responding to the transcription factor (RUNX2) released from the microparticles. The GET peptide tagged on the transcription factor will enhance cellular uptake of the molecule. The formed scaffold can serve as a host for the stem cells. The differentiation markers (early, mid and late markers) were comparable in both; scaffolds containing P21-RUNX2-8R loaded microparticles and samples seeded in osteo-inductive media. Significant differentiation was observed in the loaded scaffolds compared to negative control samples. The advantage of this delivery system is to provide localized release of GET-tagged therapeutic molecules with minimized risk of systemic dosing that may lead to non-targeted activity.

PLGA/PEG particles formula was optimised to be 3D printable, by addition of PF-127, and the sintering time was shortened by addition of tri-acetin as an external plasticiser. 3D printing of PLGA/PEG particles can provide complex bone structure for various applications, and can be utilised in future for incorporation of loaded PLGA MPs for controlled release implants.

Chapter V:

Final Conclusion and Future Work

5. Final Conclusion and Future Work

5.1. Conclusions

Successful regenerative medicine strategies often rely on exquisite control of the biological microenvironment and supplementation of extrinsic therapeutic molecules to direct cellular behaviour. Cellular processes like migration, proliferation, adhesion and differentiation occur in response to chemical cues present within the microenvironment such as interaction with extracellular matrix (ECM) and stimulation with morphogens or growth factors [243, 244]. These macromolecules trigger intracellular signal transduction pathways, with complex cross-talk between the cascades and eventual programming of cell behaviour through transcription factors [244-246]. A recent technology has shown that recombinant transcription factors can be expressed, purified and delivered efficiently to control cell behaviour for regenerative medicine strategies [81]. Such systems will allow the biological control of cells and promote regeneration of tissues if it is supplied at a functional dose, duration and location to be effective.

The developed technology named glycosaminoglycan (GAG) enhanced transduction (GET) [81]. GET technology is a series of novel fusion proteins that couple a membrane-docking peptide to heparan sulfate glycosaminoglycans (GAGs) with a PTD. It was demonstrated that this technology can enhance intracellular transduction upon coupling CPPs with a GAG-binding peptide (the composite peptide termed GET peptide).

The work presented in this thesis aimed to develop delivery system based on PLGA MPs to encapsulate these GET peptide (tagged with other molecules) and release them in the needed dose at the needed time.

5.1.1. Development of a method to encapsulate GET peptide

The aim of the first experimental chapter was to utilise a double emulsion method to create GET peptide loaded PLGA MPs. Double emulsion method is the most used approach to create PLGA MPs [116, 165, 166]. Self-reporter protein (mR) was used to directly assess activity of GET peptide after encapsulation in PLGA MPs. Results showed that GET peptide are sensitive to shear force (i.e. homogenisation) used to create emulsions during the process, and therefore PLGA MPs need to be fabricated the minimum shear force. Accordingly, S/O/W emulsion method was optimised to create PLGA loaded MPs. This approach employed PEG to create protein particles to be suspended in the organic phase, and encapsulate them in the solid form (removing the risk of water-organic interface present in W/O/W double emulsion). Vortexing was followed to create emulsion (instead of homogenisation), removing the harsh conditions that destroy the GET peptide.

The method optimised in this chapter was robust and efficient (high encapsulation efficiency) and demonstrates minimal harsh conditions to fabricate PLGA MPs, which considered optimal for loading GET peptide into the polymeric microparticles.

5.1.2. Formulation optimisation to accelerate GET peptide release and evaluate their biological activity

The work presented in the second experimental chapter aimed to optimise GET peptide release profile and to test the biological activity of these GET peptide. Release profile found to be low at the first 21 days, it was previously reported that the release in this type of MPs usually starts after 21 days [169].

The aim was to release GET peptide within 7 days (matching the optimal dose of RUNX2). Accordingly, GET peptide release was accelerated by making the PLGA MPs porous by incorporation of PBS during PLGA MPs fabrication. PBS will work as a porogen [183] and will create channels within and on the surface of PLGA MPs, which facilitates the diffusion of the encapsulated molecule from MPs. Making porous MPs was a successful strategy and the release profile was accelerated achieving around 90% release within 7 days.

It was critical after that to demonstrate that the released GET peptide maintained their biological activity. The transduction activity was tested using NIH 3t3 cells. The results showed gradual decrease of GET peptide activity (i.e. the protein released at the first day showed 80% activity, while the protein released at day 7 was below 30%). Accordingly, an investigation was started. The results showed that the carboxylic acid results from PLGA degradation is affecting GET peptide activity (either by interacting with the positively charged GET peptide) or by detaching GET peptide form the protein). Stabilisation approach, using co-encapsulation of L-Histidine was followed. The results showed that GET peptide activity maintained in presence of L-Histidine upon released from PLGA MPs. This was confirmed by simulation study using various weak and strong acids.

The work presented in this chapter resulted in optimised formulation of GET peptide loaded PLGA MPs, with optimised released profile as well as maintaining the biological activity of the released GET peptide above 70% at all studied time points.

5.1.3. Induce stem cells differentiation through controlled release of GET-RUNX2 molecule on temperature-sensitive scaffold

The work presented in the third experimental chapter aimed to utilise the previously developed fabrication method of GET loaded PLGA MPs, to encapsulate osteogenic transcription factor RUNX2.

A validation about RUNX2 release and biological activity was done before proceeding to differentiation study. The results showed efficient encapsulation (around 60%) as well as maintained biological activity of released GET-RUNX2 molecule.

A previously developed temperature sensitive PLGA/PEG particles [204] were used to create scaffolds. These particles were mixed with GET-RUNX2 loaded PLGA MPs, providing a template for stem cells as well as controlled release delivery system of osteogenic transcription factor.

Differentiation study results showed efficient delivery of biologically GET-RUNX2 molecule. Moreover, the results were compared to the employed positive control (Dexamethasone), which is used in most osteogenic differentiation approaches [230-232]. This finding clearly demonstrates the efficiency of the developed delivery system as well as bio-compatibility between all the ingredients and the stem cells (hMSCs).

Finally, a 3D printing approach was followed to create complex structures of bone, as well as modified porosity, for future applications. Sintering time was shortened through the use of tri-acetin. More characterisation of the use of pluronic (F-127) as well as tri-acetin is needed to understand the interactions between molecules. The controlled release system can be incorporated in such formula as previously shown [158], providing a controlled release system of therapeutic molecule as well as compatible template for the cells.

5.2. Future Directions

The work presented in this thesis has provided a controlled release system for GET peptide tagged to different proteins. This technology can be applied for therapeutic molecules. PLGA MPs release profile can be modulated to provide the needed dose for each molecule. The addition of thermosensitive microparticles would localise the release and give mechanical support to the structure.

Sterilisation of the material is an important factor in the development of a new medical device. There are a number of sterilisation techniques including gamma, electron beam and ultraviolet irradiation as well as ethylene oxide treatment and these may affect the material especially with regard to chain scission and a reduction in molecular weight. Studies to understand the change in material characteristics and effect on release profiles would need to be performed post sterilisation prior to the material entering in-vivo studies.

In vivo study can be done to verify the robustness of the system once applied inside the body, bone defect can be created to match the scaffold shape for a proof of concept study.

3D printing is a promising approach to provide complex structure and irregular shape scaffolds. The combination of scaffold material and loaded MPs need to be printed and release profile and activity of the released molecule needs to be validated for future use.

Chapter VI:

References

6. References

[1] Maradit Kremers H, Larson DR, Crowson CS, Kremers WK, Washington RE, Steiner CA, Jiranek WA, Berry DJ. Prevalence of Total Hip and Knee Replacement in the United States. The Journal of bone and joint surgery American volume 2015;97:1386-97.
[2] Habibovic P, de Groot K. Osteoinductive biomaterials--properties and relevance in bone repair. Journal of tissue engineering and regenerative medicine 2007;1:25-32.
[3] Vacanti CA. History of tissue engineering and a glimpse into its future. Tissue engineering 2006;12:1137-42.
[4] Vacanti JP. Beyond transplantation. Third annual Samuel Jason Mixter lecture. Archives of surgery (Chicago, Ill : 1960) 1988;123:545-9.
[5] Langer R, Vacanti JP. Tissue engineering. Science (New York, NY) 1993;260:920-6.
[6] Green H, Rheinwald JG, Sun TT. Properties of an epithelial cell type in culture: the epidermal keratinocyte and its dependence on products of the fibroblast. Progress in clinical and biological research 1977;17:493-500.
[7] Evans CH, Palmer GD, Pascher A, Porter R, Kwong FN, Gouze E, Gouze JN, Liu F, Steinert A, Betz O, Betz V, Vrahas M, Ghivizzani SC. Facilitated endogenous repair: making tissue engineering simple, practical, and economical. Tissue engineering 2007;13:1987-93.
[8] Kini U, Nandeesh BN. Physiology of Bone Formation, Remodeling, and Metabolism. In: Fogelman I, Gnanasegaran G, van der Wall H, editors. Radionuclide and Hybrid Bone Imaging. Berlin, Heidelberg: Springer Berlin Heidelberg; 2012. p. 29-57.
[9] Taichman RS. Blood and bone: two tissues whose fates are intertwined to create the hematopoietic stem-cell niche. Blood 2005;105:2631-9.
[10] Bayraktar HH, Morgan EF, Niebur GL, Morris GE, Wong EK, Keaveny TM. Comparison of the elastic and yield properties of human femoral trabecular and cortical bone tissue. Journal of Biomechanics 2004;37:27-35.
[11] Bayliss L, Mahoney DJ, Monk P. Normal bone physiology, remodelling and its hormonal regulation. Surgery (Oxford) 2012;30:47-53.
[12] Crockett JC, Rogers MJ, Coxon FP, Hocking LJ, Helfrich MH. Bone remodelling at a glance. Journal of cell science 2011;124:991-8.
[13] Jahagirdar R, Scammell BE. Principles of fracture healing and disorders of bone union. Surgery (Oxford) 2009;27:63-9.
[14] Griffin XL, Costa ML, Parsons N, Smith N. Electromagnetic field stimulation for treating delayed union or non-union of long bone fractures in adults. Cochrane Database of Systematic Reviews 2011.
[15] Shin M, Abukawa H, Troulis MJ, Vacanti JP. Development of a biodegradable scaffold with interconnected pores by heat fusion and its application to bone tissue engineering. Journal of biomedical materials research Part A 2008;84:702-9.
[16] Sammarco VJ, Chang L. Modern issues in bone graft substitutes and advances in bone tissue technology. Foot and ankle clinics 2002;7:19-41.
[17] Haidukewych GJ, Berry DJ. Nonunion of fractures of the subtrochanteric region of the femur. Clinical orthopaedics and related research 2004:185-8.

[18] Schepers E, de Clercq M, Ducheyne P, Kempeneers R. Bioactive glass particulate material as a filler for bone lesions. Journal of oral rehabilitation 1991;18:439-52.
[19] Jones JR, Ehrenfried LM, Hench LL. Optimising bioactive glass scaffolds for bone tissue engineering. Biomaterials 2006;27:964-73.
[20] Borrelli J, Jr., Prickett WD, Ricci WM. Treatment of nonunions and osseous defects with bone graft and calcium sulfate. Clinical orthopaedics and related research 2003:245-54.
[21] Daculsi G. Biphasic calcium phosphate concept applied to artificial bone, implant coating and injectable bone substitute. Biomaterials 1998;19:1473-8.
[22] J Blom E, Klein-Nulend J, P. A. T. Klein C, Kurashina K, A. J. van Waas M, H Burger E. Transforming Growth Factor-β1 Incorporated During Setting in Calcium Phosphate Cement Stimulates Bone Cell Differentiation In Vitro2000.
[23] Zhao J, Shen G, Liu C, Wang S, Zhang W, Zhang X, Zhang X, Ye D, Wei J, Zhang Z, Jiang X. Enhanced healing of rat calvarial defects with sulfated chitosan-coated calcium-deficient hydroxyapatite/bone morphogenetic protein 2 scaffolds. Tissue engineering Part A 2012;18:185-97.
[24] Hou Q, De Bank PA, Shakesheff KM. Injectable scaffolds for tissue regeneration. Journal of Materials Chemistry 2004;14:1915-23.
[25] Amini AR, Laurencin CT, Nukavarapu SP. Bone Tissue Engineering: Recent Advances and Challenges. Critical reviews in biomedical engineering 2012;40:363-408.
[26] Cancedda R, Giannoni P, Mastrogiacomo M. A tissue engineering approach to bone repair in large animal models and in clinical practice. Biomaterials 2007;28:4240-50.
[27] Wang RN, Green J, Wang Z, Deng Y, Qiao M, Peabody M, Zhang Q, Ye J, Yan Z, Denduluri S, Idowu O, Li M, Shen C, Hu A, Haydon RC, Kang R, Mok J, Lee MJ, Luu HL, Shi LL. Bone Morphogenetic Protein (BMP) signaling in development and human diseases. Genes & Diseases 2014;1:87-105.
[28] James AW, LaChaud G, Shen J, Asatrian G, Nguyen V, Zhang X, Ting K, Soo C. A Review of the Clinical Side Effects of Bone Morphogenetic Protein-2. Tissue Engineering Part B: Reviews 2016;22:284-97.
[29] Carragee EJ, Mitsunaga KA, Hurwitz EL, Scuderi GJ. Retrograde ejaculation after anterior lumbar interbody fusion using rhBMP-2: a cohort controlled study. The Spine Journal;11:511-6.
[30] Xu J, Li Z, Hou Y, Fang W. Potential mechanisms underlying the Runx2 induced osteogenesis of bone marrow mesenchymal stem cells. American Journal of Translational Research 2015;7:2527-35.
[31] Luu HH, Song WX, Luo X, Manning D, Luo J, Deng ZL, Sharff KA, Montag AG, Haydon RC, He TC. Distinct roles of bone morphogenetic proteins in osteogenic differentiation of mesenchymal stem cells. Journal of orthopaedic research : official publication of the Orthopaedic Research Society 2007;25:665-77.
[32] McKay B, Sandhu HS. Use of recombinant human bone morphogenetic protein-2 in spinal fusion applications. Spine 2002;27:S66-85.
[33] McKay B, Peckham S, Scifert J. Chapter 9 - Biologics to Promote Spinal Fusion. Spine Technology Handbook. Burlington: Academic Press; 2006. p. 241-79.

[34] Chen G, Deng C, Li Y-P. TGF-β and BMP Signaling in Osteoblast Differentiation and Bone Formation. International Journal of Biological Sciences 2012;8:272-88.
[35] Komori T. Regulation of osteoblast differentiation by transcription factors. Journal of Cellular Biochemistry 2006;99:1233-9.
[36] Komori T. Regulation of skeletal development by the Runx family of transcription factors. Journal of Cellular Biochemistry 2005;95:445-53.
[37] Dalle Carbonare L, Innamorati G, Valenti MT. Transcription Factor Runx2 and its Application to Bone Tissue Engineering. Stem Cell Reviews and Reports 2012;8:891-7.
[38] Cohen Jr MM. Perspectives on RUNX genes: An update. American Journal of Medical Genetics Part A 2009;149A:2629-46.
[39] Kanatani N, Fujita T, Fukuyama R, Liu W, Yoshida CA, Moriishi T, Yamana K, Miyazaki T, Toyosawa S, Komori T. Cbf beta regulates Runx2 function isoform-dependently in postnatal bone development. Developmental biology 2006;296:48-61.
[40] Komori T. Regulation of Osteoblast Differentiation by Runx2. In: Choi Y, editor. Osteoimmunology: Interactions of the Immune and skeletal systems II. Boston, MA: Springer US; 2010. p. 43-9.
[41] Komori T. Regulation of Osteoblast and Odontoblast Differentiation by RUNX2. Journal of Oral Biosciences 2010;52:22-5.
[42] Song L, Webb NE, Song Y, Tuan RS. Identification and functional analysis of candidate genes regulating mesenchymal stem cell self-renewal and multipotency. Stem Cells 2006;24:1707-18.
[43] Penick KJ, Solchaga LA, Welter JF. High-throughput aggregate culture system to assess the chondrogenic potential of mesenchymal stem cells. BioTechniques 2005.
[44] Zhao Z, Zhao M, Xiao G, Franceschi RT. Gene transfer of the Runx2 transcription factor enhances osteogenic activity of bone marrow stromal cells in vitro and in vivo. Molecular therapy : the journal of the American Society of Gene Therapy 2005;12:247-53.
[45] Zheng H, Guo Z, Ma Q, Jia H, Dang G. Cbfa1/osf2 Transduced Bone Marrow Stromal Cells Facilitate Bone Formation In Vitro and In Vivo. Calcified Tissue International 2004;74:194-203.
[46] Byers BA, Guldberg RE, Garcia AJ. Synergy between genetic and tissue engineering: Runx2 overexpression and in vitro construct development enhance in vivo mineralization. Tissue engineering 2004;10:1757-66.
[47] Gersbach CA, Le Doux JM, Guldberg RE, Garcia AJ. Inducible regulation of Runx2-stimulated osteogenesis. Gene Ther 2006;13:873-82.
[48] Kumar A, Singh TD, Singh SK, Prakash S. Methods, potentials, and limitations of gene delivery to regenerate central nervous system cells. Biologics : Targets & Therapy 2009;3:245-56.
[49] Curtin JF, Candolfi M, Xiong W, Lowenstein PR, Castro MG. Turning the gene tap off; implications of regulating gene expression for cancer therapeutics. Molecular cancer therapeutics 2008;7:439-48.
[50] Jo J, Hong S, Choi WY, Lee DR. Cell-penetrating peptide (CPP)-conjugated proteins is an efficient tool for manipulation of human mesenchymal stromal cells. Scientific Reports 2014;4:4378.
[51] Auman JT. Gene therapy: Have the risks associated with viral vectors been solved? Current opinion in molecular therapeutics 2010;12:637-8.

[52] Baldo A, van den Akker E, Bergmans HE, Lim F, Pauwels K. General Considerations on the Biosafety of Virus-derived Vectors Used in Gene Therapy and Vaccination. Current Gene Therapy 2013;13:385-94.
[53] Thomas CE, Ehrhardt A, Kay MA. Progress and problems with the use of viral vectors for gene therapy. Nature reviews Genetics 2003;4:346-58.
[54] Ravindran S, Snee PT, Ramachandran A, George A. Acidic Domain in Dentin Phosphophoryn Facilitates Cellular Uptake: IMPLICATIONS IN TARGETED PROTEIN DELIVERY. The Journal of biological chemistry 2013;288:16098-109.
[55] Thiagarajan L, Abu-Awwad HAM, Dixon JE. Osteogenic Programming of Human Mesenchymal Stem Cells with Highly Efficient Intracellular Delivery of RUNX2. Stem cells translational medicine 2017;6:2146-59.
[56] Um SH. Delivering Factors for Reprogramming a Somatic Cell to Pluripotency. International Journal of Stem Cells 2012;5:6-11.
[57] Bucher C, Gazdhar A, Benneker LM, Geiser T, Gantenbein-Ritter B. Nonviral Gene Delivery of Growth and Differentiation Factor 5 to Human Mesenchymal Stem Cells Injected into a 3D Bovine Intervertebral Disc Organ Culture System. Stem Cells International 2013;2013:326828.
[58] Halim NSSA, Fakiruddin KS, Ali SA, Yahaya BH. A Comparative Study of Non-Viral Gene Delivery Techniques to Human Adipose-Derived Mesenchymal Stem Cell. International Journal of Molecular Sciences 2014;15:15044-60.
[59] Zhang X, Godbey WT. Viral vectors for gene delivery in tissue engineering. Advanced drug delivery reviews 2006;58:515-34.
[60] Audouy S, Hoekstra D. Cationic lipid-mediated transfection in vitro and in vivo (review). Molecular membrane biology 2001;18:129-43.
[61] Crombez L, Morris MC, Dufort S, Aldrian-Herrada G, Nguyen Q, Mc Master G, Coll JL, Heitz F, Divita G. Targeting cyclin B1 through peptide-based delivery of siRNA prevents tumour growth. Nucleic acids research 2009;37:4559-69.
[62] Wadia JS, Dowdy SF. Protein transduction technology. Current opinion in biotechnology 2002;13:52-6.
[63] Schwarze SR, Ho A, Vocero-Akbani A, Dowdy SF. In vivo protein transduction: delivery of a biologically active protein into the mouse. Science (New York, NY) 1999;285:1569-72.
[64] Frankel AD, Pabo CO. Cellular uptake of the tat protein from human immunodeficiency virus. Cell 1988;55:1189-93.
[65] Green M, Loewenstein PM. Autonomous functional domains of chemically synthesized human immunodeficiency virus tat trans-activator protein. Cell 1988;55:1179-88.
[66] Copolovici DM, Langel K, Eriste E, Langel Ü. Cell-Penetrating Peptides: Design, Synthesis, and Applications. ACS Nano 2014;8:1972-94.
[67] Heitz F, Morris MC, Divita G. Twenty years of cell-penetrating peptides: from molecular mechanisms to therapeutics. British journal of pharmacology 2009;157:195-206.
[68] Eguchi A, Dowdy SF. siRNA delivery using peptide transduction domains. Trends in pharmacological sciences 2009;30:341-5.
[69] Mae M, Langel U. Cell-penetrating peptides as vectors for peptide, protein and oligonucleotide delivery. Current opinion in pharmacology 2006;6:509-14.

[70] Jarver P, Mager I, Langel U. In vivo biodistribution and efficacy of peptide mediated delivery. Trends in pharmacological sciences 2010;31:528-35.
[71] Taylor BN, Mehta RR, Yamada T, Lekmine F, Christov K, Chakrabarty AM, Green A, Bratescu L, Shilkaitis A, Beattie CW, Das Gupta TK. Noncationic peptides obtained from azurin preferentially enter cancer cells. Cancer research 2009;69:537-46.
[72] Johansson HJ, El-Andaloussi S, Holm T, Mae M, Janes J, Maimets T, Langel U. Characterization of a novel cytotoxic cell-penetrating peptide derived from p14ARF protein. Molecular therapy : the journal of the American Society of Gene Therapy 2008;16:115-23.
[73] Milletti F. Cell-penetrating peptides: classes, origin, and current landscape. Drug Discovery Today 2012;17:850-60.
[74] Fu A, Tang R, Hardie J, Farkas ME, Rotello VM. Promises and Pitfalls of Intracellular Delivery of Proteins. Bioconjugate Chemistry 2014;25:1602-8.
[75] Nakase I, Takeuchi T, Tanaka G, Futaki S. Methodological and cellular aspects that govern the internalization mechanisms of arginine-rich cell-penetrating peptides. Advanced drug delivery reviews 2008;60:598-607.
[76] Wadia JS, Stan RV, Dowdy SF. Transducible TAT-HA fusogenic peptide enhances escape of TAT-fusion proteins after lipid raft macropinocytosis. Nature medicine 2004;10:310-5.
[77] Torchilin V. Intracellular delivery of protein and peptide therapeutics. Drug Discovery Today: Technologies 2008;5:e95-e103.
[78] Erazo-Oliveras A, Najjar K, Dayani L, Wang T-Y, Johnson GA, Pellois J-P. Protein delivery into live cells by incubation with an endosomolytic agent. Nat Meth 2014;11:861-7.
[79] Liu NQ, Lossinsky AS, Popik W, Li X, Gujuluva C, Kriederman B, Roberts J, Pushkarsky T, Bukrinsky M, Witte M, Weinand M, Fiala M. Human immunodeficiency virus type 1 enters brain microvascular endothelia by macropinocytosis dependent on lipid rafts and the mitogen-activated protein kinase signaling pathway. Journal of virology 2002;76:6689-700.
[80] Kim D, Kim CH, Moon JI, Chung YG, Chang MY, Han BS, Ko S, Yang E, Cha KY, Lanza R, Kim KS. Generation of human induced pluripotent stem cells by direct delivery of reprogramming proteins. Cell stem cell 2009;4:472-6.
[81] Dixon JE, Osman G, Morris GE, Markides H, Rotherham M, Bayoussef Z, El Haj AJ, Denning C, Shakesheff KM. Highly efficient delivery of functional cargoes by the synergistic effect of GAG binding motifs and cell-penetrating peptides. Proceedings of the National Academy of Sciences of the United States of America 2016;113:E291-E9.
[82] Munoz EM, Linhardt RJ. Heparin-binding domains in vascular biology. Arteriosclerosis, thrombosis, and vascular biology 2004;24:1549-57.
[83] Varde NK, Pack DW. Microspheres for controlled release drug delivery. Expert Opinion on Biological Therapy 2004;4:35-51.
[84] Sinha VR, Trehan A. Biodegradable microspheres for protein delivery. Journal of Controlled Release 2003;90:261-80.
[85] Wise DL, Trantolo DJ, Marino RT, Kitchell JP. Immunoliposomes in VivoOpportunities and challenges in the design of implantable biodegradable polymeric systems for the delivery of antimicrobial agents and vaccines. Advanced drug delivery reviews 1988;1:269.

[86] Kim J-H, Taluja A, Knutson K, Han Bae Y. Stability of bovine serum albumin complexed with PEG-poly(l-histidine) diblock copolymer in PLGA microspheres. Journal of Controlled Release 2005;109:86-100.
[87] Kim KK, Pack DW. Microspheres for Drug Delivery. In: Ferrari M, Lee AP, Lee LJ, editors. BioMEMS and Biomedical Nanotechnology: Volume I Biological and Biomedical Nanotechnology. Boston, MA: Springer US; 2006. p. 19-50.
[88] Liechty WB, Kryscio DR, Slaughter BV, Peppas NA. Polymers for drug delivery systems. Annu Rev Chem Biomol Eng 2010;1:149-73.
[89] Uhrich KE, Cannizzaro SM, Langer RS, Shakesheff KM. Polymeric systems for controlled drug release. Chemical reviews 1999;99:3181-98.
[90] Reis RL, Cunha AM, Allan PS, Bevis MJ. Mechanical behavior of injection-molded starch-based polymers. Polymers for Advanced Technologies 1996;7:784-90.
[91] Seal BL, Otero TC, Panitch A. Polymeric biomaterials for tissue and organ regeneration. Materials Science and Engineering: R: Reports 2001;34:147-230.
[92] Di Martino A, Sittinger M, Risbud MV. Chitosan: a versatile biopolymer for orthopaedic tissue-engineering. Biomaterials 2005;26:5983-90.
[93] Lee SB, Kim YH, Chong MS, Hong SH, Lee YM. Study of gelatin-containing artificial skin V: fabrication of gelatin scaffolds using a salt-leaching method. Biomaterials 2005;26:1961-8.
[94] Mohanty AK, Misra M, Hinrichsen G. Biofibres, biodegradable polymers and biocomposites: An overview. Macromolecular Materials and Engineering 2000;276-277:1-24.
[95] Amit Jagannath G, Harshal Ashok P. - Synthetic Biodegradable Polymers Used in Controlled Drug Delivery System: An Overview.
[96] Alam AS, Parrott EL. Effect of aging on some physical properties of hydrochlorothiazide tablets. Journal of Pharmaceutical Sciences 1971;60:263-6.
[97] Makadia HK, Siegel SJ. Poly Lactic-co-Glycolic Acid (PLGA) as Biodegradable Controlled Drug Delivery Carrier. Polymers 2011;3:1377-97.
[98] Bouissou C, Rouse JJ, Price R, van der Walle CF. The Influence of Surfactant on PLGA Microsphere Glass Transition and Water Sorption: Remodeling the Surface Morphology to Attenuate the Burst Release. Pharmaceutical Research 2006;23:1295-305.
[99] Jain RA. The manufacturing techniques of various drug loaded biodegradable poly(lactide-co-glycolide) (PLGA) devices. Biomaterials 2000;21:2475-90.
[100] Ruhe PQ, Hedberg EL, Padron NT, Spauwen PH, Jansen JA, Mikos AG. rhBMP-2 release from injectable poly(DL-lactic-co-glycolic acid)/calcium-phosphate cement composites. The Journal of bone and joint surgery American volume 2003;85-A Suppl 3:75-81.
[101] Wu XS, Wang N. Synthesis, characterization, biodegradation, and drug delivery application of biodegradable lactic/glycolic acid polymers. Part II: biodegradation. Journal of biomaterials science Polymer edition 2001;12:21-34.
[102] Lu L, Peter SJ, Lyman MD, Lai HL, Leite SM, Tamada JA, Uyama S, Vacanti JP, Langer R, Mikos AG. In vitro and in vivo degradation of porous poly(DL-lactic-co-glycolic acid) foams. Biomaterials 2000;21:1837-45.
[103] Lu L, Garcia CA, Mikos AG. In vitro degradation of thin poly(DL-lactic-co-glycolic acid) films. Journal of biomedical materials research 1999;46:236-44.

[104] Park TG. Degradation of poly(lactic-co-glycolic acid) microspheres: effect of copolymer composition. Biomaterials 1995;16:1123-30.
[105] Park TG. Degradation of poly(d,l-lactic acid) microspheres: effect of molecular weight. Journal of Controlled Release 1994;30:161-73.
[106] Liggins RT, Burt HM. Paclitaxel loaded poly(L-lactic acid) microspheres: properties of microspheres made with low molecular weight polymers. International journal of pharmaceutics 2001;222:19-33.
[107] Schliecker G, Schmidt C, Fuchs S, Wombacher R, Kissel T. Hydrolytic degradation of poly(lactide-co-glycolide) films: effect of oligomers on degradation rate and crystallinity. International journal of pharmaceutics 2003;266:39-49.
[108] Witt C, Kissel T. Morphological characterization of microspheres, films and implants prepared from poly(lactide-co-glycolide) and ABA triblock copolymers: is the erosion controlled by degradation, swelling or diffusion? European journal of pharmaceutics and biopharmaceutics : official journal of Arbeitsgemeinschaft fur Pharmazeutische Verfahrenstechnik eV 2001;51:171-81.
[109] Grizzi I, Garreau H, Li S, Vert M. Hydrolytic degradation of devices based on poly(DL-lactic acid) size-dependence. Biomaterials 1995;16:305-11.
[110] Han FY, Thurecht KJ, Whittaker AK, Smith MT. Bioerodable PLGA-Based Microparticles for Producing Sustained-Release Drug Formulations and Strategies for Improving Drug Loading. Frontiers in Pharmacology 2016;7:185.
[111] Patel RP, Patel MP, Suthar AM. Spray Drying Technology: an overview2009.
[112] Yeo Y, Chen AU, Basaran OA, Park K. Solvent exchange method: a novel microencapsulation technique using dual microdispensers. Pharm Res 2004;21:1419-27.
[113] Zhu L, Li Y, Zhang Q, Wang H, Zhu M. Fabrication of monodisperse, large-sized, functional biopolymeric microspheres using a low-cost and facile microfluidic device. Biomedical microdevices 2010;12:169-77.
[114] Walstra P. Principles of emulsion formation. Chemical Engineering Science 1993;48:333-49.
[115] p. http://people.umass.edu/mcclemen/FoodEmulsions2008/Presentations.
[116] Morita T, Sakamura Y, Horikiri Y, Suzuki T, Yoshino H. Protein encapsulation into biodegradable microspheres by a novel S/O/W emulsion method using poly(ethylene glycol) as a protein micronization adjuvant. Journal of controlled release : official journal of the Controlled Release Society 2000;69:435-44.
[117] Castellanos IJ, Carrasquillo KG, Lopez JD, Alvarez M, Griebenow K. Encapsulation of bovine serum albumin in poly(lactide-co-glycolide) microspheres by the solid-in-oil-in-water technique. The Journal of pharmacy and pharmacology 2001;53:167-78.
[118] Wischke C, Schwendeman SP. Principles of encapsulating hydrophobic drugs in PLA/PLGA microparticles. International journal of pharmaceutics 2008;364:298-327.
[119] Dawes GJ, Fratila-Apachitei LE, Mulia K, Apachitei I, Witkamp GJ, Duszczyk J. Size effect of PLGA spheres on drug loading efficiency and release profiles. Journal of materials science Materials in medicine 2009;20:1089-94.

[120] Bible E, Chau DY, Alexander MR, Price J, Shakesheff KM, Modo M. Attachment of stem cells to scaffold particles for intra-cerebral transplantation. Nature protocols 2009;4:1440-53.
[121] Sah H. Protein behavior at the water/methylene chloride interface. J Pharm Sci 1999;88:1320-5.
[122] Fu K, Klibanov AM, Langer R. Protein stability in controlled-release systems. Nat Biotech 2000;18:24-5.
[123] Ye M, Kim S, Park K. Issues in long-term protein delivery using biodegradable microparticles. Journal of controlled release : official journal of the Controlled Release Society 2010;146:241-60.
[124] van de Weert M, Hennink WE, Jiskoot W. Protein Instability in Poly(Lactic-co-Glycolic Acid) Microparticles. Pharmaceutical Research 2000;17:1159-67.
[125] Fu K, Pack DW, Klibanov AM, Langer R. Visual Evidence of Acidic Environment Within Degrading Poly(lactic-co-glycolic acid) (PLGA) Microspheres. Pharmaceutical Research 2000;17:100-6.
[126] Shao PG, Bailey LC. Stabilization of pH-Induced Degradation of Porcine Insulin in Biodegradable Polyester Microspheres. Pharmaceutical Development and Technology 1999;4:633-42.
[127] Liu WR, Langer R, Klibanov AM. Moisture-induced aggregation of lyophilized proteins in the solid state. Biotechnology and Bioengineering 1991;37:177-84.
[128] Pérez C, Griebenow K. Improved activity and stability of lysozyme at the water/CH2CI2 interface: enzyme unfolding and aggregation and its prevention by polyols. Journal of Pharmacy and Pharmacology 2001;53:1217-26.
[129] Pérez C, De Jesús P, Griebenow K. Preservation of lysozyme structure and function upon encapsulation and release from poly(lactic-co-glycolic) acid microspheres prepared by the water-in-oil-in-water method. International journal of pharmaceutics 2002;248:193-206.
[130] Kang F, Jiang G, Hinderliter A, DeLuca PP, Singh J. Lysozyme Stability in Primary Emulsion for PLGA Microsphere Preparation: Effect of Recovery Methods and Stabilizing Excipients. Pharmaceutical Research 2002;19:629-33.
[131] Pérez-Rodriguez C, Montano N, Gonzalez K, Griebenow K. Stabilization of α-chymotrypsin at the CH2Cl2/water interface and upon water-in-oil-in-water encapsulation in PLGA microspheres. Journal of Controlled Release 2003;89:71-85.
[132] Morita T, Sakamura Y, Horikiri Y, Suzuki T, Yoshino H. Protein encapsulation into biodegradable microspheres by a novel S/O/W emulsion method using poly(ethylene glycol) as a protein micronization adjuvant. Journal of Controlled Release 2000;69:435-44.
[133] Jiang W, Schwendeman SP. Stabilization and Controlled Release of Bovine Serum Albumin Encapsulated in Poly(D, L-lactide) and Poly(ethylene glycol) Microsphere Blends. Pharmaceutical Research 2001;18:878-85.
[134] Marinina J, Shenderova A, Mallery SR, Schwendeman SP. Stabilization of Vinca Alkaloids Encapsulated in Poly(lactide-co-glycolide) Microspheres. Pharmaceutical Research 2000;17:677-83.
[135] Zhu G, Mallery SR, Schwendeman SP. Stabilization of proteins encapsulated in injectable poly (lactide- co-glycolide). Nat Biotech 2000;18:52-7.

[136] Kaibara K, Okazaki T, Bohidar HB, Dubin PL. pH-Induced Coacervation in Complexes of Bovine Serum Albumin and Cationic Polyelectrolytes. Biomacromolecules 2000;1:100-7.
[137] Xia J, Dubin PL, Kokufuta E, Havel H, Muhoberac BB. Light scattering, CD, and ligand binding studies of ferrihemoglobin–polyelectrolyte complexes. Biopolymers 1999;50:153-61.
[138] Gao JY, Dubin PL. Binding of proteins to copolymers of varying hydrophobicity. Biopolymers 1999;49:185-93.
[139] Tormala P, Pohjonen T, Rokkanen P. Bioabsorbable polymers: materials technology and surgical applications. Proceedings of the Institution of Mechanical Engineers Part H, Journal of engineering in medicine 1998;212:101-11.
[140] Agrawal CM. Reconstructing the human body using biomaterials. JOM 1998;50:31-5.
[141] Quatela VC, Chow J. Synthetic facial implants. Facial plastic surgery clinics of North America 2008;16:1-10, v.
[142] Chen G, Ushida T, Tateishi T. Scaffold Design for Tissue Engineering. Macromolecular Bioscience 2002;2:67-77.
[143] Landers R, Pfister A, Hübner U, John H, Schmelzeisen R, Mülhaupt R. Fabrication of soft tissue engineering scaffolds by means of rapid prototyping techniques. Journal of Materials Science 2002;37:3107-16.
[144] Pérez-Pomares JM, Mironov V, Guadix JA, Macías D, Markwald RR, Muñoz-Chápuli R. In vitro self-assembly of proepicardial cell aggregates: An embryonic vasculogenic model for vascular tissue engineering. The Anatomical Record Part A: Discoveries in Molecular, Cellular, and Evolutionary Biology 2006;288A:700-13.
[145] Drury JL, Mooney DJ. Hydrogels for tissue engineering: scaffold design variables and applications. Biomaterials 2003;24:4337-51.
[146] Kakudo N, Shimotsuma A, Miyake S, Kushida S, Kusumoto K. Bone tissue engineering using human adipose-derived stem cells and honeycomb collagen scaffold. Journal of biomedical materials research Part A 2008;84:191-7.
[147] Zhang L, Ao Q, Wang A, Lu G, Kong L, Gong Y, Zhao N, Zhang X. A sandwich tubular scaffold derived from chitosan for blood vessel tissue engineering. Journal of biomedical materials research Part A 2006;77:277-84.
[148] Elkayam T, Amitay-Shaprut S, Dvir-Ginzberg M, Harel T, Cohen S. Enhancing the drug metabolism activities of C3A--a human hepatocyte cell line--by tissue engineering within alginate scaffolds. Tissue engineering 2006;12:1357-68.
[149] Seeherman H, Wozney JM. Delivery of bone morphogenetic proteins for orthopedic tissue regeneration. Cytokine & Growth Factor Reviews 2005;16:329-45.
[150] Jarcho M. Calcium phosphate ceramics as hard tissue prosthetics. Clinical orthopaedics and related research 1981:259-78.
[151] Hutmacher DW. Scaffolds in tissue engineering bone and cartilage. Biomaterials 2000;21:2529-43.
[152] Dhillon A, Schneider P, Kuhn G, Reinwald Y, White LJ, Levchuk A, Rose FRAJ, Müller R, Shakesheff KM, Rahman CV. Analysis of sintered polymer scaffolds using concomitant synchrotron computed tomography and in situ

mechanical testing. Journal of Materials Science: Materials in Medicine 2011;22:2599-605.
[153] G. Hamilton L, Quirk R, Shakesheff K. An Injectable Scaffold for Cell and Growth Factor Delivery. Journal of Pharmacy and Pharmacology 2010;62:1498-9.
[154] V. Rahman C, C. Cox H, G. Hamilton L, Quirk R, R. A. J. Rose F, Shakesheff K. Injectable Scaffold for Bone Tissue Engineering Applications. Journal of Pharmacy and Pharmacology 2010;62:1508-9.
[155] Kretlow JD, Klouda L, Mikos AG. Injectable matrices and scaffolds for drug delivery in tissue engineering. Advanced drug delivery reviews 2007;59:263-73.
[156] Suggs LJ, Shive MS, Garcia CA, Anderson JM, Mikos AG. In vitro cytotoxicity and in vivo biocompatibility of poly(propylene fumarate-co-ethylene glycol) hydrogels. Journal of biomedical materials research 1999;46:22-32.
[157] Burdick JA, Mason MN, Hinman AD, Thorne K, Anseth KS. Delivery of osteoinductive growth factors from degradable PEG hydrogels influences osteoblast differentiation and mineralization. Journal of controlled release : official journal of the Controlled Release Society 2002;83:53-63.
[158] Sawkins MJ, Mistry P, Brown BN, Shakesheff KM, Bonassar LJ, Yang J. Cell and protein compatible 3D bioprinting of mechanically strong constructs for bone repair. Biofabrication 2015;7:035004.
[159] Bose S, Vahabzadeh S, Bandyopadhyay A. Bone tissue engineering using 3D printing. Materials Today 2013;16:496-504.
[160] Wen Y, Xun S, Haoye M, Baichuan S, Peng C, Xuejian L, Kaihong Z, Xuan Y, Jiang P, Shibi L. 3D printed porous ceramic scaffolds for bone tissue engineering: a review. Biomaterials Science 2017;5:1690-8.
[161] Seitz H, Rieder W, Irsen S, Leukers B, Tille C. Three-dimensional printing of porous ceramic scaffolds for bone tissue engineering. Journal of biomedical materials research Part B, Applied biomaterials 2005;74:782-8.
[162] Do A-V, Khorsand B, Geary SM, Salem AK. 3D Printing of Scaffolds for Tissue Regeneration Applications. Advanced healthcare materials 2015;4:1742-62.
[163] Peltola SM, Melchels FP, Grijpma DW, Kellomaki M. A review of rapid prototyping techniques for tissue engineering purposes. Annals of medicine 2008;40:268-80.
[164] Cho DID, Yoo HJ. Microfabrication Methods for Biodegradable Polymeric Carriers for Drug Delivery System Applications: A Review. Journal of Microelectromechanical Systems 2015;24:10-8.
[165] Rosca ID, Watari F, Uo M. Microparticle formation and its mechanism in single and double emulsion solvent evaporation. Journal of Controlled Release 2004;99:271-80.
[166] Kemala T, Budianto E, Soegiyono B. Preparation and characterization of microspheres based on blend of poly(lactic acid) and poly(ε-caprolactone) with poly(vinyl alcohol) as emulsifier. Arabian Journal of Chemistry 2012;5:103-8.
[167] van de Weert M, Hennink W, Jiskoot W. Protein Instability in Poly(Lactic-co-Glycolic Acid) Microparticles. An Official Journal of the American Association of Pharmaceutical Scientists 2000;17:1159-67.

[168] Kirby GTS, White LJ, Rahman CV, Cox HC, Qutachi O, Rose FRAJ, Hutmacher DW, Shakesheff KM, Woodruff MA. PLGA-Based Microparticles for the Sustained Release of BMP-2. Polymers 2011;3:571.
[169] White LJ, Kirby GTS, Cox HC, Qodratnama R, Qutachi O, Rose FRAJ, Shakesheff KM. Accelerating protein release from microparticles for regenerative medicine applications. Materials Science and Engineering: C 2013;33:2578-83.
[170] Sah H. A new strategy to determine the actual protein content of poly(lactide-co-glycolide) microspheres. Journal of Pharmaceutical Sciences 1997;86:1315-8.
[171] Morita T, Horikiri Y, Suzuki T, Yoshino H. Applicability of various amphiphilic polymers to the modification of protein release kinetics from biodegradable reservoir-type microspheres. European Journal of Pharmaceutics and Biopharmaceutics 2001;51:45-53.
[172] Eltaher HM, Yang J, Shakesheff KM, Dixon JE. Highly efficient intracellular transduction in three-dimensional gradients for programming cell fate. Acta Biomaterialia 2016;41:181-92.
[173] Bhatt Y, Shah D. Influence of additives on fabrication and release from protein loaded PLGA microparticles2012.
[174] Sharma N, Madan P, Lin S. Effect of process and formulation variables on the preparation of parenteral paclitaxel-loaded biodegradable polymeric nanoparticles: A co-surfactant study. Asian Journal of Pharmaceutical Sciences 2016;11:404-16.
[175] Mu L, Feng SS. A novel controlled release formulation for the anticancer drug paclitaxel (Taxol): PLGA nanoparticles containing vitamin E TPGS. Journal of controlled release : official journal of the Controlled Release Society 2003;86:33-48.
[176] Zambaux MF, Bonneaux F, Gref R, Dellacherie E, Vigneron C. Preparation and characterization of protein C-loaded PLA nanoparticles. Journal of Controlled Release 1999;60:179-88.
[177] Elias CB, Joshi JB. Role of hydrodynamic shear on activity and structure of proteins. Advances in biochemical engineering/biotechnology 1998;59:47-71.
[178] Thomas CR, Geer D. Effects of shear on proteins in solution. Biotechnology Letters 2010;33:443-56.
[179] Azizi M, Farahmandghavi F, Joghataei M, Zandi M, Imani M, Bakhtiary M, Dorkoosh FA, Ghazizadeh F. Fabrication of protein-loaded PLGA nanoparticles: effect of selected formulation variables on particle size and release profile. Journal of Polymer Research 2013;20:110.
[180] Jiang G, Woo BH, Kang F, Singh J, DeLuca PP. Assessment of protein release kinetics, stability and protein polymer interaction of lysozyme encapsulated poly(d,l-lactide-co-glycolide) microspheres. Journal of Controlled Release 2002;79:137-45.
[181] Klose D, Siepmann F, Elkharraz K, Krenzlin S, Siepmann J. How porosity and size affect the drug release mechanisms from PLGA-based microparticles. International journal of pharmaceutics 2006;314:198-206.
[182] Mao S, Xu J, Cai C, Germershaus O, Schaper A, Kissel T. Effect of WOW process parameters on morphology and burst release of FITC-dextran loaded PLGA microspheres. International journal of pharmaceutics 2007;334:137-48.

[183] Qutachi O, Vetsch JR, Gill D, Cox H, Scurr DJ, Hofmann S, Müller R, Quirk RA, Shakesheff KM, Rahman CV. Injectable and porous PLGA microspheres that form highly porous scaffolds at body temperature. Acta Biomaterialia 2014;10:5090-8.
[184] Estey T, Kang J, Schwendeman SP, Carpenter JF. BSA Degradation Under Acidic Conditions: A Model For Protein Instability During Release From PLGA Delivery Systems. Journal of Pharmaceutical Sciences;95:1626-39.
[185] Jiang G, Woo BH, Kang F, Singh J, DeLuca PP. Assessment of protein release kinetics, stability and protein polymer interaction of lysozyme encapsulated poly(d,l-lactide-co-glycolide) microspheres. Journal of Controlled Release 2002;79:137-45.
[186] Mitragotri S, Burke PA, Langer R. Overcoming the challenges in administering biopharmaceuticals: formulation and delivery strategies. Nat Rev Drug Discov 2014;13:655-72.
[187] Jeon BJ, Jeong SY, Koo AN, Kim B-C, Hwang Y-S, Lee SC. Fabrication of porous PLGA microspheres with BMP-2 releasing polyphosphate-functionalized nano-hydroxyapatite for enhanced bone regeneration. Macromolecular Research 2012;20:715-24.
[188] Nicolete R, Santos DFd, Faccioli LH. The uptake of PLGA micro or nanoparticles by macrophages provokes distinct in vitro inflammatory response. International Immunopharmacology 2011;11:1557-63.
[189] Singh M, Kazzaz J, Chesko J, Soenawan E, Ugozzoli M, Giuliani M, Pizza M, Rappouli R, O'Hagan DT. Anionic microparticles are a potent delivery system for recombinant antigens from Neisseria meningitidis serotype B. J Pharm Sci 2004;93:273-82.
[190] Bruderer M, Richards RG, Alini M, Stoddart MJ. Role and regulation of runx2 in osteogenesis. European Cells and Materials 2014;28:269-86.
[191] Hayrapetyan A, Jansen JA, van den Beucken JJ. Signaling pathways involved in osteogenesis and their application for bone regenerative medicine. Tissue Eng Part B Rev 2015;21:75-87.
[192] Birmingham E, Niebur GL, Mchugh PE, Shaw G, Barry FP, McNamara LM. Osteogenic differentiation of mesenchymal stem cells is regulated by osteocyte and osteoblast cells in a simplified bone niche. European Cells and Materials 2012;23:13-27.
[193] Rahman MS, Akhtar N, Jamil HM, Banik RS, Asaduzzaman SM. TGF-beta/BMP signaling and other molecular events: regulation of osteoblastogenesis and bone formation. Bone Res 2015;3:15005.
[194] Phillips JE, Burns KL, Le Doux JM, Guldberg RE, García AJ. Engineering graded tissue interfaces. Proceedings of the National Academy of Sciences 2008;105:12170-5.
[195] Gould TWA, Birchall JP, Mallick AS, Alliston T, Lustig LR, Shakesheff KM, Rahman CV. Development of a porous poly(DL-lactic acid-co-glycolic acid)-based scaffold for mastoid air-cell regeneration. The Laryngoscope 2013;123:3156-61.
[196] Murphy SV, Atala A. 3D bioprinting of tissues and organs. Nat Biotech 2014;32:773-85.
[197] Malda J, Visser J, Melchels FP, Jüngst T, Hennink WE, Dhert WJA, Groll J, Hutmacher DW. 25th Anniversary Article: Engineering Hydrogels for Biofabrication. Advanced Materials 2013;25:5011-28.

[198] Dixon JE, Osman G, Morris GE, Markides H, Rotherham M, Bayoussef Z, El Haj AJ, Denning C, Shakesheff KM. Highly efficient delivery of functional cargoes by the synergistic effect of GAG binding motifs and cell-penetrating peptides. Proceedings of the National Academy of Sciences of the United States of America 2016;113:E291-9.
[199] Abu-Awwad HA-DM, Thiagarajan L, Dixon JE. Controlled release of GAG-binding enhanced transduction (GET) peptides for sustained and highly efficient intracellular delivery. Acta Biomaterialia 2017;57:225-37.
[200] Zhang H, Pan Y, Zheng L, Choe C, Lindgren B, Jensen ED, Westendorf JJ, Cheng L, Huang H. FOXO1 Inhibits Runx2 Transcriptional Activity and Prostate Cancer Cell Migration and Invasion. Cancer Research 2011.
[201] Dixon JE, Dick E, Rajamohan D, Shakesheff KM, Denning C. Directed Differentiation of Human Embryonic Stem Cells to Interrogate the Cardiac Gene Regulatory Network. Molecular Therapy;19:1695-703.
[202] Dhillon A, Rahman C, White L, Scammell B, Shakesheff K. Physical and Biological Characterisation of a Novel Injectable Scaffold Formulation2010.
[203] Song L, Webb NE, Song Y, Tuan RS. Identification and Functional Analysis of Candidate Genes Regulating Mesenchymal Stem Cell Self-Renewal and Multipotency. STEM CELLS 2006;24:1707-18.
[204] Dhillon A, Schneider P, Kuhn G, Reinwald Y, White LJ, Levchuk A, Rose FR, Muller R, Shakesheff KM, Rahman CV. Analysis of sintered polymer scaffolds using concomitant synchrotron computed tomography and in situ mechanical testing. Journal of materials science Materials in medicine 2011;22:2599-605.
[205] Marom R, Shur I, Solomon R, Benayahu D. Characterization of adhesion and differentiation markers of osteogenic marrow stromal cells. Journal of Cellular Physiology 2005;202:41-8.
[206] Golub EE, Boesze-Battaglia K. The role of alkaline phosphatase in mineralization. Current Opinion in Orthopaedics 2007;18:444-8.
[207] Granéli C, Thorfve A, Ruetschi U, Brisby H, Thomsen P, Lindahl A, Karlsson C. Novel markers of osteogenic and adipogenic differentiation of human bone marrow stromal cells identified using a quantitative proteomics approach. Stem Cell Research 2014;12:153-65.
[208] Duong LT, Rodan GA. Regulation of Osteoclast Formation and Function*. Reviews in Endocrine and Metabolic Disorders 2001;2:95-104.
[209] Nakamura A, Dohi Y, Akahane M, Ohgushi H, Nakajima H, Funaoka H, Takakura Y. Osteocalcin secretion as an early marker of in vitro osteogenic differentiation of rat mesenchymal stem cells. Tissue engineering Part C, Methods 2009;15:169-80.
[210] Zohar R, Cheifetz S, McCulloch CA, Sodek J. Analysis of intracellular osteopontin as a marker of osteoblastic cell differentiation and mesenchymal cell migration. European journal of oral sciences 1998;106 Suppl 1:401-7.
[211] Gioffredi E, Boffito M, Calzone S, Giannitelli SM, Rainer A, Trombetta M, Mozetic P, Chiono V. Pluronic F127 Hydrogel Characterization and Biofabrication in Cellularized Constructs for Tissue Engineering Applications. Procedia CIRP 2016;49:125-32.
[212] Brunet-Maheu J-M, C Fernandes J, A V de Lacerda C, Shi Q, Benderdour M, Lavigne P. Pluronic F-127 as a Cell Carrier for Bone Tissue Engineering2008.

[213] Fedorovich NE, Swennen I, Girones J, Moroni L, van Blitterswijk CA, Schacht E, Alblas J, Dhert WJ. Evaluation of photocrosslinked Lutrol hydrogel for tissue printing applications. Biomacromolecules 2009;10:1689-96.
[214] Khattak SF, Bhatia SR, Roberts SC. Pluronic F127 as a cell encapsulation material: utilization of membrane-stabilizing agents. Tissue engineering 2005;11:974-83.
[215] Vieira MGA, da Silva MA, dos Santos LO, Beppu MM. Natural-based plasticizers and biopolymer films: A review. European Polymer Journal 2011;47:254-63.
[216] Fringant C, Rinaudo M, Foray MF, Bardet M. Preparation of mixed esters of starch or use of an external plasticizer: Two different ways to change the properties of starch acetate films1998.
[217] Simmons CA, Alsberg E, Hsiong S, Kim WJ, Mooney DJ. Dual growth factor delivery and controlled scaffold degradation enhance in vivo bone formation by transplanted bone marrow stromal cells. Bone 2004;35:562-9.
[218] Green DW, Mann S, Oreffo ROC. Mineralized polysaccharide capsules as biomimetic microenvironments for cell, gene and growth factor delivery in tissue engineering. Soft Matter 2006;2:732-7.
[219] Shi S, Cheng X, Wang J, Zhang W, Peng L, Zhang Y. RhBMP-2 Microspheres-Loaded Chitosan/Collagen Scaffold Enhanced Osseointegration: An Experiment in Dog. Journal of Biomaterials Applications 2009;23:331-46.
[220] Lutolf MP, Hubbell JA. Synthetic biomaterials as instructive extracellular microenvironments for morphogenesis in tissue engineering. Nature biotechnology 2005;23:47-55.
[221] Chen FM, Zhao YM, Wu H, Deng ZH, Wang QT, Zhou W, Liu Q, Dong GY, Li K, Wu ZF, Jin Y. Enhancement of periodontal tissue regeneration by locally controlled delivery of insulin-like growth factor-I from dextran-co-gelatin microspheres. Journal of controlled release : official journal of the Controlled Release Society 2006;114:209-22.
[222] Patel ZS, Young S, Tabata Y, Jansen JA, Wong ME, Mikos AG. Dual delivery of an angiogenic and an osteogenic growth factor for bone regeneration in a critical size defect model. Bone 2008;43:931-40.
[223] Park H, Temenoff JS, Tabata Y, Caplan AI, Mikos AG. Injectable biodegradable hydrogel composites for rabbit marrow mesenchymal stem cell and growth factor delivery for cartilage tissue engineering. Biomaterials 2007;28:3217-27.
[224] Chen RR, Silva EA, Yuen WW, Mooney DJ. Spatio-temporal VEGF and PDGF delivery patterns blood vessel formation and maturation. Pharm Res 2007;24:258-64.
[225] Kimura Y, Hokugo A, Takamoto T, Tabata Y, Kurosawa H. Regeneration of anterior cruciate ligament by biodegradable scaffold combined with local controlled release of basic fibroblast growth factor and collagen wrapping. Tissue engineering Part C, Methods 2008;14:47-57.
[226] Lee ES, Kwon MJ, Na K, Bae JH. Protein release behavior from porous microparticle with lysozyme/hyaluronate ionic complex. Colloids and Surfaces B: Biointerfaces 2007;55:125-30.
[227] Tomoda K, Kojima S, Kajimoto M, Watanabe D, Nakajima T, Makino K. Effects of pulmonary surfactant system on rifampicin release from rifampicin-loaded PLGA microspheres. Colloids and Surfaces B: Biointerfaces 2005;45:1-6.

[228] Bernkop-Schnürch A, Egger C, Elhassan Imam M, Krauland AH. Preparation and in vitro characterization of poly(acrylic acid)–cysteine microparticles. Journal of Controlled Release 2003;93:29-38.
[229] Ungaro F, De Rosa G, Miro A, Quaglia F, La Rotonda MI. Cyclodextrins in the production of large porous particles: Development of dry powders for the sustained release of insulin to the lungs. European Journal of Pharmaceutical Sciences 2006;28:423-32.
[230] Chang JK, Li CJ, Wu SC, Yeh CH, Chen CH, Fu YC, Wang GJ, Ho ML. Effects of anti-inflammatory drugs on proliferation, cytotoxicity and osteogenesis in bone marrow mesenchymal stem cells. Biochemical pharmacology 2007;74:1371-82.
[231] Li X, Jin L, Cui Q, Wang GJ, Balian G. Steroid effects on osteogenesis through mesenchymal cell gene expression. Osteoporosis international : a journal established as result of cooperation between the European Foundation for Osteoporosis and the National Osteoporosis Foundation of the USA 2005;16:101-8.
[232] Phillips JE, Gersbach CA, Wojtowicz AM, Garcia AJ. Glucocorticoid-induced osteogenesis is negatively regulated by Runx2/Cbfa1 serine phosphorylation. Journal of cell science 2006;119:581-91.
[233] Choi KM, Seo YK, Yoon HH, Song KY, Kwon SY, Lee HS, Park JK. Effect of ascorbic acid on bone marrow-derived mesenchymal stem cell proliferation and differentiation. Journal of bioscience and bioengineering 2008;105:586-94.
[234] Al-Salleeh F, Beatty MW, Reinhardt RA, Petro TM, Crouch L. Human osteogenic protein-1 induces osteogenic differentiation of adipose-derived stem cells harvested from mice. Archives of oral biology 2008;53:928-36.
[235] Bronckers AL, Gay S, Finkelman RD, Butler WT. Developmental appearance of Gla proteins (osteocalcin) and alkaline phosphatase in tooth germs and bones of the rat. Bone and mineral 1987;2:361-73.
[236] Cao T, Heng BC, Ye CP, Liu H, Toh WS, Robson P, Li P, Hong YH, Stanton LW. Osteogenic differentiation within intact human embryoid bodies result in a marked increase in osteocalcin secretion after 12 days of in vitro culture, and formation of morphologically distinct nodule-like structures. Tissue & cell 2005;37:325-34.
[237] Kim H, Kim HW, Suh H. Sustained release of ascorbate-2-phosphate and dexamethasone from porous PLGA scaffolds for bone tissue engineering using mesenchymal stem cells. Biomaterials 2003;24:4671-9.
[238] Zhang J, Li J, Jia G, Jiang Y, Liu Q, Yang X, Pan S. Improving osteogenesis of PLGA/HA porous scaffolds based on dual delivery of BMP-2 and IGF-1 via a polydopamine coating. RSC Advances 2017;7:56732-42.
[239] Kim TH, Yun YP, Park YE, Lee SH, Yong W, Kundu J, Jung JW, Shim JH, Cho DW, Kim SE, Song HR. In vitro and in vivo evaluation of bone formation using solid freeform fabrication-based bone morphogenic protein-2 releasing PCL/PLGA scaffolds. Biomedical materials (Bristol, England) 2014;9:025008.
[240] Ramsey LB, Pounds S, Cheng C, Cao X, Yang W, Smith C, Karol SE, Liu C, Panetta JC, Inaba H, Rubnitz JE, Metzger ML, Ribeiro RC, Sandlund JT, Jeha S, Pui CH, Evans WE, Relling MV. Genetics of pleiotropic effects of dexamethasone. Pharmacogenetics and genomics 2017;27:294-302.

[241] Yang J, Shi P, Tu M, Wang Y, Liu M, Fan F, Du M. Bone morphogenetic proteins: Relationship between molecular structure and their osteogenic activity. Food Science and Human Wellness 2014;3:127-35.
[242] Mekonnen T, Mussone P, Khalil H, Bressler D. Progress in bio-based plastics and plasticizing modifications. Journal of Materials Chemistry A 2013;1:13379-98.
[243] Sant S, Hancock MJ, Donnelly JP, Iyer D, Khademhosseini A. BIOMIMETIC GRADIENT HYDROGELS FOR TISSUE ENGINEERING. Can J Chem Eng 2010;88:899-911.
[244] Ashe HL, Briscoe J. The interpretation of morphogen gradients. Development 2006;133:385-94.
[245] Nguyen EH, Schwartz MP, Murphy WL. Biomimetic Approaches to Control Soluble Concentration Gradients in Biomaterials. Macromolecular bioscience 2011;11:483-92.
[246] Wolpert L. One hundred years of positional information. Trends in Genetics 1996;12:359-64.